

Alessio Filippi
via Scapacchiò est 5
35030 Saccolongo (PD)
Italien

Non-conventional multi-carrier air interface for mobile radio systems

deutscher Titel:
**Nicht-konventionelle Multiträger-Luftschnittstelle für
Mobilfunksysteme**

Vom Fachbereich Elektrotechnik und Informationstechnik
der Technischen Universität Kaiserslautern
zur Verleihung des akademischen Grades
Doktor der Ingenieurwissenschaften (Dr.-Ing.)
genehmigte Dissertation

von
Ing. Alessio Filippi
D 386

Tag der Einreichung: 22. Oktober 2004
Tag der mündlichen Prüfung: 9. February 2005

Dekan des Fachbereichs: Prof. Dr.-Ing. G. Huth

Vorsitzender der
Prüfungskommission: Prof. Dr.-Ing. Tielert

1. Berichterstatter: Prof. Dr.-Ing. habil. Dr.-Ing. E.h. P.W. Baier
2. Berichterstatter: Prof. Dr.rer.nat. Dr.h.c. H. Rohling

Vorwort

This work was carried out at Siemens AG, Munich, Germany, from April 2002 to December 2004. I worked there as an external PhD candidate of professor P.W. Baier, University of Kaiserslautern. I would like to thank all the people who have given me the possibility, strength and support to complete this PhD thesis.

I thank Prof. Dr.-Ing. habil. Dr.-Ing. E.h. P.W. Baier for the useful guidelines and the fruitful discussions. I have learnt a lot from him, both from the professional and human point of view.

Warm thanks are extended to Prof. Dr.rer.nat. Dr.h.c. H. Rohling for acting as a reviewer of my thesis and for his comments, which lead to important improvements.

I am very grateful to Siemens AG, ICM N PG NT RC FR who supported my studies during this three-year long experience. Particular thanks go to the colleagues working at ICM N PG NT RC FR and particularly to Dr. E. Schulz. Special thanks to Dr. M. Weckerle for the useful tips on the Kaiserslautern's rules and above all to Dr. E. Costa for the technical discussions, the endless support and the friendship.

Thanks to Jessie, Guixia, Dan, Roger and Maran who are sharing my same experience at Siemens AG.

Last but not least, I would like to thank my family. In Italy: my mother, my father, my brothers and all my relatives in Saccolongo. In Germany: my wife Corinna to whom this thesis is dedicated.

München, October 2004

Alessio Filippi

Contents

| | | |
|----------|--------------------------------------------------------------------|-----------|
| 1 | Introduction | 1 |
| 1.1 | Multi-carrier modulation | 1 |
| 1.1.1 | General | 1 |
| 1.1.2 | Orthogonal Frequency Division Multiplexing | 3 |
| 1.1.3 | A more general framing | 4 |
| 1.1.4 | Data symbol specific transmit signature | 8 |
| 1.1.5 | State of the art | 9 |
| 1.2 | Goals of the thesis | 15 |
| 1.3 | Contents and important results | 16 |
| 2 | Modelling of linear transmission systems | 18 |
| 2.1 | Introduction | 18 |
| 2.2 | General system model | 19 |
| 2.2.1 | System structure | 19 |
| 2.2.2 | Transmitter | 19 |
| 2.2.3 | Transmission over the channel | 20 |
| 2.2.4 | Receiver | 20 |
| 2.3 | Receiver | 21 |
| 2.3.1 | Matched filter estimate | 21 |
| 2.3.2 | Noise covariance matrix | 22 |
| 2.3.3 | Post processing | 23 |
| 2.4 | Proposed classification | 24 |
| 2.4.1 | General | 24 |
| 2.4.2 | Single carrier | 25 |
| 2.4.3 | Multi-carrier | 26 |
| 2.4.4 | Hybrid systems | 27 |
| 2.4.5 | Generalised hybrid systems | 28 |
| 2.5 | Conventional OFDM framed as hybrid system | 29 |
| 2.5.1 | General | 29 |
| 2.5.2 | Transmit signal generation and receive signal processing | 29 |
| 2.5.3 | Mathematical modelling | 30 |
| 2.6 | Quality criteria | 33 |
| 2.6.1 | General | 33 |
| 2.6.2 | Rate | 33 |
| 2.6.3 | SNR-degradation | 35 |
| 2.6.4 | Bounds of the SNR-degradation | 37 |
| 2.6.5 | Example of trade-off | 39 |
| 2.6.6 | Measures for conventional OFDM | 41 |
| 2.7 | On the structure of the system matrix \mathbf{A} | 44 |
| 2.7.1 | General | 44 |

| | | |
|----------|--------------------------------------------------------------------------|-----------|
| 2.7.2 | Existing symmetries | 44 |
| 2.7.3 | Channel impact on the system matrix $\underline{\mathbf{A}}$ | 48 |
| 2.8 | Special setting of the model | 49 |
| 2.8.1 | General | 49 |
| 2.8.2 | Point to multi-point | 50 |
| 2.8.3 | Multi-point to point | 53 |
| 3 | Considered system implementations | 54 |
| 3.1 | General | 54 |
| 3.2 | Reference system | 54 |
| 3.2.1 | General | 54 |
| 3.2.2 | Parameters for 4 th generation mobile radio systems | 56 |
| 3.2.3 | OFDM over an AWGN channel | 59 |
| 3.2.4 | SC, MC and HY systems with equal resource consumption | 60 |
| 3.3 | Choice of parameters | 62 |
| 3.3.1 | General | 62 |
| 3.3.2 | Fixed parameters | 63 |
| 3.3.3 | Variable parameters | 66 |
| 3.3.4 | Gaussian basic transmit signature | 69 |
| 3.3.5 | Proposed values | 74 |
| 3.3.6 | Choice of an AWGN channel | 74 |
| 3.4 | Evaluation of the proposed approach | 77 |
| 3.4.1 | General | 77 |
| 3.4.2 | Channel capacity in the proposed modelling | 77 |
| 4 | Simulations | 81 |
| 4.1 | General | 81 |
| 4.2 | Single carrier systems | 82 |
| 4.2.1 | Rectangular basic transmit signature | 82 |
| 4.2.2 | Sinc shaped basic transmit signature | 84 |
| 4.2.3 | Gaussian basic transmit signature | 85 |
| 4.2.4 | Square root raised cosine basic transmit signature | 87 |
| 4.3 | Multi-carrier systems | 89 |
| 4.3.1 | Rectangular basic transmit signature | 89 |
| 4.3.2 | Sinc shaped basic transmit signature | 92 |
| 4.3.3 | Gaussian basic transmit signature | 93 |
| 4.3.4 | Square root raised cosine basic transmit signature | 94 |
| 4.3.5 | SC and MC duality | 96 |
| 4.4 | Hybrid systems | 97 |
| 4.4.1 | General | 97 |
| 4.4.2 | Rectangular basic transmit signature | 97 |
| 4.4.3 | Sinc shaped basic transmit signature | 100 |

| | | |
|----------|------------------------------------------------------------------|------------|
| 4.4.4 | Gaussian basic transmit signature | 102 |
| 4.4.5 | Square root raised cosine basic transmit signature | 104 |
| 4.5 | Proposed approach as increment of the channel capacity | 106 |
| 4.5.1 | General | 106 |
| 4.5.2 | Single carrier systems | 107 |
| 4.5.3 | Multi-carrier systems | 112 |
| 4.5.4 | Hybrid systems | 114 |
| 5 | Discussion on simulations: Recommendations | 119 |
| 5.1 | General | 119 |
| 5.2 | SC system with rectangular basic transmit signature | 119 |
| 5.2.1 | Properties | 119 |
| 5.2.2 | Channel capacity | 122 |
| 5.2.3 | Possible applications | 124 |
| 5.3 | Recommendations | 127 |
| 6 | Summary | 128 |
| 6.1 | English | 128 |
| 6.2 | German | 129 |
| | Appendix | 130 |
| A.1 | Abbreviations | 130 |
| A.2 | Symbols | 131 |
| | References | 136 |

1 Introduction

1.1 Multi-carrier modulation

1.1.1 General

The key requirements for future wireless communication systems are the capability to support high data rate and high user mobility and to allow a great flexibility in the allocation of the available resources [FaK01, FaK02, FaK03, RGG01, RMB99]. These requirements are pursued through the search of new air interfaces and through the development of system models capable of integrating different technologies under the same concept. The integration process should bring to the definition of a general common platform flexible enough to include existing as well as future systems still to be developed [FaK03].

The rising of the supported data rate goes along with the increment of the bandwidth usage [Pro95]. As a consequence, the potential candidates for the radio interface of fourth generation (4G) [BaM02, FaK03, RGG01, RMB99] systems have to efficiently support broadband communications. Moreover, given the high cost of the electromagnetic spectrum, techniques capable of efficiently using the available bandwidth should be employed [Lu02, Wec02]. The most promising candidate for a 4G radio interface is based on orthogonal frequency division multiplexing (OFDM), a multi-carrier modulation scheme which has been widely studied [RGG01, RMB99] and applied both in wireline [CTC91] and wireless communications [Bin90]. Recently, other multi-carrier systems have been proposed [BeT02c, Bol99, CEO02, Ton01, Vai01] as alternative solutions to OFDM whose success is mainly due to the low implementation complexity.

This thesis investigates a novel approach to better exploit the transmission resources in time and frequency. The price to be paid for such a better exploitation is an increase of the required transmit power. We utilize the flexibility of multi-carrier systems different from OFDM, hereafter referred to as non-conventional multi-carrier systems, to investigate the advantages and disadvantages of the novel approach. In this chapter, we review the contributions that different fields of research have given to the development of non-conventional multi-carrier systems and outline those related to our work. In this way, we show the generality of the multi-carrier principle and frame the thesis' contribution in a more general context.

In digital communication systems with the increasing of the transmission data rate, the time separation T between consecutive transmitted symbols decreases [Pro95, Rap99]. Moreover, in wireless digital communications the signal transmitted over the air reaches the receiver through different paths generated by the reflection on environment obstacles such as buildings, trees, mountains etc. [Pro95, Rap99]. If the time separation T

is longer than the sum of the excess delay τ_{\max} of the last signal replica that arrives at the receiver and of the time duration T_0 of the associated waveform, then there is no interference among consecutive symbols. If the time separation $T \leq \tau_{\max} + T_0$, then the received symbol is corrupted by the delayed replicas of the previous symbols. This kind of interference is referred to as intersymbol interference (ISI) and it becomes larger and larger with the increasing of the transmission data rate. ISI can be removed at the receiver through the deployment of an equalizer [BeC02, Pro95]. Depending of the particular equalization method, the equalizer eliminates all the interference or just a part of it.

In broadband single carrier (SC) systems the problem of ISI removal becomes very complex because of the high data rate [BeC02, Pro95]. Multi-carrier modulation offers a possible simplification by applying an approach similar to the Latin motto “divide et impera”, i.e. to separate your enemies and face them one at the time. In this case, the enemy is broadband SC transmission because it generates a great amount of ISI. Therefore, the broadband transmission is divided in many narrowband transmissions, by splitting the original data stream into many low data rate streams, hereafter referred to as sub-streams, see Fig. 1.1. Then, instead of modulating a single carrier frequency with

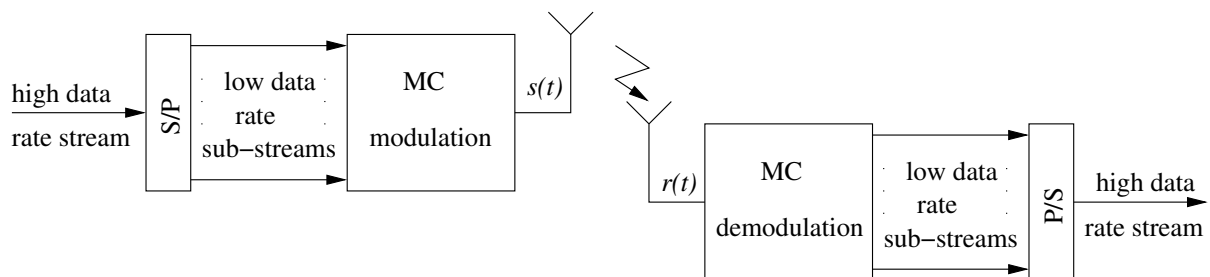


Fig. 1.1. Multi-carrier wireless system.

a high data rate stream, many carrier frequencies, namely sub-carriers, are modulated in parallel with low data rate sub-streams. With the decreasing of the data rate, the time separation T of the symbols of each sub-stream is increased. If T is longer than $\tau_{\max} + T_0$, then there is no ISI to be removed in the single sub-carrier narrowband transmission and the complex problem of ISI removal is solved introducing the challenge of multi-carrier modulation and multi-carrier demodulation. If these operations are simpler than the broadband equalization, multi-carrier systems demand lower complexity than broadband SC systems. Besides the complexity issue, we should consider also other trade-offs between SC and multi-carrier. In particular, multi-carrier exhibits the key advantage of enabling adaptive power and bit allocation, e.g. through the deployment of the so called “water filling” technique [Gal68] and loading algorithms [CCB95]. This capability has

been recognized to be one of the most significant benefits yielded by multi-carrier modulation [Bin90, WaG00]. Additionally, multi-carrier modulation shows a great flexibility and adaptability to different propagation conditions, mainly due to the possibility of adjusting the number of sub-carriers [RMB99].

The rest of this chapter is organized as follows. In Subsection 1.1.2, we review the development of OFDM. In Subsection 1.1.3 we present the contribution of the signal processing community and of the mathematics theory on series expansions on the development of multi-carrier systems recalling the connections between the different fields of research. Subsection 1.1.4 describes our approach to non-conventional multi-carrier systems. We define the main parameters that characterize different system configurations and recognize the differences and similarities with respect to the approaches described in the previous subsections. A review of the state of the art concerning the topic of the thesis is given in Subsection 1.1.5. This chapter ends with the statement of the goals of the thesis, in Section 1.2, followed by an outline of the thesis' structure with the attained results in Section 1.3.

1.1.2 Orthogonal Frequency Division Multiplexing

Among the possible multi-carrier modulation schemes OFDM is the most studied, known and used. A rich literature covers all the aspects of this modulation technique and some exhaustive reviews can be found in [NeP00, RGG01, RMB99, ZoW95]. Here, we briefly recall the main steps of its development [CEO00, NeP00, ZoW95].

The key characteristic of OFDM is that the separation in the frequency domain among the different sub-carriers is achieved through the deployment of overlapping and orthogonal sub-carrier spectra [BeC02]. Therefore, the frequency division multiplex (FDM) of the sub-streams is not achieved by disjoint spectra. The first system in which a concept similar to OFDM could be recognized is the Kineplex [MoC58], an application to the high-frequency modems deployed by the military. However, the key idea of OFDM was first published in [Cha66] and patented by the same author. Soon after, another approach of overlapping FDM transmission was published [Sal67]. In this case, the frequency separation was achieved through an offset quadrature amplitude modulation (O-QAM) and an analog implementation was proposed. The efficient implementation of OFDM via discrete Fourier transform (DFT) was developed in [WeE71]. There, the deployment of a cyclical extension of the signal, often referred to as guard interval or cyclic prefix [NeP00], was also suggested. During the 1980ies, OFDM was considered as a possible modulation technique for digital radio broadcasting [Cim85] as well as for high speed modems [Hir81]. In the 1990ies, it was further studied and developed for wireline communications as applied to asynchronous digital subscriber line (ADSL) and to very high speed digital subscriber line (VDSL) [CTC91]. Regarding wireless communications, it was proposed for wideband

digital broadcasting [CaL91]. OFDM evolution culminates in its standardisation as transmission technique for Digital Video and Audio Broadcasting (DVB and DAB) [ETS01a], [ETS01b], as well as for the wireless local area network (LAN) IEEE 802.11a standard [IEE99] and for the ETSI HIPERLAN/Type 2 [ETS99] systems. Currently, OFDM is considered as the most promising candidate for a new radio interface for future 4G cellular mobile radio systems [FaK03, RGG01, RMB99].

The great success of OFDM is mainly due to its very efficient all digital implementation. However, OFDM has some drawbacks which should be kept in mind when considering alternative solutions. We have mentioned that OFDM uses a cyclic signal extension. This technique on the one hand simplifies the equalization at the receiver, on the other hand it introduces an efficiency loss due to the transmission of redundant data. Moreover, the amount of redundancy depends on the maximum excess delay τ_{\max} of the channel, which is a given parameter in the system design. Another limitation is given by the high peak to average power ratio (PAPR) which characterizes the OFDM signal. The power amplifier at the transmitter has to operate at a large input back-off to avoid out of band interference and in band distortion so that a high quality and, therefore, expensive power amplifier is required for OFDM. An additional drawback is given by the high sensitivity to time and frequency synchronisation. If not perfectly synchronised, the overlapping spectra lose their orthogonality and generate intercarrier interference (ICI) which may cause a significant performance loss. We have also to mention that the limitations due to the guard interval, the PAPR and the sensitivity to synchronisation errors have been all faced and solutions to bound the performance degradation have been proposed in the literature [NeP00, RGG01, RMB99, ZoW95]. Nevertheless, these issues are due to the particular nature of the OFDM transmission technique, e.g. the overlapping sub-carrier signals.

1.1.3 A more general framing

Lately, other multi-carrier modulation techniques have been proposed as alternative solutions to OFDM [BoH95, BoI99, BTT01, CEO02, KoM98, TLP00a, ToP02, Vai01]. We can recognize them as belonging to two main families. One is strictly related to the works on transmultiplexers (TMUXs) [BeD74] and filter banks (FBs) [Vai93], the other to the works on series expansions [VeK95]. In what follows, we explain the basic principles of TMUXs and FBs and then we give an overview of series expansions. The application of FBs theory and series expansions to communications generates alternative multi-carrier modulation schemes. The relationship existing among the two different families is stressed out at the end of this subsection.

With the name TMUX we refer to a device, see Fig. 1.2, which synthesizes a signal from N_f signals through a synthesis stage, and then recovers the original N_f signals through

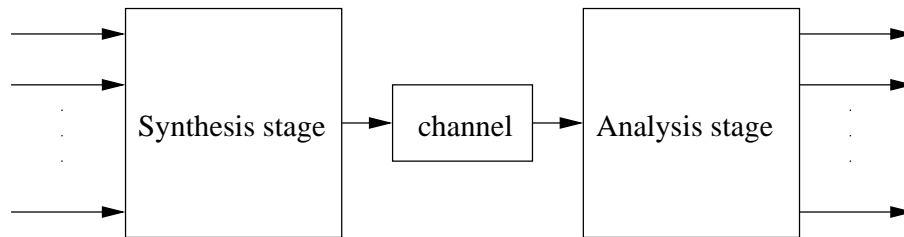


Fig. 1.2. Transmultiplexer.

an analysis stage [BeD74]. TMUXs were initially studied in communications to accommodate many users sharing the same channel. The idea was to separate the users by multiplexing their signals in time, i.e. time division multiplexing (TDM), or in frequency, i.e. FDM. From Fig. 1.1 and Fig. 1.2, we infer that multi-carrier modulation can be seen as a particular TMUX because it also multiplexes N_f signals into one signal. However, while in the TMUX this is the main goal, for multi-carrier modulation the main goal is to shape the original signal in order to better adapt it to the transmission over the channel. In a TMUX, each of the N_f input signals is interpolated by adding M zeros between consecutive samples [Vai93], filtered and then summed up with the other signals. The combination of the interpolator and the filter impulse responses is referred to as the digital function characterizing the analysis or the synthesis stage of the TMUX. A key aspect is the relationship between the number of multiplexed signals N_f and the interpolation factor M . If $M \geq N_f$ the synthesized signal can convey the whole information of the N_f signals. If $M = N_f$ the system is critically sampled and every N_f discrete input samples, the synthesis stage produces exactly $M = N_f$ discrete output samples. If $M > N_f$ the system is not critically sampled. This means that the TMUX introduces some amount of redundancy in the synthesised signal, thus generating $M > N_f$ output samples every N_f input samples. The introduced redundancy is basically used to build a signal with some desired properties. For instance in the OFDM case, the redundancy is introduced in form of cyclic prefix, cf. Subsection 1.1.2, to allow a simple channel equalization [NeP00]. If $M < N_f$, then the synthesized signal does not convey the complete information of the original N_f signals [Bol99].

The general scheme of a FB is depicted in Fig. 1.3. By comparing Fig. 1.2 and Fig. 1.3, it is apparent that TMUXs and FBs are very similar although the order of the analysis and synthesis stages is changed. FBs do not multiplex many signals in one single signal, but they split an input discrete time signal in its spectral components through the deployment of a bank of filters that constitutes the analysis stage. The distinct spectral components of the signals are then combined together to recover the original signal through the synthesis stage. If the synthesized signal at the output of a FB is exactly the same as the signal

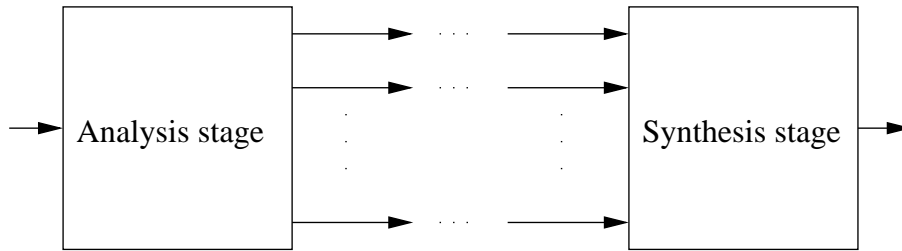


Fig. 1.3. Filter bank.

at the input of the analysis stage, then the FB is a perfect reconstruction (PR) FB. The resort to FB may allow a more efficient implementation of some class of algorithms. For instance, signal compression algorithms are usually implemented through a FB because in this way they achieve better compression without requiring additional complexity. FBs are also used for sub-band coding [VeK95]. In this case, the signal is cut in its spectral components, i.e. sub-bands, and each component is encoded independently. The relationship between the parameters N_f and M has the same meaning explained in the case of TMUXs and, depending on it, the FB has different properties. In the critically sampled case, $M = N_f$, PR FBs exist and the conditions on the digital functions to obtain a PR FB are known [Vai93]. In the not critically sampled case, $M > N_f$, the conditions on the digital functions to obtain PR conditions are established as well and they are in general relaxed so that a larger set of selections is available. FBs are and widely studied [Vai93]. In the framework of the thesis, we are interested in its contributions to communications [Vai01].

FBs are not only highly related to TMUXs and, as a consequence, to multi-carrier modulation, but also to the series expansions. To clarify this connection we introduce the principles of series expansions mainly through the well-known Fourier analysis which yields an example of series expansion. A rigorous analysis on the existing relation between series expansions and FBs can be found in [VeK95].

The theory of series expansions studies the possibility of representing a space of signals, or functions in general, through linear combinations of a specific set of functions. If the set generates all the signals belonging to the space, then it is a basis for this space. A basis is complete if all its elements are linearly independent or overcomplete if at least one of its elements is linearly dependent on the others. An overcomplete basis with some specific properties [CvV98, Uns00] is referred to as frame. In what follows, frame and overcomplete basis are used as synonyms. The reasons to represent a set of signals with respect to a different basis could be many, especially if the basis is “good”, i.e. it offers a less complex processing and/or a compact representation of the signals. The most famous series

expansion is given by the Fourier series which enables to represent the space of periodic signals through linear combinations of harmonic sines and cosines. Therefore, the Fourier series offers a good and complete basis for the space of periodic signals. Representing a signal in terms of the Fourier basis can be useful for analysis purpose, i.e. to characterize its spectral behaviour, as well as for computational purpose since the convolution of two periodic signals comes out to be simply a multiplication in the Fourier domain. The most obvious limitation of Fourier series is related to the periodicity of the involved signals, because in general we are not only interested in periodic signals. Another very common series expansion is the wavelets transform. In this case the basis is made of scaled and shifted versions of a basic impulse shape. Such a series expansion turns out to offer a good orthogonal basis. Moreover, the wavelet expansion was the first to be efficiently computed through a FB algorithm, thus showing the close interaction between FBs and series expansions [VeK95].

The relation between FBs and series expansions has been investigated, for instance in [CvV98, VeK95], and it was shown that under some constraints [CvV98] FBs offer the discrete time analogue of series expansions. A rigorous treatment of the relationship is beyond the scope of this chapter. It is important here to recall that a strict relationship exists and that FBs can be in general used for an efficient implementation of the corresponding continuous time series expansion coefficients. The difference between the twos is determined by the fact that FB theory is more related to implementation issues while series expansion is more related to mathematical theory. Another important aspect involves the relationship between the FB parameters N_f and M and the series expansion parameters F and T as summarised in Table 1.1. The product FT plays a key role on

Table 1.1. Relationship between series expansions and filter banks.

| Series expansions | | Filter banks | |
|-------------------|----------|--------------|--------------------------|
| frame | $FT > 1$ | $M > N_f$ | not critically sampled |
| complete basis | $FT = 1$ | $M = N_f$ | critically sampled |
| not a basis | $FT < 1$ | $M < N_f$ | under critically sampled |

the characteristics of the series expansion. If $FT = 1$, the set of time-frequency shifted versions of the basic impulse shape can offer a complete basis, but the basic impulse has no good property regarding its time and frequency occupation. The most cited example of basic impulse shape that offers a complete basis for $FT = 1$ is the rectangular shape of duration $T_0 = T$ which is used in OFDM. If $FT > 1$ the series expansion considers also linearly dependent elements and the set of functions becomes a frame. The degrees of freedom gained by choosing $FT > 1$ allow to look for alternative impulse shapes offering a good overcomplete basis. Moreover, the designer is free to impose some other constraints such as, for example, a better frequency containment. Given the relationship between

FBs and series expansions [Bol99], the equivalent discrete time realization of the series expansions with $FT = 1$ is given by a critically sampled FB with $M = N_f$. If the series expansion is achieved through a frame, then the equivalent discrete realization is given by a not critically sampled case FB with $M > N_f$. The mathematical theory dealing with series expansions in which the set of functions is a frame, is referred to as frame theory.

Lately, a lot of work has been applying the results of frame theory to communication systems [BHF98, BoH95, BoH98, Bol99, KoM98] generating a new class of multi-carrier systems currently under investigation. The focus is on how to exploit the condition $FT > 1$ to design alternative basic impulse shapes and gain in robustness with respect to the time and frequency dispersion introduced by the communication channel. The condition $FT < 1$ was never considered in the literature because the synthesised signal offers an incomplete representation of the input signals [Bol99].

All the works exploiting the multi-carrier principle, applied to communications, to series expansions or to signal processing, mainly show the importance that the multi-carrier principle covers in many different fields. Recognising the common guidelines in different research activities is important to enable the reuse of significant results and to frame the topic of the thesis as a more general contribution. In particular, our focus is on multi-carrier communications and our aim is to investigate their sensitivity to the reduction of the time separation T and frequency separation F among the sub-carriers, cf. Table 1.1.

1.1.4 Data symbol specific transmit signature

We have seen that the multi-carrier principle is used in different fields. As a consequence, different notations and modelling have been developed. Since we are focused on communications, we use the multi-carrier concept to split an original high data rate stream into many low data rate sub-streams, cf. Subsection 1.1.2, which modulate in parallel a number N_f of sub-carriers. The synthesis and analysis stages of our model are depicted in Fig. 1.4. Our approach applies some notations derived from the series expansions and FBs and TMUXs. As in the series expansions, the functions of the synthesis stage are defined in the continuous time and we refer to them as data symbol specific transmit signatures $\underline{c}_n(t)$, $n = 1 \dots N$. As in the FB theory, the analysis stage is defined as a bank of N filters whose properties are discussed later on, cf. Chapter 2. We note that there is no assumption on the data symbol specific transmit signatures $\underline{c}_n(t)$. Any communication system can be framed in such a general modelling and, in particular, OFDM as well as any non-conventional multi-carrier system.

Within the whole set of non-conventional multi-carrier systems we have to discern among different configurations and to evaluate their peculiar properties. Three key parameters of non-conventional multi-carrier systems, see Fig. 1.4, are well suited for this scope:

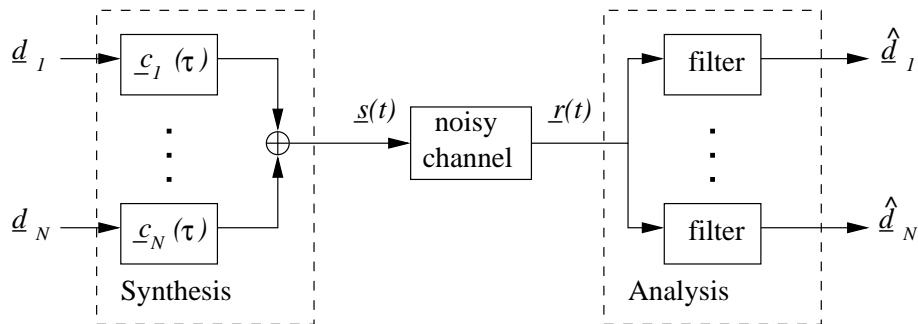


Fig. 1.4. Our model framed within filter bank, multi-carrier modulation and frame theory.

- The data symbol specific transmit signature $\underline{c}_n(t)$, $n = 1 \dots N$, which is the waveform associated to the transmit data symbol \underline{d}_n , $n = 1 \dots N$, see Fig. 1.4. The definition of $\underline{c}_n(t)$ determines the key characteristics of the transmitted signal such as its frequency and time occupation and its sensitivity to distortion generated in frequency and/or time. By changing the data symbol specific transmit signatures $\underline{c}_n(t)$ we change the communication system under consideration.
- The frequency separation F , which determines the location of the sub-carriers under the assumption of equally spaced sub-carriers. We consider F as a variable parameter and the performance of non-conventional multi-carrier systems is evaluated as a function of F .
- The time separation T between consecutive symbols on each sub-carrier. We consider T as a variable parameter and evaluate the system performance as a function of T .

The parameters T and F are the same used to describe the series expansions in the previous subsection. The data symbol specific transmit signature $\underline{c}_n(t)$ can be seen as the analogous continuous time equivalents of the digital functions of the FB. Therefore, the product FT holds the same role as described in Subsection 1.1.3 and summarised in Table 1.1.

1.1.5 State of the art

Subsection 1.1.2 briefly recalls the main steps in the evolution of OFDM, whereas Subsection 1.1.3 shows that the multi-carrier principle has roots in different fields. This

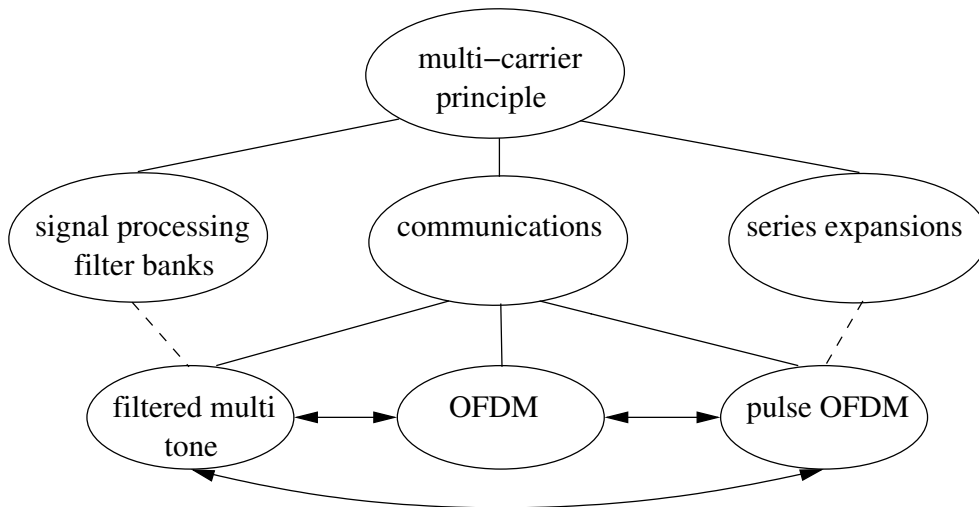


Fig. 1.5. Overview of relations between multi-carrier systems.

subsection proposes a semantic organization of the literature regarding the application of the multi-carrier principle to communications. As depicted in Fig. 1.5, we consider the multi-carrier principle as the general concept which joins different fields of research, namely signal processing and filter bank, cf. Subsection 1.1.3, communication, cf. Subsection 1.1.2 to 1.1.4, and series expansions, cf. Subsection 1.1.3. Since the thesis is focused on the application of the multi-carrier principle to communications, the communication field in Fig. 1.5 holds the central position whereas the others are considered in terms of their contributions to communications. The numerous communication systems deploying the multi-carrier principle are arranged in three families namely filtered multi tone (FMT) [BeC02], OFDM and pulse OFDM. They are highly related to each other so that a multi-carrier system framed within one family can be studied with the techniques and naming conventions developed for another family. For instance the conventional OFDM system, whose importance and history motivates its own family, can be framed as a special pulse OFDM [KPU00] as well as an FMT system [BeC02].

In Tables 1.2 and 1.3, we report the literature highly related to this thesis thus establishing its background. We follow the organization proposed in Fig. 1.5 grouping the contributions as belonging to the three different families of Fig. 1.5.

Within FMT family, we frame the works regarding FBs and TMUXs, cf. Table 1.2. The main reference for FBs is [Vai93] in which the theory of FBs and multirate systems is extensively developed. The main contribution of FBs to communication regards the implementation approaches. In [BeD74] and [BBC79] the authors propose an all digital fast implementation of TMUXs and critically sampled FBs based on fast Fourier transform (FFT) and polyphase decomposition of the involved filter impulse responses. More

Table 1.2. Contributions on multi-carrier modulation. FMT and pulse OFDM.

| multi-carrier modulation | reference | remarks |
|--------------------------|--------------------------------------------------------------------------------------------------------|------------------------------------------------------------------------------------------------------------------------------------------------------------------------------------------------------------------------------------------------------------------------------------------|
| filter multi tone | [Vai93] [BeD74],[BBC79], [WeS00] [BoH97] | Filter Banks - main reference - fast implementations - oversampled FBs to increase the design space of the filters - importance in communications |
| | [Vai01] | |
| | [SGB99a], [SGB99b], [SGB99c], [SGB99d] | FBs as precoding |
| | [CEO99], [CEO00], [CEO02] [BCT00],[BTT01] [CFO03] [CFW03] [Tom01] [Ton01] [ATT03] | FMT versus OFDM - FMT applied to wireline - FMT applied to wireless - sensitivity to asynchronism - sensitivity to multipath - CDMA on FMT - theoretical ISI/ICI - sensitivity to phase noise |
| pulse OFDM | [VeK95] [BoI99] [BoH95] [BoH98] [CvV98], [BHF98] [KPU00] | FB and frames - overview - FT in relationship with oversampled and critically sampled FB - relationship between Gabor series and DFT - Gabor and oversampled FBs - conditions on the equivalence between FBs and frame expansions - OFDM framed as a Gabor expansion |
| | [KoM98] [LaA03] [Pfs01] [SMH02] [STS03], [BeS01] | alternative impulse shape - non-orthogonal - trade-off between ISI and ICI - with higher energy concentration around the sub-carrier - fast implementation - jointly ISI/ICI minimization |

recently, not critically sampled FBs have drawn a lot of attention. [WeS00] derives a fast implementation for the not critically sampled FBs. In [BoH97], the not critically sampled FBs are considered to relax the tight conditions which ensure PR and new constraints

Table 1.3. Contributions on multi-carrier modulation. OFDM.

| multi-carrier modulation | reference | remarks |
|--------------------------|-----------------------------------------------------------------------------------------------------|------------------------------------------------------------------------------------------------------------------------------------------------------------------------------------------------------------|
| OFDM | [Bin90], [NeP00] [RGG01], [RMB99] [Cha66], [Sal67], [WeE71], [Hir81] [ZoW95] [KeH99] | General - overview and principles - significant development steps - importance of coding - pre-equalization in OFDM |
| | [RGG01], [RMB99] [FaK01],[FaK02], [FaK03] [Kai98] [BBT03] [CHS02], [TCF03] | OFDM for 4G - to wireless cellular systems - CDMA combined with OFDM - overview of MC-CDMA - pre-equalization MC-CDMA for up-link - adaptive multi-user allocation - adaptive coding |
| | [FAB02] [SGH02] [BTT02] [Ana01] | OFDM versus single carrier - frequency domain equalization - guard interval removal - compared with FMT - complexity |
| | [ETS01a], [ETS01b], [IEE99], [ETS99], [IAV00] | applications and standards |

are proposed to increase the system robustness. A particular application of FBs, named precoding, is proposed in [SGB99a, SGB99b, SGB99c, SGB99d]. The transmitter can be recognized to be a very flexible multi-carrier modulator that introduces redundancy into the signal through a particular FB called precoder. This is designed to optimize the signal to noise ratio (SNR) at the input of the detector under the assumption of a given power constraint and a perfectly known channel at the transmitter. Precoders can also be seen as a representation of the traditional coder such as block or convolutional coders [Vai01]. In [Vai01], the author discusses the most important applications of FBs to communications giving a complete literature review of the state of the art. The contribution of FB theory to communications becomes evident in the works in which FMT is compared to OFDM. Among them, [CEO99, CEO00] propose FMT as applied to wireline communications. The authors introduce on purpose a given amount of redundancy through the choice of $M > N_f$, to gain in robustness with respect to interference generated by other sub-carriers, i.e. ICI. In [CEO02], where FMT is investigated as a potential candidate

for VDSL, a novel efficient implementation of both the transmitter and the receiver is also derived which differs from the one in [WeS00]. A similar approach is considered in [BCT00, BTT01], where the comparison between OFDM and FMT is carried out in a wireless environment. In particular, the authors propose a simplification of the per sub-carrier equalizer required by FMT modulation. Another FMT scheme is compared to OFDM in [CFO03] in terms of sensitivity to asynchronism and in [CFW03] the authors consider also the effects of the multipath channel. The potential of FMT is investigated also in combination with code division multiple access (CDMA) [Ver98] in [Tom01]. A more theoretical contribution can be found in [Ton01] in which the author investigates the performance of an FMT system in an up-link asynchronous multi-user scenario, deriving the analytical expression of ISI and ICI. In [ATT03] the authors further study the potential of FMT by studying its sensitivity to phase noise.

In the family denoted pulse OFDM, cf. Table 1.2, we group all the works regarding multi-carrier modulation which are highly related to series expansions, in that they make use of mathematical results derived in that field to propose new multi-carrier communication systems. The literature dealing with this topic mainly considers continuous time functions and faces the problem of representing a signal as a linear combination of a convenient set of functions. The relationship between series expansions and communications was first investigated in terms of connection between the series expansions and FBs as pointed out in the introduction of [VeK95]. In [Bol99] the relationship between the parameters T and F of the series expansions and the parameters M and N_f , cf. Table 1.1, of the FBs is derived. The author shows the equivalence between Gabor expansions and DFT in [BoH95] and investigates the relationship existing between Gabor expansions and oversampled FBs in [BoH98]. In two different publications, [BHF98] and [CvV98], the conditions to meet the equivalence between FBs and frame expansions are derived. In [KPU00], OFDM is framed as a particular Gabor expansion, showing explicitly the strict connection among the different fields of research. Among the alternative multi-carrier communication systems employing the mathematical tools developed in the framework of series expansions of particular interest is that presented in [KoM98]. The authors propose non-orthogonal impulse shapes claiming that orthogonality is the optimum solution only when an additive white Gaussian noise (AWGN) channel is considered. In [LaA03], various multi-carrier schemes are compared with a particular focus on the trade-off between ISI and ICI. [SMH02] proposes a fast implementation of pulse OFDM modulation with $FT > 1$ in which the additional redundancy is exploited to minimize ISI and ICI under the assumption of a time-varying channel. [STS03] jointly minimizes ISI and ICI with $FT > 1$, too. However, the assumptions are quite unrealistic for a communication system because the authors study the case $FT = 2$ which implies the transmission of a redundant symbol every information bearing symbol. In [BeS01] a general framework of pulse OFDM is presented for $FT > 1$. Once more, the goal is to minimize jointly ISI and ICI for a doubly dispersive channel.

In Table 1.3, we report a brief collection of the literature regarding OFDM. A general and detailed overview of the OFDM principles is given in [NeP00], together with the design issues, the pros and cons, the known problems and available solutions. [Bin90] is one of the most cited articles regarding OFDM. It presents an overview of the key characteristics of OFDM, the advantage of using numerous sub-carriers, the achievable performance, the techniques to face the channel impairments and the application of coding. Another good and more up-to-date overview can be found in [RGG01, RMB99]. The state of the art is presented together with a review of the known limits of OFDM and of the most promising solutions proposed in the literature. The authors explain the potential of OFDM and the reasons that brought OFDM to be the leading candidate for the air interface for the 4G communication systems. The authors of [RGG01, RMB99] belong to a research group who has been working on OFDM since 1992. They have investigated many aspects of OFDM as shown in [GaR02, GBR00, MBG96, MRE98, RBG97, ReR94, RGM97, RoG96a, RoG96b, RoG97, RoG98, RoM97]. From a more historical point of view, [Cha66, Hir81, Sal67, WeE71] represent the most significant steps in the evolution of OFDM, cf. Subsection 1.1.3. [ZoW95] shows the importance of coding in OFDM based systems to exploit the diversity gain ensured by the high number N_f of sub-carriers. The exploitation of the channel knowledge at the transmitter side is studied in [KeH99] through the investigation of a sub-band pre-equalized scheme. OFDM is proposed as a candidate for the radio interface of 4G communication systems also in [FaK01, FaK02, FaK03] in which the main focus is on the combination of CDMA with OFDM. An overview of the different possible combinations of OFDM and CDMA is found in [Kai98], whose focus is on the so called MC-CDMA systems. Focusing on OFDM based 4G systems, different proposals on how to exploit the channel knowledge at the transmitter in an MC-CDMA system are investigated in [BBT03, CHS02, TCF03]. Regarding the comparison between SC and OFDM, [FAB02] investigates an SC system similar to OFDM, in that a block-wise transmission is carried out with the insertion of a guard interval at the transmitter and its removal at the receiver. In this way, a cyclic signal structure is obtained and a frequency domain equalization can be implemented via an FFT and inverse FFT (IFFT). In [SGH02], the guard interval typical of OFDM is removed and alternative equalization techniques are proposed. OFDM is compared to FMT in [BTT02] whose conclusions are in favour of OFDM in most of the application scenarios. In [Ana01], the comparison between OFDM and SC systems is carried out in terms of required complexity. Finally, in [ETS01a, ETS01b, ETS99, IEE99] some examples of standards deploying OFDM as modulation technique are given, cf. Subsection 1.1.2.

The strict relationship between the different fields of application of the multi-carrier principle has motivated the need of considering all of them and shows the great interest arisen by multi-carrier systems.

1.2 Goals of the thesis

Throughout the literature, we recognize the similarities between multi-carrier modulation, FBs and series expansions. Moreover, multi-carrier modulation is considered the most promising candidate for the new air interface of 4G mobile radio systems [RGG01] mainly because it efficiently faces the problem of ISI increment in very high data rate systems. The interest on this subject motivates the need of a deeper study of the potential offered by multi-carrier modulation especially as compared to SC modulation. Therefore, the first objective of this work is to propose a common framing for any multi-carrier and SC system. To this end, we develop a rigorous system model in which any of the described approaches can be framed. Generally speaking, an important goal of the thesis consists in studying the impact of working with non-orthogonal data symbol specific transmit signatures $\underline{c}_n(t)$. This question is relevant e.g. with respect to the multi-carrier transmission over time-varying radio channels. However, in the simulations in the thesis, non-orthogonality is not produced by the radio channel, which is assumed to be of the type AWGN, but by the form of the signatures $\underline{c}_n(t)$ and by their spectral and/or temporal separation. Moreover, the system model developed in the thesis could be also used in other cases of practical interests as e.g. characterized by the occurrence of time varying channels. In the thesis, we propose a novel term of comparison. We evaluate the dependency of the SNR at the output of the post processing stage, cf. Chapter 2, on the increment of the system load. The latter is increased through the reduction of the frequency separation F and/or time separation T among the data symbol specific transmit signatures $\underline{c}_n(t)$ below the minimum values able to ensure absence of ISI in an AWGN channel, i.e. $FT < 1$, cf. Subsection 1.1.4 and Table 1.1. As a consequence, this thesis deals with ISI. However, not ISI caused by multipath channels is considered since the assumed channels are AWGN channels. ISI is generated on purpose by moving the data symbol specific transmit signatures $\underline{c}_n(t)$ closer together in the temporal and/or the spectral domain. We do this to better exploit the time and/or frequency transmission resources. The price to be paid for such a better exploitation is an increase of the required transmit power. The main goal of the thesis is the investigation of how the said beneficial and the said disadvantageous effects work out depending on the system lay-out, and how they can be advantageously balanced against each other.

The goals of the thesis are achieved by pursuing the following intermediate steps:

- Development of a general system modelling capable to describe any multi-carrier and SC system. In this way, we build a common platform for comparison.
- Framing of the multi-carrier systems already known in literature as special cases of the proposed system modelling. In this way, we do not only validate the modelling, but also show its potential and clarify its structure. Moreover, other well known transmission systems can be recognised in our model so that the algorithms

developed in the framework of different research fields can be transferred to our system.

- Proposal of quality criteria to take into account the trade-off between the distortion of the received data and the effort invested in the data transmission. This method shall determine the quality of the system under investigation as a function of the increased system load.
- Proposal of two possible approaches to increase the transmission rate. The load of the system can be increased by reducing the time separation T and/or the frequency separation F among the data specific transmit signatures $\underline{c}_n(t)$. Depending on the considered multi-carrier system, the system performance could be more sensitive to the reduction of the time or of the frequency separation.
- Choice of a set of promising system designs to carry out a fair comparison among different system configurations. Among the multi-carrier systems, OFDM shall be always present to ensure a well known reference for comparison of the performance of other candidates.
- Derivation of an approximation of the Shannon channel capacity formula [Sha48] $C = \text{ld}(1+\text{SNR})$ to take into account the trade-off between the increment in terms of resource usage and the decrement of SNR due to the reduction of the time separation T and/or the frequency separation F .
- Presentation and discussion of simulation results. Some recommendations should be derived on the basis of the attained results in order to narrow down the range of the potential candidates for the radio interface of 4G radio systems.
- Discussion about the most promising configurations and proposal of an interpretation of the related simulation results.

1.3 Contents and important results

Apart from the Introduction, the thesis is composed of seven other chapters.

In Chapter 2, we introduce the proposed system modelling and describe in more detail three configurations named SC, multi-carrier (MC) and Hybrid (HY) systems. Conventional OFDM systems are framed within the modelling to confirm its flexibility and validity. We outline the quality criteria to assess the system performance, investigate their properties and apply them to conventional OFDM systems to determine the bounds for comparison purposes. Then, we examine the structure of the system matrix of the proposed modelling and recognize two main components. The first is a made only of phase terms and the second of a block structured matrix. The chapter ends showing how

a point to multi-point and a multi-point to point transmission can be framed within the modelling. By doing so, we show how the developed system model can be extended to include more general configurations.

There is no agreement on what to expect for 4G mobile radio systems. Therefore, Chapter 3 introduces the author's vision of 4G systems, describes the expected system parameters and introduces a possible design of a conventional OFDM system which is considered the most promising candidate for future radio systems. Based on the designed conventional OFDM system, we determine the reference time and frequency values used throughout the thesis to normalize the parameters. We propose the scope of parameters to investigate a wide range of possible system configurations. Among all, we resort to a Gaussian basic transmit signature $\underline{c}_0(t)$ and derive the analytical expression of the relationship between the receive and the transmit data symbols. The last section of the chapter presents an evaluation of the proposed approach of increasing the resource usage by resorting to a modified expression of the Shannon channel capacity C .

The effects of the increment of the resource usage are presented in Chapter 4, in which we show the simulation results and justify the similarities among them. For SC systems we consider the entire scope of parameters, verify the attained results through some reasoning and justify the similarities among the different system configurations. For MC systems, we recognize the duality between the time and frequency domain. In particular we derive the hypothesis needed to obtain the same performance in SC and MC systems. For HY systems, we only depict the simulation results of a subset of the scope of parameters. The evaluation of the proposed approach introduced in Chapter 3 is used to investigate, through computer simulation, if there exist any configurations able to improve the channel capacity C . The results are reported and discussed in the last section of Chapter 4.

Chapter 5 focuses on the most promising configurations among those investigated in Chapter 4 and proposes a justification of the unexpected results. The chapter ends with some short recommendations on the possible applications of the proposed method of increasing the usage of the available resources. We underline the importance of a further investigation of the method to fully exploit its potential.

The thesis ends with Chapter 6 in which we report a summary of the most significant results in English and German.

2 Modelling of linear transmission systems

2.1 Introduction

Investigation of bandpass transmission systems can be beneficially performed based on system models established in the equivalent low-pass domain [Pro95]. In the case of bandpass transmission systems utilizing linear modulation, such system models become particularly simple and easy to handle if they are organized in two parts [Ver98, Kal95]:

- A physical transmission model. This represents in its interior the physical signal transmission and establishes, with respect to its input and output, the relation between the data symbols fed into the transmitter (Tx) and the raw data estimates available in the receiver (Rx). Consequently, this model has to work time continuously in its interior and time discretely with respect to its input and output.
- An optional post-processor in the Rx with the task to provide improved data estimates based on the raw estimates.

In this chapter this approach to system modelling is worked out. The physical transmission model consists of a generator for the physical signal to be sent by the Tx, of the channel (Ch) and of a matched filter (MF) [Pro95] front end at the Rx. The MF front end consists of a bank of MFs and a vector sampler. The time discrete raw estimates at the output of the vector sampler are fed into the post-processor for possible improvement.

In what follows, first a general model on the above outlined basis is presented in Section 2.2. Then, in Section 2.3 the receiver structure is described in more detail. Section 2.4 proposes the classification of four different classes of transmission systems, namely SC systems [Pro95], MC systems, HY [BeC02] and generalised hybrid (G-HY) systems. Within the HY systems, we frame the well known OFDM system [NeP00, RGG01] in Section 2.5 pointing out the differences and similarities between conventional OFDM and the proposed modelling. In Section 2.6 the rate R and the SNR-degradation δ are defined and proposed as quality criteria suited to judge the system performance. We investigate the structure of the system matrix $\underline{\mathbf{A}}$ in Section 2.7 showing the existing symmetries. Finally, in Section 2.8, the point to multi-point and multi-point to point scenarios are derived as special settings of the model.

Complex quantities are characterized by underlining, vectors and matrices are represented by bold face letters. For matrix operations, with $(\cdot)^T$, $(\cdot)^*$ and $(\cdot)^H$ we indicate the transpose, the conjugate and the Hermitian [Wha71], respectively. Variable quantities are indicated in italics. The expressions $\text{diag}(\cdot)$, $\mathbf{E}\{\cdot\}$ and $\text{tr}\{\cdot\}$ denote the diagonal matrix containing the diagonal elements of the matrix in the argument, the expectation operation and trace operation, respectively.

2.2 General system model

2.2.1 System structure

Fig. 2.1 shows the general structure of a bandpass transmission system in the equivalent

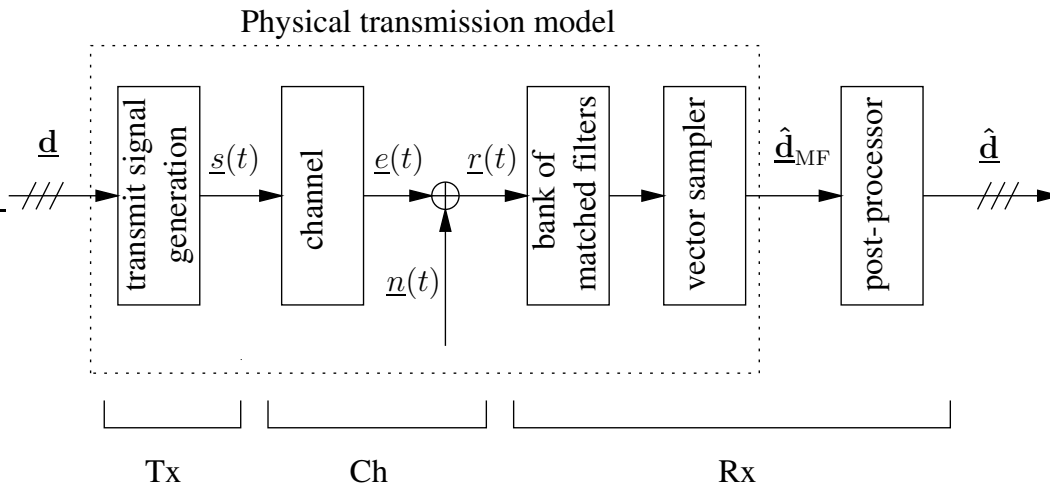


Fig. 2.1. Equivalent low-pass model for band-pass transmission systems utilizing linear modulation.

low-pass domain [BeC02, Pro95]. This system consists of the Tx, the Ch and the Rx. We assume that N complex data symbols \underline{d}_n , $n = 1 \dots N$, which are stacked in the data vector

$$\underline{d} = (\underline{d}_1 \dots \underline{d}_N)^T \quad (2.1)$$

are fed into the Tx and shall be transmitted over the Ch to the Rx.

At the output of the Rx an estimate $\hat{\underline{d}}$ of \underline{d} of (2.1) is aspired, which should deviate from \underline{d} as little as possible. The blocks and the signals involved in Fig. 2.1 are described in what follows.

2.2.2 Transmitter

In order to physically transmit the data symbols by a linear bandpass transmission system, each data symbol \underline{d}_n is represented by the product $\underline{d}_n \underline{c}_n(t)$ of \underline{d}_n and the data symbol specific transmit signature $\underline{c}_n(t)$, which is the complex envelope of a corresponding bandpass signal form. The signal radiated by the Tx into the Ch becomes

$$\underline{s}(t) = \sum_{n=1}^N \underline{d}_n \underline{c}_n(t). \quad (2.2)$$

The generation of $\underline{s}(t)$ of (2.2) is part of the task of the physical transmission model.

2.2.3 Transmission over the channel

The Ch is assumed to be linear and time variant and, therefore, can be characterized by the channel impulse response $\underline{h}(\tau, t)$ [Rap99]. By convolution of $\underline{c}_n(t)$ and $\underline{h}(\tau, t)$ we can introduce the N data symbol specific receive signatures

$$\underline{c}_{r,n}(t) = \int_{-\infty}^{+\infty} \underline{c}_n(t - \tau) \underline{h}(\tau, t) d\tau, \quad n = 1 \dots N. \quad (2.3)$$

With these signatures, from the linearity of the convolution and from (2.2), the useful signal at the Ch output can be written as

$$\underline{e}(t) = \int_{-\infty}^{+\infty} \underline{s}(t - \tau) \underline{h}(\tau, t) d\tau = \sum_{n=1}^N \underline{d}_n \underline{c}_{r,n}(t). \quad (2.4)$$

The channel is assumed to be causal and to have a channel impulse response of finite duration given by the maximum excess delay τ_{\max} [Rap99] so that $h(\tau, t) \neq 0$ only for $\tau \in [0, \tau_{\max}]$.

The consideration of the effect of the Ch as described by (2.3) and (2.4) is part of the task of the physical transmission model.

2.2.4 Receiver

Before entering the Rx, $\underline{e}(t)$ of (2.4) is assumed to be corrupted by the AWGN $\underline{n}(t)$ with the one sided noise power spectral density N_0 [Pro95] so that with (2.4) the signal to be processed in the Rx reads

$$\underline{r}(t) = \underline{e}(t) + \underline{n}(t) = \sum_{n=1}^N \underline{d}_n \underline{c}_{r,n}(t) + \underline{n}(t). \quad (2.5)$$

We shall assume that in the Rx $\underline{r}(t)$ of (2.5) is first fed into a bank of N parallel filters with each of these filters being matched to one of the N data symbol specific receive signatures $\underline{c}_{r,n}(t)$ of (2.3). The filter bank plus a vector sampler form the MF Rx front end shown in Fig. 2.2. The impulse response of the MF for $\underline{c}_{r,n}(t)$ is given by [Pro95]

$$\underline{h}_n(\tau) = \underline{c}_{r,n}^*(-\tau). \quad (2.6)$$

The N MFs characterized by (2.6) are non-causal, which, however, is irrelevant for our considerations, in which absolute timing relations between transmitted and received signals do not play a role.

Filtering with the MFs described by (2.6) belongs to the task of the physical transmission model.

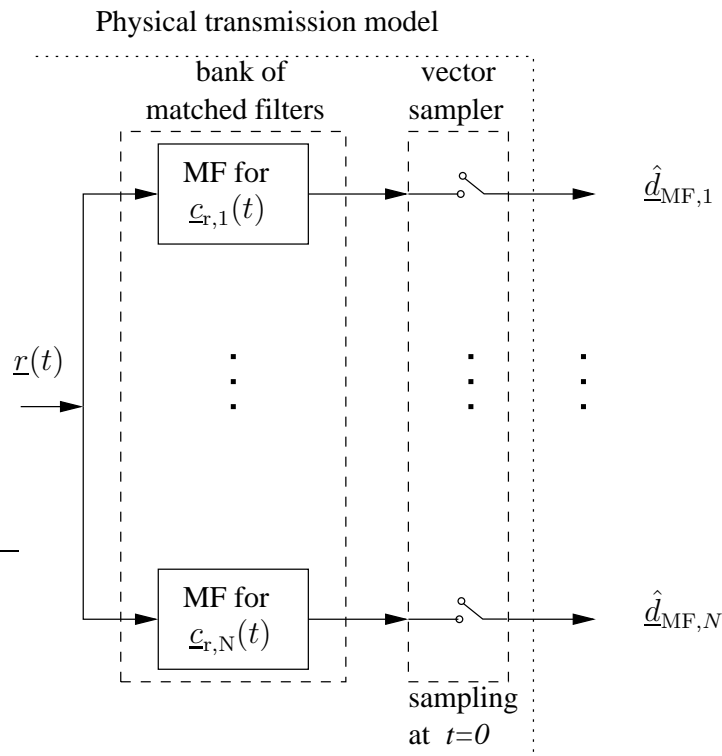


Fig. 2.2. Matched filter receiver front end.

2.3 Receiver

2.3.1 Matched filter estimate

The outputs of the N MFs are sampled at $t = 0$ by a vector sampler, which also belongs to the physical transmission model, see Fig. 2.2. This yields the MF estimate

$$\hat{\underline{\mathbf{d}}}_{\text{MF}} = (\hat{d}_{\text{MF},1} \cdots \hat{d}_{\text{MF},N})^{\text{T}} \quad (2.7)$$

as a raw data estimate of $\underline{\mathbf{d}}$ of (2.1). $\hat{\underline{\mathbf{d}}}_{\text{MF}}$ of (2.7) is a sufficient set of statistics [Kay93] for the transmitted data symbols. Therefore, no information on these data symbols is lost on the way from the Rx input to the outputs of the data vector sampler. $\hat{\underline{\mathbf{d}}}_{\text{MF}}$ of (2.7) is the sum of a useful part originating in the received desired signal $\underline{\mathbf{e}}(t)$ of (2.4) and of a noise part

$$\underline{\mathbf{n}}_{\text{MF}} = (\underline{n}_{\text{MF},1} \cdots \underline{n}_{\text{MF},N})^{\text{T}} \quad (2.8)$$

stemming from the received noise signal $\underline{\mathbf{n}}(t)$ introduced in (2.5).

Under consideration of (2.6), the contribution of the transmitted data symbol $\underline{d}_{n'}$, $n' = 1 \dots N$, to the MF estimate $\hat{d}_{\text{MF},n}$ of \underline{d}_n can be expressed as

$$\underline{d}_{n'} \int_{-\infty}^{+\infty} \underline{c}_{r,n'}(t - \tau) \underline{h}_n(\tau) d\tau \Big|_{t=0} = \underline{d}_{n'} \int_{-\infty}^{+\infty} \underline{c}_{r,n'}(\tau) \underline{c}_{r,n}^*(\tau) d\tau. \quad (2.9)$$

Consequently, with the noise contribution

$$\underline{n}_{\text{MF},n} = \int_{-\infty}^{+\infty} \underline{n}(t-\tau)\underline{h}_n(\tau)d\tau \Big|_{t=0} = \int_{-\infty}^{+\infty} \underline{n}(\tau)\underline{c}_{r,n}^*(\tau)d\tau \quad (2.10)$$

to $\hat{\underline{d}}_{\text{MF},n}$, we can write

$$\hat{\underline{d}}_{\text{MF},n} = \sum_{n'=1}^N \underline{d}_{n'} \int_{-\infty}^{+\infty} \underline{c}_{r,n'}(t)\underline{c}_{r,n}^*(t)dt + \underline{n}_{\text{MF},n}. \quad (2.11)$$

We now introduce the correlation coefficients

$$\underline{A}_{n,n'} = \int_{-\infty}^{+\infty} \underline{c}_{r,n'}(t)\underline{c}_{r,n}^*(t)dt \quad (2.12)$$

of the N data symbol specific receive signatures $\underline{c}_{r,n}(t)$ of (2.3). Then, (2.11) can be re-written as

$$\hat{\underline{d}}_{\text{MF},n} = \sum_{n'=1}^N \underline{d}_{n'}\underline{A}_{n,n'} + \underline{n}_{\text{MF},n}. \quad (2.13)$$

With $\underline{A}_{n,n'}$ of (2.12) we can form the $N \times N$ system matrix

$$\underline{\mathbf{A}} = \begin{pmatrix} \underline{A}_{1,1} & \cdots & \underline{A}_{1,N} \\ \vdots & \ddots & \vdots \\ \underline{A}_{N,1} & \cdots & \underline{A}_{N,N} \end{pmatrix}. \quad (2.14)$$

The raw data estimate $\hat{\underline{d}}_{\text{MF}}$ of (2.7) can now be expressed as

$$\hat{\underline{d}}_{\text{MF}} = \underline{\mathbf{A}}\underline{\mathbf{d}} + \underline{\mathbf{n}}_{\text{MF}}. \quad (2.15)$$

(2.15) represents the transition from $\underline{\mathbf{d}}$ of (2.1) to $\hat{\underline{d}}_{\text{MF}}$ of (2.7) to be performed by the physical transmission model, see Fig. 2.1. The element $\underline{A}_{n,n'}$ in position (n, n') of $\underline{\mathbf{A}}$ of (2.14) represents the contribution of the transmitted data symbol $\underline{d}_{n'}$ to the receive data symbol estimate $\hat{\underline{d}}_{\text{MF},n}$. For $n = n'$, $\underline{A}_{n,n'}$ represents the useful part. For $n \neq n'$, $\underline{A}_{n,n'}$ represents the ISI [Pro95] generated by the presence of transmitted symbols different from the symbol to be recovered.

2.3.2 Noise covariance matrix

From (2.10), the covariance coefficients of the noise at the output of the MF front end are determined by

$$\begin{aligned} \text{E} \{ \underline{n}_{\text{MF},n} \underline{n}_{\text{MF},n'}^* \} &= \text{E} \left\{ \int_{-\infty}^{+\infty} \int_{-\infty}^{+\infty} \underline{c}_{r,n'}(x) \underline{n}^*(x) \underline{n}(y) \underline{c}_{r,n}^*(y) dx dy \right\} \\ &= \int_{-\infty}^{+\infty} \int_{-\infty}^{+\infty} \underline{c}_{r,n'}(x) \text{E} \{ \underline{n}^*(x) \underline{n}(y) \} \underline{c}_{r,n}^*(y) dx dy. \end{aligned} \quad (2.16)$$

Since $\underline{n}(t)$ is assumed to be white with the one sided noise power spectral density N_0 [Pro95],

$$\text{E} \{ \underline{n}^*(x) \underline{n}(y) \} = N_0 \delta(x - y) \quad (2.17)$$

holds. The substitution of (2.17) into (2.16) yields

$$\text{E} \{ \underline{n}_{\text{MF},n} \underline{n}_{\text{MF},n'}^* \} = N_0 \int_{-\infty}^{+\infty} \underline{c}_{r,n'}(t) \underline{c}_{r,n}^*(t) dt \quad (2.18)$$

so that with $\underline{A}_{n,n'}$ of (2.12) we can write

$$\text{E} \{ \underline{n}_{\text{MF},n} \underline{n}_{\text{MF},n'}^* \} = N_0 \underline{A}_{n,n'}. \quad (2.19)$$

With (2.19) and \underline{A} of (2.14) the covariance matrix of $\underline{\mathbf{n}}_{\text{MF}}$ of (2.8) becomes

$$\underline{\mathbf{R}}_{\mathbf{n}} = \text{E} \{ \underline{\mathbf{n}}_{\text{MF}} \underline{\mathbf{n}}_{\text{MF}}^{\text{H}} \} = N_0 \underline{\mathbf{A}}. \quad (2.20)$$

The noise covariance matrix $\underline{\mathbf{R}}_{\mathbf{n}}$ of (2.20) is given by the system matrix $\underline{\mathbf{A}}$ of (2.12) scaled by the one sided noise power spectral density N_0 . This particular structure is determined by the chosen model in which the noise contribution is coloured by the filter with impulse response $\underline{h}_n(\tau)$ of (2.6) matched to the data symbol specific receive signature $\underline{c}_{r,n}(t)$ of (2.3), i.e. the convolution of the data symbol specific transmit signature $\underline{c}_n(t)$ of (2.2) and the channel impulse response $\underline{h}(\tau, t)$ of (2.3).

2.3.3 Post processing

In the Rx, the raw data estimate $\hat{\underline{\mathbf{d}}}_{\text{MF}}$ of (2.15) could already serve as the aspired estimate of $\underline{\mathbf{d}}$ of (2.1). However, by digital post-processing this estimate can be improved. The optimum algorithm for this post-processing [Kle96] would be the Maximum-a-Posteriori-Probability (MAP) algorithm, which would need the knowledge of the a priori probabilities of the data symbols \underline{d}_n of (2.1), or the Maximum-Likelihood (ML) algorithm, which does without this knowledge. In addition, each of these algorithms would need the knowledge of the probability density function of the noise $\underline{\mathbf{n}}_{\text{MF}}$ of (2.8). Both the MAP and the ML algorithms are non-linear, and, therefore, tend to be computationally expensive. Less expensive are the linear algorithms, which realize a linear transformation of $\underline{\mathbf{d}}_{\text{MF}}$ according to a given equalization algorithm. The most important linear equalizers are the Zero Forcing Block Linear Equalizer (ZF-BLE) and the Minimum Mean Square Error Block Linear Equalizer (MMSE-BLE) [Kle96, Kal95, KKB96]. In the case of ZF-BLE, with the raw estimate $\hat{\underline{\mathbf{d}}}_{\text{MF}}$ of (2.15) and $\underline{\mathbf{A}}$ of (2.14) the final estimate $\hat{\underline{\mathbf{d}}}$ of $\underline{\mathbf{d}}$ of (2.1) is determined by

$$\hat{\underline{\mathbf{d}}} = (\underline{\mathbf{A}}^{\text{H}} \underline{\mathbf{R}}_{\mathbf{n}}^{-1} \underline{\mathbf{A}})^{-1} \underline{\mathbf{A}}^{\text{H}} \underline{\mathbf{R}}_{\mathbf{n}}^{-1} \hat{\underline{\mathbf{d}}}_{\text{MF}} = \underline{\mathbf{A}}^{-1} \hat{\underline{\mathbf{d}}}_{\text{MF}}. \quad (2.21)$$

In the case of the MMSE-BLE, by assuming $\underline{\mathbf{d}}$ to be stationary with the covariance matrix

$$\underline{\mathbf{R}}_{\mathbf{d}} = \text{E} \{ \underline{\mathbf{d}} \underline{\mathbf{d}}^{\text{H}} \}, \quad (2.22)$$

with $\underline{\mathbf{R}}_n$ of (2.20), the final estimate is

$$\begin{aligned}\hat{\underline{\mathbf{d}}} &= (\underline{\mathbf{A}}^H \underline{\mathbf{R}}_n^{-1} \underline{\mathbf{A}} + \underline{\mathbf{R}}_d^{-1})^{-1} \underline{\mathbf{A}}^H \underline{\mathbf{R}}_n^{-1} \hat{\underline{\mathbf{d}}}_{\text{MF}} \\ &= \left(\mathbf{I} + \underline{\mathbf{A}}^{-1} \underline{\mathbf{R}}_n (\underline{\mathbf{A}}^H)^{-1} \underline{\mathbf{R}}_d^{-1} \right)^{-1} \underline{\mathbf{A}}^{-1} \hat{\underline{\mathbf{d}}}_{\text{MF}}.\end{aligned}\tag{2.23}$$

The performance of linear signal processing schemes as those described by (2.21) or (2.23) can be enhanced by introducing a feedback feature and, thus, the signal processing schemes may become non-linear [Kle96, WeM02].

2.4 Proposed classification

2.4.1 General

The system model elaborated in Sections 2.2 to 2.3 can serve to describe any linear transmission system. In this section, a classification of the linear transmission systems is proposed, namely

- single carrier (SC) systems,
- multi-carrier (MC) systems,
- hybrid (HY) systems, and
- generalised hybrid (G-HY) systems.

The classification is reported in Fig. 2.3 where the time-frequency extension of the radiated signal $\underline{\mathbf{s}}(t)$ is shown. Each data symbol specific transmit signature $\underline{\mathbf{c}}_n(t)$ of (2.2) is indicated as a rectangle with a given time and frequency occupation. From Fig. 2.3a, in SC systems $\underline{\mathbf{c}}_n(t)$ has the same frequency occupation for each value of $n = 1 \dots N$, while, as shown in Fig. 2.3b, in MC systems $\underline{\mathbf{c}}_n(t)$ has the same time occupation for each value of $n = 1 \dots N$. HY systems of Fig. 2.3c can be seen as the direct combination of the SC and MC systems and G-HY of Fig. 2.3d as a generalisation of HY systems, in which the frequency and time occupation is not equally distributed among the data symbol specific transmit signatures $\underline{\mathbf{c}}_n(t)$, $n = 1 \dots N$.

In the following we give a more detailed description of the characteristics of the classified systems.

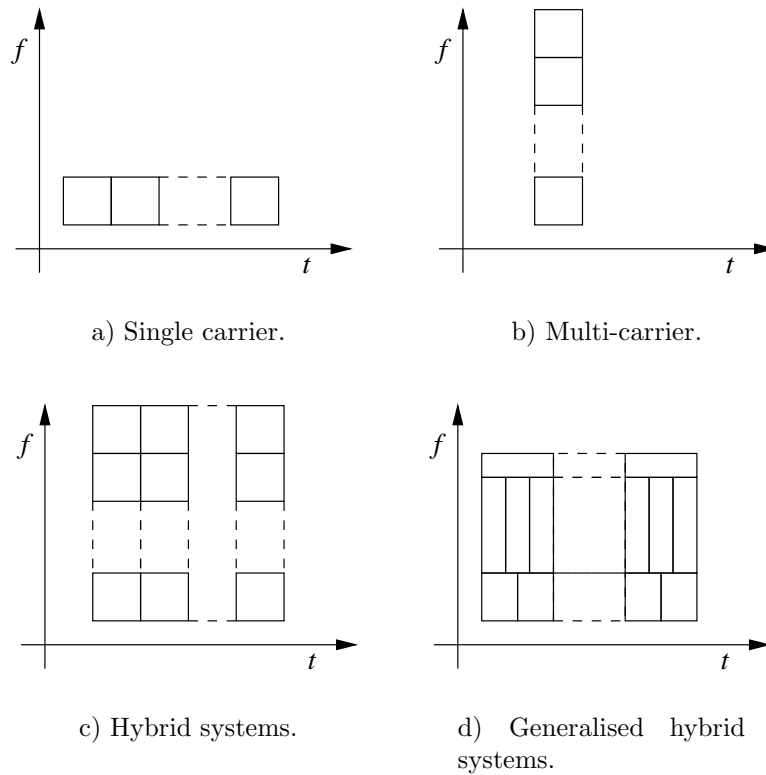


Fig. 2.3. Proposed classification. Each data symbol specific transmit signature $\underline{c}_n(t)$ of (2.2) is represented by a rectangle.

2.4.2 Single carrier

In the case of SC systems, see Fig. 2.3a, we set out from a basic transmit signature $\underline{c}_0(t)$ and generate the data symbol specific transmit signatures $\underline{c}_n(t)$ occurring in (2.2) with the time separation T of successive symbols according to

$$\underline{c}_n(t) = \underline{c}_0[t - (n - 1)T]. \quad (2.24)$$

The signal radiated into the channel becomes, cf. (2.2),

$$\underline{s}(t) = \sum_{n=1}^N \underline{d}_n \underline{c}_0[t - (n - 1)T]. \quad (2.25)$$

Typically [Pro95], $\underline{c}_0(t)$ in (2.25) is chosen such that $\underline{c}_{\text{eq}}(t) = \int_{-\infty}^{+\infty} \underline{c}_0(t - \tau) c_0(\tau) d\tau$ is a Nyquist impulse.

We designate the 3 dB bandwidth [Pro95] of $\underline{c}_0(t)$ by B_0 . Then, for the total bandwidth in the case of SC transmission we can assume

$$B_{\text{tot}} = B_0. \quad (2.26)$$

In analogy to B_0 we can introduce the 3 dB duration T_0 of $\underline{c}_0(t)$. Then, the total time required for the transmission of the N data symbols \underline{d}_n of (2.1) by this transmission scheme can be quantified by

$$T_{\text{tot}} = (N - 1)T + T_0. \quad (2.27)$$

The design space of the SC systems is outlined by the choices of

- the basic transmit signature $\underline{c}_0(t)$ including B_0 and T_0 ,
- the time separation T of successive symbols.

2.4.3 Multi-carrier

In the case of MC systems, see Fig. 2.3b, we again rely on a basic transmit signature $\underline{c}_0(t)$, but we generate the data symbol specific transmit signatures $\underline{c}_n(t)$ occurring in (2.2) with the frequency separation F according to

$$\underline{c}_n(t) = \underline{c}_0(t) \exp [j2\pi(n - 1)Ft]. \quad (2.28)$$

Each value of n corresponds to a different sub-carrier $\exp [j2\pi(n - 1)Ft]$. The entire radiated signal $\underline{s}(t)$ of (2.2) reads

$$\underline{s}(t) = \sum_{n=1}^N \underline{d}_n \underline{c}_0(t) \exp [j2\pi(n - 1)Ft], \quad (2.29)$$

and it occupies a single temporal slot.

In the case of an MC system, we can define the total bandwidth

$$B_{\text{tot}} = (N - 1)F + B_0 \quad (2.30)$$

and the total transmission duration

$$T_{\text{tot}} = T_0. \quad (2.31)$$

The design space of MC systems is outlined by the choice of

- the basic transmit signature $\underline{c}_0(t)$ including B_0 and T_0 and
- the frequency separation F of the sub-carriers.

2.4.4 Hybrid systems

In the case of HY systems, see Fig. 2.3c, let us assume that the number N of data symbols \underline{d}_n of (2.1) can be expressed as the product

$$N = N_t N_f \quad (2.32)$$

of the two integers N_t and N_f . Similarly, let us define the two functions $n_t(n)$ and $n_f(n)$ as

$$\begin{aligned} n_t(n) &= \left\lfloor \frac{n-1}{N_f} \right\rfloor + 1 & n = 1 \dots N \\ n_f(n) &= n - N_f \left\lfloor \frac{n-1}{N_f} \right\rfloor & n = 1 \dots N, \end{aligned} \quad (2.33)$$

where with $\lfloor \cdot \rfloor$ we indicate the closest lower integer. We note that each n , $n = 1 \dots N$, corresponds to the two values $n_t(n)$ and $n_f(n)$ of (2.33). The function $n_t(n)$ of (2.33) can assume values from 1 to N_t of (2.32). The function $n_f(n)$ of (2.33) can assume values from 1 to N_f of (2.32).

We choose a basic transmit signature $\underline{c}_0(t)$ and with (2.33) we determine the data symbol specific transmit signatures $\underline{c}_n(t)$ according to

$$\begin{aligned} \underline{c}_n(t) &= \underline{c}_0(t - (n_t(n) - 1)T) \exp[j2\pi(n_f(n) - 1)Ft], \\ &\text{with } n_t(n) = 1 \dots N_t, \quad n_f(n) = 1 \dots N_f. \end{aligned} \quad (2.34)$$

The frequency separation F in (2.34) is also referred to as sub-carrier spacing, cf. (2.28). It can be observed that N_t and N_f quantify the extensions of $\underline{s}(t)$ of (2.2) along the time and frequency axes, respectively. As a consequence, N_f is also referred to as the number of sub-carriers and N_t as the number of MC symbols, i.e. the number of the data symbols carried by the same sub-carrier. From (2.33) and (2.34), the role of $n_t(n)$ and $n_f(n)$ can be identified as the time index of the symbols modulating a given sub-carrier, i.e. the symbol slot index, and as the sub-carrier index, respectively.

The transmit signal $\underline{s}(t)$ of (2.2) reads now as

$$\underline{s}(t) = \sum_{n=1}^N \underline{d}_n \underline{c}_0(t - (n_t(n) - 1)T) \exp[j2\pi(n_f(n) - 1)Ft]. \quad (2.35)$$

For HY systems we can define the total bandwidth

$$B_{\text{tot}} = (N_f - 1)F + B_0 \quad (2.36)$$

and the total transmit duration

$$T_{\text{tot}} = (N_t - 1)T + T_0. \quad (2.37)$$

The design space of HY systems is given by the choices of

- the integers N_t and N_f ,
- the basic transmit signature $\underline{c}_0(t)$ including B_0 and T_0 ,
- the time separation T between any pair of data symbols carried by the same sub-carrier, and
- the frequency separation F between any pair of sub-carriers.

By assuming $N_t = 1$ or equivalently $N_f = N$, there is no time separation, i.e. $T = 0$, between consecutive transmit data symbols, and the HY system collapses into an MC system, cf. Subsection 2.4.3. On the other hand, by assuming $N_f = 1$ or equivalently $N_t = N$, there is no frequency separation, i.e. $F = 0$, between consecutive transmit data symbols, and the HY system collapses into an SC system, cf. Subsection 2.4.2.

2.4.5 Generalised hybrid systems

The G-HY systems considered here, cf. Fig. 2.3d, represent an extension of the HY systems presented in Subsection 2.4.4. We assume (2.32) valid and we choose N_f basic transmit signatures namely $\underline{c}_{0,n_f(n)}(t)$, with $n_f(n)$ of (2.33), with time extension $T_{0,n_f(n)}$ and frequency extension $B_{0,n_f(n)}$. We relax the assumption of equal sub-carrier separation through the definition of the sub-carriers $F_{n_f(n)}$, with $n_f(n)$ of (2.33), such that $F_{n_f(n)} \geq F_{n_f(n)-1}$. Similarly, we define the time separation $T_{n_f(n)}$, with $n_f(n)$ of (2.33). Without loss of generality, we assume that the data symbols \underline{d}_n of (2.1) modulating the sub-carrier $F_{n_f(n)}$ are spaced apart of $T_{n_f(n)}$. Therefore, the data symbol specific transmit signatures $\underline{c}_n(t)$ are given by

$$\underline{c}_n(t) = \underline{c}_{0,n_f(n)}(t - (n_t(n) - 1)T_{n_f(n)}) \exp[j2\pi F_{n_f(n)}t] \quad (2.38)$$

with $n_t(n), n_f(n)$ of (2.33)

For the G-HY systems we can define the total bandwidth

$$B_{\text{tot}} = F_{N_f} - F_1 + B_0, \quad (2.39)$$

and the total transmission duration as

$$T_{\text{tot}} = \max_{\substack{n_f(n)=1\dots N_f \\ n'_f(n)=1\dots N_f}} \{(N_t - 1)T_{n_f(n)} + T_{0,n'_f(n)}\}. \quad (2.40)$$

The design space is given by the choices of

- the integers N_t and N_f ,

- the N_f basic signatures $\underline{c}_{0,n_f(n)}(t)$, including their time extension $T_{0,n_f(n)}$ and frequency extension $B_{0,n_f(n)}$,
- the time separation $T_{n_f(n)}$ of the data symbols carried by the sub-carrier $F_{n_f(n)}$,
- the sub-carrier locations $F_{n_f(n)}$.

The G-HY systems can describe any system and can be easily reduced to the SC, to the MC or to the HY systems presented in the previous sections.

In particular, the flexibility of the G-HY systems allows the representation of different systems under the same model. This capability could be exploited to evaluate, for instance, the interference generating from different systems operating in the same environment, e.g. the effects due to the co-existence of second generation (2G) cellular systems with third generation (3G) cellular systems.

2.5 Conventional OFDM framed as hybrid system

2.5.1 General

In this section, conventional OFDM systems [NeP00, RGG01] are put into relation to the system model introduced in Sections 2.2 to 2.3. We assume that the radio channel is time invariant with the channel impulse response $\underline{h}(\tau)$ and the maximum excess delay τ_{\max} , and that the time separation T of the successive data symbols fulfils

$$T \geq \tau_{\max}. \quad (2.41)$$

We define the channel transfer function $\underline{H}(f)$ as the Fourier transform of the time invariant radio channel, i.e. $\underline{H}(f) = \int_{-\infty}^{+\infty} h(\tau) \exp[j2\pi f\tau] d\tau$.

2.5.2 Transmit signal generation and receive signal processing

Concerning the transmit signal $\underline{s}(t)$, a conventional OFDM system is a special version of the HY system introduced in Subsection 2.4.4 characterised by [NeP00]

- the choice

$$\underline{c}_0(t) = \frac{1}{\sqrt{T}} \text{rect} \left(\frac{t}{T} \right) = \begin{cases} 1/\sqrt{T} & 0 \leq |t| \leq T/2, \\ 0 & \text{else,} \end{cases} \quad (2.42)$$

of the basic transmit signature and

- the choice

$$F = \frac{1}{T - \tau_{\max}} \quad (2.43)$$

of the frequency separation in (2.34).

The time separation T for a conventional OFDM system is equal to the duration T of the basic transmit signature $\underline{c}_0(t)$ of (2.42). T can be considered as the 3 dB duration T_0 of $\underline{c}_0(t)$ of (2.42). Let us term the value of the radio channel transfer function $\underline{H}(f)$ for sub-carrier $n_f(n)$, cf. (2.33), as $\underline{H}_{n_f(n)}$. Then, the choice of $\underline{c}_0(t)$ according to (2.42) and the choice of F according to (2.43) guarantee that the data symbol specific receive signatures $\underline{c}_{r,n}(t)$ of (2.3) contain mutually orthogonal sinusoidal sections of duration $T - \tau_{\max}$ with constant envelope [NeP00].

Following (2.3), $\underline{c}_0(t)$ of (2.42) leads to the data symbol specific receive signature $\underline{c}_{r,n}(t)$ of duration $T + \tau_{\max}$. With respect to conventional OFDM we now define with $n_t(n)$ and $n_f(n)$ of (2.33) a modified data symbol specific receive signature

$$\tilde{\underline{c}}_{r,n}(t) = \underline{H}_{n_f(n)} \cdot \frac{1}{\sqrt{T}} \text{rect} \left(\frac{t - (n_t(n) - 1)T - \tau_{\max}/2}{T - \tau_{\max}} \right) \exp [j2\pi(n_f(n) - 1)Ft], \quad (2.44)$$

which is considered at the receiver. The interference introduced by the channel is removed, if conventional OFDM receive signal processing is applied.

Concerning the signal processing in the receiver, conventional OFDM differs from the system model developed in Sections 2.2 to 2.4 and illustrated in Fig. 2.1 and Fig. 2.2. This difference consists in choosing in the receiver, instead of filters matched to the data symbol specific receive signatures $\underline{c}_{r,n}(t)$ of (2.3), filters matched to the modified data symbol specific receive signatures $\tilde{\underline{c}}_{r,n}(t)$ of (2.44), see Fig. 2.4. This kind of signal processing in the receiver has the well known advantage that it can be implemented at low cost by FFT [NeP00]. However, it has the disadvantage that not the total received energy is utilised.

2.5.3 Mathematical modelling

With $\tilde{\underline{c}}_{r,n}(t)$ of (2.44) we obtain instead of $\underline{A}_{n,n'}$ of (2.12), now

$$\tilde{\underline{A}}_{n,n'} = \int_{-\infty}^{+\infty} \underline{c}_{r,n'}(t) \tilde{\underline{c}}_{r,n}^*(t) dt. \quad (2.45)$$

With the choice of $\underline{c}_0(t)$ of (2.42) and of $\tilde{\underline{c}}_{r,n}(t)$ of (2.44), (2.45) can be evaluated in closed form. By substituting (2.42) and (2.44) in (2.45) and explicitly writing $\underline{c}_{r,n}(t)$ of (2.3) we

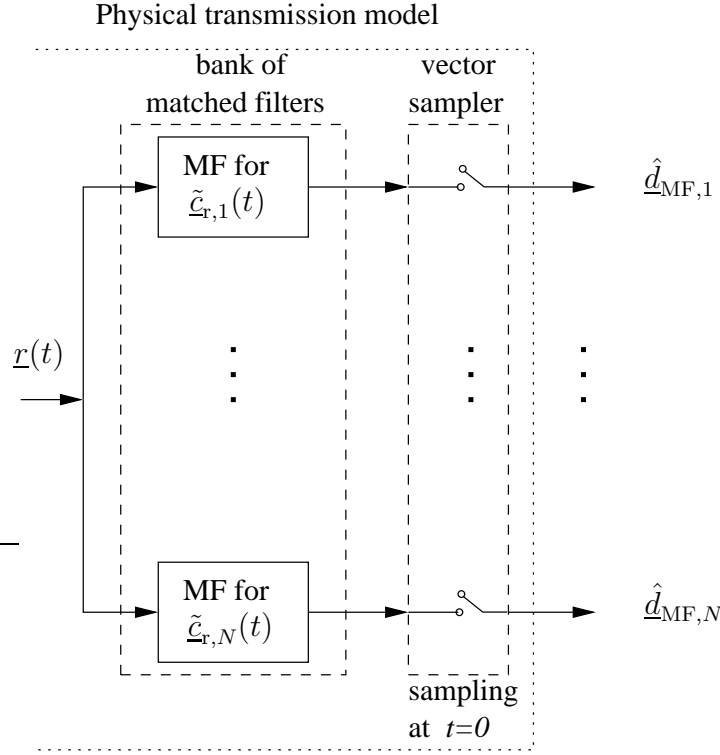


Fig. 2.4. OFDM receiver front end.

obtain

$$\begin{aligned} \tilde{A}_{n,n'} = & \int_{-\infty}^{+\infty} \int_0^{\tau_{\max}} \frac{1}{\sqrt{T}} \text{rect} \left(\frac{t - (n_t(n') - 1)T - \tau}{T} \right) \exp [j2\pi(n_f(n') - 1)F(t - \tau)] \cdot \\ & \cdot \underline{h}(\tau) d\tau \frac{1}{\sqrt{T}} \underline{H}_{n_f(n)}^* \text{rect} \left(\frac{t - (n_t(n) - 1)T - \tau_{\max}/2}{T - \tau_{\max}} \right) \exp [-j2\pi(n_f(n) - 1)Ft] dt. \end{aligned} \quad (2.46)$$

The first $\text{rect}(\cdot)$ function depending on $n_t(n')$ implies that (2.46) is different from zero if and only if

$$\tau + (n_t(n') - 1)T - T/2 \leq t \leq \tau + (n_t(n') - 1)T + T/2. \quad (2.47)$$

Similarly, the second $\text{rect}(\cdot)$ function depending on $n_t(n)$ implies that (2.46) is different from zero if and only if

$$(n_t(n) - 1)T + \tau_{\max} - T/2 \leq t \leq (n_t(n) - 1)T + T/2. \quad (2.48)$$

Under consideration of (2.47) and (2.48), it is apparent that $\tilde{A}_{n,n'}$ of (2.46) is different from zero if and only if $n_t(n') = n_t(n)$. As a consequence no ISI occurs. With some algebra we can simplify (2.46) as

$$\begin{aligned} \tilde{A}_{n,n'} = & \frac{1}{T} \underline{H}_{n_f(n)}^* \int_{(n_t(n)-1)T+\tau_{\max}-T/2}^{(n_t(n)-1)T+T/2} \exp [j2\pi(n_f(n') - n_f(n))Ft] dt \cdot \\ & \cdot \int_0^{\tau_{\max}} \underline{h}(\tau) \exp [-j2\pi(n_f(n') - 1)F\tau] d\tau. \end{aligned} \quad (2.49)$$

By recalling (2.43), the integral over t of (2.49) always extends over a full period of a sinusoid function. Therefore, it gives a non-zero contribution only if $n_f(n') = n_f(n)$ and no ICI occurs. The integral over τ of (2.49) returns the value of the radio channel transfer function $\underline{H}(f)$ for the sub-carrier $n_f(n)$, i.e. $\underline{H}_{n_f(n)}$. Then, we can further simplify (2.49) as

$$\tilde{\underline{A}}_{n,n'} = \begin{cases} |\underline{H}_{n_f(n)}|^2 (T - \tau_{\max})/T & \text{for } n' = n, \\ 0 & \text{else} \end{cases} \quad (2.50)$$

and the system matrix reads, instead of (2.14),

$$\tilde{\underline{A}} = \begin{pmatrix} \tilde{\underline{A}}_{1,1} & \cdots & 0 \\ \vdots & \ddots & \vdots \\ 0 & \cdots & \tilde{\underline{A}}_{N,N} \end{pmatrix}. \quad (2.51)$$

The data estimate at the output of the receive front end of Fig. 2.4 reads

$$\hat{\underline{\mathbf{d}}}_{\text{MF}} = \tilde{\underline{A}} \underline{\mathbf{d}} + \tilde{\underline{\mathbf{n}}}. \quad (2.52)$$

The noise vector $\tilde{\underline{\mathbf{n}}}$ has elements determined by, cf. (2.10),

$$\tilde{\underline{\mathbf{n}}}_n = \int_{-\infty}^{+\infty} \underline{\mathbf{n}}(\tau) \tilde{\underline{\mathcal{C}}}_{r,n}^*(\tau) d\tau. \quad (2.53)$$

The noise covariance matrix is determined by, cf. Subsection 2.3.2,

$$\tilde{\underline{\mathbf{R}}}_{n,n'} = N_0 \int_{-\infty}^{+\infty} \tilde{\underline{\mathcal{C}}}_{r,n'}(t) \tilde{\underline{\mathcal{C}}}_{r,n}^*(t) dt, \quad (2.54)$$

which is slightly different from (2.45). Nevertheless, with some algebra similar to (2.46) to (2.50) we derive that

$$\tilde{\underline{\mathbf{R}}}_n = N_0 \tilde{\underline{A}}. \quad (2.55)$$

With this approach conventional OFDM is framed within the proposed modelling.

In Subsection 2.5.2 we have mentioned that conventional OFDM does not recover all the energy of the transmitted symbol. The energy loss can be quantitatively expressed as

$$L_n = \frac{\int_{-\infty}^{+\infty} |\underline{\mathcal{C}}_{r,n}(t)|^2 dt}{\int_{-\infty}^{+\infty} |\tilde{\underline{\mathcal{C}}}_{r,n}(t)|^2 dt} = \frac{\int_{-\infty}^{+\infty} |\underline{\mathcal{C}}_{r,n}(t)|^2 dt}{|\underline{H}_{n_f(n)}|^2 (T - \tau_{\max})/T} \geq 1. \quad (2.56)$$

The value L_n of (2.56) is treated in Subsection 2.6.6 where we put it in relation to the quality criteria introduced to evaluate the system performance. In the case τ_{\max} equal to zero, L_n of (2.56) attains its minimum value one.

2.6 Quality criteria

2.6.1 General

In order to assess the quality of a transmission system, performance criteria are required. In the next subsections, we derive the rate R and the SNR-degradation δ under the hypothesis of SC, MC, HY and G-HY systems. The rate R and the SNR-degradation δ represent a trade-off in the system design. By increasing the rate R , the system increases the resource usage. By increasing the SNR-degradation δ the system performs worse in terms of quality of service. Ideally, we would like to have a high rate R and a low SNR-degradation δ . Actually, the two parameters are strictly related to each other in that with an increase of the rate R the SNR-degradation δ increases. Hence, the goal of the system design is to find the optimum trade-off between the two quantities.

The parameter δ is derived both for the ZF-BLE and the MMSE-BLE [Kle96]. The rate R is independent of the receiver.

2.6.2 Rate

With the number N of data symbols, cf. (2.1), the total transmission bandwidth B_{tot} of (2.26), (2.30), (2.36) and (2.39), respectively, and the total transmission duration T_{tot} of (2.27), (2.31), (2.37) and (2.40), respectively, the rate R will be defined as

$$R = \frac{N}{B_{\text{tot}}T_{\text{tot}}}. \quad (2.57)$$

R represents the ratio between the number N of transmitted data symbols \underline{d}_n in $\underline{\mathbf{d}}$ of (2.1) and the total capital invested in the transmission in terms of bandwidth and time.

In the case of an SC system, from (2.26) and (2.27), (2.57) becomes

$$R^{(\text{SC})} = \frac{N}{B_0[(N-1)T + T_0]}. \quad (2.58)$$

We can make some assumptions to characterize (2.58). If N is large enough, then the time duration T_0 of the basic transmit signature $\underline{c}_0(t)$ can be omitted in the denominator of (2.58) and $(N-1)T \approx NT$ holds so that (2.58) can be re-written as

$$R^{(\text{SC})} \approx \frac{N}{B_0NT} = \frac{1}{B_0T}. \quad (2.59)$$

If the sampling theorem [Pro95] shall be addressed, which is not an indispensable condition in the considered transmission systems, $B_0 \geq 1/T$ has to be fulfilled. As a consequence,

with N large enough to make valid the assumptions used in (2.59), the rate R of (2.57) of an SC system keeping the sampling theorem would be

$$R^{(\text{SC})} \leq 1. \quad (2.60)$$

As soon as R does not satisfy (2.60), the system performance is expected to degrade significantly.

In the case of an MC system, cf. Subsection 2.4.3, by substituting (2.30) and (2.31) in (2.57), the rate R of (2.57) becomes

$$R^{(\text{MC})} = \frac{N}{T_0 [(N-1)F + B_0]}. \quad (2.61)$$

By assuming N large enough, (2.61) can be simplified to

$$R^{(\text{MC})} \approx \frac{1}{T_0 F}. \quad (2.62)$$

The rate R of (2.62) now depends on the frequency separation F . As soon as the frequency separation F becomes smaller than the 3 dB bandwidth B_0 of the basic transmit signature $\underline{c}_0(t)$ we expect a significant performance degradation.

In the case of a HY system as introduced in Subsection 2.4.4, by substituting (2.32), (2.36) and (2.37) in (2.57), the rate R becomes

$$R^{(\text{HY})} = \frac{N_t N_f}{[(N_f - 1)F + B_0] \cdot [(N_t - 1)T + T_0]}. \quad (2.63)$$

By assuming N_t and N_f large enough, (2.63) can be simplified to

$$R^{(\text{HY})} \approx \frac{1}{TF}. \quad (2.64)$$

As before, if the sampling theorem should be addressed, to transmit with a period T , we would need at least a bandwidth of $1/T$. As a consequence, to avoid interference among adjacent sub-carriers, the frequency separation F should be $F \geq 1/T$. It follows that, as for the SC system, the rate R would be

$$R^{(\text{HY})} \leq 1. \quad (2.65)$$

If (2.65) is not verified we expect a significant increment of the SNR-degradation δ , cf. Subsection 2.6.3. (2.65) is not a necessary condition, but a value of the rate R at which we expect a significant change in the SNR-degradation δ trend.

For the G-HY systems the simplification is not straightforward. From (2.39) and (2.40) the rate R is derived as

$$R^{(\text{G-HY})} = \frac{N}{(F_{N_f} - F_1 + B_0) \max_{\substack{n_f(n)=1\dots N_f \\ n'_f(n)=1\dots N_f}} \{(N_t - 1)T_{n_f(n)} + T_{0,n'_f(n)}\}}. \quad (2.66)$$

The generalisation introduced in the G-HY system definition does not let us simplify (2.66), without introducing assumptions that would reduce the G-HY system to a HY, an SC or an MC system.

2.6.3 SNR-degradation

The SNR-degradation δ [Kle96, Lu02] is defined as the ratio between the SNR γ_{MF} at the MF output under neglect of interference and the SNR at the post processor output. In an AWGN channel, the MF is the best possible solution with respect to the SNR [Pro95], therefore the SNR-degradation δ gives a measure of how far the detection algorithm is from the best solution achievable in absence of interference.

From [Kle96] and [Lu02], if the detection algorithm is a ZF-BLE, then the mean SNR-degradation δ with $\underline{\mathbf{A}}$ of (2.14) and $\underline{\mathbf{R}}_n$ of (2.20) reads

$$\delta_{\text{ZF}} = \frac{1}{N} \sum_{n=1}^N [\underline{\mathbf{A}}^H \underline{\mathbf{R}}_n^{-1} \underline{\mathbf{A}}]_{n,n} \left[(\underline{\mathbf{A}}^H \underline{\mathbf{R}}_n^{-1} \underline{\mathbf{A}})^{-1} \right]_{n,n}. \quad (2.67)$$

We notice that in the proposed system modelling, the filter matched to the channel is included in the matrix elements $\underline{\mathbf{A}}_{n,n'}$, cf. (2.3) and (2.12). This has influence on the noise covariance matrix $\underline{\mathbf{R}}_n$ of (2.20).

By substituting (2.20) in (2.67) we obtain

$$\delta_{\text{ZF}} = \frac{1}{N} \sum_{n=1}^N [\underline{\mathbf{A}}^H]_{n,n} [(\underline{\mathbf{A}}^H)^{-1}]_{n,n}, \quad (2.68)$$

which is valid only for the proposed system modelling. In the OFDM case, cf. Section 2.5, the simplification of (2.68) is also valid but with a slight modification, cf. Subsection 2.6.6.

In the case of MMSE-BLE some work is needed for the derivation of the SNR-degradation δ . We notice that the MMSE-BLE does not completely eliminate the interference so that at the output of the post processing unit we have to evaluate the signal to noise plus interference ratio (SNIR). In what follows, the SNR-degradation δ in the MMSE-BLE case is assessed as the ratio between an SNR and an SNIR.

From [Wha71] the symbol estimates of the MMSE-BLE are given by

$$\hat{\underline{\mathbf{d}}}_{\text{MMSE}} = (\underline{\mathbf{A}}^H \underline{\mathbf{R}}_n^{-1} \underline{\mathbf{A}} + \underline{\mathbf{R}}_d^{-1})^{-1} \underline{\mathbf{A}}^H \underline{\mathbf{R}}_n^{-1} \hat{\underline{\mathbf{d}}}_{\text{MF}}. \quad (2.69)$$

(2.69) can be written as [Kle96]

$$\hat{\underline{\mathbf{d}}}_{\text{MMSE}} = \left(\mathbf{I} + (\underline{\mathbf{R}}_d \underline{\mathbf{A}}^H \underline{\mathbf{R}}_n^{-1} \underline{\mathbf{A}})^{-1} \right)^{-1} (\underline{\mathbf{A}}^H \underline{\mathbf{R}}_n^{-1} \underline{\mathbf{A}})^{-1} \underline{\mathbf{A}}^H \underline{\mathbf{R}}_n^{-1} \hat{\underline{\mathbf{d}}}_{\text{MF}}, \quad (2.70)$$

in which the term

$$\underline{\mathbf{W}}_0 = \left(\mathbf{I} + (\underline{\mathbf{R}}_d \underline{\mathbf{A}}^H \underline{\mathbf{R}}_n^{-1} \underline{\mathbf{A}})^{-1} \right)^{-1} \quad (2.71)$$

is referred to as Wiener estimator [Kle96] and the other term $(\underline{\mathbf{A}}^H \underline{\mathbf{R}}_n^{-1} \underline{\mathbf{A}})^{-1} \underline{\mathbf{A}}^H \underline{\mathbf{R}}_n^{-1}$ is recognized as the ZF-BLE in (2.21). In [Kle96], the SINR γ_{MMSE} at the output of the MMSE-BLE is found to be

$$\gamma_{\text{MMSE},n} = \frac{\left| [\underline{\mathbf{W}}_0]_{n,n} \right|^2 \text{E} \{ |d_n|^2 \}}{\left[\underline{\mathbf{W}}_0 \underline{\mathbf{R}}_d \right]_{n,n} - 2 \text{Re} \left\{ [\underline{\mathbf{W}}_0 \underline{\mathbf{R}}_d]_{n,n} [\underline{\mathbf{W}}_0]_{n,n}^* \right\} + \left| [\underline{\mathbf{W}}_0]_{n,n} \right|^2 \text{E} \{ |d_n|^2 \}}. \quad (2.72)$$

We can substitute $\underline{\mathbf{R}}_d = \mathbf{I}$, cf. (2.22), and with some matrix algebra we obtain from (2.72)

$$\gamma_{\text{MMSE},n} = \frac{[\underline{\mathbf{W}}_0]_{n,n}^*}{1 - [\underline{\mathbf{W}}_0]_{n,n}^*}. \quad (2.73)$$

From (2.71), (2.73) becomes

$$\gamma_{\text{MMSE},n} = \frac{\left[\left(\mathbf{I} + (\underline{\mathbf{A}}^H \underline{\mathbf{R}}_n^{-1} \underline{\mathbf{A}})^{-1} \right)^{-1} \right]_{n,n}^*}{1 - \left[\left(\mathbf{I} + (\underline{\mathbf{A}}^H \underline{\mathbf{R}}_n^{-1} \underline{\mathbf{A}})^{-1} \right)^{-1} \right]_{n,n}^*}. \quad (2.74)$$

We assume now the noise covariance matrix $\underline{\mathbf{R}}_n$ of (2.20). From the definition of the SNR-degradation δ , from (2.20) from (2.67) it is straightforward to write the mean SNR-degradation δ of the MMSE-BLE as

$$\delta_{\text{MMSE}} = \frac{1}{N} \sum_{n=1}^N N_0^{-1} [\underline{\mathbf{A}}^H]_{n,n} \frac{1 - \left[\left(\mathbf{I} + N_0 (\underline{\mathbf{A}}^H)^{-1} \right)^{-1} \right]_{n,n}^*}{\left[\left(\mathbf{I} + N_0 (\underline{\mathbf{A}}^H)^{-1} \right)^{-1} \right]_{n,n}^*}. \quad (2.75)$$

To further simplify (2.75), we consider the term $1 - \left[\left(\mathbf{I} + N_0 (\underline{\mathbf{A}}^H)^{-1} \right)^{-1} \right]_{n,n}^*$ in (2.75). It can be written as

$$\left[\mathbf{I} - \left(\mathbf{I} + N_0 (\underline{\mathbf{A}}^H)^{-1} \right)^{-1} \right]_{n,n}^*,$$

which becomes, after applying some matrix algebra,

$$N_0 \left[(\underline{\mathbf{A}}^H + N_0 \mathbf{I})^{-1} \right]_{n,n}^*.$$

By substituting in (2.75) and after applying some matrix algebra on the denominator, we obtain the SNR-degradation of the MMSE-BLE

$$\delta_{\text{MMSE}} = \frac{1}{N} \sum_{n=1}^N [\underline{\mathbf{A}}^H]_{n,n} \frac{\left[(\underline{\mathbf{A}}^H + N_0 \mathbf{I})^{-1} \right]_{n,n}^*}{\left[(\underline{\mathbf{A}}^H + N_0 \mathbf{I})^{-1} \underline{\mathbf{A}}^H \right]_{n,n}^*}, \quad (2.76)$$

which is valid only for the proposed system modelling.

2.6.4 Bounds of the SNR-degradation

δ_{ZF} of (2.68) and δ_{MMSE} of (2.76) can be further analysed to derive their expected behaviour. Under the assumptions of an AWGN channel and of basic transmit signatures $\underline{c}_0(t)$ with energy equal to one, i.e. $\int_{-\infty}^{+\infty} |\underline{c}_0(t)|^2 dt = 1$, the diagonal elements of the system matrix $\underline{\mathbf{A}}$ in (2.68) and (2.76) are equal to one. In particular, the SNR-degradation δ_{ZF} of (2.68) reads

$$\delta_{\text{ZF}} = \frac{1}{N} \sum_{n=1}^N \left[(\underline{\mathbf{A}}^{\text{H}})^{-1} \right]_{n,n}. \quad (2.77)$$

(2.77) can be written as

$$\delta_{\text{ZF}} = \frac{1}{N} \text{tr} \left\{ (\underline{\mathbf{A}}^{\text{H}})^{-1} \right\}. \quad (2.78)$$

With the eigenvalues λ_n , $n = 1 \dots N$, of $\underline{\mathbf{A}}$, the trace of $(\underline{\mathbf{A}}^{\text{H}})^{-1}$ becomes

$$\text{tr} \left\{ (\underline{\mathbf{A}}^{\text{H}})^{-1} \right\} = \sum_{n=1}^N \frac{1}{\lambda_n^*}. \quad (2.79)$$

Therefore, we can write instead of (2.78)

$$\delta_{\text{ZF}} = \frac{1}{N} \sum_{n=1}^N \frac{1}{\lambda_n^*}. \quad (2.80)$$

If $FT = 1$ and the basic transmit signature $\underline{c}_0(t)$ satisfies the Nyquist conditions [Pro95], then $\underline{\mathbf{A}}$ is an identity matrix and the SNR-degradation δ_{ZF} is equal to 1. If $FT < 1$, δ_{ZF} is expected to increase because of the rising of the overlapping among the data symbol specific transmit signatures $\underline{c}_n(t)$. In particular, if both $F = 0$ and $T = 0$, then the transmitted data symbols \underline{d}_n of (2.1) have the same time and frequency location. The elements of the system matrix $\underline{\mathbf{A}}$ of (2.14) are expected to be all equal to one so that $(\underline{\mathbf{A}}^{\text{H}})^{-1}$ does not exist. With $T \rightarrow 0$ and/or $F \rightarrow 0$, the matrix $\underline{\mathbf{A}}^{\text{H}}$ tends to be singular or, equivalently, all the eigenvalues but one tend to zero. Therefore, the SNR-degradation δ_{ZF} of (2.80) tends to infinity and we can write

$$1 \leq \delta_{\text{ZF}} < +\infty. \quad (2.81)$$

(2.81) does not give any information about the way δ_{ZF} increases with $T \rightarrow 0$ and/or $F \rightarrow 0$.

The SNR-degradation δ of the MMSE-BLE of (2.76) depends not only on the system matrix $\underline{\mathbf{A}}$ of (2.14), but also on the one sided noise power spectral density N_0 . We first investigate the influence of N_0 . We start from (2.74) and assume that the noise covariance matrix $\underline{\mathbf{R}}_n$ in (2.74) is obtained by colouring a white noise with a linear transformation, cf. (2.20). This is always the case in the presence of any linear detector and AWGN

$\underline{n}(t)$ at the input of the receiver. With this assumption we can write $\underline{\mathbf{R}}_n = N_0 \underline{\mathbf{A}}_n$. From the definition of the SNR-degradation δ and from (2.67) it is straightforward to write the mean SNR-degradation δ of the MMSE-BLE as

$$\delta_{\text{MMSE}} = \frac{1}{N} \sum_{n=1}^N N_0^{-1} [\underline{\mathbf{A}}^H \underline{\mathbf{A}}_n^{-1} \underline{\mathbf{A}}]_{n,n} \frac{1 - \left[\left(\mathbf{I} + N_0 (\underline{\mathbf{A}}^H \underline{\mathbf{A}}_n^{-1} \underline{\mathbf{A}})^{-1} \right)^{-1} \right]_{n,n}^*}{\left[\left(\mathbf{I} + N_0 (\underline{\mathbf{A}}^H \underline{\mathbf{A}}_n^{-1} \underline{\mathbf{A}})^{-1} \right)^{-1} \right]_{n,n}^*}. \quad (2.82)$$

From (2.82) and following the same reasoning of (2.75) to (2.76), we obtain

$$\delta_{\text{MMSE}} = \frac{1}{N} \sum_{n=1}^N [\underline{\mathbf{A}}^H \underline{\mathbf{A}}_n^{-1} \underline{\mathbf{A}}]_{n,n} \frac{\left[\left(\mathbf{I} + N_0 (\underline{\mathbf{A}}^H \underline{\mathbf{A}}_n^{-1} \underline{\mathbf{A}})^{-1} \right)^{-1} (\underline{\mathbf{A}}^H \underline{\mathbf{A}}_n^{-1} \underline{\mathbf{A}})^{-1} \right]_{n,n}^*}{\left[\left(\mathbf{I} + N_0 (\underline{\mathbf{A}}^H \underline{\mathbf{A}}_n^{-1} \underline{\mathbf{A}})^{-1} \right)^{-1} \right]_{n,n}^*}. \quad (2.83)$$

Let us now consider the case in which N_0 is very large, i.e. $N_0 \rightarrow +\infty$. In this case, the identity matrix in $\left(\mathbf{I} + N_0 (\underline{\mathbf{A}}^H \underline{\mathbf{A}}_n^{-1} \underline{\mathbf{A}})^{-1} \right)^{-1}$ can be assumed to have no influence so that

$$\delta_{\text{MMSE}} \xrightarrow{N_0 \rightarrow +\infty} 1. \quad (2.84)$$

(2.84) shows that in case of high N_0 the MMSE-BLE performs as the MF bound in the absence of other interference. In other words, if the one sided noise power spectral density N_0 is very high, then the effect of the interference is negligible and the MMSE-BLE performs as the MF.

Let us now focus on the case in which the one sided noise power spectral density N_0 is approximating the zero value. From (2.83), with $N_0 \rightarrow 0$, the matrixes multiplied by N_0 do not give any contribution and (2.83) reads

$$\delta_{\text{MMSE}} \xrightarrow{N_0 \rightarrow 0} \frac{1}{N} \sum_{n=1}^N [\underline{\mathbf{A}}^H \underline{\mathbf{A}}_n^{-1} \underline{\mathbf{A}}]_{n,n} \left[(\underline{\mathbf{A}}^H \underline{\mathbf{A}}_n^{-1} \underline{\mathbf{A}})^{-1} \right]_{n,n}, \quad (2.85)$$

which is the SNR-degradation δ obtained for the ZF-BLE in (2.68) under the assumption that $\underline{\mathbf{R}}_n = N_0 \underline{\mathbf{A}}_n$. As expected [KKB96], without any noise in the system the MMSE-BLE approximates the ZF-BLE.

The SNR-degradation δ_{MMSE} of (2.76) depends also on the system matrix $\underline{\mathbf{A}}$ of (2.14), but it does not require the inversion of system matrix $\underline{\mathbf{A}}$ of (2.14) as the ZF-BLE. If $FT = 1$ and the Nyquist assumption are verified [Pro95], then $\underline{\mathbf{A}} = \mathbf{I}$ and from (2.76) we obtain $\delta_{\text{MMSE}} = 1$. We then consider the same assumptions as in the ZF-BLE, i.e. $T = 0$ and $F = 0$, an AWGN noise channel and a basic transmit signature $\underline{c}_0(t)$ with energy equal to one. From (2.76), with $\underline{A}_{n,n'} = 1$ for each n, n' , we obtain

$$[\underline{\mathbf{A}}^H + N_0 \mathbf{I}]_{n,n'} = \begin{cases} 1 + N_0 & \text{for } n' = n, \\ 1 & \text{for } n' \neq n. \end{cases} \quad (2.86)$$

Given the particular structure of the matrix in (2.86), with some matrix and algebra manipulation we can derive the inverse in a closed form, i.e.

$$\left[(\underline{\mathbf{A}}^H + N_0 \mathbf{I})^{-1} \right]_{n,n'} = \begin{cases} \frac{N_0 + N - 1}{N_0(N_0 + N)} & \text{for } n' = n, \\ -\frac{1}{N_0(N_0 + N)} & \text{for } n' \neq n. \end{cases} \quad (2.87)$$

Through (2.87), we can derive the elements of the numerator of (2.76). Also the denominator can be written in a closed form since the matrix $\underline{\mathbf{A}}$ has all elements equal to one. As a consequence, from (2.76) and (2.87) we obtain

$$\left[(\underline{\mathbf{A}}^H + N_0 \mathbf{I})^{-1} \underline{\mathbf{A}}^H \right]_{n,n} = \sum_{n'=1}^N \left[(\underline{\mathbf{A}}^H + N_0 \mathbf{I})^{-1} \right]_{n,n'} = \frac{1}{N_0 + N}. \quad (2.88)$$

With (2.87) and (2.88), (2.76) can be written as

$$\delta_{\text{MMSE}} \Big|_{T=0, F=0} = \frac{N_0 + N - 1}{N_0}. \quad (2.89)$$

Therefore, the bounds of the SNR-degradation δ_{MMSE} of (2.76) are given by

$$1 \leq \delta_{\text{MMSE}} < \frac{N_0 + N - 1}{N_0}. \quad (2.90)$$

From (2.90), we infer that for a block transmission the δ_{MMSE} does not diverge toward infinity but is upper bounded by a factor which depends on the one sided noise power spectral density N_0 and on the number N of transmitted data symbols \underline{d}_n . The upper bound of δ_{MMSE} of (2.76) is proportional to N . When evaluating the performance through simulations we will be able to verify the just derived bounds.

2.6.5 Example of trade-off

As a tendency, a large rate R of (2.57) goes along with a large mean SNR-degradation δ of (2.67) and (2.82). In practical system layout, an acceptable compromise between R and δ has to be found.

To show how these two measures are related to each other, let us consider an example. Let us assume an MC system with $N = 2$. The basic transmit signature $\underline{c}_0(t)$ is chosen as a square root raised cosine (rrcos) with a roll-off factor α and a reference time T_{ref} [BeC02, Pro95], i.e.

$$\underline{c}_0(t) = \frac{1}{\sqrt{T_{\text{ref}}}} \frac{\sin [\pi(1 - \alpha)t/T_{\text{ref}}] + 4\alpha t/T_{\text{ref}} \cos [\pi(1 + \alpha)t/T_{\text{ref}}]}{\pi [1 - (4\alpha t/T_{\text{ref}})^2] t/T_{\text{ref}}}. \quad (2.91)$$

As a consequence we have two data symbol specific transmit signatures $\underline{c}_n(t)$, cf. (2.28), which read

$$\begin{aligned} \underline{c}_1(t) &= \underline{c}_0(t) \\ \underline{c}_2(t) &= \underline{c}_0(t) \cdot \exp[j2\pi Ft]. \end{aligned} \quad (2.92)$$

The 3 dB duration T_0 of $\underline{c}_0(t)$ is defined as the time duration during which $|\underline{c}_0(t)| \geq \max_t |\underline{c}_0(t)|/2$ [BeC02]. Since $\underline{c}_0(t)$ of (2.91) is symmetric, i.e. $\underline{c}_0(t) = \underline{c}_0(-t)$, and it assumes its maximum absolute value for $t = 0$, we first determine the positive value t_0 for which

$$|\underline{c}_0(t_0)| = \left| \frac{\underline{c}_0(0)}{2} \right|. \quad (2.93)$$

Then, with t_0 of (2.93) the 3 dB duration T_0 is

$$T_0 = 2t_0. \quad (2.94)$$

Equivalently, if we indicate with $\underline{C}_0(f)$ the Fourier transform of the basic transmit signature $\underline{c}_0(t)$, then the 3 dB bandwidth B_0 is defined as the set of frequencies in which $|\underline{C}_0(f)| \geq \max_f |\underline{C}_0(f)|/2$ [BeC02]. With $\underline{c}_0(t)$ of (2.91), $\underline{C}_0(f)$ is Hermitian symmetric, i.e. $\underline{C}_0(f) = \underline{C}_0^*(-f)$ and it assumes its maximum absolute value for $f = 0$. Therefore, we first determine the positive value f_0 for which

$$|\underline{C}_0(f_0)| = \left| \frac{\underline{C}_0(0)}{2} \right|. \quad (2.95)$$

Then, with f_0 of (2.95) the 3 dB bandwidth B_0 is

$$B_0 = 2f_0. \quad (2.96)$$

The 3 dB duration T_0 of $\underline{c}_0(t)$ of (2.91) cannot be expressed in a closed form. With (2.91), (2.93) and (2.94) and through numerical approximation, we determine

$$T_0 \approx \frac{4}{3} T_{\text{ref}}. \quad (2.97)$$

The 3 dB bandwidth B_0 of $\underline{c}_0(t)$ of (2.91) can be determined in a closed form [BeC02, Pro95]. With (2.91), (2.95) and (2.96) we obtain

$$B_0 = \frac{\alpha + 3}{3T_{\text{ref}}}. \quad (2.98)$$

With T_0 of (2.97) and B_0 of (2.98), we derive from (2.30) and (2.31)

$$\begin{aligned} T_{\text{tot}} &= T_0, \\ B_{\text{tot}} &= F + B_0. \end{aligned} \quad (2.99)$$

From (2.97) to (2.99) the value of R of (2.57) can be written

$$R = \frac{9}{6FT_{\text{ref}} + 2\alpha + 6}. \quad (2.100)$$

The system matrix $\underline{\mathbf{A}}$ of (2.14) has two rows and two columns, hence the SNR-degradation δ of (2.68) can be expressed as

$$\delta_{\text{ZF}} = \frac{1}{2} \frac{|A_{1,1}|^2 + |A_{2,2}|^2}{A_{1,1}^* A_{2,2}^* - \underline{A}_{1,2}^* \underline{A}_{2,1}^*}. \quad (2.101)$$

Under the assumption of data symbol specific receive signatures $\underline{c}_{r,n}(t)$ of (2.3) with normalized energy [Pro95], (2.101) reduces to

$$\delta_{\text{ZF}} = \frac{1}{1 - \underline{A}_{1,2}^* \underline{A}_{2,1}^*} = \frac{1}{1 - |\underline{A}_{1,2}|^2}. \quad (2.102)$$

By recalling (2.12), in (2.102) it is shown that with the increasing of the interference between the two adjacent sub-carriers, i.e. the increase of the terms outside the main diagonal of $\underline{\mathbf{A}}$ of (2.14), an increment of δ_{ZF} can be observed.

We consider now two possibilities:

1. **We do not admit degradation:** In this case we impose $\delta = 1$, i.e. $\underline{A}_{1,2}^* = \underline{A}_{2,1}^* = 0$. With the choice made in (2.92), to avoid any interference we have to choose the frequency separation $F \geq (1 + \alpha)/T_{\text{ref}}$ to ensure that the data symbol specific transmit signatures $\underline{c}_n(t)$ of (2.92) do not overlap in frequency [BeC02, Pro95]. By substituting $F \geq (1 + \alpha)/T_{\text{ref}}$ in (2.100), we obtain

$$R \leq \frac{9}{12 + 8\alpha}. \quad (2.103)$$

The rate R decreases as α increases so the best choice under ideal assumptions is in this case $\alpha = 0$. We note that, by imposing no SNR-degradation δ , (2.103) yields an upper bound of the highest possible achievable rate R .

2. **We do admit degradation:** In this case $\delta \geq 1$, i.e. $\underline{A}_{1,2}^* \neq 0$, $\underline{A}_{2,1}^* \neq 0$, and we can admit $F \leq (1 + \alpha)/T_{\text{ref}}$. This case is specular with respect to the previous one and (2.103) becomes

$$R \geq \frac{9}{12 + 8\alpha}, \quad (2.104)$$

which gives a lower bound. By admitting a SNR-degradation $\delta > 1$, we can increase the rate R .

2.6.6 Measures for conventional OFDM

The quality criteria proposed in Subsection 2.6.2 and 2.6.3 are used also to evaluate the performance of conventional OFDM. As described in Section 2.5, conventional OFDM

systems cannot be directly framed in the proposed system modelling, hence also the quality measures could vary.

The rate R of (2.57) does not depend on the data symbol specific receive signature $\underline{c}_{r,n}(t)$, therefore it assumes the same value both for the proposed modelling and for the conventional OFDM. The SNR-degradation δ of (2.67) depends on the system matrix and it represents the degradation introduced by the detection algorithm with respect to the optimum receiver. In Section 2.5 we have mentioned that conventional OFDM is a sub-optimum solution and the modified system matrix $\tilde{\mathbf{A}}$ of (2.51) has a slightly different structure with respect to the system matrix \mathbf{A} of (2.14) obtained for the proposed modelling. Also the modified noise covariance matrix $\tilde{\mathbf{R}}_n$ of (2.55) of conventional OFDM system is different from the noise covariance matrix \mathbf{R}_n of (2.20). To measure the SNR-degradation δ of the conventional OFDM systems due to the deployment of the guard interval τ_{\max} of (2.43), we define an SNR-degradation $\tilde{\delta}$ as the ratio between the SNR γ_{MF} obtained by the optimum solution of the proposed modelling, cf. Section 2.4, and the SNR $\tilde{\gamma}_{\text{MF}}$ obtained by the conventional OFDM system. With this characterization we can define the SNR-degradation δ of conventional OFDM when deploying the MF as

$$\tilde{\delta}_{\text{MF}} = \frac{\gamma_{\text{MF}}}{\tilde{\gamma}_{\text{MF}}}, \quad (2.105)$$

the degradation of conventional OFDM when deploying the ZF-BLE as

$$\tilde{\delta}_{\text{ZF}} = \frac{\gamma_{\text{MF}}}{\tilde{\gamma}_{\text{ZF}}}, \quad (2.106)$$

and the degradation of OFDM when deploying the MMSE-BLE as

$$\tilde{\delta}_{\text{MMSE}} = \frac{\gamma_{\text{MF}}}{\tilde{\gamma}_{\text{MMSE}}}. \quad (2.107)$$

From (2.52) and (2.67), we can write (2.105) as

$$\tilde{\delta}_{\text{MF}} = \frac{1}{N} \sum_{n=1}^N \frac{[\mathbf{A}^H \mathbf{R}_n^{-1} \mathbf{A}]_{n,n}}{[\tilde{\mathbf{A}}^H \tilde{\mathbf{R}}_n^{-1} \tilde{\mathbf{A}}]_{n,n}}. \quad (2.108)$$

Similarly, we can derive the expressions of the measures of (2.106) and (2.107) as

$$\tilde{\delta}_{\text{ZF}} = \frac{1}{N} \sum_{n=1}^N [\mathbf{A}^H \mathbf{R}_n^{-1} \mathbf{A}]_{n,n} \left[\left(\tilde{\mathbf{A}}^H \tilde{\mathbf{R}}_n^{-1} \tilde{\mathbf{A}} \right)^{-1} \right]_{n,n} \quad (2.109)$$

and as

$$\tilde{\delta}_{\text{MMSE}} = \frac{1}{N} \sum_{n=1}^N [\mathbf{A}^H \mathbf{R}_n^{-1} \mathbf{A}]_{n,n} \frac{1 - \left[\left(\mathbf{I} + \left(\tilde{\mathbf{A}}^H \tilde{\mathbf{R}}_n^{-1} \tilde{\mathbf{A}} \right)^{-1} \right)^{-1} \right]_{n,n}^*}{\left[\left(\mathbf{I} + \left(\tilde{\mathbf{A}}^H \tilde{\mathbf{R}}_n^{-1} \tilde{\mathbf{A}} \right)^{-1} \right)^{-1} \right]_{n,n}^*}, \quad (2.110)$$

respectively.

In Subsection 2.5.3 we have seen that the modified system matrix $\tilde{\mathbf{A}}$ of (2.51) of conventional OFDM systems has a diagonal structure, cf. (2.50), and we have introduced the energy loss factors L_n in (2.56). Based on these observations we can derive the SNR-degradation $\tilde{\delta}$ as defined in (2.108), (2.109) and (2.110) in a closed form. The expression of $\tilde{\mathbf{A}}$ of (2.51) is determined in Subsection 2.5.3. Here, we determine the expression of the system matrix \mathbf{A} of (2.14) for a HY system deploying the basic transmit signature $\underline{c}_0(t)$ of (2.42). From (2.3), (2.12) and (2.42) we obtain

$$\begin{aligned} \underline{c}_{r,n}(t) &= \int_{-\infty}^{+\infty} \frac{1}{\sqrt{T}} \text{rect} \left(\frac{t - (n_t(n) - 1)T - \tau}{T} \right) \exp [j2\pi(n_f(n) - 1)F(t - \tau)] h(\tau) d\tau = \\ &= \frac{1}{\sqrt{T}} \exp [j2\pi(n_f(n) - 1)Ft] \int_{(n_t(n)-1)T-T/2}^{(n_t(n)-1)T+T/2+\tau_{\max}} \text{rect} \left(\frac{t - (n_t(n) - 1)T - \tau}{T} \right) \cdot \\ &\quad \cdot \exp [-j2\pi(n_f(n) - 1)F\tau] h(\tau) d\tau. \end{aligned} \quad (2.111)$$

Under the assumption of $T \gg \tau_{\max}$ and from the definition of $\underline{H}_{n_f(n)}$ of Subsection 2.5.3, then (2.111) can be approximated as

$$\underline{c}_{r,n}(t) \approx \underline{H}_{n_f(n)} \frac{1}{\sqrt{T}} \text{rect} \left(\frac{t - (n_t(n) - 1)T}{T + \tau_{\max}} \right) \exp [j2\pi(n_f(n) - 1)Ft]. \quad (2.112)$$

With (2.112) we derive

$$\underline{A}_{n,n} \approx |\underline{H}_{n_f(n)}|^2 \frac{T + \tau_{\max}}{T}. \quad (2.113)$$

By substituting (2.20) and (2.55) in (2.108) we obtain

$$\tilde{\delta}_{\text{MF}} = \frac{1}{N} \sum_{n=1}^N \frac{[\mathbf{A}^{\text{H}}]_{n,n}}{[\tilde{\mathbf{A}}^{\text{H}}]_{n,n}}, \quad (2.114)$$

and with (2.50) and (2.113)

$$\tilde{\delta}_{\text{MF}} = \frac{T + \tau_{\max}}{T - \tau_{\max}}, \quad (2.115)$$

which is the closed form of the SNR-degradation δ of (2.68) for conventional OFDM systems as defined in (2.105). By recalling the energy loss factors L_n of (2.56) it is now apparent that it has the same value of the SNR-degradation δ of (2.115), i.e.

$$L_n = \tilde{\delta}_{\text{MF}}, \quad n = 1 \dots N, \quad (2.116)$$

holds.

The diagonal structure of $\tilde{\mathbf{A}}$ of (2.51) implies that the degradation is always the same for the different detection schemes so that

$$\tilde{\delta}_{\text{MF}} = \tilde{\delta}_{\text{ZF}} = \tilde{\delta}_{\text{MMSE}}. \quad (2.117)$$

The SNR-degradation $\tilde{\delta}$ of conventional OFDM does not depend on the detection algorithm because the deployment of the guard interval avoids a priori the presence of ISI and ICI. Additionally, we observe that the measures (2.108) to (2.110) differ from the usual definition of SNR-degradation δ [Lu02], because they compare two systems with a different system matrix $\underline{\mathbf{A}}$. However, they allow taking into account the SNR-degradation introduced by the deployment of the guard interval and, as a consequence, to consider conventional OFDM as a reference in the assessment of other HY systems.

To derive (2.113) to (2.117), we used the assumption that the approximation of (2.112) holds true. This is always the case in conventional OFDM systems [NeP00, RGG01] in which the system is designed so that $T \gg \tau_{\max}$.

2.7 On the structure of the system matrix $\underline{\mathbf{A}}$

2.7.1 General

In Subsection 2.6.3, we have seen how the system matrix $\underline{\mathbf{A}}$ of (2.14) influences the SNR-degradation δ of (2.68) and (2.76). From (2.12), we can derive the inner structure of $\underline{\mathbf{A}}$ and propose some simplifications. We consider the data symbol specific transmit signatures $\underline{c}_n(t)$ of (2.2) of the HY systems so that we can easily trace the results for the SC and MC case, cf. Subsection 2.4.4. Moreover, we assume the presence of an AWGN channel, cf. Subsection 2.2.3. In this way, the data symbol specific receive signatures $\underline{c}_{r,n}(t)$ of (2.3) are equal to the data symbol specific transmit signatures $\underline{c}_n(t)$ of (2.2). The presence of the channel will be considered in Subsection 2.7.3.

2.7.2 Existing symmetries

From (2.12) and (2.33) to (2.34) and under the assumption that $\underline{c}_{r,n}(t) = \underline{c}_n(t)$, we derive

$$\begin{aligned} \underline{A}_{n,n'} = & \int_{-\infty}^{+\infty} \underline{c}_0 [t' - (n_t(n') - 1)T] \exp [j2\pi(n_f(n') - 1)Ft'] \cdot \\ & \cdot \underline{c}_0 [t' - (n_t(n) - 1)T] \exp [-j2\pi(n_f(n) - 1)Ft'] dt'. \end{aligned} \quad (2.118)$$

We write the exponential factors as one single factor and substitute the variable $t = t' - (n_t(n') - 1)T$ to obtain

$$\begin{aligned} \underline{A}_{n,n'} = & \int_{-\infty}^{+\infty} \underline{c}_0(t) \underline{c}_0 [t - (n_t(n) - n_t(n'))T] \cdot \\ & \cdot \exp [-j2\pi(n_f(n) - n_f(n'))F(t + (n_t(n') - 1)T)] dt. \end{aligned} \quad (2.119)$$

We define the relative time distance between the data symbol specific transmit signatures $\underline{\mathbf{c}}_n(t)$ and $\underline{\mathbf{c}}_{n'}(t)$ as

$$\Delta_t(n, n') = n_t(n) - n_t(n') \quad (2.120)$$

and equivalently the relative frequency distance as

$$\Delta_f(n, n') = n_f(n) - n_f(n'). \quad (2.121)$$

By substituting (2.120) and (2.121) in (2.119) we obtain

$$\begin{aligned} \underline{\mathbf{A}}_{n,n'} = & \exp[-j2\pi\Delta_f(n, n')FT(n_t(n') - 1)] \cdot \\ & \cdot \int_{-\infty}^{+\infty} \underline{\mathbf{c}}_0(t)\underline{\mathbf{c}}_0[t - \Delta_t(n, n')T] \exp[-j2\pi\Delta_f(n, n')Ft] dt. \end{aligned} \quad (2.122)$$

We notice that each element $\underline{\mathbf{A}}_{n,n'}$ of the system matrix $\underline{\mathbf{A}}$ of (2.14) consists of a phase factor $\exp[-j2\pi\Delta_f(n, n')FT(n_t(n') - 1)]$ multiplied by an integral, cf. (2.122). For a given T , F and $\underline{\mathbf{c}}_0(t)$, the phase factor depends on the relative frequency separation $\Delta_f(n, n')$ of (2.121) and on the time index $n_t(n')$ of (2.33). The integral depends only on the relative time separation $\Delta_t(n, n')$ and frequency separation $\Delta_f(n, n')$, cf. (2.120) and (2.121). Therefore, we can define a highly symmetric and block structured matrix $\hat{\underline{\mathbf{A}}}$ with elements

$$\hat{\underline{\mathbf{A}}}_{n,n'} = \int_{-\infty}^{+\infty} \underline{\mathbf{c}}_0(t)\underline{\mathbf{c}}_0[t - \Delta_t(n, n')T] \exp[-j2\pi\Delta_f(n, n')Ft] dt, \quad (2.123)$$

which depend only on $\Delta_t(n, n')$ and $\Delta_f(n, n')$. From (2.33), (2.120) and (2.121), we can derive the values assumed by $\Delta_t(n, n')$ and $\Delta_f(n, n')$ for each n, n' . Hence, the $N \times N$ matrix of the relative time separation $\underline{\mathbf{\Delta}}_t$ with elements $\Delta_t(n, n')$ reads

$$\underline{\mathbf{\Delta}}_t = \left(\begin{array}{ccc|ccc|ccc} 0 & \dots & 0 & -1 & \dots & -1 & & -N_t + 1 & \dots & -N_t + 1 \\ \vdots & \ddots & \vdots & \vdots & \ddots & \vdots & \dots & \vdots & \ddots & \vdots \\ 0 & \dots & 0 & -1 & \dots & -1 & & -N_t + 1 & \dots & -N_t + 1 \\ \hline 1 & \dots & 1 & 0 & \dots & 0 & & & & \\ \vdots & \ddots & \vdots & \vdots & \ddots & \vdots & \dots & & \vdots & \\ 1 & \dots & 1 & 0 & \dots & 0 & & & & \\ \hline & \vdots & & & & & \ddots & & \vdots & \\ \hline N_t - 1 & \dots & N_t - 1 & & & & & 0 & \dots & 0 \\ \vdots & \ddots & \vdots & & \dots & & \dots & \vdots & \ddots & \vdots \\ N_t - 1 & \dots & N_t - 1 & & & & & 0 & \dots & 0 \end{array} \right) \quad (2.124)$$

We have organized the matrix $\underline{\mathbf{\Delta}}_t$ in $N_t \times N_t$ sub-matrices with dimension $N_f \times N_f$. In this way its block Toeplitz structure becomes evident. Each sub-matrix has all elements assuming the same value.

Similarly, we can write the $N \times N$ matrix of the relative frequency separation Δ_f which reads

$$\Delta_f = \left(\begin{array}{cccc|cccc|c} 0 & -1 & \dots & -N_f + 1 & 0 & -1 & \dots & -N_f + 1 & \\ 1 & 0 & \dots & -N_f + 2 & 1 & 0 & \dots & -N_f + 2 & \\ \vdots & \ddots & \vdots & \vdots & \vdots & \ddots & \vdots & \vdots & \dots \\ N_f - 1 & N_f - 2 & \dots & 0 & N_f - 1 & N_f - 2 & \dots & 0 & \\ \hline & & & \vdots & \ddots & & & & \dots \\ 0 & -1 & \dots & -N_f + 1 & 0 & -1 & \dots & -N_f + 1 & \\ 1 & 0 & \dots & -N_f + 2 & 1 & 0 & \dots & -N_f + 2 & \\ \vdots & \ddots & \vdots & \vdots & \vdots & \ddots & \vdots & \vdots & \dots \\ N_f - 1 & N_f - 2 & \dots & 0 & N_f - 1 & N_f - 2 & \dots & 0 & \end{array} \right) \quad (2.125)$$

The matrix Δ_f also consists of $N_t \times N_t$ sub-matrices with dimension $N_f \times N_f$. In this case the sub-matrices are Toeplitz, i.e. their elements are a function of the difference between the row index and the column index, and equal.

From (2.123), (2.124) and (2.125) we can infer the inner structure of the matrix $\hat{\underline{\mathbf{A}}}$ of (2.123). We consider the matrix $\hat{\underline{\mathbf{A}}}$ of (2.123) organized in sub-matrices $\hat{\underline{\mathbf{A}}}_{\text{sub}}^{(n_t, n'_t)}$, $n_t = 1 \dots N_t$, $n'_t = 1 \dots N_t$ of dimension $N_f \times N_f$. Each element of a sub-matrix experiences the same relative time separation $\Delta_t(n, n')$. Then, the matrix $\hat{\underline{\mathbf{A}}}$ can be re-written as

$$\hat{\underline{\mathbf{A}}} = \begin{pmatrix} \hat{\underline{\mathbf{A}}}_{\text{sub}}^{(1,1)} & \hat{\underline{\mathbf{A}}}_{\text{sub}}^{(1,2)} & \dots & \hat{\underline{\mathbf{A}}}_{\text{sub}}^{(1,N_t)} \\ \hat{\underline{\mathbf{A}}}_{\text{sub}}^{(2,1)} & \hat{\underline{\mathbf{A}}}_{\text{sub}}^{(2,2)} & \dots & \hat{\underline{\mathbf{A}}}_{\text{sub}}^{(2,N_t-1)} \\ \vdots & \vdots & \ddots & \vdots \\ \hat{\underline{\mathbf{A}}}_{\text{sub}}^{(N_t,1)} & \dots & \hat{\underline{\mathbf{A}}}_{\text{sub}}^{(N_t,N_t-1)} & \hat{\underline{\mathbf{A}}}_{\text{sub}}^{(N_t,N_t)} \end{pmatrix}. \quad (2.126)$$

Let us now focus on a single sub-matrix $\hat{\underline{\mathbf{A}}}_{\text{sub}}^{(n_t, n'_t)}$ with elements $\hat{\underline{\mathbf{A}}}_{\text{sub}}^{(n_t, n'_t)}(n_f, n'_f)$, $n_f = 1 \dots N_f$, $n'_f = 1 \dots N_f$, in which all elements experience the same relative time shift. For a given $\Delta_t(n, n')$ we define

$$\hat{\underline{\mathbf{c}}}_{0, \Delta_t}(t) = \underline{\mathbf{c}}_0(t) \underline{\mathbf{c}}_0(t - \Delta_t(n, n')T) \quad (2.127)$$

and its Fourier transform

$$\hat{\underline{\mathbf{C}}}_{0, \Delta_t}(f) = \int_{-\infty}^{+\infty} \hat{\underline{\mathbf{c}}}_{0, \Delta_t}(t) \exp[-j2\pi ft] dt. \quad (2.128)$$

We then notice that the integral of (2.123) can be read as the Fourier transform $\hat{\underline{\mathbf{C}}}_{0, \Delta_t}(f)$ of (2.128) evaluated at the frequencies $f = \Delta_f(n, n')F$. Moreover, if the basic transmit signature $\underline{\mathbf{c}}_0(t)$ is real, $\hat{\underline{\mathbf{c}}}_{0, \Delta_t}(t)$ is real too and its Fourier transform becomes Hermitian symmetric, i.e. $\hat{\underline{\mathbf{C}}}_{0, \Delta_t}(f) = \hat{\underline{\mathbf{C}}}_{0, \Delta_t}^*(-f)$ [Car96]. As a consequence, each sub-matrix $\hat{\underline{\mathbf{A}}}_{\text{sub}}^{(n_t, n'_t)}$ is not only Toeplitz, but also Hermitian, i.e. $\hat{\underline{\mathbf{A}}}_{\text{sub}}^{(n_t, n'_t)} = \hat{\underline{\mathbf{A}}}_{\text{sub}}^{(n'_t, n_t)H}$, and its elements are

determined by, cf. (2.128),

$$\hat{\underline{\mathbf{A}}}_{\text{sub}}^{(n_t, n'_t)}(n_f, n'_f) = \hat{\underline{\mathbf{C}}}_{0, \Delta_t}(f) \Big|_{f=(n_f - n'_f)F}. \quad (2.129)$$

(2.129) is particularly useful for calculation purposes since all the elements of a sub-matrix $\hat{\underline{\mathbf{A}}}_{\text{sub}}^{(n_t, n'_t)}$ are obtained through the sampling of a Fourier transform.

We have determined the structure of each sub-matrix $\hat{\underline{\mathbf{A}}}_{\text{sub}}^{(n_t, n'_t)}$. The difference among the sub-matrices is only given by the different relative time separation. As a consequence, the matrix $\hat{\underline{\mathbf{A}}}$ is block Toeplitz. Another characteristic of the matrix $\hat{\underline{\mathbf{A}}}$ can be derived from (2.123) under the common assumption that $\underline{c}_0(t) = \underline{c}_0(-t)$. From (2.127) we notice that the inversion of the time axis in $\hat{\underline{c}}_{0, \Delta_t}(t)$ is equivalent to considering a relative time separation Δ_t with opposite sign. In the Fourier transform domain, the inversion of the time axis is equivalent to the inversion of the frequency axis in the frequency domain. Moreover, the Fourier transform is Hermitian symmetric, and considering the inversion of the frequency axis is equivalent to take the complex conjugate. By recalling that the elements of the sub-matrices are given by the samples of the Fourier transform, cf. (2.128) and (2.129), we infer that the sub-matrices with relative time distances with opposite sign are one the complex conjugate of the other, i.e. $\hat{\underline{\mathbf{A}}}_{\text{sub}}^{(n_t, n'_t)} = \hat{\underline{\mathbf{A}}}_{\text{sub}}^{(n_t, n'_t)*}$. Therefore, the matrix $\hat{\underline{\mathbf{A}}}$ is not only block Toeplitz, but the blocks in opposite position with respect to the main block diagonal are the complex conjugate of each other. We can define this matrix as block Toeplitz and block-conjugate.

Taking into account the overall symmetries of the matrix $\hat{\underline{\mathbf{A}}}$, many sub-matrices $\hat{\underline{\mathbf{A}}}_{\text{sub}}^{(n_t, n'_t)}$ of $\hat{\underline{\mathbf{A}}}$ of (2.126) are equal or related to each other. There are only N_t different sub-matrices that we indicate with $\hat{\underline{\mathbf{A}}}_{\text{sub}}^{(n'_t)}$. The overall structure reads as

$$\hat{\underline{\mathbf{A}}} = \begin{pmatrix} \hat{\underline{\mathbf{A}}}_{\text{sub}}^{(1)} & \hat{\underline{\mathbf{A}}}_{\text{sub}}^{(2)} & \cdots & \hat{\underline{\mathbf{A}}}_{\text{sub}}^{(N_t)} \\ \hat{\underline{\mathbf{A}}}_{\text{sub}}^{(2)*} & \hat{\underline{\mathbf{A}}}_{\text{sub}}^{(1)} & \cdots & \hat{\underline{\mathbf{A}}}_{\text{sub}}^{(N_t-1)} \\ \vdots & \vdots & \ddots & \vdots \\ \hat{\underline{\mathbf{A}}}_{\text{sub}}^{(N_t)*} & \hat{\underline{\mathbf{A}}}_{\text{sub}}^{(N_t-1)*} & \cdots & \hat{\underline{\mathbf{A}}}_{\text{sub}}^{(1)} \end{pmatrix}, \quad (2.130)$$

with each sub-matrix $\hat{\underline{\mathbf{A}}}_{\text{sub}}^{(n'_t)}$ being Toeplitz and Hermitian. From (2.129) and (2.130) and by adding the phase factor of (2.122) we determine the system matrix $\underline{\mathbf{A}}$ avoiding redundant calculation, thus reducing the computational complexity required by the post-processing stage.

From Subsection 2.4.4, the relation between SC, MC and HY systems lets us derive the structure of the system matrix $\underline{\mathbf{A}}$ for the SC and MC systems starting from the more general structure obtained for a HY system. In particular, for both SC and MC systems the phase factor in (2.122) is equal to one. In the SC systems this is true because the

term $\Delta_f(n, n')$ is always zero, in the MC systems because the term $n_t(n')$ is always equal to one. Therefore, we can focus on (2.123) and consider one system at the time.

In SC systems there is no frequency separation. Under the assumptions of a real and symmetric basic transmit signature $\underline{c}_0(t)$, the integral in (2.123) has no exponential factor and it always returns a real value. The matrix structure can be derived by setting $N_f = 1$ and repeating the reasoning made from (2.123) to (2.130). The result is a system matrix $\underline{\mathbf{A}}$ as in (2.130), where the sub-matrices $\hat{\underline{\mathbf{A}}}_{\text{sub}}^{(n'_t)}$ have only a single real element, i.e. they are numbers, not matrices. The overall system matrix $\hat{\underline{\mathbf{A}}}$ in the SC case is therefore real and symmetric.

In MC systems there is no time separation. Therefore, the system matrix $\underline{\mathbf{A}}$ has the same structure as a single sub-matrix $\hat{\underline{\mathbf{A}}}_{\text{sub}}^{(n'_t)}$. It is no longer real because the integral of (2.123) can extend over a not integer number of sinusoidal sections. Its elements are given by the samples of the Fourier transform as in (2.129). The system matrix $\underline{\mathbf{A}}$ of MC systems is complex and Hermitian.

2.7.3 Channel impact on the system matrix $\underline{\mathbf{A}}$

By considering the presence of the channel, cf. Subsection 2.2.3, the data symbol receive signatures $\underline{c}_{r,n}(t)$ of (2.3) are not equal to the data symbol specific transmit signature $\underline{c}_n(t)$ and (2.118) does not hold true. We can proceed by considering the SC, MC and HY systems separately.

By considering SC systems, cf. Subsection 2.4.2 and (2.24), and by recalling the properties of the convolution as well as (2.3), we infer that the presence of the channel does not preclude the derivation of the structure of the system matrix $\underline{\mathbf{A}}$ of (2.14). As a matter of fact, if we define the basic receive signature $\underline{c}_{r,0}(t)$, cf. (2.3) and (2.24), as

$$\underline{c}_{r,0}(t) = \int_{-\infty}^{+\infty} \underline{c}_0(t - \tau) \underline{h}(\tau, t) d\tau, \quad (2.131)$$

then, due to the linearity of the convolution operation, we can derive that for the SC systems the data symbol specific receive signatures $\underline{c}_{r,n}(t)$ read

$$\underline{c}_{r,n}(t) = \underline{c}_{r,0}[t - (n - 1)T]. \quad (2.132)$$

Therefore, the reasoning of the previous subsection is still valid; it is only required to consider the data symbol specific receive signature $\underline{c}_{r,n}(t)$ of (2.132) instead of the data symbol specific transmit signature $\underline{c}_n(t)$. In particular, the overall system matrix $\underline{\mathbf{A}}$ of (2.14) in the SC case and in the presence of the channel is a complex Hermitian matrix.

In MC and HY systems the presence of the channel can be modelled as in conventional OFDM systems, cf. Section 2.5. We shall assume that the number of sub-carriers in MC and HY systems is large enough so that each sub-carrier experiences a flat fading channel. Under this assumption, we can model the channel experienced by each sub-carrier as in Subsection 2.5.2, and the data symbol specific receive signature $\underline{c}_{r,n}(t)$ reads

$$\underline{c}_{r,n}(t) = \underline{H}_n \underline{c}_n(t), \quad (2.133)$$

for the MC systems, and

$$\underline{c}_{r,n}(t) = \underline{H}_{n_f(n)} \underline{c}_n(t), \quad (2.134)$$

for the HY systems. The channel selected by the data symbol specific transmit signature $\underline{c}_n(t)$ is described by a constant complex factor; therefore, the elements of the system matrix $\underline{\mathbf{A}}$ read, cf. (2.118),

$$\begin{aligned} \underline{A}_{n,n'} = & \underline{H}_{n_f(n)}^* \underline{H}_{n_f(n')} \int_{-\infty}^{+\infty} \underline{c}_0 [t' - (n_t(n') - 1)T] \exp [j2\pi(n_f(n') - 1)Ft'] \cdot \\ & \cdot \underline{c}_0 [t' - (n_t(n) - 1)T] \exp [-j2\pi(n_f(n) - 1)Ft'] dt'. \end{aligned} \quad (2.135)$$

By comparing (2.135) and (2.118) it is apparent that the derivation of Subsection 2.8.2 can be extended to the case of including the channel. Moreover, the properties of the system matrix $\underline{\mathbf{A}}$ of (2.14) for MC systems remain the same, i.e. it is complex and Hermitian. In HY systems, the properties of the sub-matrix $\hat{\underline{\mathbf{A}}}_{\text{sub}}^{(n'_t)}$ remain unchanged as well.

The channel can be included in the derivation of the structure of the system matrix $\underline{\mathbf{A}}$ of MC and HY systems only if (2.133) and (2.134) hold true, respectively. Therefore, (2.135) represents an approximation and it is valid only if the time duration T_0 of the data symbol specific transmit signatures $\underline{c}_n(t)$ is much larger than the maximum excess delay τ_{max} of the channel, cf. Subsection 2.6.6.

2.8 Special setting of the model

2.8.1 General

The modelling proposed in Section 2.2 and 2.3 is valid for many different system configurations at the cost of slight modifications. Until now, the model has been developed for a point to point scenario, in which the data vector $\underline{\mathbf{d}}$ of (2.1) and the received data vector $\underline{\mathbf{d}}_{\text{MF}}$ of (2.7) belong to a single user. The model can be extended to consider a point to multi-point scenario and a multi-point to point scenario. In both cases, we assume the presence of K users in the system, each transmitting the same number N_K of complex data symbols $\underline{d}_n^{(k)}$, $n = 1 \dots N_K$, $k = 1 \dots K$. We then define the user data vectors, cf. (2.1), as

$$\underline{\mathbf{d}}^{(k)} = \left(\underline{d}_1^{(k)} \dots \underline{d}_{N_K}^{(k)} \right)^T. \quad (2.136)$$

The concatenation of the K user data vectors of (2.136) gives the multi-user data vector

$$\underline{\mathbf{d}}^{(\text{MU})} = \left(\underline{\mathbf{d}}^{(1)\text{T}} \ \dots \ \underline{\mathbf{d}}^{(K)\text{T}} \right)^{\text{T}}. \quad (2.137)$$

In the Subsections 2.8.2 to 2.8.3, we describe the point to multi-point and the multi-point to point scenario, respectively, framing them within the modelling proposed in Section 2.2 to 2.3.

2.8.2 Point to multi-point

Fig. 2.5 represents the point to multi-point scenario. A single transmitter broadcasts a

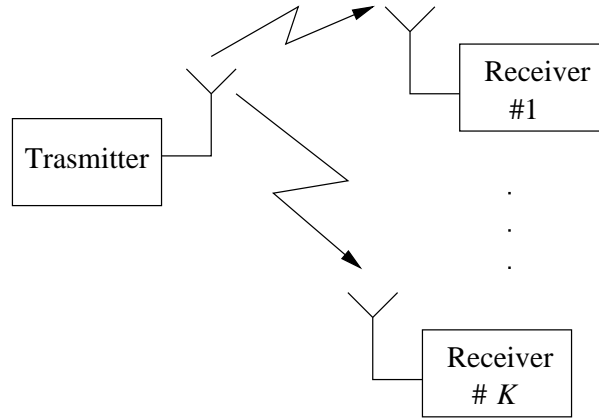


Fig. 2.5. Point to multi-point scenario.

signal $\underline{\mathbf{s}}(t)$ made up by the data addressed to all K users. Each user k , $k = 1 \dots K$ usually receives also the data belonging to other users. From the receiver point of view, the signals addressed to all the users are affected by the same channel. This scenario describes the typical down-link (DL) transmission of a cellular system in which the base station is the transmitter and the mobile terminals are the K receivers.

To take into account this scenario, we assume that each user complex data symbol $\underline{d}_n^{(k)}$ of (2.136) of user k , $k = 1 \dots K$ is associated to a data symbol specific transmit signature $\underline{c}_n^{(k)}(t)$ of user k . Then, we define the transmitted signal conveying the user complex data symbols $\underline{d}_n^{(k)}$ of (2.136) of user k , $k = 1 \dots K$ as, cf. (2.2) and (2.136),

$$\underline{\mathbf{s}}^{(k)}(t) = \sum_{n=1}^{N_K} \underline{d}_n^{(k)} \underline{c}_n^{(k)}(t). \quad (2.138)$$

Then, we define the data symbol specific receive signature of user k as

$$\underline{c}_{r,n}^{(k)}(t) = \int_{-\infty}^{+\infty} \underline{c}_n^{(k)}(t - \tau) \underline{h}(\tau, t) d\tau, \quad (2.139)$$

and the useful signal of user k at the input of the Rx as in (2.4)

$$\underline{e}^{(k)}(t) = \int_{-\infty}^{+\infty} \underline{s}^{(k)}(t-\tau) \underline{h}(\tau, t) d\tau = \sum_{n=1}^{N_K} \underline{d}_n^{(k)} \underline{c}_{r,n}^{(k)}(t). \quad (2.140)$$

The useful signals of the K users are superimposed at the receiver antenna and corrupted by AWGN, cf. Subsection 2.2.4, so that the signal to be processed by the receiver reads as, cf. (2.5),

$$\underline{r}(t) = \sum_{k=1}^K \underline{e}^{(k)}(t) + \underline{n}(t) = \sum_{k=1}^K \sum_{n=1}^{N_K} \underline{d}_n^{(k)} \underline{c}_{r,n}^{(k)}(t) + \underline{n}(t). \quad (2.141)$$

The receive signal $\underline{r}(t)$ is then filtered by the bank of filters matched to the data symbol specific receive signatures of user k , $\underline{c}_{r,n}^{(k)}(t)$. As in (2.10) the noise is coloured by the receive MFs, but it is user dependant and reads as

$$\underline{n}_{\text{MF},n}^{(k)} = \int_{-\infty}^{+\infty} \underline{n}(\tau) \underline{c}_{r,n}^{(k)*}(\tau) d\tau. \quad (2.142)$$

(2.142) can be arranged in the noise vector of user k

$$\underline{\mathbf{n}}_{\text{MF}}^{(k)} = \left(\underline{n}_{\text{MF},1}^{(k)} \cdots \underline{n}_{\text{MF},N_K}^{(k)} \right)^{\text{T}}, \quad (2.143)$$

which, by considering all the users, gives the multi-user noise vector

$$\underline{\mathbf{n}}_{\text{MF}}^{(\text{MU})} = \left(\underline{\mathbf{n}}_{\text{MF}}^{(1)\text{T}} \cdots \underline{\mathbf{n}}_{\text{MF}}^{(K)\text{T}} \right)^{\text{T}}. \quad (2.144)$$

We can write the contribution of the transmitted symbol $\underline{d}_{n'}^{(k')}$, $n' = 1 \dots N_K$, of user k' , $k' = 1 \dots K$ on the received symbol $\hat{\underline{d}}_{\text{MF},n}^{(k)}$ of user k as, cf. (2.9),

$$\underline{d}_{n'}^{(k')} \int_{-\infty}^{+\infty} \underline{c}_{r,n'}^{(k')}(\tau) \underline{c}_{r,n}^{(k)*}(\tau) d\tau,$$

to derive the MF estimate $\hat{\underline{d}}_{\text{MF},n}^{(k)}$ of user k as

$$\hat{\underline{d}}_{\text{MF},n}^{(k)} = \sum_{k'=1}^K \sum_{n'=1}^{N_K} \underline{d}_{n'}^{(k')} \int_{-\infty}^{+\infty} \underline{c}_{r,n'}^{(k')}(\tau) \underline{c}_{r,n}^{(k)*}(\tau) d\tau + \underline{n}_{\text{MF},n}^{(k)}. \quad (2.145)$$

The MF estimate of user k can be arranged in a vector, cf. (2.7),

$$\hat{\underline{\mathbf{d}}}_{\text{MF}}^{(k)} = \left(\hat{\underline{d}}_{\text{MF},1}^{(k)} \cdots \hat{\underline{d}}_{\text{MF},N_K}^{(k)} \right)^{\text{T}}, \quad (2.146)$$

which can be used to write the multi-user MF estimate as

$$\hat{\underline{\mathbf{d}}}_{\text{MF}}^{(\text{MU})} = \left(\hat{\underline{\mathbf{d}}}_{\text{MF}}^{(1)\text{T}} \cdots \hat{\underline{\mathbf{d}}}_{\text{MF}}^{(K)\text{T}} \right)^{\text{T}}. \quad (2.147)$$

We can now introduce the correlation coefficients similar to (2.12), but user dependent

$$\underline{A}_{n,n'}^{(k,k')} = \int_{-\infty}^{+\infty} \underline{c}_{r,n'}^{(k')}(t) \underline{c}_{r,n}^{(k)*}(t) dt, \quad (2.148)$$

to form the $N_K \times N_K$ matrix from user k' to user k

$$\underline{\mathbf{A}}^{(k,k')} = \begin{pmatrix} \underline{A}_{1,1}^{(k,k')} & \cdots & \underline{A}_{1,N}^{(k,k')} \\ \vdots & \ddots & \vdots \\ \underline{A}_{N,1}^{(k,k')} & \cdots & \underline{A}_{N,N}^{(k,k')} \end{pmatrix}. \quad (2.149)$$

$\underline{\mathbf{A}}^{(k,k')}$ of (2.149) expresses the linear transformation between the symbol data vector $\underline{\mathbf{d}}^{(k')}$ of user k' , $k' = 1 \dots K$ and the matched filter estimate vector $\hat{\underline{\mathbf{d}}}_{\text{MF}}^{(k)}$ of user k , $k = 1 \dots K$. To consider the effect of the interference generated by the presence of many users, we introduce the matrix $\underline{\mathbf{A}}^{(k)}$ of user k , as the concatenation of the matrixes defined in (2.149) with $k' = 1 \dots K$. The resulting matrix of user k reads as

$$\underline{\mathbf{A}}^{(k)} = (\underline{\mathbf{A}}^{(k,1)} \quad \dots \quad \underline{\mathbf{A}}^{(k,K)}). \quad (2.150)$$

From (2.150), (2.146) and (2.137) we can write the raw data estimate of (2.146) as

$$\hat{\underline{\mathbf{d}}}_{\text{MF}}^{(k)} = \underline{\mathbf{A}}^{(k)} \underline{\mathbf{d}}^{(\text{MU})} + \underline{\mathbf{n}}_{\text{MF}}^{(k)}. \quad (2.151)$$

(2.151) represents the linear transformation between the multi-user data vector $\underline{\mathbf{d}}^{(\text{MU})}$ and the raw data vector $\hat{\underline{\mathbf{d}}}_{\text{MF}}^{(k)}$ of user k . We can consider the system as a whole by introducing the multi-user matrix $\underline{\mathbf{A}}^{(\text{MU})}$ as

$$\underline{\mathbf{A}}^{(\text{MU})} = (\underline{\mathbf{A}}^{(1)} \quad \dots \quad \underline{\mathbf{A}}^{(K)})^T \quad (2.152)$$

and by writing the multi-user raw data estimate of (2.145) as

$$\hat{\underline{\mathbf{d}}}_{\text{MF}}^{(\text{MU})} = \underline{\mathbf{A}}^{(\text{MU})} \underline{\mathbf{d}}^{(\text{MU})} + \underline{\mathbf{n}}_{\text{MF}}^{(\text{MU})}. \quad (2.153)$$

By framing a multi-user scenario in the developed system model, we show its generality. In particular, (2.153) has the same structure as (2.15) which implies that the measures proposed to evaluate the system performance are valid also in the multi-user scenario. The main difference is given by the nature of the distortion in the receive data symbols and by the inner structure of the system matrix. As a matter of fact, the system matrix $\underline{\mathbf{A}}^{(\text{MU})}$ in the multi-user case can be read in a block-wise fashion to recognize the multi-user interference (MUI), the ISI or the ICI.

Another important aspect regards the considered multiple access method. In the proposed modelling, each user has its own set of data symbol specific transmit signatures $\underline{c}_n^{(k)}(t)$. Hence, the model consists in a signature division multiple access (SIDMA). Depending on the characteristics of the signatures $\underline{c}_n^{(k)}(t)$ assigned to each user, different multiple access schemes can be taken into account such as time division multiple access (TDMA), frequency division multiple access (FDMA), code division multiple access (CDMA) [Kle96] or any combination of these three.

2.8.3 Multi-point to point

From Subsection 2.8.2, it is now straightforward to extend the proposed modelling to a multi-point to point scenario. As shown in Fig. 2.6, in this scenario K transmitters aim to communicate with the same receiver. The scenario describes the typical up-link (UL)

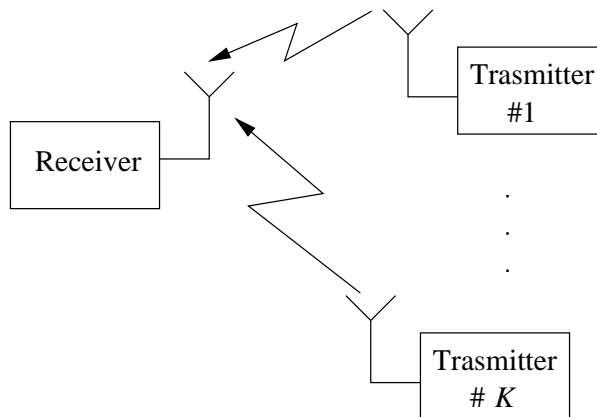


Fig. 2.6. Multi-point to point scenario.

of a cellular system, in which K mobile terminals, i.e. the K transmitters, communicate with a single base station, i.e. the single receiver of Fig. 2.6.

As compared with the point to multi-point scenario of Subsection 2.8.2, now the single receiver sees the signal transmitted by the single users $\underline{s}^{(k)}(t)$ corrupted by the channel that goes from each user to the receiver. This difference affects the derivation of Subsection 2.8.2 only within (2.140) which now reads as

$$\underline{e}^{(k)}(t) = \int_{-\infty}^{+\infty} \underline{s}^{(k)}(t - \tau) \underline{h}^{(k)}(\tau, t) d\tau = \sum_{n=1}^{N_K} \underline{d}_n^{(k)} \underline{c}_{r,n}^{(k)}(t). \quad (2.154)$$

The symbol specific receive signature of user k , $\underline{c}_{r,n}^{(k)}(t)$ depends also on the particular channel experienced by the user k . The rest of the derivation follows Subsection 2.8.2, (2.141) to (2.153).

3 Considered system implementations

3.1 General

In this chapter, we propose the scope of parameters to be chosen when investigating the dependency between the rate R of (2.57) and the SNR-degradation δ of (2.68) and (2.76), respectively. To this end, in Section 3.2 we introduce our vision of 4G system requirements and frame the work of the thesis as a contribution to the development of future mobile radio systems. We recognize conventional OFDM [RGG01], cf. Chapter 1, as the leading candidate for the radio interface of 4G systems and, from the expected channel characteristics, we define the values of the time separation T and the frequency separation F in conventional OFDM systems. We propose a reasonable frame structure and show the relationship between the transmission model of Chapter 2 and a more detailed scheme of a point-to-point transmission system. We determine the values of the SNR-degradation δ of (2.67) and of the rate R of (2.57) in conventional OFDM systems and introduce the relationship between the reference time separation T_{ref} and the reference frequency separation F_{ref} . The role of T_{ref} and F_{ref} is strictly related to the goal of the thesis presented in Section 1.2. As a matter of fact, the main focus of the thesis can be interpreted as the investigation of the effects of choosing $T < T_{\text{ref}}$ and/or $F < F_{\text{ref}}$ on the rate R of (2.57) and on the SNR-degradation δ of (2.68) and (2.76). In Section 3.3, the parameters involved in the system design are organized in two classes. The fixed parameters include the basic transmit signature $\underline{c}_0(t)$ and the relative time-frequency location of consecutive data symbol specific transmit signatures $\underline{c}_n(t)$ of (2.28). The variable parameters include the time separation T and the frequency separation F . Then, we present the set of basic transmit signatures $\underline{c}_0(t)$ considered within this thesis. Among them, we include a $\underline{c}_0(t)$ with a Gaussian shape so that we can derive the elements of the system matrix $\underline{\mathbf{A}}$ of (2.14) in a closed form. Finally, in Section 3.4, we derive an approximation of the Shannon channel capacity formula [Sha48] to explicitly show its dependency on the rate R of (2.57) and the SNR-degradation δ of (2.68) and (2.76). Based in the modified channel capacity we will determine the potential of the proposed method of increasing the rate R of (2.57) at the cost of an increment in SNR-degradation δ .

3.2 Reference system

3.2.1 General

The path to 4G systems, cf. Chapter 1, started around the years 2000/2001 [FaK01, RGG01], when 3G systems were not even at the commercial stage. In 2004, the first 3G

terminals can be found in the European market, but with a significant delay with respect to the expected roll-out time [FaK01]. Nevertheless, telecommunication manufacturers are investing on research towards 4G since the user service requirements will soon increase beyond the capability of 3G systems.

The potential user of a 4G system is expected to ask for an ubiquitous and transparent system, which ensures a global roaming with a coverage at least as complete as that offered by 3G systems with some additional services. The 4G user would require mobility up to 500 km/h and a location service achieved, for instance, through the current global positioning system (GPS) or the European Galileo system [HGI02]. The services offered by next generation systems shall be more sophisticated than the ones advertised for 3G systems. Security and quality of service (QoS) configurability shall be guaranteed. For instance, if the user wanted to watch a movie, he would be able to choose among different quality formats with different prices and characteristics. With the increasing of the offered services, the user terminals are expected to include not only cellular/video phones but also laptops and PDAs. Hence, many user terminals are expected to be proposed in the market with different functionalities, prices, sizes and performance. For all of them, the battery consumption will be a key parameter so that the designer should carefully take into account the power required by the different terminal components. From a more engineering perspective, 4G systems shall basically support a higher data rate with flexible and controllable QoS parameters such as the overall delay or the peak data rate. Depending on the actual service, the system shall be able to fulfil the necessary constraints. For instance, a voice data stream might require a low data rate of 16 kbit/s but with a delay less than 100 ms, while a very high quality multimedia service might require up to 100 Mbit/s with a much less stringent delay requirement. The flexibility shall also concern the system design, taking into account the importance of backward compatibility and coexistence with 3G systems already present in the territory. The backward compatibility is an issue coming also from a more economical requirement of the telecommunication providers. As compared to 3G systems, 4G systems give more importance to the costs of the infrastructure and of the mobile terminals, looking for cheap and reliable communications. The system developers shall also take into account the issues related to the coexistence of many operators and of different communication systems which should be all included in the modelling/vision/concept of 4G systems. Among the included systems, we shall consider almost all the technology available at the present day.

In this thesis, we are focused on the physical layer design and on the implications of our vision of 4G systems on this are many. The most significant is the dimension of the bandwidth which is expected to be around 100 MHz to support peak data rate as high as 1 Gbit/s in downlink applications, e.g. for movies download. The goal of the physical layer design is to develop a radio interface capable of supporting such high data rate under the constraints of low cost and low complexity devices. Actually, the complexity can be assumed higher than that required by 3G devices because we expect an improvement

in terms of chip performance. Nevertheless, the complexity is bounded especially by the power constraints needed to ensure a longer battery life. In the UL communications, from the single user to the network, a lower data rate can be assumed. Therefore, the implications of asymmetric DL and UL capacity requirements should be taken into account in the choice of the duplex scheme [Pro95], i.e. time division duplex (TDD) and frequency division duplex (FDD). Realistically, pure FDD is not very attractive, because it requires higher costs and power consumption due to the presence of two separated analog radio frequency interfaces. TDD or probably a combination of TDD with FDD is more likely to be chosen. The asymmetric data rate requirements would justify the TDD component to avoid the use of a sophisticated radio interface to transmit low data rate streams.

The most promising candidate, cf. Chapter 1, for DL transmission in 4G systems is OFDM deployed over an available bandwidth of 100 MHz. For UL applications, OFDM is again the leading candidate but limited to hot spot scenarios where mobility is very low and a very high data rate is required. For UL applications with wide area coverage, the discussion is still open. Based on the different capacity requirements, a bandwidth of 20 MHz or 40 MHz is expected for the UL, which is lower than the 100 MHz required for the DL. Nevertheless, also in this scenario OFDM is a possible modulation scheme.

Our work contributes to the proposal of a candidate for 4G radio interface in an UL scenario. We choose a conventional OFDM system designed for the UL as a reference system. Then, we consider SC, MC and HY systems as alternative solutions and investigate their potential. Among the possible terms of comparison, we define a very particular one. We exploit the flexibility of the system modelling introduced in Chapter 2 to study the trade-off between the increment of resource usage and the corresponding performance degradation in SC, MC and HY systems.

3.2.2 Parameters for 4th generation mobile radio systems

[RGG01] proposes a physical layer system design for OFDM as a candidate for 4G systems. This proposal fits well to our vision of the UL scenario of 4G systems. Therefore, we report here the setting given in [RGG01], although considering some slight modifications. The prominent parameter in the design of an OFDM system is the number N_f of sub-carriers, cf. Subsection 2.4.4. With the increasing of N_f , the energy loss factors L_n of (2.56) decreases, but the system becomes more and more sensitive to synchronization errors, especially to those due to carrier frequency misalignments or to phase noise [NeP00, RGG01]. Moreover, the PAPR, cf. Subsection 1.1.2, and the time separation T increase with N_f . If T is too long, then the channel may vary within T causing a significant loss in performance [NeP00]. A lower number N_f of sub-carriers, on the other hand, may contribute to gain in robustness with respect to frequency misalignments and to reduce the loss due to the insertion of the pilot symbols required for channel estimation

[Pro95]. However, a lower N_f generates higher energy loss factors L_n , cf. (2.116), and it implies a reduction of the time separation T . If T is too short, the channel selected by each sub-carrier might be frequency selective, thus invalidating the simple receiver scheme typical of conventional OFDM. Other constraints more related to implementation issues exist, e.g. regarding the computational complexity, the hardware requirements, the practical size of the OFDM symbol as related to the higher layer packet dimension. There are many trade-offs, and the number N_f should be carefully chosen taking into account especially the nature of the radio channel, cf. Subsection 3.3.6.

The parameters of the considered channel of conventional OFDM systems are summarized in Table 3.1 [RGG01]. The bandwidth B of 20 MHz is defined around the carrier

Table 3.1. 4G radio uplink channel parameters.

| Parameters | Value |
|----------------------|--------------------------------|
| Bandwidth | $B = 20$ MHz |
| Carrier frequency | $f_c = 5$ GHz |
| Maximum excess delay | $\tau_{\max} = 2.5\mu\text{s}$ |
| Power delay profile | exponential |

frequency f_c of 5 GHz. A maximum excess delay τ_{\max} of $2.5 \mu\text{s}$ is assumed with an exponentially decreasing power delay profile [Kan04, Rap99, RGG01]. Based on the channel parameters of Table 3.1, we propose a conventional OFDM system with $N_f = 512$ and, consequently, with a fixed sub-carrier spacing

$$F = \frac{B}{N_f} \approx 39 \text{ kHz}. \quad (3.1)$$

We note that the sub-carrier spacing has the same role as the frequency separation F as defined for HY systems in Subsection 2.4.3. From (2.43) the time separation T among consecutive symbols which includes the guard interval reads

$$T = \frac{1}{F} + \tau_{\max} = 28.1 \mu\text{s}. \quad (3.2)$$

The transmitted data vector $\underline{\mathbf{d}}$ of (2.1) contains in general not only information data symbols, but also known data such as pilot symbols and null values. The latter are transmitted on the virtual sub-carriers [NeP00] at the spectrum border. Therefore, the data vector $\underline{\mathbf{d}}$ can be referred to as frame. We propose a possible frame structure as the concatenation of $N_t = 24$ OFDM symbols so that the vector $\underline{\mathbf{d}}$ consists of $N_t N_f$ data symbols, see Fig. 3.1. At the beginning of each frame we additionally consider a pilot sequence for the purpose of time and frequency synchronization as well as channel estimation [Kan04]. The choice of $N_t = 24$ OFDM symbols is due to the scalability of

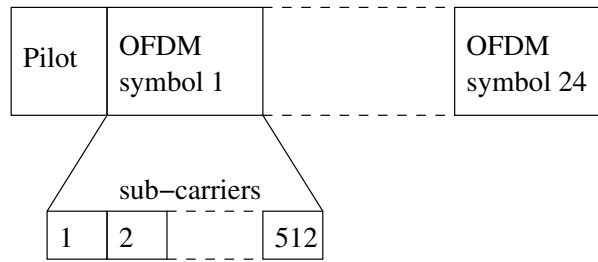


Fig. 3.1. OFDM frame structure.

the number 24 which, having different divisors, allows a higher flexibility in the resource allocation. The resulting frame is depicted in Fig. 3.1. It has a duration of

$$T_{\text{fr}} = 6.74 \text{ ms} + T_{\text{pilot}}, \quad (3.3)$$

where T_{pilot} is the duration of the pilot sequence needed for synchronization.

Under consideration of the frame structure, a block diagram of the end-to-end communication chain is depicted in Fig. 3.2. A data source generates a sequence of data bit

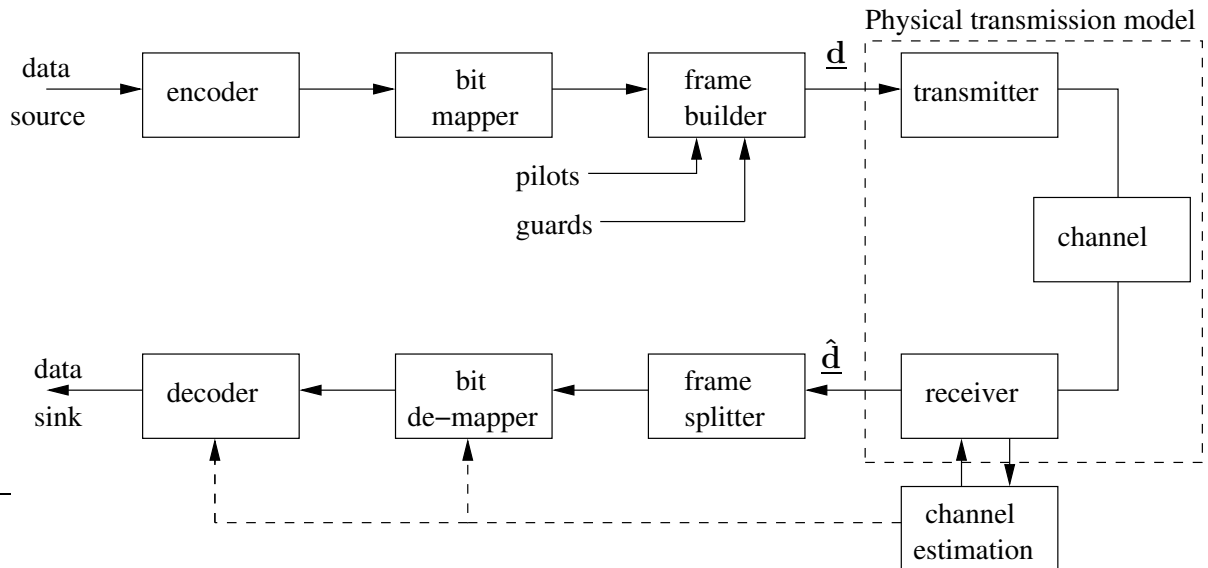


Fig. 3.2. Block structure of a point to point transmission system.

which is then encoded through a forward error correcting (FEC) encoder [Bos99, Pro95] to improve the overall system performance. Within the encoder block we also include an interleaver which scrambles the bits and whose dimension and performance are related to the specific type of the encoder and of the channel [Bos99]. The output of the encoder is a bit sequence which is mapped to a complex symbol data sequence, e.g. through an M_d -QAM bit-mapper [BeC02, Pro95]. The complex data sequence enters a frame builder which inserts the proper pilot sequences as well as the guard intervals to obtain the desired frame structure, see Fig. 3.1. The output of the frame builder is the transmitted

data symbol vector $\underline{\mathbf{d}}$ of (2.1). As shown in Fig. 3.2, the cascade of transmitter, channel and receiver matches the equivalent low-pass physical transmission model of Fig. 2.1. We have additionally included a channel estimation block that, based on the knowledge of the pilot sequence, estimates the channel impulse response or its frequency response [BPH99, Kan04, PSW99]. In the proposed modelling, cf. Chapter 2, we assume a perfect channel knowledge available at the receiver for data detection purposes. Therefore, we have omitted any consideration regarding channel estimation. The channel information is usually exploited also by the decoder and by the inverse bit-mapper in case a soft information is required, see Fig. 3.2, [Bos99].

3.2.3 OFDM over an AWGN channel

Since OFDM is the leading candidate for a 4G radio interface, cf. Subsections 1.1.1 to 1.1.2 and Subsections 3.2.1 to 3.2.2, we choose as a reference the OFDM system designed in Subsection 3.2.2 and we assume that it operates over an AWGN channel. In this case, the insertion of a guard interval is not necessary [NeP00] and the energy loss factors L_n of (2.56) are one since $\tau_{\max} = 0$. Therefore, we obtain an ideal reference HY system with a frequency separation F_{ref} and a time separation T_{ref} satisfying

$$F_{\text{ref}}T_{\text{ref}} = 1. \quad (3.4)$$

Under this assumption, the SNR-degradation δ of (2.115) is equal to one. From the definition of the basic transmit signature $\underline{c}_0(t)$ of (2.42), we determine the 3 dB duration T_0 and the 3 dB bandwidth B_0 of a rect basic transmit signature $\underline{c}_0(t)$ of (2.42) as shown in Subsection 2.6.5. T_0 can be easily expressed in closed form as

$$T_0 = T_{\text{ref}}, \quad (3.5)$$

while B_0 can be only determined through numerical approximation. It reads as

$$B_0 \approx 6/(5T_{\text{ref}}). \quad (3.6)$$

The rate R of (2.63), with T_0 of (3.5), B_0 of (3.6), $T = T_{\text{ref}}$, $F = F_{\text{ref}}$ and N_t and N_f large enough becomes

$$R \approx \frac{5N_f}{5N_f + 6} \approx 1. \quad (3.7)$$

Both the SNR-degradation δ of (2.68) and the rate R of (2.63) of the conventional OFDM do not vary because the frequency and time separation and the basic transmit signature $\underline{c}_0(t)$ are kept fixed.

For the considerations in Chapter 4 to 5 the numerical value of T_{ref} and F_{ref} of (3.4) are irrelevant. It is only required that these two quantities fulfil (3.4). Therefore, in the

rest of the thesis, we consider two arbitrary values of T_{ref} and F_{ref} under the constraint that (3.4) holds. In conventional modulation schemes [BeC02, Pro95], the time separation T and the frequency separation F are usually chosen as $T = T_{\text{ref}}$ and $F = F_{\text{ref}}$, respectively. Our main focus, cf. Subsection 1.2 and Section 3.1, is on how much we deviate the time separation T from T_{ref} and on how much we deviate the frequency separation F from F_{ref} .

With T_{ref} and F_{ref} of (3.4), in Table 3.2, we show the relationship between the main

Table 3.2. Relationship between normalized and absolute quantities.

| absolute | normalized values |
|----------|----------------------|
| f | f/F_{ref} |
| F | F/F_{ref} |
| B_0 | B_0/F_{ref} |
| t | t/T_{ref} |
| T | T/T_{ref} |
| T_0 | T_0/T_{ref} |

absolute and normalized time and frequency variables. The normalized quantities are used to report the simulation results in Chapter 4.

3.2.4 SC, MC and HY systems with equal resource consumption

In Section 2.5, we framed the proposed reference system as a particular HY system. However, we are considering different possible configurations, namely SC systems, MC systems and HY systems, cf. Subsections 2.4.2 to 2.4.4, in which the time-frequency locations of the data symbol specific transmit signatures $\underline{c}_n(t)$ of (2.2) significantly differ. If we assume that the resource consumption in terms of total transmit duration T_{tot} and total bandwidth B_{tot} are the same for all three system configurations, then we shall address how the time separation T and the frequency separation F change depending on the system configurations. In Fig. 3.3 we graphically represent the three different strategies of assignment of the available resources to the data symbol specific transmit signatures $\underline{c}_n(t)$ of (2.2). We set out a very simple configuration with $N = 8$ transmitted data symbols \underline{d}_n of $\underline{\mathbf{d}}$ of (2.1). In the HY systems of Fig. 3.3c, $N = 8$ is expressed as $N = N_t N_f$ with $N_t = 2$ and $N_f = 4$. Fig. 3.3 is similar to Fig. 2.3, but now, through the definition of the total bandwidth B_{tot} in (2.26), (2.30) and (2.36) and the total transmit duration T_{tot} in (2.27), (2.31) and (2.37) and under the assumption of the same B_{tot} and T_{tot} for the three system configurations, the relation between the parameters is specified. In SC systems of Fig. 3.3a, each data symbol specific signature $\underline{c}_n(t)$ of (2.24) occupies

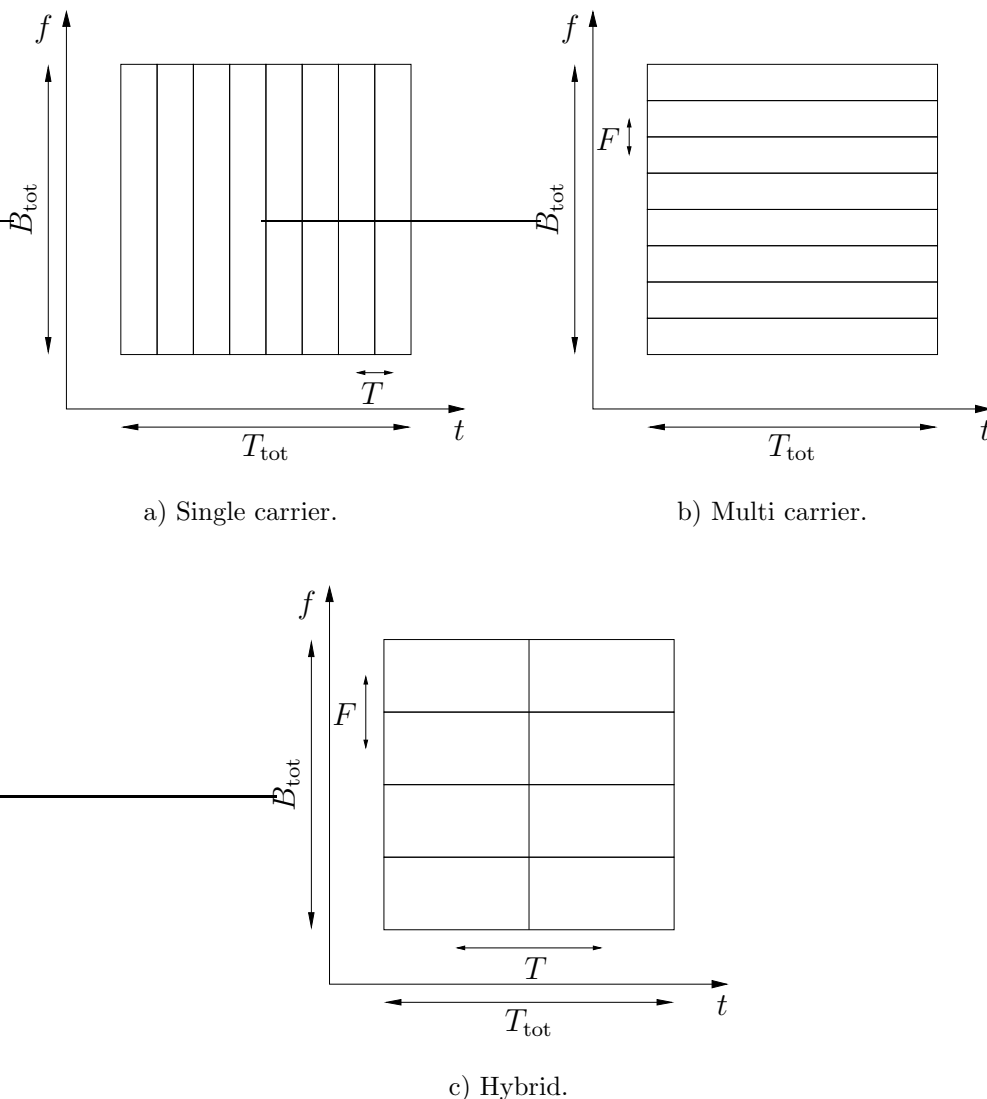


Fig. 3.3. Time-frequency occupation of SC, MC and HY systems with equal resource consumption. Each data symbol specific transmit signature $\underline{c}_n(t)$ of (2.2) is represented by a rectangle. $N = 8$, $N_f = 4$, $N_t = 2$.

the entire total bandwidth determined by the 3 dB bandwidth B_0 of the basic transmit signature $\underline{c}_0(t)$. Moreover, each $\underline{c}_n(t)$ of (2.24) has the same frequency location. In MC systems of Fig. 3.3b each data symbol specific signature $\underline{c}_n(t)$ of (2.28) occupies the entire total transmit duration T_{tot} and only a portion of the available bandwidth. All the transmitted symbols occupy the same time location, cf. (2.28). HY systems of Fig. 3.3c are a combination of SC and MC systems so that each data symbol specific transmit signature $\underline{c}_n(t)$ of (2.34) has its own time and frequency location. The time separation T and the frequency separation F , although having the same meaning in SC, MC and HY systems, assume different values depending on the given configuration. With N_t and N_f large enough, cf. Subsection 2.6.2, from Fig. 3.3, we can infer the relationship between the

time separation $T^{(\text{SC})}$ of an SC system and the time separation $T^{(\text{HY})}$ of an HY systems as

$$T^{(\text{SC})} \approx \frac{T^{(\text{HY})}}{N_f}. \quad (3.8)$$

In a similar way, we infer the relationship between the frequency separation $F^{(\text{MC})}$ in MC systems and the frequency separation $F^{(\text{HY})}$ in HY systems as

$$F^{(\text{MC})} \approx \frac{F^{(\text{HY})}}{N_t}. \quad (3.9)$$

We also notice, cf. Fig. 3.3, that the same basic transmit signature $\underline{c}_0(t)$ should have different B_0 and T_0 in SC, MC and HY systems. (3.8) and (3.9) shall be considered if we compare SC, MC and HY systems under the requirements of equal resource consumption. However, when considering the sensitivity of the reduction of T and/or F , we are not interested in (3.8) and (3.9).

3.3 Choice of parameters

3.3.1 General

The main goal of the thesis is that of evaluating the trade-off between the performance degradation and the increase of resource usage generated by the reduction of the frequency and/or time separation among data symbol specific signatures $\underline{c}_n(t)$ of (2.2), cf. Section 2.2. As a consequence, we shall consider a set of parameters which yields different combinations of time and frequency overlapping of the data symbol specific signatures $\underline{c}_n(t)$ of (2.2). The parameters are organized in two main families:

- **Fixed parameters:** These include the basic transmit signatures $\underline{c}_0(t)$ of (2.24), (2.28) and (2.34) and the relative time-frequency location of consecutive data symbol specific transmit signatures $\underline{c}_n(t)$. The former characterizes the system sensitivity to the variation of the time and frequency separation, the latter determines if we have an SC, an MC or a HY transmission system. In general, with a time limited basic transmit signature $\underline{c}_0(t)$, the system is expected to be less sensitive to time overlapping than to frequency overlapping.
- **Variable parameters:** These include the time separation T and the frequency separation F among data symbol specific signatures $\underline{c}_n(t)$.

We evaluate the system performance through the rate R of (2.57) and the SNR-degradation δ of (2.67) and (2.74). Both these quality criteria are functions of the time separation T and/or the frequency separation F .

3.3.2 Fixed parameters

The fixed parameters determine the system under consideration by fixing the basic transmit signature $\underline{c}_0(t)$ and the relative time-frequency location of the data symbol specific transmit signatures $\underline{c}_n(t)$ of (2.2). According to the latter parameter, we can have the three cases described in (2.24), (2.28) and (2.34), corresponding to an SC, an MC or a HY system, respectively. For each system, we may have different choices of the basic transmit signature $\underline{c}_0(t)$. We expect a significant influence of $\underline{c}_0(t)$ on the system performance, especially of its time and frequency extension.

The investigation of the dependency of the SNR-degradation δ of (2.68) and (2.76) on the increasing of the rate R of (2.57) beyond the value $R = 1$ represents a novel aspect of this thesis. In particular, with $R > 1$ the Nyquist conditions [Pro95] cannot be satisfied so that the system under investigation is affected by ISI also in the presence of an AWGN channel. To the author's knowledge, there is no work dealing with this assumption. Therefore, the effect of the basic transmit signature $\underline{c}_0(t)$ in this case has never been investigated. We choose a set of commonly used shapes [Pro95] with different spectral characteristics. The set of the proposed basic transmit signatures $\underline{c}_0(t)$ is reported in Table 3.3 with the naming convention and some key remarks on their properties.

Table 3.3. Considered basic transmit signatures $\underline{c}_0(t)$.

| $\underline{c}_0(t)$ | equation | remarks |
|----------------------|----------|-------------------------------------------------------------------------------------------|
| rect | (3.10) | rectangular; Nyquist impulse, time limited. |
| sinc | (3.13) | sinc shaped; Nyquist impulse, frequency limited. |
| gauss | (3.18) | Gaussian; limited both in time and frequency: Three values of variance σ^2 . |
| rrcos | (3.21) | square root raised cosine; frequency limited: Two values of roll-off factor α . |

The 3 dB duration T_0 and the 3 dB bandwidth B_0 of the basic transmit signatures $\underline{c}_0(t)$ of Table 3.3 are computed following the procedure presented in Subsection 2.6.5. If there is no closed form expression, then we approximate the values via numerical simulation.

With rect we indicate the rectangular impulse with duration T_{ref} and unitary energy, i.e., cf. (2.42),

$$\underline{c}_0(t) = \frac{1}{\sqrt{T_{\text{ref}}}} \text{rect} \left(\frac{t}{T_{\text{ref}}} \right). \quad (3.10)$$

$\underline{c}_0(t)$ of (3.10) has the 3 dB duration, cf. (3.5),

$$T_0 = T_{\text{ref}}. \quad (3.11)$$

and the 3 dB bandwidth, cf. (3.6),

$$B_0 \approx 6/(5T_{\text{ref}}). \quad (3.12)$$

It is time limited and it allows perfect reconstruction under the Nyquist assumptions [Pro95]. It is the basic impulse used in conventional OFDM systems, cf. Section 2.5. We assume a duration T_{ref} so that, over an AWGN channel, if $T = T_{\text{ref}}$ and $F = 1/T_{\text{ref}}$, cf. (3.4) the performance should perfectly match that of the reference system, cf. Subsection 3.2.3.

The sinc is frequency limited, has infinite time duration and is defined as

$$\underline{c}_0(t) = \frac{1}{\sqrt{T_{\text{ref}}}} \text{sinc}\left(\frac{\pi t}{T_{\text{ref}}}\right) = \frac{1}{\sqrt{T_{\text{ref}}}} \frac{\sin(\pi t/T_{\text{ref}})}{\pi t/T_{\text{ref}}}. \quad (3.13)$$

$\underline{c}_0(t)$ of (3.13) has the 3 dB duration

$$T_0 \approx 6T_{\text{ref}}/5 \quad (3.14)$$

and the 3 dB bandwidth

$$B_0 = 1/T_{\text{ref}}. \quad (3.15)$$

$\underline{c}_0(t)$ of (3.13) allows the perfect reconstruction of the transmitted symbols if the Nyquist assumptions are satisfied [Pro95]. The sinc function of (3.13) assumes zero values at the multiple of T_{ref} . In SC systems, if $T = T_{\text{ref}}$, in an AWGN channel the sinc ensures that there is no SNR-degradation δ of (2.68) and (2.76) [Pro95]. The Fourier transform of the sinc(t) function has a rectangular shape. In MC systems, if $F = F_{\text{ref}}$, there is no SNR-degradation δ . The decreasing of the frequency separation F is expected to have less influence than the decreasing of the time separation T on the SNR-degradation δ since the basic transmit signature $\underline{c}_0(t)$ of (3.13) is frequency limited. An MC system with a sinc basic transmit signature $\underline{c}_0(t)$ of (3.13) and an SC system with a rect basic transmit signature $\underline{c}_0(t)$ of (3.10) are expected to have the same sensitivity to the reduction of the time separation T and of the frequency separation F , respectively. We note that, in the former the interference is generated by the time overlapping of the data symbol specific transmit signatures $\underline{c}_n(t)$, while, in the latter, by their frequency overlapping. The effects of the post-processing stage on the noise enhancement due to interference removal might be influenced by the time or frequency origin of the interference. This aspect will be clarified through the discussion of the simulation results, cf. Chapter 4 and Chapter 5.

A basic transmit signature $\underline{c}_0(t)$ with a Gaussian shape, with the normalization factor D , with variance σ^2 and the reference time T_{ref} is defined as [BeC02, Pap91, Pro95]

$$\underline{c}_0(t) = D \cdot \exp\left[-\frac{1}{2} \left(\frac{t}{\sigma T_{\text{ref}}}\right)^2\right]. \quad (3.16)$$

We choose the factor D in order to normalize the energy to one, cf. Subsection 2.6.2, so that the main diagonal of the system matrix $\underline{\mathbf{A}}$ of (2.14) is given by ones. From the knowledge of the area of a Gaussian function [BeC02, Pap91, Pro95], i.e. $\int_{-\infty}^{+\infty} \exp\left[-\frac{1}{2}\left(\frac{t}{\sigma}\right)^2\right] dt = \sqrt{2\pi}\sigma$, by imposing

$$\int_{-\infty}^{+\infty} |\underline{\mathcal{C}}_0(t)|^2 dt = D^2 \int_{-\infty}^{+\infty} \exp\left[-\frac{1}{2}\left(\frac{t}{\sigma T_{\text{ref}}/\sqrt{2}}\right)^2\right] dt = D^2 \sqrt{\pi}\sigma T_{\text{ref}} = 1, \quad (3.17)$$

we derive the desired normalization factor D . Therefore, we define the gauss basic transmit signature as

$$\underline{\mathcal{C}}_0(t) = \sqrt{\frac{1}{\sqrt{\pi}\sigma T_{\text{ref}}}} \exp\left[-\frac{1}{2}\left(\frac{t}{\sigma T_{\text{ref}}}\right)^2\right]. \quad (3.18)$$

$\underline{\mathcal{C}}_0(t)$ of (3.18) has the 3 dB duration [BeC02, Pap91, Pro95]

$$T_0 = 2\sigma\sqrt{2\ln(2)}T_{\text{ref}}. \quad (3.19)$$

and the 3 dB bandwidth

$$B_0 = \frac{\sqrt{2\ln(2)}}{\pi\sigma T_{\text{ref}}}. \quad (3.20)$$

Both (3.19) and (3.20) are determined following Subsection 2.6.5. The gauss basic transmit signature $\underline{\mathcal{C}}_0(t)$ of (3.18) can be considered to be time and frequency limited with a good approximation, although it does not satisfy the Nyquist theorem [Pro95]. We choose three values of variance σ^2 so that we can consider the case in which the Gaussian impulse is essentially time limited, the case in which it is essentially frequency limited or the case in which it is approximately both time and frequency limited. The main property of the gauss of (3.18) is its nice analytical formula which allows the derivation of theoretical results. These are important to validate the computer simulations and to justify the interpretation of the results. In Subsection 3.3.4, we derive the analytical expression of the ISI and of the ICI in a HY system deploying a gauss basic transmit signature $\underline{\mathcal{C}}_0(t)$ of (3.18).

The rrcos indicates the basic transmit signature [BeC02], cf. (2.91),

$$\underline{\mathcal{C}}_0(t) = \frac{1}{\sqrt{T_{\text{ref}}}} \frac{\sin[\pi(1-\alpha)t/T_{\text{ref}}] + 4\alpha t/T_{\text{ref}} \cos[\pi(1+\alpha)t/T_{\text{ref}}]}{\pi[1-(4\alpha t/T_{\text{ref}})^2]t/T_{\text{ref}}}. \quad (3.21)$$

$\underline{\mathcal{C}}_0(t)$ of (3.21) has the 3 dB duration, cf. (2.97) in Subsection 2.6.5,

$$T_0 \approx \frac{4}{3}T_{\text{ref}} \quad (3.22)$$

and the 3 dB bandwidth, cf. (2.98),

$$B_0 = \frac{\alpha + 3}{3T_{\text{ref}}}. \quad (3.23)$$

$\underline{c}_0(t)$ of (3.21) with $\alpha = 0$ coincides to the sinc of (3.13) and it is the most commonly used Nyquist impulse in SC communication systems. It is frequency limited, but it implies an excess bandwidth depending on the roll-off factor α [Pro95]. We choose this basic transmit signature because, by controlling the extension of the excess bandwidth [Pro95] through the roll-off factor α , we can investigate the influence of different degrees of overlapping in the frequency domain. We consider in particular the two values $\alpha = 0.1$ and $\alpha = 0.3$.

The basic transmit signatures $\underline{c}_0(t)$ of (3.10), (3.13), (3.18) and (3.21) depend on the reference time T_{ref} . In what follows we set

$$T_{\text{ref}} = 1/F_{\text{ref}} = 1. \quad (3.24)$$

If we want to adapt our results to systems with values T_{ref} and F_{ref} different from the values in (3.24), then we have to multiply all time quantities by T_{ref} and to divide all frequency quantities by T_{ref} . T_{ref} is the reference time of the systems under consideration. In some cases, cf. Section 3.3, we still indicate T_{ref} and F_{ref} to highlight their effects.

3.3.3 Variable parameters

We indicate with variable parameters the parameters which may vary, so determining the system performance in terms of the quality criteria introduced in Section 2.6. The variable parameters are defined in Table 3.4.

Table 3.4. Variable parameters.

| Parameter | remarks |
|--------------------------|---------------------------------------------------|
| time separation T | time separation between consecutive symbols |
| frequency separation F | frequency separation between simultaneous symbols |

The considered range of T and F allows us to evaluate the system performance both when the Nyquist assumptions can be verified, i.e. $FT \geq 1$, and when they cannot be verified, i.e. $FT < 1$. The main focus is on the latter case which is equivalent to consider $R > 1$, cf. (2.63).

By varying F and T of Table 3.4, we influence the values assumed by the quality criteria R of (2.57) and δ of (2.68) and (2.76) used to evaluate the system performance presented in Table 3.5. The SNR-degradation δ_{MMSE} of (2.76) depends on the one sided

Table 3.5. Quality criteria.

| Criterion | equation | remarks |
|----------------------------------------|----------|------------------------------------------------------------------------------------------------------------------------------------------------|
| rate R | (2.57) | number N of transmitted data symbols divided by total transmission duration T_{tot} and total bandwidth occupation B_{tot} |
| SNR-degradation δ_{ZF} | (2.68) | SNR-degradation of the ZF-BLE |
| SNR-degradation δ_{MMSE} | (2.76) | SNR-degradation of the MMSE-BLE: Two values of SNR |

noise power spectral density N_0 at the input of the receiver, cf. Subsection 2.6.3. Therefore, two values of SNR, i.e. SNR=10 dB and SNR=30 dB, are considered to validate the analytical derivation of the bounds derived in Subsections 2.6.3 and 2.6.5.

When considering SC systems the quality criteria R of (2.57) and δ of (2.68) and (2.76) mainly depend on the time separation T since the dependency on the number of data symbols N , on the 3 dB duration T_0 and on the 3 dB bandwidth B_0 can be made particularly small by choosing N large enough, cf. Subsections 2.6.2 to 2.6.6. Time limited basic transmit signatures $\underline{c}_0(t)$ are expected to show better performance, cf. Chapter 5. In the case of MC systems, R of (2.57) and δ of (2.68) and (2.76) mainly depend on F and, in contrast to SC systems, frequency limited basic transmit signatures $\underline{c}_0(t)$ are expected to yield better performance. In the case of HY systems there is an additional degree of freedom because R of (2.57) and δ of (2.68) and (2.76) depend on both F and T . Moreover, there are many combinations of frequency and time separations offering the same value of R . In Fig. 3.4 the dependency of R of (2.57) on T and F for a HY system is depicted. We consider (2.63) with $N_t = 8$, $N_f = 8$, B_0 and T_0 as the 3 dB bandwidth and the 3 dB duration of a rect of (3.10), respectively. The two dimensional surface $R(F, T)$ grows very similarly with the decreasing of F and T . If $F = 0$ and $T = 0$, it assumes the expected value, cf. (2.63), (3.11) and (3.12),

$$R|_{T=0, F=0} = \frac{N_f N_t}{T_0 B_0} = \frac{160}{3} \approx 53. \quad (3.25)$$

(3.25), although derived for HY systems, holds true also for SC and MC systems under the assumption, always verified, that $N = N_t N_f$, cf. Subsection 2.4.4. By recalling Subsection 2.6.4, we notice that with T and F close to zero, the SNR-degradation δ of (2.68) and (2.76) is expected to diverge to very high values. These are of no interest since the SNR-degradation δ gives a measure of how much one should increase the transmitted power to maintain the same performance in terms of average bit error probability (P_b) [Sk104]. If the SNR-degradation δ is higher than 80 dB, then it would be required to increase the transmitted power by 8 orders of magnitude which is not acceptable in any real system. In general, we will depict the SNR-degradation δ of (2.68) and (2.76) as a function of T

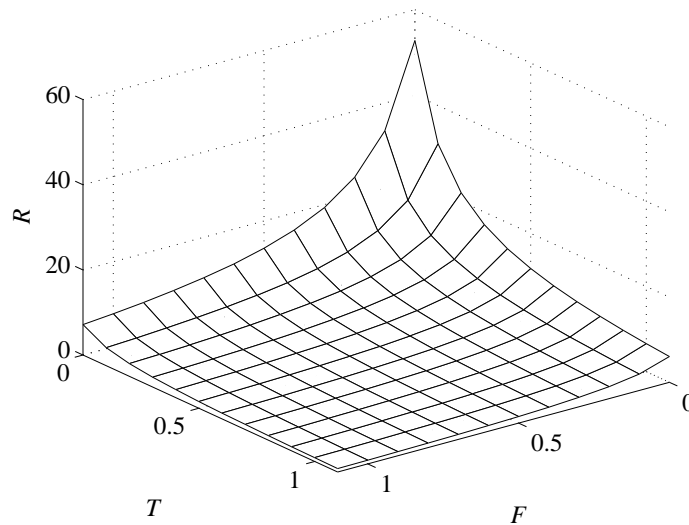


Fig. 3.4. Rate R of (2.57) in a HY system as a function of the time separation T and the frequency separation F ; rect basic transmit signature $\underline{c}_0(t)$ of (3.10); $N_t = N_f = 8$; $T_{\text{ref}} = 1/F_{\text{ref}} = 1$; $0 \leq T \leq 1.1$; $0 \leq F \leq 1.1$.

and F together with the corresponding function $R(F, T)$. For a given value of R of (2.57), i.e. for a given resource usage, there might be different combinations of F and T and, as a consequence, different values of the SNR-degradation δ . To clarify this dependency, we report some of the numerical values of Fig. 3.4 in Table 3.6. We consider now, for

Table 3.6. Rate R of (2.57) in a HY system as a function versus T and F ; rect basic transmit signature $\underline{c}_0(t)$ of (3.10); $T_{\text{ref}} = 1/F_{\text{ref}} = 1$; $N_t = N_f = 8$.

| T | Rate R | | | | | | |
|-----|----------|-----|------|------|------|------|-----|
| 0 | 7.8 | 9.4 | 11.8 | 15.9 | 24.6 | 53.1 | |
| 0.2 | 3.2 | 3.9 | 4.9 | 6.7 | 10.2 | 22.1 | |
| 0.4 | 2.1 | 2.5 | 3.1 | 4.2 | 6.4 | 13.9 | |
| 0.6 | 1.5 | 1.8 | 2.3 | 3.1 | 4.7 | 10.2 | |
| 0.8 | 1.2 | 1.4 | 1.8 | 2.4 | 3.7 | 8.0 | |
| 1.0 | 0.9 | 1.2 | 1.5 | 2.0 | 3.1 | 6.6 | |
| | 1.0 | 0.8 | 0.6 | 0.4 | 0.2 | 0 | F |

instance, the value $R \approx 1.5$. From Table 3.6 we infer that the couples $(F = 0.6, T = 1.0)$, $(F = 1.0, T = 0.6)$ and $(F = 0.8, T = 0.8)$ return approximately $R = 1.5$. For a frequency unlimited and time limited basic transmit signature $\underline{c}_0(t)$, we would expect that the couple with the lowest value of F , i.e. $(F = 0.6, T = 1.0)$, returns the highest SNR-degradation δ of (2.68) and (2.76) since the frequency overlapping has a major impact on the generation of the interference, cf. Chapter 4.

It is possible to explicitly investigate the relationship between rate R of (2.57) and SNR-degradation δ of (2.68) and (2.76) also in the HY systems by inverting (2.63) so that

$$T = \frac{1}{N_t - 1} \left[\frac{N_t N_f}{R [(N_f - 1)F + B_0]} - T_0 \right] \quad (3.26)$$

is obtained. In Chapter 4, where we present the simulation results, we will see the advantages given by (3.26).

3.3.4 Gaussian basic transmit signature

As anticipated in the Subsection 3.3.2, the gauss basic transmit signature $\underline{c}_0(t)$ of (3.18) allows a theoretical derivation of the ISI and ICI so that the elements of the system matrix $\underline{\mathbf{A}}$ of (2.14) can be evaluated in a closed form. The interference is generated in general both in time, i.e. ISI, and in frequency, i.e. ICI, and it is given by the elements of the system matrix $\underline{\mathbf{A}}$ as defined in (2.12). In Subsection 2.7.2, the dependency of the system matrix elements $\underline{A}_{n,n'}$ on the basic transmit signature $\underline{c}_0(t)$ and on the time and frequency location of the data symbol specific transmit signatures $\underline{c}_n(t)$ of (2.28) is worked out first in the case of an AWGN channel and then by taking into account the time-invariant channel impulse response $\underline{h}(t)$. In this subsection, we assume the channel to be an AWGN channel, cf. Subsections 2.7.2 to 2.7.3. From (2.120) to (2.122) and from (3.18) the interference in a HY system with a gauss basic transmit signature $\underline{c}_0(t)$ of (3.18) reads

$$\begin{aligned} \underline{A}_{n,n'} = & \frac{1}{\sqrt{\pi}\sigma T_{\text{ref}}} \exp[-j2\pi\Delta_f(n,n')FT(n_t(n')-1)] \int_{-\infty}^{+\infty} \exp\left[-\frac{1}{2}\left(\frac{t}{\sigma T_{\text{ref}}}\right)^2\right] \cdot \\ & \cdot \exp\left[-\frac{1}{2}\left(\frac{t - \Delta_t(n,n')T}{\sigma T_{\text{ref}}}\right)^2\right] \exp[-j2\pi\Delta_f(n,n')Ft] dt. \end{aligned} \quad (3.27)$$

We consider now the product of the two Gaussian functions inside the integral. It is known [BeC02, Pap91, Pro95] that the product of two Gaussian functions is still a Gaussian function multiplied by a constant factor. With some algebra we obtain

$$\begin{aligned} \underline{A}_{n,n'} = & \frac{1}{\sqrt{\pi}\sigma T_{\text{ref}}} \exp[-j2\pi\Delta_f(n,n')FT(n_t(n')-1)] \exp\left[\frac{(\Delta_t(n,n')T)^2}{4\sigma^2 T_{\text{ref}}^2}\right] \cdot \\ & \cdot \int_{-\infty}^{+\infty} \exp\left[-\frac{1}{\sigma^2 T_{\text{ref}}^2} \left(\frac{t - \Delta_t(n,n')T}{2}\right)^2\right] \exp[-j2\pi\Delta_f(n,n')Ft] dt. \end{aligned} \quad (3.28)$$

The integral in (3.28) can be interpreted as the Fourier transform of a Gaussian function evaluated at the frequencies $f = \Delta_f(n,n')F$, cf. (2.129). Therefore, by applying

the relationship existing between the Gaussian functions in time and frequency domain [BeC02, Pap91, Pro95], i.e. $\int_{-\infty}^{+\infty} \exp[-\pi t^2] \exp[-j2\pi ft] dt = \exp[-\pi f^2]$, we can write (3.28) as

$$\begin{aligned} \underline{A}_{n,n'} = & \frac{1}{\sqrt{\pi}\sigma T_{\text{ref}}} \exp[-j2\pi\Delta_f(n,n')FT(n_t(n')-1)] \exp\left[-\frac{(\Delta_t(n,n')T)^2}{4\sigma^2 T_{\text{ref}}^2}\right] \cdot \\ & \cdot \sqrt{\pi}\sigma T_{\text{ref}} \exp\left[-(\pi\sigma T_{\text{ref}}\Delta_f(n,n')F)^2\right] \exp[-j2\pi\Delta_f(n,n')F\Delta_t(n,n')T/2], \end{aligned} \quad (3.29)$$

which, by recalling (3.4), can be rearranged as

$$\begin{aligned} \underline{A}_{n,n'} = & \exp[-j2\pi\Delta_f(n,n')FT(n_t(n')-1)] \exp[-j2\pi\Delta_f(n,n')\Delta_t(n,n')FT/2] \cdot \\ & \cdot \exp\left[-\left(\frac{\Delta_t(n,n')T}{2\sigma T_{\text{ref}}}\right)^2\right] \exp\left[-(\pi\sigma\Delta_f(n,n')F/F_{\text{ref}})^2\right]. \end{aligned} \quad (3.30)$$

(3.30) gives the analytical expression of the system matrix $\underline{\mathbf{A}}$ of (2.14) when a gauss basic transmit signature $\underline{c}_0(t)$ of (3.18) is deployed and an AWGN channel is assumed.

In the case of an SC system, there is no frequency separation. Therefore $\Delta_f(n,n') = 0$ and (3.30) reduces to

$$\underline{A}_{n,n'} = \exp\left[-\left(\frac{\Delta_t(n,n')T}{2\sigma T_{\text{ref}}}\right)^2\right]. \quad (3.31)$$

In the case of an MC system, there is no time separation, $\Delta_t(n,n') = 0$ and moreover the function $n_t(n) = 1$ for each $n = 1 \dots N$ because the symbols do not extend in the time direction. As a consequence (3.30) for MC systems becomes

$$\underline{A}_{n,n'} = \exp\left[-(\pi\sigma\Delta_f(n,n')F/F_{\text{ref}})^2\right]. \quad (3.32)$$

The phase factor in (3.30) plays a role only in HY systems, cf. Subsection 2.7.2, when the effects of the data symbol specific transmit signatures $\underline{c}_n(t)$ of (2.28) allocated at different time and frequency location can be seen. We also notice that if the product FT turns out to be an integer, as it is widely assumed in the frame theory, cf. Subsection 1.1.3 and [KoM98], then the phase factor becomes real. If FT is even, then the phase factor disappears. If FT is odd, then the phase factor can assume the values plus or minus one depending on $\Delta_f(n,n')\Delta_t(n,n')$. (3.30) is bounded by minus one and one and depends on the time separation T , the frequency separation F , the standard deviation σ , the time index $n_t(n)$, the time distance $\Delta_t(n,n')$ and the frequency distance $\Delta_f(n,n')$.

Based on (3.30), we now determine a set of interesting values of the 3 dB bandwidth B_0 of the gauss basic transmit signature $\underline{c}_0(t)$ of (3.18). From (3.18) to (3.20) [BeC02, Pap91, Pro95], we derive that the 3 dB bandwidth B_0 and the 3 dB duration T_0 are related to σ of

(3.18). With a larger B_0 , the 3 dB duration T_0 of the gauss basic transmit signature $\underline{c}_0(t)$ of (3.18) decreases [BeC02, Pap91, Pro95]. Therefore, the data symbol specific transmit signatures $\underline{c}_n(t)$ of (2.28) overlap more in time or in frequency depending on the value of B_0 . The influence of B_0 depends also on the system configuration, i.e. if we consider an SC, an MC or a HY system. To better explain the nature of the overlapping, we assume a HY system with $N = 64$, $N_t = 8$, $N_f = 8$, and depict the corresponding time-frequency plane in Fig. 3.5. Each data symbol specific transmit signature $\underline{c}_n(t)$ of (2.28) has a time

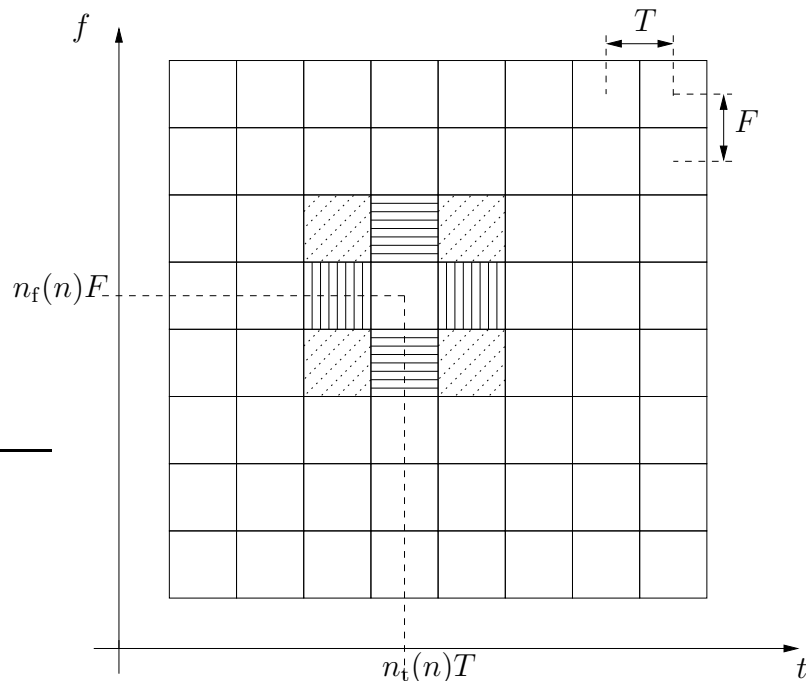


Fig. 3.5. Time and frequency plane occupation for a HY system; $N_f = 8$, $N_t = 8$. Most of the interference affecting the basic transmit signature $\underline{c}_0(t)$ in location $n_t(n)T$, $n_f(n)F$ is generated by the adjacent symbols in time, frequency and both time and frequency.

and frequency location determined by $n_t(n)T$ and $n_f(n)F$, respectively. Let us focus on the data symbol specific transmit signature $\underline{c}_{28}(t)$, i.e. $n_t(28) = 4$, $n_f(28) = 4$. Since the gauss of (3.18) can be assumed both time and frequency limited, cf. Subsection 3.3.2, we infer that the interference is mainly generated by data symbol specific transmit signatures $\underline{c}_n(t)$ of (2.28) located in adjacent time slots, indicated with vertical lines in Fig. 3.5, in adjacent sub-carriers, indicated with horizontal lines in Fig. 3.5, and in adjacent time and frequency slots as indicated by the dotted diagonal squares in Fig. 3.5. In the aforementioned positions, we expect the majority of the interference to be concentrated. We verify this intuition by considering (3.30). We have seen that the interference depends on many parameters. To avoid the complex effects of the phase factors in (3.30) and the dependency on the symbol index $n_t(n')$, we choose $FT = 1$. We consider three possible values of normalized 3 dB bandwidth B_0 as reported in Table 3.7 and analytically evaluate the system matrix $\underline{\mathbf{A}}$ through (3.30) under the assumption of the parameter set summarized in Table 3.8. We plot the row 28, see Fig. 3.5, of the system matrix $\underline{\mathbf{A}}$ of (2.14) in Fig. 3.6.

Table 3.7. 3 dB bandwidth B_0 of the gauss basic transmit signatures $\underline{c}_0(t)$ of (3.18) under investigation versus σ .

| σ | B_0 |
|----------|----------------------|
| 0.54 | $0.7/T_{\text{ref}}$ |
| 0.42 | $0.9/T_{\text{ref}}$ |
| 0.31 | $1.2/T_{\text{ref}}$ |

In Fig. 3.6, we first notice that for $n' = n = 28$, the normalized energy of the useful

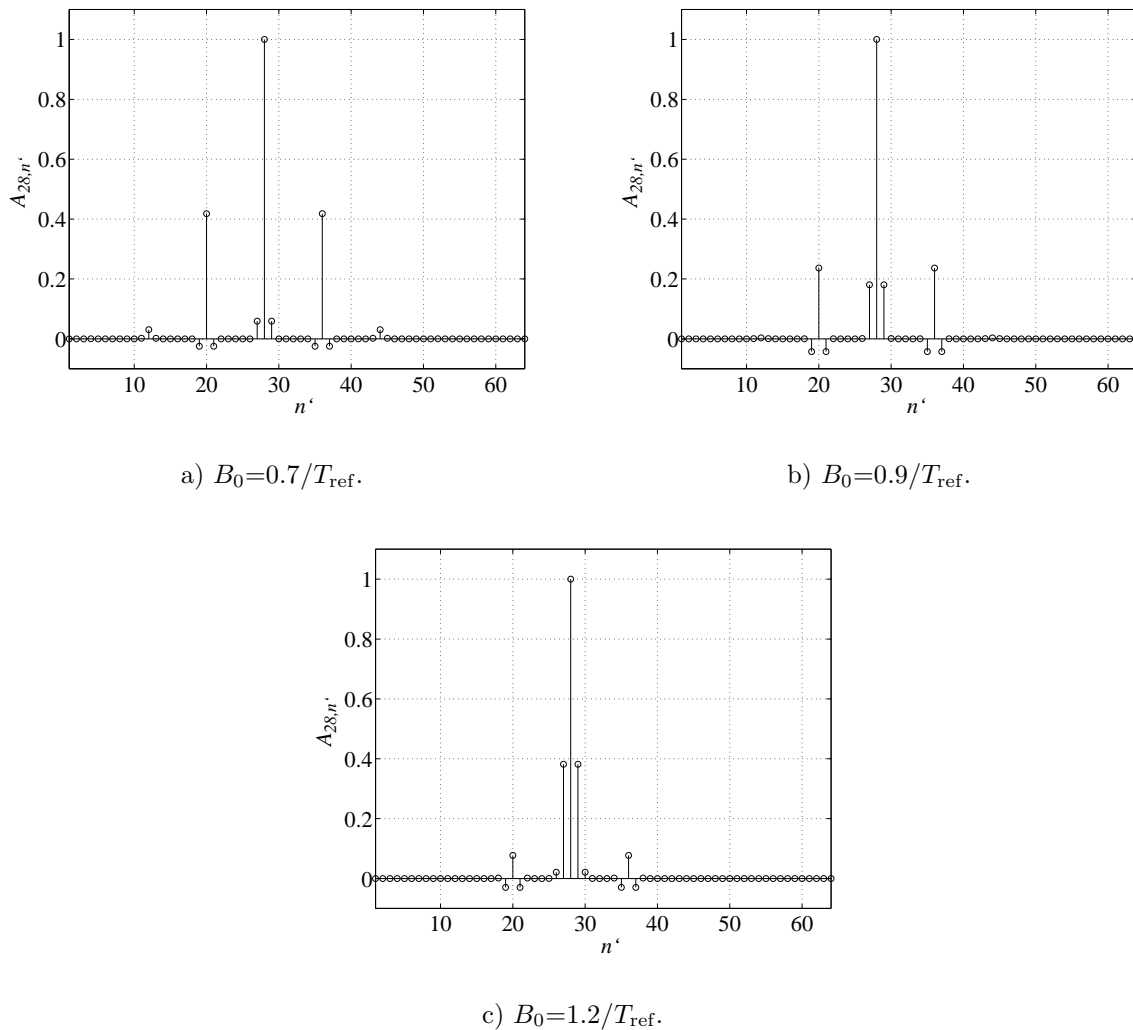


Fig. 3.6. Row 28 of the system matrix $\underline{\mathbf{A}}$ of a HY system with $N_t = 8$, $N_f = 8$ and a Gaussian basic transmit signature $\underline{c}_0(t)$ of (3.18) with 3 dB bandwidth B_0 .

received symbol is equal to one. By recalling the functions $n_t(n)$ and $n_f(n)$ of (2.32), we can read the distribution of the interference as follows. In Fig. 3.6a, the low frequency

Table 3.8. Parameter values for the HY system with gauss basic transmit signature $\underline{c}_0(t)$ of (3.18).

| Parameters | Value |
|----------------------|------------------|
| $\underline{c}_0(t)$ | gauss of (3.18) |
| T | T_{ref} |
| F | F_{ref} |
| N | 64 |
| N_t | 8 |
| N_f | 8 |

extension ensures a low level of ICI shown in the positions $n' = 27$ and $n' = 29$. The data symbol specific transmit signatures $\underline{c}_n(t)$ of (2.28) represented by horizontal lines in Fig. 3.5 do not overlap with $\underline{c}_{28}(t)$. In positions $n' = 20$ and $n' = 36$, the ISI contribution of the adjacent symbols is clearly the strongest. It corresponds to the interference generated by the data symbol specific transmit signatures $\underline{c}_n(t)$ of (2.28) indicated with vertical lines in Fig. 3.5. A particular behaviour can be observed in positions $n' = 19$ and $n' = 21$ as well as in their symmetric counterparts, i.e. the dotted diagonal square of Fig. 3.5. The phase factor of (3.30) turns to be minus one thus generating a negative contribution. The effects of the phase factors become more complicated when FT is not integer and may let the interference sum up constructively or destructively. With the increment of B_0 in Fig. 3.6b and Fig. 3.6c the interference migrate from the time to the frequency direction, but the observations regarding the effects of the adjacent symbols remain in principle the same. In Fig. 3.6b, we notice that the interference is quite equally distributed both in the time and the frequency direction.

From the investigation of the analytical expression of the system matrix $\underline{\mathbf{A}}$ of (2.14) we can conclude that the three chosen values of B_0 , cf. Table 3.7, represent three different interference situations. In the first case, most of the interference is generated in the time direction, in the second case it is present both in the time and the frequency directions, and in the last one most of the overlapping and hence interference occurs in the frequency direction.

As soon as we consider $FT < 1$, not only the phase factor can have a strong impact on the interference, but also the overlapping among the data symbol specific transmit signatures $\underline{c}_n(t)$ of (2.28) increases more and more. With F and T close to zero, all the $\underline{c}_n(t)$ of (2.28) have the same time and frequency location so that the elements of the system matrix $\underline{\mathbf{A}}$ of (2.14) have the same value.

3.3.5 Proposed values

From Fig. 3.6 we have seen that in the specific case $FT = 1$, almost all the interference is generated by the symbols transmitted in adjacent sub-carriers or sub-slots. Nevertheless, in our case study, we should be particularly careful since, by focusing on the condition $TF < 1$, we are considering highly overlapping data symbol specific transmit signatures $\underline{c}_n(t)$ of (2.28) and not adjacent $\underline{c}_n(t)$ of (2.28) could significantly overlap. With the increasing of the overlapping, the ISI and/or the ICI increase causing an increment in the SNR-degradation δ of (2.68) and (2.76). On the other hand, the rate R of (2.57) simultaneously increases too, since the reduction of T and/or F lower the total transmission duration T_{tot} , cf. (2.27), (2.31) and (2.37), and/or the total bandwidth B_{tot} , cf. (2.26), (2.30) and (2.36). It follows that we should consider a set of parameters enabling the consideration of all different kinds of interference. From Fig. 3.6 and taking into account the dependency of the simulation results on the increment of the number N_f of sub-carriers and on the number N_t of time slots, we fix the value of $N = 64$ for the SC, the MC and the HY systems. For the HY systems we choose to equally span the transmitted signal in time and frequency, by choosing $N_f = N_t = 8$. With respect to the reference system as introduced in Subsection 3.2.3, we refer to it to derive the relationship between the time separation T_{ref} and the frequency separation F_{ref} , cf. (3.4). Then, the number N_f of sub-carriers used in the reference system is not the same used to evaluate the cross dependency between the SNR-degradation δ of (2.68) and (2.76) and the rate R of (2.57). We consider a smaller number N_f of sub-carriers to simplify the simulation, since we have seen that the results we are interested in depend on the interference generated by the adjacent sub-carrier and not on their number. Although the results will not refer directly to the reference system and to a realistic scenario, they will indicate the most promising setting which is worth to be investigated in more detail.

The overall set of parameters is summarized in Table 3.9. We notice that in the HY systems, we choose not to consider the performance of the δ_{MMSE} with SNR=10 dB. We also introduce a new function to report the results. We use (3.26) to depict the simulated SNR-degradation δ of (2.76) of HY systems as a set of two dimensional functions obtained by fixing the value of the rate R of (2.57) and considering the combination of T and F returning the chosen value of R . With this approach, the reading of the results becomes more immediate and the value of the SNR-degradation δ of (2.76) can be deduced more easily than from the three dimensional surfaces.

3.3.6 Choice of an AWGN channel

In the simulation chain, we consider only an AWGN channel. In this subsection, we recall the key aspects and characteristics of the multipath radio channel [Kan04] and justify the

Table 3.9. Parameter set.

| System | $\underline{c}_0(t)$ | equation | symbols | functions | |
|--------|-----------------------|----------|----------|---------------------------------------|------------------------------------------|
| SC | rect | (3.10) | $N = 64$ | $R(T)$ | |
| | sinc | (3.13) | | $\delta_{\text{ZF}}(T)$ | |
| | gauss, $B_0 = 0.6$ | (3.18) | | $\delta_{\text{MMSE}}(T)$, SNR=10 dB | |
| | gauss, $B_0 = 0.9$ | (3.18) | | $\delta_{\text{MMSE}}(T)$, SNR=30 dB | |
| | gauss, $B_0 = 1.2$ | (3.18) | | | |
| | rrcos, $\alpha = 0.1$ | (3.21) | | | |
| | rrcos, $\alpha = 0.3$ | (3.21) | | | |
| MC | rect | (3.10) | $N = 64$ | $R(F)$ | |
| | sinc | (3.13) | | $\delta_{\text{ZF}}(F)$ | |
| | gauss, $B_0 = 0.6$ | (3.18) | | $\delta_{\text{MMSE}}(F)$, SNR=10 dB | |
| | gauss, $B_0 = 0.9$ | (3.18) | | $\delta_{\text{MMSE}}(F)$, SNR=30 dB | |
| | gauss, $B_0 = 1.2$ | (3.18) | | | |
| | rrcos, $\alpha = 0.1$ | (3.21) | | | |
| | rrcos, $\alpha = 0.3$ | (3.21) | | | |
| HY | rect | (3.10) | $N = 64$ | $R(F, T)$ | |
| | sinc | (3.13) | | $N_{\text{f}} = 8$ | $\delta_{\text{ZF}}(F, T)$ |
| | gauss, $B_0 = 0.6$ | (3.18) | | $N_{\text{t}} = 8$ | $\delta_{\text{MMSE}}(F, T)$, SNR=30 dB |
| | gauss, $B_0 = 0.9$ | (3.18) | | | $\delta_{\text{ZF}}(F, T R)$ |
| | gauss, $B_0 = 1.2$ | (3.18) | | | |
| | rrcos, $\alpha = 0.1$ | (3.21) | | | |
| | rrcos, $\alpha = 0.3$ | (3.21) | | | |

choice of an AWGN channel.

The mobile radio channel $\underline{h}(\tau, t)$, cf. Subsection 2.2.3, places fundamental limitations on the performance of wireless communication systems. The transmission path between the transmitter and the receiver can vary from simple line-of-sight to one that is severely obstructed by buildings, mountains, and foliage. The speed of motion impacts how rapidly the signal level fades as a mobile terminal moves in space.

Through the numerous measurement campaigns performed in indoor [Zol93, Kat97] and outdoor environments [KMT96, FRB97], it is well known that in mobile radio communications a part of the electromagnetic energy radiated by the transmitter reaches the receiver by propagating through different paths [Par92, Pap00]. The performance of digital radio communication systems is strongly affected by multipath propagation in the form of scattering, reflection, and refraction. The multipath in the radio channel creates small-scale fading effects. The three most important effects of the small-scale multipath propagation are [Rap99]:

- Rapid changes in signal strength over a small travel distance or time interval,
- random frequency modulation due to varying Doppler shifts on different multipath signals,
- time dispersion caused by multipath propagation delays.

The time dispersive nature of the multipath channels is normally quantified by their delay spread σ_τ , which can be determined from their power delay profile [Rap99]. The maximum multipath propagation delay τ_{\max} of the power delay profile is defined to be the time delay beyond which multipath energy is smaller than a predefined threshold. The time variance of the multipath channels is described by the Doppler spread δ_{f_D} [Rap99]. It is defined as the range of frequencies over which the receive Doppler spectrum is essentially non-zero.

Due to the random characterization of the fading channels, it is necessary to investigate their statistical behaviour, which leads to stochastic channel models. The simplest non-degenerate class of processes which exhibits uncorrelated dispersiveness in time delay and Doppler shifts is known as the wide-sense stationary uncorrelated scattering (WSSUS) model introduced in [Bel63, Pro95, Hoe92].

Based on the WSSUS model, the statistical measures such as the coherence time T_C and the coherence bandwidth B_C can be obtained. Coherence time T_C is the time duration over which two receive signals have a strong potential for amplitude correlation. If the symbol duration T_0 of the baseband signal is significantly smaller than the channel coherence time T_C , approximately 2%, then the channel variations are slower than the baseband signal variations, therefore the channel can be considered slow fading. Otherwise the channel can be considered as fast fading. Coherence bandwidth B_C is the range of frequencies over which two frequency components have a strong potential for amplitude correlation. If the system bandwidth B is greater than the channel coherence bandwidth B_C , the channel can be considered to be frequency selective, and a broadband channel is characterized. Otherwise the channel is frequency non-selective or flat, and a narrowband channel is characterized. Frequency selective fading is due to time dispersion of the transmitted symbols within the channel. Thus the frequency selective channel induces ISI.

There is large amount of literature dealing with the radio channel characterization, modelling and simulation. At the same time, many works are focused on the distortion effects of the channel on the received signal and investigate solutions to limit the consequent performance degradation [BeC02, Kal95, Kat97, KKB96, NeP00, Pro95, Rap99]. We are aware of the importance of the multipath propagation in wireless communications, but we choose to consider only the presence of an AWGN channel. By doing so, we avoid the presence of other sources of interference and highlight the effects of the reduction of time separation T and/or of the frequency separation F on the signal distortion. The

investigation of this reduction is new and is the main focus of this work. Moreover, preliminary simulation results show that the average effects of the channel are independent of the reduction of T and F .

AWGN represents a good model also for some realistic scenarios such as cellular indoor scenarios in which the cell dimension is small, static radio links and satellite links. In general, all those radio scenarios in which the line-of-sight component is very strong as compared to the multipath reflection.

Notwithstanding the choice of an AWGN channel, we included the presence of the channel in the system modelling introduced in Section 2.2, cf. (2.3), to make it valid in a more general context.

3.4 Evaluation of the proposed approach

3.4.1 General

Throughout the thesis, we have developed a new approach to increase the rate R of (2.57). In this section, we present a possible evaluation of the proposed approach.

3.4.2 Channel capacity in the proposed modelling

If the transmitted symbols d_n of \mathbf{d} of (2.1) and the noise samples $n_{\text{MF},n}$ of \mathbf{n}_{MF} of (2.8) are statistically independent zero-mean Gaussian random variables, then with γ the SNR at the input of the receiver, the normalized channel capacity in bit/dimension is [Gal68, Pro95, Sha48]

$$C = \text{ld}(1 + \gamma). \quad (3.33)$$

In the following, we make the necessary assumptions on our modelling so that (3.33) holds true and write explicitly the dependency of C of (3.33) on the rate R of (2.57) and the SNR-degradation δ of (2.68).

With \mathbf{d} of (2.1), \mathbf{A} of (2.14), \mathbf{n}_{MF} of (2.8) and \mathbf{d}_{MF} of (2.7), the system model developed in Chapter 2 is graphically depicted in Fig. 3.7. The post processing stage can be a ZF-BLE or an MMSE-BLE. To ensure that (3.33) holds true, we consider a ZF-BLE so that all the interference is removed. The ZF-BLE consists of the inversion of the system matrix \mathbf{A} of (2.14). Therefore, it is valid only if the inverse of the system matrix \mathbf{A} exists. The final estimate $\hat{\mathbf{d}}$ of \mathbf{d} of (2.1) with a ZF-BLE is

$$\hat{\mathbf{d}} = \mathbf{d} + \mathbf{A}^{-1} \mathbf{n}_{\text{MF}}. \quad (3.34)$$

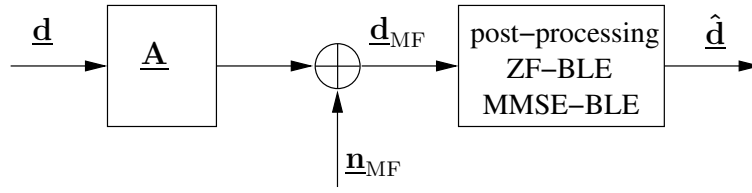


Fig. 3.7. Matrix representation of the system model introduced in Chapter 2.

The contribution $\underline{\mathbf{n}}_{\text{MF}}$ of (2.8) at the output of the MF is coloured by the post-processing stage, cf. Subsections 2.3.2 and 2.3.3. We define the equivalent noise affecting the final estimate when a ZF-BLE is employed as

$$\underline{\mathbf{n}}_{\text{ZF}} = \underline{\mathbf{A}}^{-1} \underline{\mathbf{n}}_{\text{MF}}. \quad (3.35)$$

The noise covariance matrix of $\underline{\mathbf{n}}_{\text{ZF}}$ reads, cf. (2.20),

$$\underline{\mathbf{R}}_{\text{n,ZF}} = \text{E} \{ \underline{\mathbf{n}}_{\text{ZF}} \underline{\mathbf{n}}_{\text{ZF}}^{\text{H}} \}. \quad (3.36)$$

By substituting (3.35) into (3.36) and from (2.20), we obtain

$$\underline{\mathbf{R}}_{\text{n,ZF}} = \text{E} \left\{ \underline{\mathbf{A}}^{-1} \underline{\mathbf{n}}_{\text{MF}} (\underline{\mathbf{A}}^{-1} \underline{\mathbf{n}}_{\text{MF}})^{\text{H}} \right\} = \underline{\mathbf{A}}^{-1} \underline{\mathbf{R}}_{\text{n}} (\underline{\mathbf{A}}^{-1})^{\text{H}}. \quad (3.37)$$

Finally, substituting (2.20) in (3.37), we can write

$$\underline{\mathbf{R}}_{\text{n,ZF}} = N_0 (\underline{\mathbf{A}}^{-1})^{\text{H}}. \quad (3.38)$$

With the ZF-BLE and the definition of the equivalent noise at the output of the post-processing stage, the system model of Fig. 3.7 can be further simplified as shown in Fig. 3.8. The model of Fig. 3.8 fits to the model used to derive (3.33) if the noise samples $n_{\text{ZF},n}$ of $\underline{\mathbf{n}}_{\text{ZF}}$ of (3.35) are statistically independent zero-mean Gaussian random variables. Therefore, we assume the presence of an interleaver which scrambles the transmitted data symbols at the transmitter side. We also assume the presence of a de-interleaver at the receiver which matches the interleaver. If the interleavers are properly designed, then the

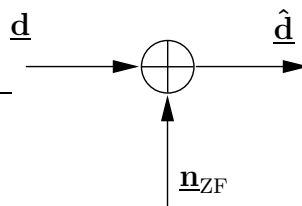


Fig. 3.8. Equivalent representation of the system model introduced in Chapter 2; ZF-BLE.

noise samples at the receiver can be considered to be uncorrelated.

From (3.38) and Fig. 3.8, we obtain the SNR

$$\gamma_{\text{ZF},n} = \frac{\text{E} \{ |\underline{d}_n|^2 \}}{N_0 \left[(\underline{\mathbf{A}}^{-1})^{\text{H}} \right]_{n,n}} = \frac{\text{E} \{ |d_n|^2 \} \left[\underline{\mathbf{A}}^{\text{H}} \right]_{n,n}}{N_0 \left[\underline{\mathbf{A}}^{\text{H}} \right]_{n,n} \left[(\underline{\mathbf{A}}^{-1})^{\text{H}} \right]_{n,n}} \quad (3.39)$$

of the final estimate $\hat{\underline{d}}_n$. From [Kle96] and from (2.20), the SNR at the output of the MF reads

$$\gamma_{\text{MF},n} = \text{E} \{ |\underline{d}_n|^2 \} [\underline{\mathbf{A}}^H \underline{\mathbf{R}}_n^{-1} \underline{\mathbf{A}}]_{n,n} = \text{E} \{ |\underline{d}_n|^2 \} N_0^{-1} [\underline{\mathbf{A}}^H]_{n,n} \quad (3.40)$$

so that (3.39) can be re-written as

$$\gamma_{\text{ZF},n} = \frac{\gamma_{\text{MF},n}}{\left[(\underline{\mathbf{A}}^{-1})^H \right]_{n,n} [\underline{\mathbf{A}}^H]_{n,n}}. \quad (3.41)$$

Since the inverse of the Hermitian is the Hermitian of the inverse, from (2.68) we can write (3.41) as

$$\gamma_{\text{ZF},n} = \frac{\gamma_{\text{MF},n}}{\delta_{\text{ZF},n}}. \quad (3.42)$$

From (3.42), we infer that the SNR of the equivalent model of Fig. 3.8 can be read as the ratio between the SNR γ_{MF} at the output of the MF and the SNR-degradation δ_{ZF} determined by the ZF-BLE. However, we notice that (3.42) depends on the transmitted symbol index n . The SNR-degradation δ defined in (2.68) is the average value of $\delta_{\text{ZF},n}$. Since, due to the presence of the interleaver/de-interleaver the noise samples are uncorrelated, we can infer that each noise sample has the same statistics. Therefore, the SNR γ_n becomes independent on the symbol index n , and (3.42) reads

$$\gamma_{\text{ZF}} = \frac{\gamma_{\text{MF}}}{\delta_{\text{ZF}}}. \quad (3.43)$$

The increment in the SNR is due to the noise enhancement caused by the ZF-BLE when removing the interference.

This additional interference is introduced by the reduction of T and/or F . However, the reduction of T and/or F does not only increase the SNR-degradation δ of (2.68), but also increases the rate R of (2.57) which influences the channel capacity C of (3.33). Indeed, (3.33) is derived [Pro95] under the assumption that the total number of transmitted symbols N is $N = B_{\text{tot}} T_{\text{tot}}$, i.e. the rate $R = 1$. Following the derivation of (3.33) in [Pro95] for a band limited channel, and writing $N = R B_{\text{tot}} T_{\text{tot}}$, cf. (2.57), we can show the dependency of the channel capacity on the rate R of (2.57).

From (3.33), (3.43) and $N = R B_{\text{tot}} T_{\text{tot}}$ we can approximate the channel capacity C of the system model of Fig. 3.8 as

$$C \approx R \cdot \text{ld} \left(1 + \frac{\gamma_{\text{MF}}}{\delta_{\text{ZF}}} \right). \quad (3.44)$$

On the one hand, the channel capacity C of (3.44) increases with the increment of the rate R of (2.57), on the other hand it decreases with the increasing of the SNR-degradation δ of (2.68). It also depends on the specific value of the SNR γ_{MF} at the output of the MF. When the Nyquist conditions are satisfied, the system matrix $\underline{\mathbf{A}}$ of (2.14) is diagonal, the

rate $R = 1$ and the SNR-degradation $\delta = 1$ so that (3.44) reduces to (3.33) as expected. When the rate R of (2.57) significantly increases, the SNR-degradation δ of (2.68) diverges towards infinity. For very large δ_{ZF} we can linearly approximate the logarithmic to obtain

$$C|_{\delta \rightarrow +\infty} \approx R \cdot \frac{\gamma_{MF}}{\delta_{ZF}}. \quad (3.45)$$

R of (2.57) is upper bounded, cf. (3.25), δ of (2.68) tends to infinity, therefore the channel capacity C of (3.44) tends to zero. This could be expected because, if R is very large, then T and/or F are very small, and we are trying to transmit all the data at the same time location and at the same frequency location. Under these conditions, the data symbol receive signatures $\underline{c}_n(t)$ of (2.2) could be separated at the receiver only if they have particular properties, e.g. they are spreading sequences. Within the considered scope of parameters, cf. Table 3.9, when F and T are very close to zero, the channel capacity is zero because there is no possibility to establish a reliable communication.

From (3.44), we infer that the proposed reduction of T and F can be interpreted as a possible way to influence the channel capacity C . There might be some configurations allowing a specific combination of R of (2.57) and δ of (2.68) so that C of (3.44) is larger than C of (3.33). We investigate this aspect through simulation results combining the rate R of (2.57) and the SNR-degradation δ of (2.68) obtained for the scope of parameters presented in this chapter and summarized in Table 3.9.

4 Simulations

4.1 General

Chapter 4 presents the simulation results for the considered systems under the assumptions of Chapter 3. In particular, the parameter values of Table 3.9 are considered. The overall set of presented figures is summarized in Table 4.1, cf. Table 3.9. For all configu-

Table 4.1. List of functions and figures for SC, MC and HY systems

| $c_0(t)$ | SC | | MC | | HY | |
|---------------------------------------|-------------|-----------|-------------|------------------|------------------------------|------------|
| | Function | Figure | Function | Figure | Function | Figure |
| rect of (3.10) | $R(T)$ | Fig. 4.1a | $R(F)$ | Fig. 4.8a | $R(F, T)$ | Fig. 4.14a |
| | $\delta(T)$ | Fig. 4.1b | $\delta(F)$ | Fig. 4.8b | $\delta_{\text{ZF}}(F, T)$ | Fig. 4.14b |
| | $C(T)$ | Fig. 4.23 | | | $\delta_{\text{MMSE}}(F, T)$ | Fig. 4.15a |
| | | | | | $\delta(F, T R)$ | Fig. 4.15b |
| | | | | | $C(F, T)$ | Fig. 4.32 |
| sinc of (3.13) | $R(T)$ | Fig. 4.2a | $R(F)$ | Fig. 4.9a | $R(F, T)$ | Fig. 4.16a |
| | $\delta(T)$ | Fig. 4.2b | $\delta(F)$ | Fig. 4.9b | $\delta_{\text{ZF}}(F, T)$ | Fig. 4.16b |
| | $C(T)$ | Fig. 4.24 | | | $\delta_{\text{MMSE}}(F, T)$ | Fig. 4.17a |
| | | | | | $\delta(F, T R)$ | Fig. 4.17b |
| | | | | | $C(F, T)$ | Fig. 4.33 |
| gauss of (3.18), $B_0 = 0.7$ | $R(T)$ | Fig. 4.3a | $R(F)$ | Fig. 4.11a | $\delta(F, T R)$ | Fig. 4.20a |
| | $\delta(T)$ | Fig. 4.3b | $\delta(F)$ | Fig. 4.11b | $C(F, T)$ | Fig. 4.34 |
| | $C(T)$ | Fig. 4.25 | | | | |
| gauss of (3.18), $B_0 = 0.9$ | $R(T)$ | Fig. 4.4a | | | $R(F, T)$ | Fig. 4.18a |
| | $\delta(T)$ | Fig. 4.4b | | | $\delta_{\text{ZF}}(F, T)$ | Fig. 4.18b |
| | $C(T)$ | Fig. 4.26 | | | $\delta_{\text{MMSE}}(F, T)$ | Fig. 4.19a |
| | | | | | $\delta(F, T R)$ | Fig. 4.19b |
| | | | | | $C(F, T)$ | Fig. 4.35 |
| gauss of (3.18), $B_0 = 1.2$ | $R(T)$ | Fig. 4.5a | | | $\delta(F, T R)$ | Fig. 4.20b |
| | $\delta(T)$ | Fig. 4.5b | | | $C(F, T)$ | Fig. 4.36 |
| | $C(T)$ | Fig. 4.27 | | | | |
| rrcos of (3.21), $\alpha = 0.1$ | $R(T)$ | Fig. 4.6a | $R(F)$ | Fig. 4.12a | $R(F, T)$ | Fig. 4.21a |
| | $\delta(T)$ | Fig. 4.6b | $\delta(F)$ | Fig. 4.12b | $\delta_{\text{ZF}}(F, T)$ | Fig. 4.21b |
| | $C(T)$ | Fig. 4.28 | $C(F)$ | Fig. 4.30 | $\delta_{\text{MMSE}}(F, T)$ | Fig. 4.22a |
| | | | | $\delta(F, T R)$ | Fig. 4.22b | |
| | | | | $C(F, T)$ | Fig. 4.37 | |
| rrcos of (3.21), $\alpha = 0.3$ | $R(T)$ | Fig. 4.7a | $R(F)$ | Fig. 4.13a | | |
| | $\delta(T)$ | Fig. 4.7b | $\delta(F)$ | Fig. 4.13b | | |
| | $C(T)$ | Fig. 4.29 | $C(F)$ | Fig. 4.31 | $C(F, T)$ | Fig. 4.38 |

rations we assume an AWGN channel, cf. Subsection 3.3.6, and the number of transmit

symbols $N = 64$. For HY systems, we consider the number of sub-carriers $N_f = 8$ and the number of time-slots $N_t = 8$, cf. Subsection 3.3.4. For SC systems, we report the rate R of (2.57), the SNR-degradation δ of (2.68) and (2.76) and the channel capacity C of (3.44) for each choice of the basic transmit signature $\underline{c}_0(t)$, cf. Table 3.3. The independent variable is the normalized time separation T/T_{ref} , cf. (3.24), with $T_{\text{ref}} = 1$. For MC systems, we consider the rate R of (2.57) and the SNR-degradation δ of (2.68) and (2.76) for all the basic transmit signatures $\underline{c}_0(t)$, cf. Table 3.3, but the gauss of (3.18) with $B_0 = 0.9$ and the gauss of (3.18) with $B_0 = 1.2$. The independent variable is the normalized frequency separation F/F_{ref} , cf. (3.24), with $F_{\text{ref}} = 1$. The channel capacity C of (3.44) is shown only for the rrcos basic transmit signature $\underline{c}_0(t)$ of (3.21) to avoid redundant simulation results. For the same reason, for HY systems, we do not report all the attained results. Moreover, to better present the three dimensional surfaces of the rate R of (2.57) and the SNR-degradation δ of (2.68) and (2.76), for each basic transmit signature $\underline{c}_0(t)$, cf. Table 3.3, we present five figures instead of the three figures used for SC and MC, cf. Table 4.1.

The rest of this chapter is organized as follows. We consider the rate R of (2.57) and the SNR-degradation δ of (2.68) and (2.76) of SC systems in Section 4.2, of MC systems in Section 4.3, and of HY systems in Section 4.4. In Section 4.5, we present the simulation results to evaluate the proposed approach as presented in Section 3.4 for SC, MC and HY systems.

4.2 Single carrier systems

4.2.1 Rectangular basic transmit signature

In Fig. 4.1 we depict the simulation results attained with an SC system with a rect basic transmit signature $\underline{c}_0(t)$ of (3.10). The rate R of (2.57) in Fig. 4.1a and the SNR-degradation δ of (2.68) and (2.76) in Fig. 4.1b are reported versus the time separation T/T_{ref} , $T_{\text{ref}} = 1$. In Fig. 4.1a, for $T = 1$, the rate R of (2.57) is $R \approx 1$ and the system does not suffer from any ISI in the presence of an AWGN channel. If T decreases, then R of (2.57) increases, since the total time occupation T_{tot} decreases, cf. (2.27). In (3.25) we have determined the upper bound of the rate R . This is not shown in Fig. 4.1a because it is larger than the selected scale axis. However, we verified that the simulation results perfectly match the bound determined in (3.25). The increment of the rate R of (2.57) is, as expected, inversely proportional to the time separation T , cf. (2.59). In Fig. 4.1b, we depict the SNR-degradation δ of the ZF-BLE and the MMSE-BLE. For the latter, since it depends on the one sided noise power spectral density N_0 , cf. (2.76), we consider two values of SNR, i.e. SNR=10 dB and SNR=30 dB. In Fig. 4.1b only two curves can be seen, because for SNR=30 dB the MMSE-BLE and the ZF-BLE perform almost the

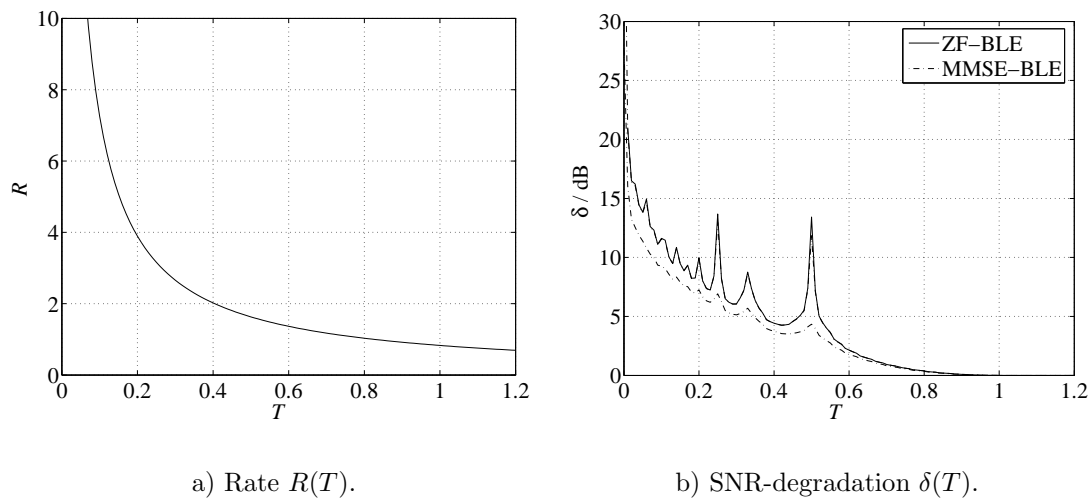


Fig. 4.1. $R(T)$ and $\delta(T)$ of an SC system with a rect basic transmit signature $\underline{c}_0(t)$ of (3.10) versus the time separation T ; $T_{\text{ref}} = 1$; ZF-BLE and MMSE-BLE; SNR=10 dB and SNR=30 dB; $N = 64$; AWGN channel.

same and cannot be distinguished with the chosen scale axis. This aspect was also shown in (2.85), where we derived the behaviour of the MMSE-BLE for very small values of N_0 . Also the bounds derived in (2.90) have been verified through simulation results. The SNR-degradation δ of Fig. 4.1b is $\delta = 0$ dB for $T \geq 1$, i.e. when there is no ISI and there is no difference between the SNR γ_{MF} at the output of the MF and the SNR γ_{ZF} at the output of the ZF-BLE. With the decreasing of T , δ of (2.68) and (2.76) increases in a quite particular way. There are some peaks at given values of T which were not expected and had not been predicted through the theoretical model. We notice that the main peaks occur at the values $T = 0.5$, $T = 0.33$ and $T = 0.25$. By recalling that the rect of (3.10) has a duration of $T = 1$, then it is straightforward to verify that the peaks correspond to the minimum value of time separation T for a fixed number of interfering symbols. If there are only two interfering symbols, i.e. the previous and the following symbols overlap with the current symbol, then T must be larger than $T = 0.5$. As soon as $T < 0.5$ two previous symbols and two following symbols are influencing the current symbol. In other words, when the number of interference symbols changes we observe a peak in the SNR-degradation δ of (2.68) and (2.76). We propose a possible interpretation of the presence of this result in Chapter 5 by observing the structure of the system matrix $\underline{\mathbf{A}}$ of (2.14). Besides the peaks, the SNR-degradation δ increases for smaller values of the time separation T because of the additional interference generated by the time overlapping data symbol specific transmit signatures $\underline{c}_n(t)$ of (2.24).

4.2.2 Sinc shaped basic transmit signature

Fig. 4.2 shows the rate R of (2.57) and the SNR-degradation δ of (2.68) and (2.76) versus the time separation T/T_{ref} , $T_{\text{ref}} = 1$, of an SC system with a sinc basic transmit signature

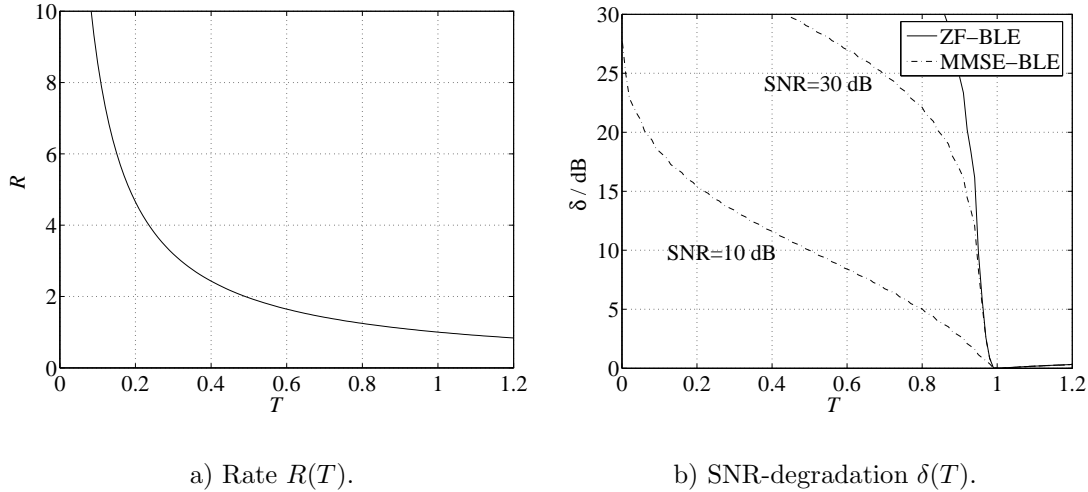


Fig. 4.2. $R(T)$ and $\delta(T)$ of an SC system with a sinc basic transmit signature $\underline{c}_0(t)$ of (3.13) versus the time separation T ; $T_{\text{ref}} = 1$; ZF-BLE and MMSE-BLE; SNR=10 dB and SNR=30 dB; $N = 64$; AWGN channel.

$\underline{c}_0(t)$ of (3.13). The considered functions are the same as the functions in Fig. 4.1 and they show the same tendency. By reducing T , the rate R of (2.57) and the SNR-degradation δ of (2.68) and (2.76) increase. Nevertheless, we can observe some differences. For a given value of T , the rate R of Fig. 4.2a is slightly higher than the rate R of Fig. 4.1a. This could be expected from (2.58) and especially from (2.59) where the rate R of an SC system under the assumption of N large enough is shown to be $R \approx 1/(B_0 T)$. Then, since the 3 dB bandwidth B_0 of (3.15) of the sinc of (3.13) is smaller than the 3 dB bandwidth B_0 of (3.12) of the rect of (3.10), it has to be expected that for the same value of T the rate R of Fig. 4.2a is larger than the rate R of Fig. 4.1a. The SNR-degradation δ of Fig. 4.2b significantly differs from the SNR-degradation δ of Fig. 4.1b. It assumes much higher values. For the ZF-BLE it grows very fast with decreasing T , since the system matrix $\underline{\mathbf{A}}$ of (2.14) tends to singularity. The MMSE-BLE shows better performance than the ZF-BLE both in the case of SNR=30 dB and in the case of SNR=10 dB. As in Subsection 4.2.1, the bounds of (2.90) are verified through simulation results. For $T = 1$ we notice that the SNR-degradation is $\delta = 0$ dB, but for $T > 1$ it does not maintain the zero value as in the case considered in Fig. 4.1b. This is due to the characteristics of the sinc of (3.13) which satisfies the Nyquist conditions of no interference in AWGN only if the zeros of the sinc of (3.13) are located exactly at the multiples of the time separation T . Therefore, for $T > 1$, ISI arises and the SNR-degradation becomes $\delta > 0$ dB. By comparing Fig. 4.1 with Fig. 4.2, we can say that for SC systems the choice of a time limited basic transmit signature $\underline{c}_0(t)$ such as

the rect of (3.10) should be preferred to the choice of a frequency limited basic transmit signature $\underline{c}_0(t)$ such as the sinc of (3.13). This is due to the fact that in an SC system, by reducing the time separation T to increase the resource usage, we introduce an overlap among the data symbol specific transmit signatures $\underline{c}_n(t)$ of (2.24). If the $\underline{c}_n(t)$ of (2.24) are time limited, then the overlap is limited to the adjacent transmitted signatures. If the $\underline{c}_n(t)$ of (2.24) are frequency limited and, as a consequence time unlimited, then the overlapping among the data symbol specific transmit signatures $\underline{c}_n(t)$ of (2.24) involves many signatures and generates a much higher amount of interference.

4.2.3 Gaussian basic transmit signature

In Figs. 4.3 to 4.5 we report the rate R of (2.57) and the SNR-degradation δ of (2.68)

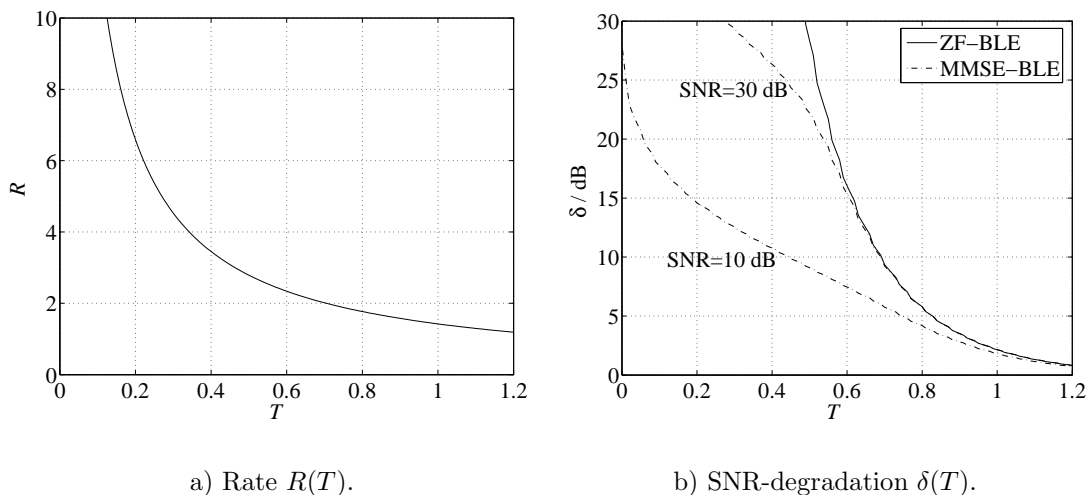


Fig. 4.3. $R(T)$ and $\delta(T)$ of an SC system with a gauss basic transmit signature $\underline{c}_0(t)$ of (3.18) versus the time separation T ; $T_{\text{ref}} = 1$; $B_0 = 0.7$; ZF-BLE and MMSE-BLE; SNR=10 dB and SNR=30 dB; $N = 64$; AWGN channel.

and (2.76) of an SC system with a gauss basic transmit signature $\underline{c}_0(t)$ of (3.18) versus the time separation T/T_{ref} , $T_{\text{ref}} = 1$. We consider three different values of standard deviation σ so that the three considered Gaussian functions have different 3 dB bandwidth B_0 of (3.20) as shown in Table 3.7. A gauss of (3.18) with $B_0 = 0.7$ is considered in Fig. 4.3, a gauss of (3.18) with $B_0 = 0.9$ in Fig. 4.4 and a gauss of (3.18) with $B_0 = 1.2$ in Fig. 4.5. For all the three figures the performance is similar. The rate R of (2.57) and the SNR-degradation δ of (2.68) and (2.76) increase with decreasing T . Moreover, as explained in the comparison between the rate R in Fig. 4.1a and in Fig. 4.2a, the rate R decreases with the increasing of the 3 dB bandwidth B_0 . This was expected from (2.59). Let us now consider Fig. 4.3a and the rate value $R = 2$. $R = 2$ is obtained by a time separation $T \approx 0.7$. By reporting the same time separation in Fig. 4.3b, we observe that for $T \approx 0.7$,

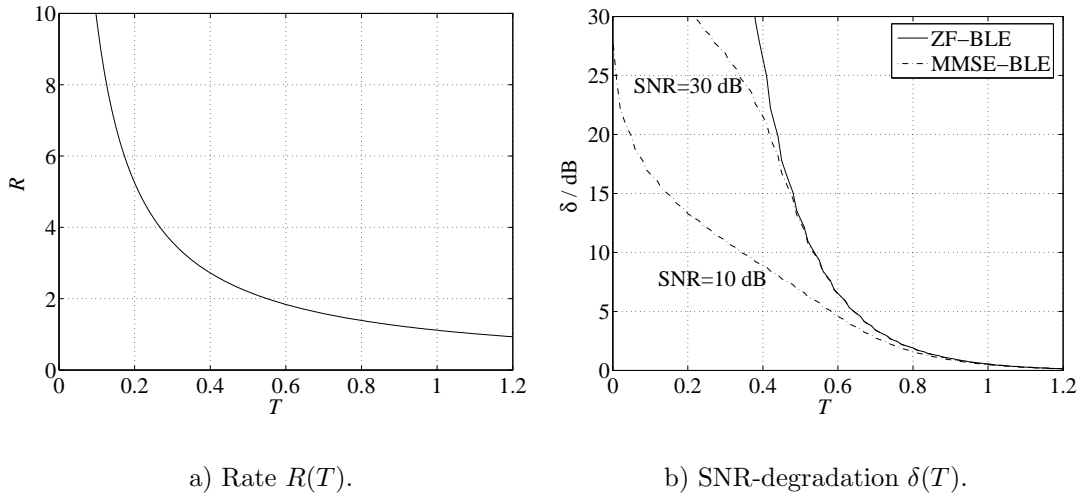


Fig. 4.4. $R(T)$ and $\delta(T)$ of an SC system with a gauss basic transmit signature $\underline{c}_0(t)$ of (3.18) versus the time separation T ; $T_{\text{ref}} = 1$; $B_0 = 0.9$; ZF-BLE and MMSE-BLE; SNR=10 dB and SNR=30 dB; $N = 64$; AWGN channel.

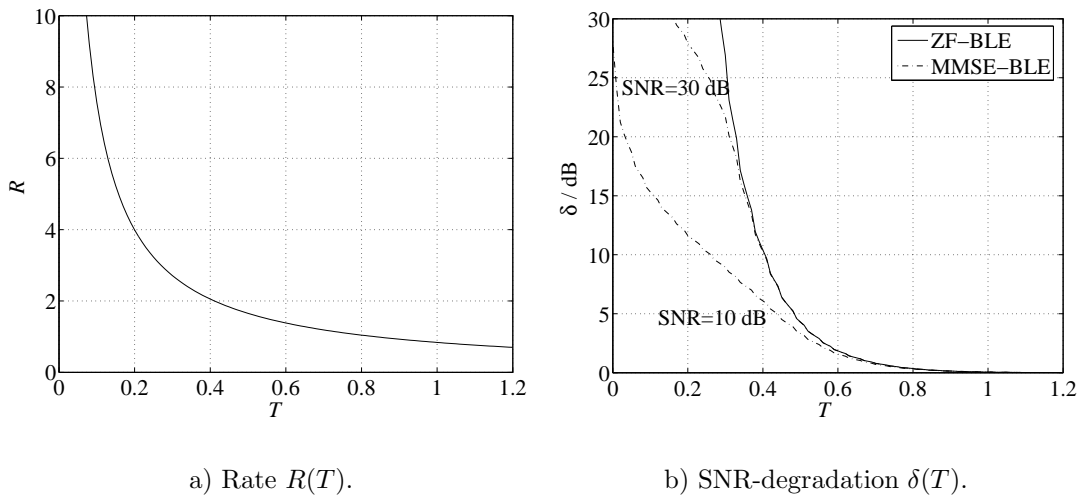


Fig. 4.5. $R(T)$ and $\delta(T)$ of an SC system with a gauss basic transmit signature $\underline{c}_0(t)$ of (3.18) versus the time separation T ; $T_{\text{ref}} = 1$; $B_0 = 1.2$; ZF-BLE and MMSE-BLE; SNR=10 dB and SNR=30 dB; $N = 64$; AWGN channel.

the SNR-degradation $\delta \approx 10$ dB is obtained. In this case δ indicates the SNR-degradation δ given by the ZF-BLE and by the MMSE-BLE with SNR=30 dB. We can say that in an SC system with a gauss basic transmit signature $\underline{c}_0(t)$ of (3.18) having $B_0 = 0.7$, increasing the rate R of (2.57) to $R = 2$ corresponds to an SNR-degradation $\delta \approx 10$ dB. In other words, if we aim at transmitting at $R = 2$ we should increase the transmitted power of 10 dB to maintain the same system performance in terms of average bit error probability P_b . Let us now focus on Fig. 4.4a and consider the same value of $R = 2$. In

this case, since the 3 dB bandwidth B_0 is larger, the rate $R = 2$ is achieved at a smaller time separation, i.e. $T \approx 0.53$, cf. (2.59). By reporting $T \approx 0.53$ in Fig. 4.4b, we notice that the SNR-degradation is $\delta \approx 10$ dB. Therefore, also with a larger B_0 , for a given value of the rate R of (2.57), the corresponding value of SNR-degradation δ of (2.68) is the same. Fig. 4.5 confirms the results of Figs. 4.3 and 4.4. The value $R = 2$ is given by the time separation $T \approx 0.4$ which corresponds to an SNR-degradation $\delta \approx 10$ dB. By investigating the results in Figs. 4.3 to 4.5, we infer that the dependency between R of (2.57) and δ of (2.68) and (2.76) in an SC system with gauss basic transmit signature $\underline{c}_0(t)$ of (3.18) is independent of the standard deviation σ of the considered Gaussian function. We can see this also from the analytical derivation of the system matrix $\underline{\mathbf{A}}$ of (2.14) in the case of a gauss basic transmit signature $\underline{c}_0(t)$ of (3.18), cf. Subsection 3.3.4. Based on the results presented in Subsection 3.3.4, we show that, if we express the SNR-degradation δ of (2.68) and (2.76) versus the rate R in an SC system with a gauss basic transmit signature $\underline{c}_0(t)$ of (3.18), then δ does not depend on σ . From (2.59) and (3.20) we can write the rate R of an SC system as

$$R = \frac{\pi \sigma T_{\text{ref}}}{T \sqrt{2 \ln(2)}} \quad (4.1)$$

We can invert the order of (4.1) and write the time separation T as

$$\frac{T}{T_{\text{ref}}} = \frac{\pi \sigma}{R \sqrt{2 \ln(2)}}. \quad (4.2)$$

Then, by substituting (4.2) in (3.31), we can write the element of the system matrix $\underline{\mathbf{A}}$ of (2.14) in position (n, n') as

$$\underline{A}_{n,n'} = \exp \left[- \left(\frac{\pi \Delta_t(n, n')}{2R \sqrt{2 \ln(2)}} \right)^2 \right]. \quad (4.3)$$

(4.3) shows that the system matrix $\underline{\mathbf{A}}$ in SC systems with a gauss basic transmit signature $\underline{c}_0(t)$ of (3.18) does not depend on the standard deviation σ of $\underline{c}_0(t)$ of (3.18). Since the SNR-degradation δ of (2.68) depends only on the system matrix $\underline{\mathbf{A}}$ of (2.14) and the SNR-degradation δ of (2.76) depends only on the system matrix $\underline{\mathbf{A}}$ of (2.14) and on the one sided noise power spectral density N_0 , it follows that δ does not depend on σ . Therefore, the trade-off between R of (2.57) and the corresponding SNR-degradation δ of (2.68) and (2.76) is independent of the σ of the gauss of (3.18). However, we recall that the proposed simplification holds true only if N is large enough. If we use the exact expression of the rate R of (2.58), then the dependency on σ remains as well as the dependency on the number N of transmitted symbols.

4.2.4 Square root raised cosine basic transmit signature

In Figs. 4.6 and 4.7 we consider an SC system with an rrcos basic transmit signature $\underline{c}_0(t)$

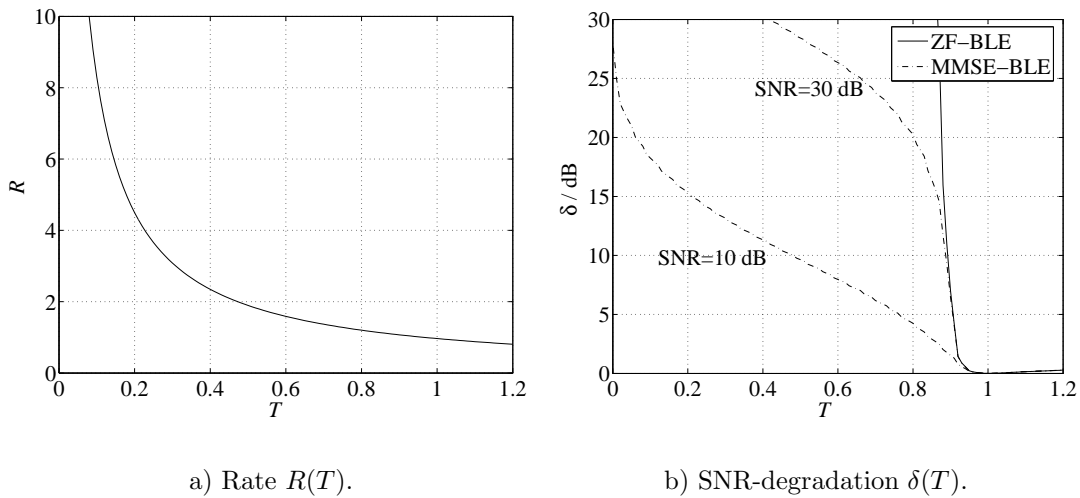


Fig. 4.6. $R(T)$ and $\delta(T)$ of an SC system with an rrcos basic transmit signature $\underline{c}_0(t)$ of (3.21) versus the time separation T ; $T_{\text{ref}} = 1$; $\alpha = 0.1$; ZF-BLE and MMSE-BLE; SNR=10 dB and SNR=30 dB; $N = 64$; AWGN channel.

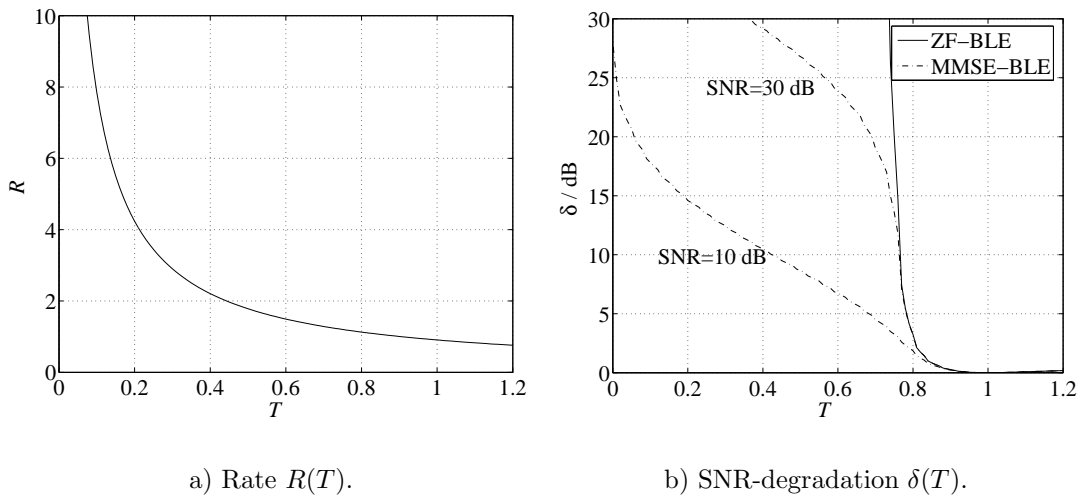


Fig. 4.7. $R(T)$ and $\delta(T)$ of an SC system with an rrcos basic transmit signature $\underline{c}_0(t)$ of (3.21) versus the time separation T ; $T_{\text{ref}} = 1$; $\alpha = 0.3$; ZF-BLE and MMSE-BLE; SNR=10 dB and SNR=30 dB; $N = 64$; AWGN channel.

of (3.21) with roll-off factors $\alpha = 0.1$ and $\alpha = 0.3$, respectively. In both cases the rate R of (2.57) and the SNR-degradation δ of (2.68) and (2.76) increase with the decreasing of the time separation T . The roll-off factor α influences the results since it changes the characteristics of the rrcos basic transmit signature $\underline{c}_0(t)$ of (3.21). Moreover, the rrcos of (3.21) is similar to the sinc of (3.13) and this is confirmed by comparing Figs. 4.6 and 4.7 with Fig. 4.2. A slightly better performance can be observed in the rrcos case. The SNR-degradation δ of (2.68) and (2.76) diverges for smaller values of T with respect to

the sinc of (3.13). The rate R is very similar for sinc of (3.13) and rrcos of (3.21) since they have very similar 3 dB bandwidths B_0 , cf. (3.15) and (3.23). Therefore, the slight difference in the SNR-degradation δ curves cannot be justified as in the case of gauss of (3.18), i.e. by resorting to the jointly consideration of R of (2.57) and δ of (2.68), cf. Subsection 4.2.3. If we take a closer look at Figs. 4.6b and 4.7b we notice that in Fig. 4.6b the SNR-degradation δ starts to increase significantly when $T \approx 0.9$, while in Fig. 4.7b the same behaviour can be observed for $T \approx 0.8$. We can explain this behaviour by recalling that with the increment of α the 3 dB bandwidth B_0 of the rrcos basic transmit signature $\underline{c}_0(t)$ of (3.21) increases, cf. (3.23). Moreover, the time duration T_0 is reduced since the time decay of the rrcos of (3.21) is a function of α , cf. (3.21). Therefore, the amount of interference induced by the reduction of T depends on α . The smaller the α , the higher the SNR-degradation δ of (2.68) and (2.76), because the data symbol specific signatures $\underline{c}_n(t)$ overlap more significantly.

Based on the simulation results presented in the SC case, we can conclude that the most interesting results are given by the choice of the rect basic transmit signature $\underline{c}_0(t)$ of (3.10) for which the values of SNR-degradation δ of (2.68) and (2.76) are quite promising. The presence of the peaks requires an additional reasoning that will be made in Chapter 5. With the choice of a gauss basic transmit signature $\underline{c}_0(t)$ of (3.18), we have also some interesting results and we have shown that they are independent of the choice of the variance σ of the Gaussian function. In the other cases, the performance is not satisfactory showing an SNR-degradation δ which diverges to very high values as soon as $T < 1$. We infer that for an SC system the best solution is given by the deployment of a time limited basic transmit signature $\underline{c}_0(t)$. With the reduction of the time separation T , if the basic transmit signature $\underline{c}_0(t)$ is time limited, the interference influences only a finite number of adjacent symbols. In contrast, if the basic transmit signature $\underline{c}_0(t)$ is time unlimited, then the reduction of T generates interference on a much higher number of data symbol specific transmit signatures $\underline{c}_n(t)$ so causing a much worse SNR-degradation δ of (2.68) and (2.76).

4.3 Multi-carrier systems

4.3.1 Rectangular basic transmit signature

In Fig. 4.8, a MC system with a rect basic transmit signature $\underline{c}_0(t)$ of (3.10) is assumed. The SNR-degradation δ of (2.68) and (2.76) is different from Fig. 4.1b, i.e. the SC system with a rect basic transmit signature $\underline{c}_0(t)$ of (3.10). The performance obtained in Fig. 4.8 is the same performance of the SC system with a sinc basic transmit signature $\underline{c}_0(t)$ of (3.13) depicted in Fig. 4.2. The similarity is due to the fact that the reduction of T in an SC system with a sinc of (3.13) generates the same kind of interference as the reduction

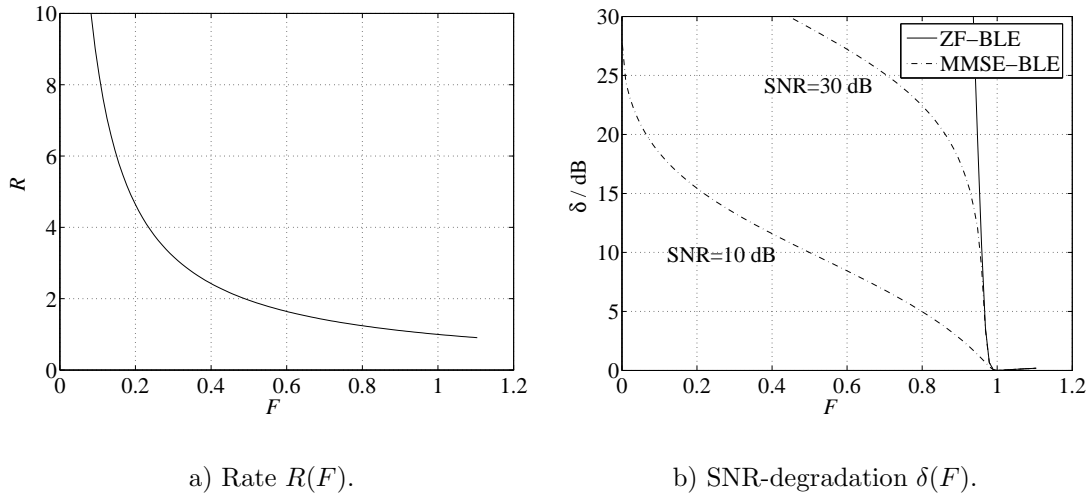


Fig. 4.8. $R(F)$ and $\delta(F)$ of an MC system with a rect basic transmit signature $\underline{c}_0(t)$ of (3.10) versus the frequency separation F ; $F_{\text{ref}} = 1$; ZF-BLE and MMSE-BLE; SNR=10 dB and SNR=30 dB; $N = 64$; AWGN channel.

of the frequency separation F in an MC system with a rect of (3.10). This is due to the duality of the rect of (3.10) and the sinc of (3.13) with respect to the Fourier transform, i.e. the Fourier transform of a $\text{rect}(t)$ is a $\text{sinc}(f)$, [Car96]. This intuitive reasoning can be supported by mathematical derivation by determining the system matrix $\underline{\mathbf{A}}$ of (2.14) in a closed form for the MC system with a rect basic transmit signature $\underline{c}_0(t)$ of (3.10) and for an SC system with a sinc basic transmit signature $\underline{c}_0(t)$ of (3.13). We consider the two cases separately.

We first consider an MC system, with a basic transmit signature (3.10),

$$\underline{c}_0(t) = \frac{1}{\sqrt{T_{\text{ref}}}} \text{rect}\left(\frac{t}{T_{\text{ref}}}\right). \quad (4.4)$$

By applying the results of Subsection 2.7.2 to the particular case of an MC system in which $\Delta_t(n, n')$ of (2.120) is always $\Delta_t(n, n') = 0$, from (2.127)-(2.129) we can write the elements of the system matrix $\underline{\mathbf{A}}$ of (2.14) as

$$\underline{A}_{n,n'} = \hat{\underline{C}}_0(f) \Big|_{f=(n-n')F}. \quad (4.5)$$

From (2.127), (2.128), (4.4) and the properties of the Fourier transform [Car96] we infer that

$$\hat{\underline{C}}_0(f) = \text{sinc}(fT_{\text{ref}}). \quad (4.6)$$

From (4.5) and (4.6) and by recalling that $T_{\text{ref}} = 1/F_{\text{ref}}$, cf. (3.4), we obtain

$$\underline{A}_{n,n'} = \text{sinc}\left((n-n')\frac{F}{F_{\text{ref}}}\right). \quad (4.7)$$

(4.7) is the analytical expression of the system matrix $\underline{\mathbf{A}}$ of (2.14) of an MC system deploying a rect basic transmit signature $\underline{c}_0(t)$ of (3.10) with energy equal to one.

Then, we consider an SC system with a basic transmit signature (3.13),

$$\underline{c}_0(t) = \frac{1}{\sqrt{T_{\text{ref}}}} \text{sinc} \left(\frac{t}{T_{\text{ref}}} \right) \quad (4.8)$$

with Fourier transform defined as [Car96]

$$\underline{C}_0(f) = \sqrt{T_{\text{ref}}} \text{rect}(T_{\text{ref}}f). \quad (4.9)$$

For SC systems, cf. Subsection 2.7.2, the elements of the system matrix $\underline{\mathbf{A}}$ of (2.14) can be written as

$$\underline{A}_{n,n'} = \int_{-\infty}^{+\infty} \underline{c}_0(t) \underline{c}_0(t - (n - n')T) dt \quad (4.10)$$

If $\underline{c}_0(t) = \underline{c}_0(-t)$ and with the change of variable $\tau = t - (n - n')T$, (4.10) can be written as

$$\underline{A}_{n,n'} = \int_{-\infty}^{-\infty} \underline{c}_0(\tau) \underline{c}_0(-(n - n')T - \tau) d\tau = \left(\int_{-\infty}^{-\infty} \underline{c}_0(\tau) \underline{c}_0(t - \tau) d\tau \right) \Big|_{t=-(n-n')T} \quad (4.11)$$

which is the convolution evaluated at the time instances $-(n - n')T$. Taking the sampling operation out of the integral operation is permitted by the regularity of the basic transmit signatures $\underline{c}_0(t)$ under consideration. The convolution can be interpreted as the inverse Fourier transform of the product of the Fourier transform of the convolved functions [Car96]. Then, from (4.9) and (4.11) we obtain

$$\underline{A}_{n,n'} = \left(\int_{-\infty}^{-\infty} \underline{C}_0(f) \underline{C}_0(f) \exp(j2\pi ft) df \right) \Big|_{t=-(n-n')T}. \quad (4.12)$$

By substituting (4.9) in (4.12), with some algebra we obtain

$$\underline{A}_{n,n'} = \text{sinc} \left((n - n') \frac{T}{T_{\text{ref}}} \right). \quad (4.13)$$

(4.7) and (4.13) are equal if $T/T_{\text{ref}} = F/F_{\text{ref}}$.

We have shown that an MC system with a rect basic transmit signature $\underline{c}_0(t)$ of (3.10) and an SC system with a sinc basic transmit signature $\underline{c}_0(t)$ of (3.13) have the same system matrix $\underline{\mathbf{A}}$ of (2.14) given the same value of frequency separation F/F_{ref} and time separation T/T_{ref} , respectively. Therefore, the SNR-degradation δ of (2.68) and (2.76) of the MC system with a rect of (3.10) and of an SC system with a sinc of (3.13) has the same dependency on F and T , respectively.

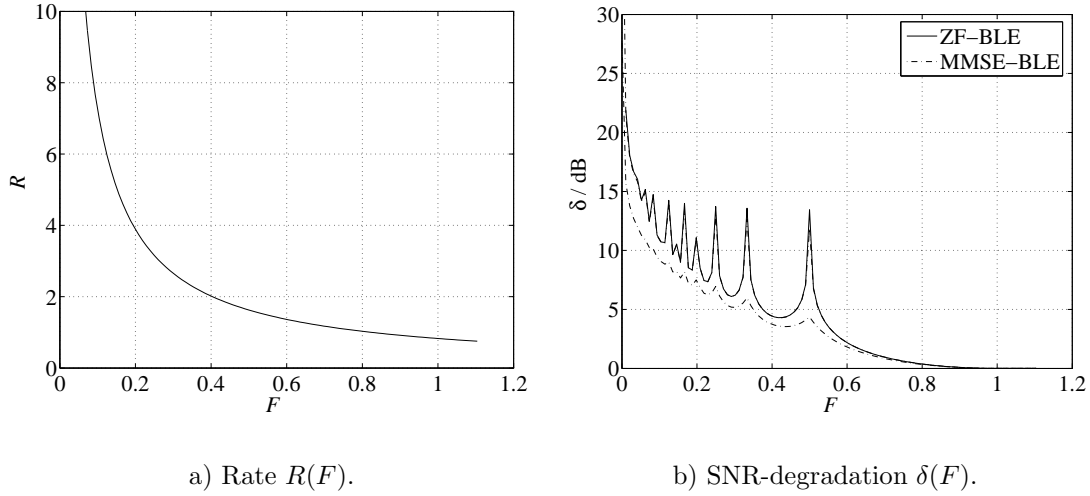


Fig. 4.9. $R(F)$ and $\delta(F)$ of an MC system with a sinc basic transmit signature $\underline{c}_0(t)$ of (3.13) versus the frequency separation F ; $F_{\text{ref}} = 1$; ZF-BLE and MMSE-BLE; SNR=10 dB and SNR=30 dB; $N = 64$; AWGN channel.

4.3.2 Sinc shaped basic transmit signature

In Fig. 4.9 the rate R of (2.57) and the SNR-degradation δ of (2.68) and (2.76) of an MC system with a sinc basic transmit signature $\underline{c}_0(t)$ of (3.13) are shown. The results are very similar to the results of Fig. 4.1 in which the rate R of (2.57) and the SNR-degradation δ of (2.68) and (2.76) of an SC system with a rect basic transmit signature $\underline{c}_0(t)$ of (3.10) are shown. We can explain this similarity by following the previous reasoning. The system matrix $\underline{\mathbf{A}}$ of (2.14) can be determined explicitly also in this case. As before, cf. Subsection 4.3.1, we consider one configuration at the time.

We first consider an MC system with a sinc basic transmit signature $\underline{c}_0(t)$ of (3.13). From (2.129), we infer that

$$\hat{\underline{C}}_0(f) = \frac{1}{T_{\text{ref}}} \int_{-\infty}^{\infty} \text{sinc}^2\left(\frac{t}{T_{\text{ref}}}\right) \exp(-j2\pi ft) dt. \quad (4.14)$$

The Fourier transform of $\text{sinc}^2(t)$ is known [BeC02, Car96] so that, by taking into account the scaling factors, (4.14) reads

$$\hat{\underline{C}}_0(f) = (1 - |T_{\text{ref}}f|) \text{rect}\left(\frac{fT_{\text{ref}}}{2}\right). \quad (4.15)$$

The function $\text{rect}(fT_{\text{ref}}/2)$ implies that $|fT_{\text{ref}}| < 1$, cf. (3.10). From (4.5) and by recalling that $F_{\text{ref}}T_{\text{ref}} = 1$, cf. (3.4), we obtain

$$\underline{A}_{n,n'} = \begin{cases} 1 - (n - n')F/F_{\text{ref}} & \text{for } |n - n'|F/F_{\text{ref}} < 1, \\ 0 & \text{else.} \end{cases} \quad (4.16)$$

which is the analytical expression of the system matrix $\underline{\mathbf{A}}$ of (2.14).

Then, we consider an SC system with a rect basic transmit signature $\underline{c}_0(t)$ of (3.10). We have to determine, cf. (2.12),

$$\underline{A}_{n,n'} = \frac{1}{T_{\text{ref}}} \int_{-\infty}^{+\infty} \text{rect}\left(\frac{t}{T_{\text{ref}}}\right) \text{rect}\left(\frac{t - (n - n')T}{T_{\text{ref}}}\right) dt. \quad (4.17)$$

To solve the integral in (4.17) in closed form let us consider Fig. 4.10 in which we report what happens when the time separation T between two rect functions of (3.10) decreases. The two rect functions of (3.10) of duration T_{ref} overlap only if $T < T_{\text{ref}}$. If there is an

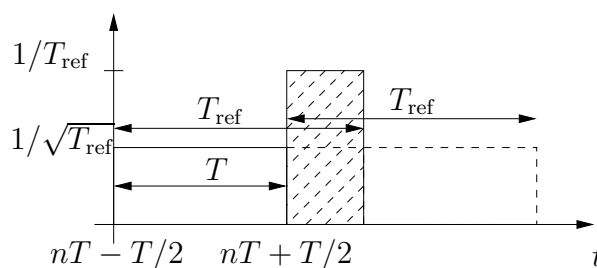


Fig. 4.10. Effect of the reduction of time separation T in SC system with a rect basic transmit signature $\underline{c}_0(t)$ of (3.10).

overlap, the resulting interference is given by the shaded rectangle. By generalizing the reasoning for all the N data symbol specific transmit signatures $\underline{c}_n(t)$ and from (4.17), we infer that

$$\underline{A}_{n,n'} = \begin{cases} 1 - (n - n')T/T_{\text{ref}} & \text{for } |n - n'|T/T_{\text{ref}} < 1, \\ 0 & \text{else.} \end{cases} \quad (4.18)$$

If $T/T_{\text{ref}} = F/F_{\text{ref}}$, then (4.16) is equal to (4.18). Therefore, we have shown by mean of analytical derivation that, if $T/T_{\text{ref}} = F/F_{\text{ref}}$, an MC system with a sinc basic transmit signature $\underline{c}_0(t)$ of (3.13) has the same system matrix $\underline{\mathbf{A}}$ of (2.14) as an SC system with a rect basic transmit signature $\underline{c}_0(t)$ of (3.10).

The difference between Fig. 4.1b and Fig. 4.9b such as the value of the peak at $T = 0.33$ in Fig. 4.1b and the value of the peak at $F = 0.33$ in Fig. 4.9b is caused by numerical errors occurring when evaluating the integral of (2.12). For SC systems the interference is determined by the temporal overlapping of rectangular functions, while for MC systems it is determined as the time integral of sinc of (3.13) with different frequency location.

4.3.3 Gaussian basic transmit signature

In Fig. 4.11, we report the rate R of (2.57) and the SNR-degradation δ of (2.68) and (2.76) of an MC system with a gauss basic transmit signature $\underline{c}_0(t)$ of (3.18). We report

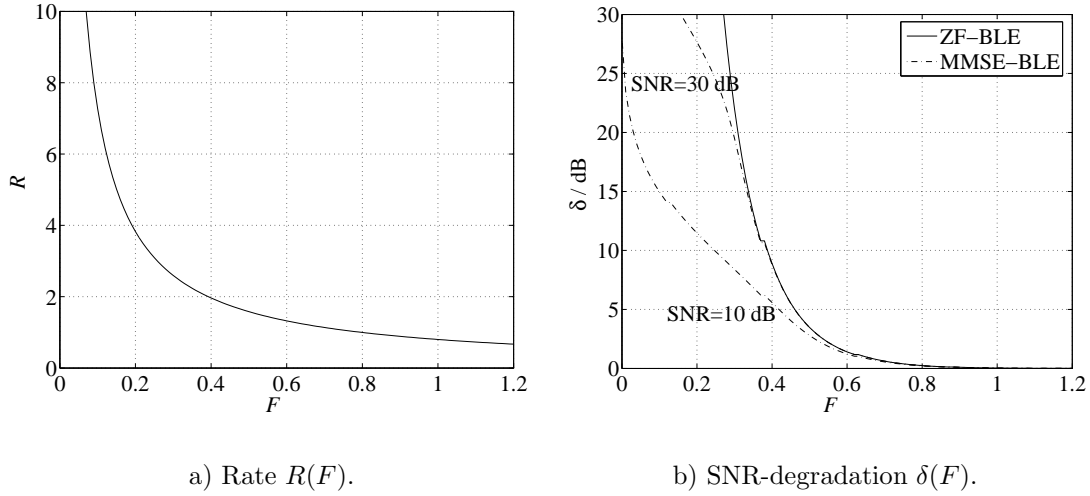


Fig. 4.11. $R(F)$ and $\delta(F)$ of an MC system with a gauss basic transmit signature $\underline{c}_0(t)$ of (3.18) versus the frequency separation F ; $F_{\text{ref}} = 1$; $B_0 = 0.7$; ZF-BLE and MMSE-BLE; SNR=10 dB and SNR=30 dB; $N = 64$; AWGN channel.

only the case of gauss of (3.18) with $B_0 = 0.7$ since, as we have shown for the SC case, see Figs. 4.3 to 4.5, the dependency between δ of (2.68) and (2.76) and R of (2.57) is not influenced by the standard deviation σ . In the case of an MC system the system matrix $\underline{\mathbf{A}}$ of (2.14) when a gauss of (3.18) is employed reads, cf. (3.32),

$$\underline{A}_{n,n'} = \exp \left[- (\pi \sigma \Delta_f(n, n') F / F_{\text{ref}})^2 \right]. \quad (4.19)$$

The rate R reads as in (2.62) and the 3 dB duration T_0 as in (3.19) so that we can write the frequency separation F/F_{ref} versus the rate R of (2.62) and (4.19) becomes

$$\underline{A}_{n,n'} = \exp \left[- \left(\frac{\pi \Delta_f(n, n')}{2R\sqrt{2\ln(2)}} \right)^2 \right]. \quad (4.20)$$

By comparing (4.3) with (4.20) and recalling that the matrix $\underline{\mathbf{\Delta}}_t$ of (2.124) for an SC system is equal to the matrix $\underline{\mathbf{\Delta}}_f$ of (2.125) for an MC system, we infer that when choosing a gauss basic transmit signature $\underline{c}_0(t)$ of (3.18) the dependency of δ of (2.68) and (2.76) on R of (2.57) is not influenced nor by the standard deviation σ neither by the SC or MC configuration. This can be also observed by investigating directly the simulation results and comparing Fig. 4.11 with Fig. 4.5.

4.3.4 Square root raised cosine basic transmit signature

In Figs. 4.12 and 4.13 the rate R of (2.57) and the SNR-degradation δ of (2.68) and (2.76) of an MC system with an rrcos basic transmit signature $\underline{c}_0(t)$ of (3.21) are shown.

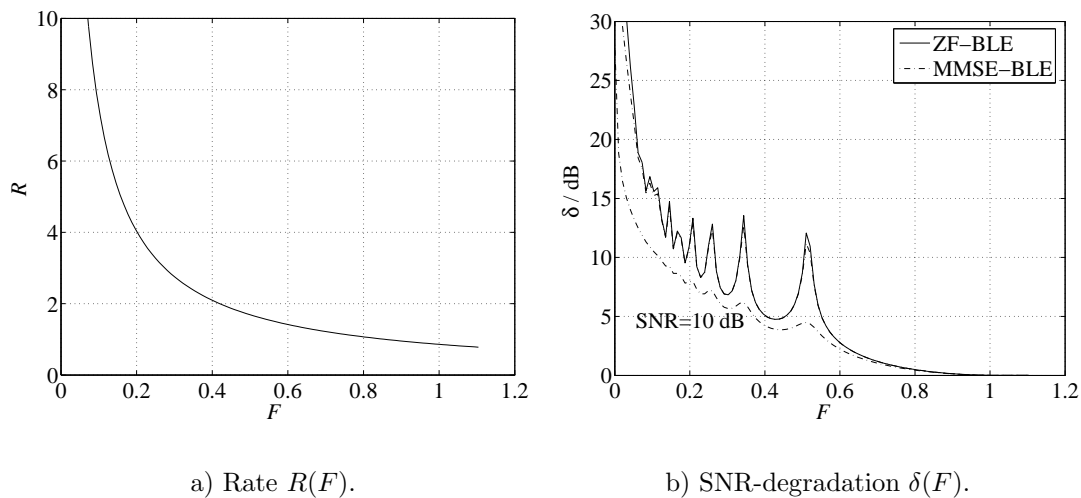


Fig. 4.12. $R(F)$ and $\delta(F)$ of an MC system with an rrcos basic transmit signature $\underline{c}_0(t)$ of (3.21) versus the frequency separation F ; $F_{\text{ref}} = 1$; $\alpha = 0.1$; ZF-BLE and MMSE-BLE; $\text{SNR}=10$ dB and $\text{SNR}=30$ dB; $N = 64$; AWGN channel.

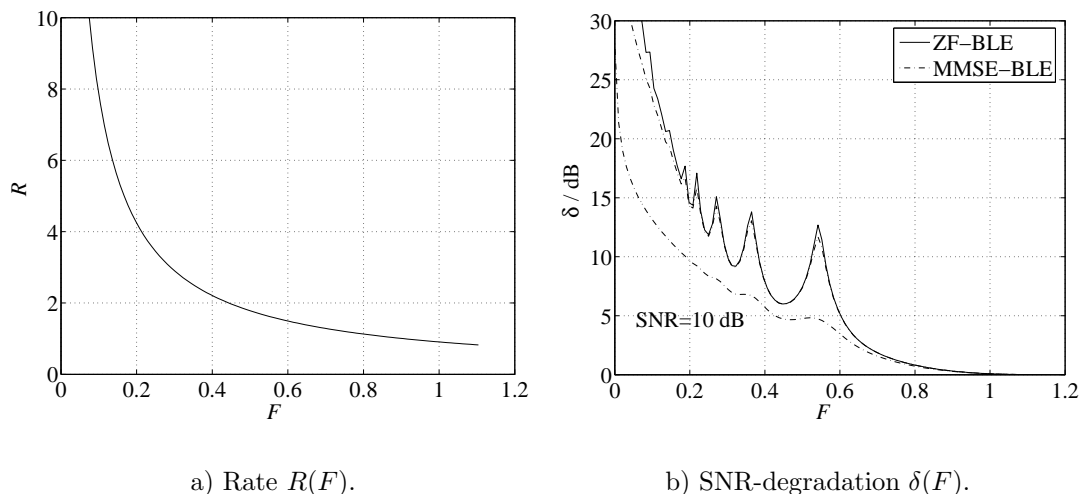


Fig. 4.13. $R(F)$ and $\delta(F)$ of an MC system with an rrcos basic transmit signature $\underline{c}_0(t)$ of (3.21) versus the frequency separation F ; $F_{\text{ref}} = 1$; $\alpha = 0.3$; ZF-BLE and MMSE-BLE; $\text{SNR}=10$ dB and $\text{SNR}=30$ dB; $N = 64$; AWGN channel.

The results are different from the SC system configuration, see Figs. 4.6 and 4.7, and are similar to the results of Fig. 4.9 in which we considered the case of a sinc basic transmit signature $\underline{c}_0(t)$ of (3.13). The similarity is not surprising since the rrcos of (3.21) tends to a sinc of (3.13) for α close to zero [BeC02]. We notice the presence of the peaks for certain values of the frequency separation F . If we compare Fig. 4.9b with Fig. 4.12b and with Fig. 4.13b, then we observe that the peaks move to the right with the increasing of the roll-off factor α . As explained before, cf. Subsection 4.2.1, the peaks indicate

the value of time separation T and/or frequency separation F for which the interference generated by a fixed number of symbols is maximum. With an rrcos of (3.21) the adjacent symbols interfere for smaller value of frequency separation F since the 3 dB bandwidth B_0 increases with the increment of α , cf. (3.23). As compared to the other choices of basic transmit signatures $\underline{c}_0(t)$, in the case of the rrcos of (3.21) we do not consider its dual in the frequency domain.

4.3.5 SC and MC duality

The duality existing between time and frequency domain has its roots in the Fourier transform and it is not only related to the specific cases considered in Subsections 4.3.1 to 4.3.3. If we indicate with $\mathcal{F}\{\cdot|f\}$ the Fourier operator that determines the Fourier transform and with $\mathcal{F}^{-1}\{\cdot|t\}$ the inverse Fourier transform, then from (4.10) to (4.12) we derive that in an SC system the system matrix $\underline{\mathbf{A}}$ of (2.14) has elements

$$\underline{A}_{n,n'} = \mathcal{F}^{-1} \left\{ |\underline{C}_0(f)|^2 |t \right\} \Big|_{t=(n-n')T}. \quad (4.21)$$

From Subsection 2.7.2, in an MC system the system matrix $\underline{\mathbf{A}}$ of (2.14) has elements

$$\underline{A}_{n,n'} = \mathcal{F} \left\{ |\underline{c}_0(t)|^2 |f \right\} \Big|_{f=(n-n')F}. \quad (4.22)$$

If SC and MC systems have the same system matrix $\underline{\mathbf{A}}$ then they have the same SNR-degradation δ of (2.68) and (2.76). (4.21) and (4.22) are given by considering some samples of a Fourier transform. To investigate when (4.21) is equal to (4.22), we can consider the following more general problem. Given two functions $\underline{x}(t)$ and $\underline{Y}(f)$, find the conditions under which the equality

$$\mathcal{F} \{ \underline{x}(t) \} = \mathcal{F}^{-1} \{ \underline{Y}(f) \} \quad (4.23)$$

holds. By applying the Fourier operator at both sides of (4.23) and by recalling the symmetry of the Fourier transform [BeC02, Car96], we obtain

$$\underline{x}(-t) = \underline{Y}(f). \quad (4.24)$$

Now, if we substitute $\underline{x}(t)$ with $|\underline{c}_0(t)|^2$ for the MC system and $\underline{Y}(f)$ with $|\underline{C}_0(f)|^2$ for the SC system, we can conclude that under the conditions

1. $\underline{c}_0(t)$ is real and $\underline{c}_0(t) = \underline{c}_0(-t)$,
2. $\underline{c}_0(t)$ in the SC system is equal to the Fourier transform of $\underline{c}_0(t)$ in the MC system,
3. $T/T_{\text{ref}} = F/F_{\text{ref}}$,

SC and MC systems have the same system matrix $\underline{\mathbf{A}}$ of (2.14). In general condition 1 is always verified in the systems under consideration. Moreover, (4.21) holds only if $\underline{c}_0(t) = \underline{c}_0(-t)$. Therefore, with the scope of parameters presented Subsection 3.3.2, if condition 2 is verified then we expect the same performance for SC and MC systems.

4.4 Hybrid systems

4.4.1 General

When considering HY systems, the dependence of the rate R of (2.57) and the SNR-degradation δ of (2.68) and (2.76) on F and T can be visualized as a three dimensional surface. From a graphical point of view, it is not straightforward to determine the exact value of a surface. Therefore, we depict the simulation results in an alternative way. The SNR-degradation δ of (2.68) of the ZF-BLE and the δ of (2.76) of the MMSE-BLE are reported in two separated figures since two three dimensional surfaces on a single figure cannot be clearly read. We consider only the value 30 dB of the SNR for the MMSE-BLE. Moreover, we change the range of the axis of the figures with respect to Sections 4.2 to 4.3 and propose a new representation of the results based on (3.26). In (3.26), we have seen that the SNR-degradation δ of (2.68) and (2.76) can be expressed as a function of both R and F to investigate how the SNR-degradation δ can vary for a chosen value of the rate R . We choose some values of R , e.g. $R = 1.0, 1.5, 2.0, 2.5, 4.0$, and for these values we report the one dimensional function $\delta(F, T|R)$.

4.4.2 Rectangular basic transmit signature

In Figs. 4.14a and 4.14b, we report the rate R of (2.57) and the SNR-degradation δ of

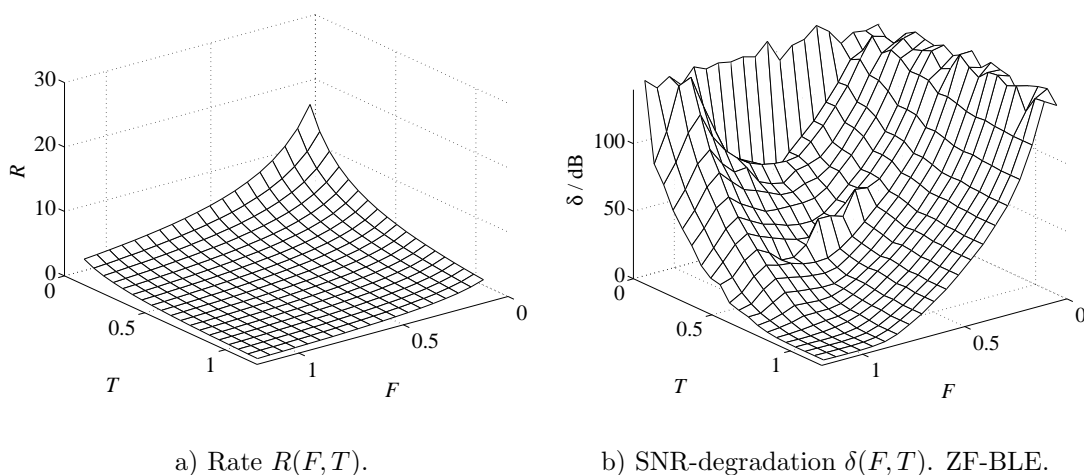


Fig. 4.14. $R(F, T)$ and $\delta(F, T)$ of a HY system with a rect basic transmit signature $\underline{c}_0(t)$ of (3.10) versus the frequency separation F and time separation T ; $T_{\text{ref}} = 1/F_{\text{ref}} = 1$; ZF-BLE; $N_t = 8$, $N_f = 8$; AWGN channel.

(2.68) for the ZF-BLE of a HY system with a rect basic transmit signature $\underline{c}_0(t)$ of (3.10), respectively. In Figs. 4.15a and 4.15b, we report, for the same system configuration and

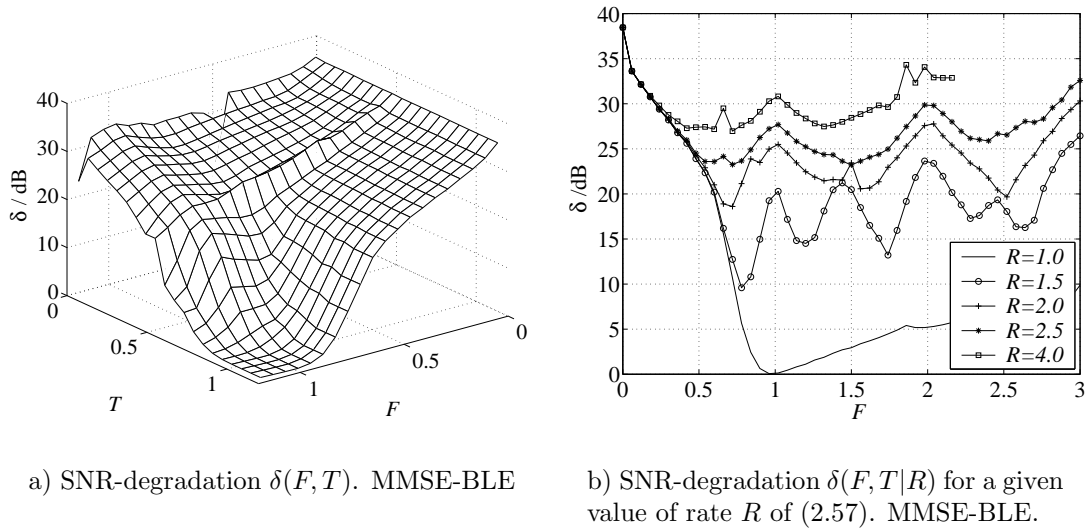


Fig. 4.15. $\delta(F, T)$ and $\delta(F, T|R)$ of a HY system with a rect basic transmit signature $\underline{c}_0(t)$ of (3.10) versus the frequency separation F and time separation T ; $T_{\text{ref}} = 1/F_{\text{ref}} = 1$; MMSE-BLE; SNR=30 dB; $N_t = 8$, $N_f = 8$; AWGN channel.

basic transmit signature $\underline{c}_0(t)$, the SNR-degradation δ of (2.76) for the MMSE-BLE with SNR=30 dB, and the two dimensional $\delta(F, T|R)$ function. The rate R of Fig. 4.14a is the surface already shown in Fig. 3.4, but here we have considered a denser grid of T and F and a smaller range of the vertical axis. The rate R of (2.57) increases smoothly with increasing T and F , and the increment is very high when T and F get close to zero. For a given value of R of (2.57) different combinations of T and F exist. In Fig. 4.14b the values of δ of (2.68) become rapidly very high with T and F decreasing, and the surface is not smooth. In particular, if we consider $F = 0.5$ and let T vary, then we observe some peaks at $T = 0.5$ and $T = 0.33$. By recalling Fig. 4.1b, we infer that the position of the peaks is the same. Let us now focus on what happens for $T > 1$. The data symbol specific transmit signatures $\underline{c}_n(t)$ of (3.10) and (2.34) are time limited and do not overlap in time for $T > 1$. Therefore, for $T > 1$ there is no interference generated in the time domain. Nevertheless, with the decreasing of F the SNR-degradation δ of (2.68) increases, since the data symbol specific transmit signatures $\underline{c}_n(t)$, which occupy the same time slot but different frequencies, generate ICI. In the range of $T > 1$ and $F > 1$, $\delta \approx 1$. This is the operational region of conventional OFDM systems. For $T = 1$ and $F = 1$ we obtain the performance of the reference conventional OFDM presented in Subsection 3.2.3, which shows no SNR-degradation δ , i.e. $\delta = 0$ dB.

In Fig. 4.15a, the SNR-degradation δ of (2.76) of the MMSE-BLE is depicted. As for SC and MC systems, the MMSE-BLE outperforms the ZF-BLE. We notice also for the MMSE-BLE the presence of a peak at $T = 0.5$. The peaks in the other positions can be hardly seen. The peaks are smoother than in SC and MC systems because they are

generated by a specific configuration of the ISI or the ICI. In HY systems, most of the times ISI and ICI coexist and a specific configuration of one type of interference does not influence so much the overall performance. Fig. 4.15b represents the SNR-degradation δ of (2.76) given by the MMSE-BLE for some fixed values of rate R of (2.57). The most important change with respect to the previous figures is the set of frequency separation F under investigation. We have considered $0 \leq F \leq 3$ to investigate also the combination of a very large frequency separation F and a very small time separation T which offers a high value of rate R of (2.57). By considering this set of F , we also verify the goodness of the choice of the range of T and F considered in the rest of the figures of HY systems, cf. Subsections 4.4.2 to 4.4.5. Besides the wider range of frequency separation F , in Fig. 4.15b we consider different values of R of (2.57). For instance, we consider $R = 1$ and for all combinations of T and F which yield $R = 1$, we determine the SNR-degradation δ of (2.76). We report the results as a function of the frequency separation F although, having fixed R , to each value of F corresponds only one value of T . In general, we can infer that by fixing R , δ depends on the combination of T and F . For $R = 1$, we notice that for $F = 1$, $\delta = 0$ dB. This is exactly the conventional OFDM reference system, cf. Subsection 3.2.3. If $F > 1$, then T shall decrease to keep R of (2.57) constant so that interference arises as well as SNR-degradation δ . For $F < 1$, the time separation T increases to keep constant the rate R of (2.57) and the increment of the SNR-degradation δ of (2.76) is generated by the interference arisen in the frequency direction. For different values of R , we can observe the same behaviour. With the decreasing of F , the SNR-degradation δ curves converge together. This has two implications:

- The SNR-degradation δ of (2.76) versus R of (2.57) is lower bounded by the SNR-degradation δ given by the lower value of R under consideration. Therefore, for any value of $R > 1$, the corresponding value of SNR-degradation δ is always higher than the SNR-degradation δ obtained by $R = 1$.
- With the increasing of the time and frequency overlapping, the dependency of δ of (2.76) on the value of R of (2.57) becomes less and less stringent. As a matter of fact, for $F \approx 0.4$, for the different considered values of R , the SNR-degradation δ is the same. The low value of F implies a large time separation T and the data symbol specific transmit signatures $\underline{c}_n(t)$ of (2.34) do not overlap in the time direction. If we increase the rate R of (2.57) while keeping fixed the small frequency separation F , we reduce the time separation T . As far as the reduction of T does not cause any overlapping in the time domain, we observe the same SNR-degradation δ for the different values of R .

Let us now focus on the curve $R = 1.5$. For $F \approx 1$, $\delta \approx 20$ dB, for $F \approx 0.8$, $\delta \approx 10$ dB. There is a difference of 10 dB of SNR-degradation δ of (2.76) for the same value of rate R of (2.57). This means that if we aim at transmitting at a higher rate R , we shall take

into consideration the best combination of T and F since the difference might be very significant. We also notice that by considering $F > 1$, the SNR-degradation δ increases. The minimum is given by $F = 0.8$. Through (3.26) we can determine the corresponding value of $T = 0.75$. The considered ranges $0 \leq F \leq 1.2$ and $0 \leq T \leq 1.2$ span the most interesting values of the trade-offs between R of (2.57) and δ since for $1.2 < F < 3$ there is no improvement in the SNR-degradation δ .

4.4.3 Sinc shaped basic transmit signature

In Figs. 4.16 and 4.17, we consider a HY system with a sinc basic transmit signature

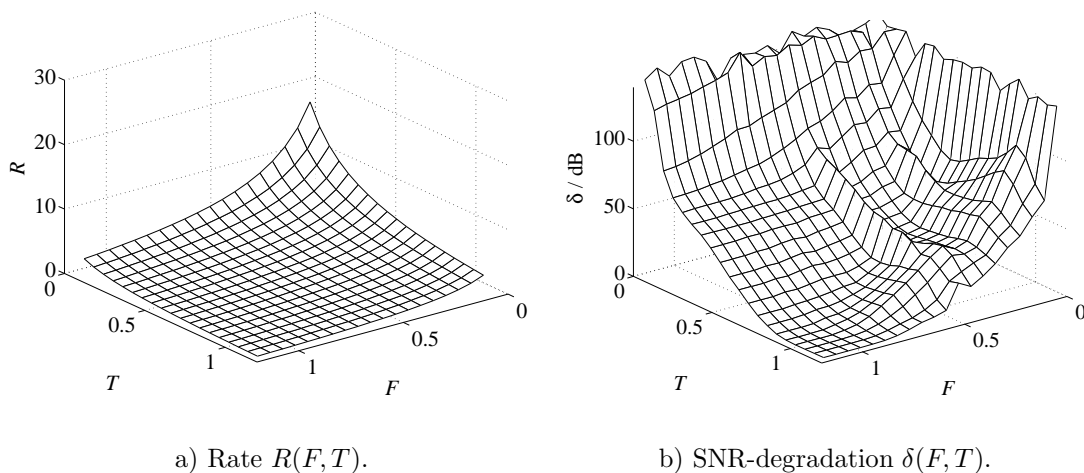


Fig. 4.16. $R(F, T)$ and $\delta(F, T)$ of a HY system with a sinc basic transmit signature $\underline{c}_0(t)$ of (3.13) versus the frequency separation F and time separation T ; $T_{\text{ref}} = 1/F_{\text{ref}} = 1$; ZF-BLE; $N_t = 8$, $N_f = 8$; AWGN channel.

$\underline{c}_0(t)$ of (3.13). The rate R of Fig. 4.16a is exactly as the rate R of Fig. 4.14a also from the analytical point of view, since we are considering $N_t = N_f$, cf. (2.63), and the sinc of (3.13) is dual of the rect of (3.10), cf. Subsection 4.3.2. Figs. 4.16b and 4.17a seem symmetric to Figs. 4.14b and 4.15a, respectively. Therefore, we infer that the SNR-degradation δ of (2.68) and (2.76) of a HY system with a rect basic transmit signature $\underline{c}_0(t)$ of (3.10) and the SNR-degradation δ of (2.68) and (2.76) of a HY system with a sinc basic transmit signature $\underline{c}_0(t)$ of (3.13) differ only in the fact that the dependency on T and F is exchanged. As a matter of fact, for the HY system with a sinc basic transmit signature $\underline{c}_0(t)$ of (3.13) we notice the peaks for $F = 0.5$ as we noticed in correspondence of $T = 0.5$ for the rect basic transmit signature $\underline{c}_0(t)$ of (3.10) in Fig. 4.14b. These observations might suggest a complete duality between the rect of (3.10) and the sinc of (3.13) similar to the duality considered for the SC and MC systems, cf. Subsections 4.3.1 to 4.3.2. However, in this case the system matrix $\underline{\mathbf{A}}$ of (2.14) is not the same for a given

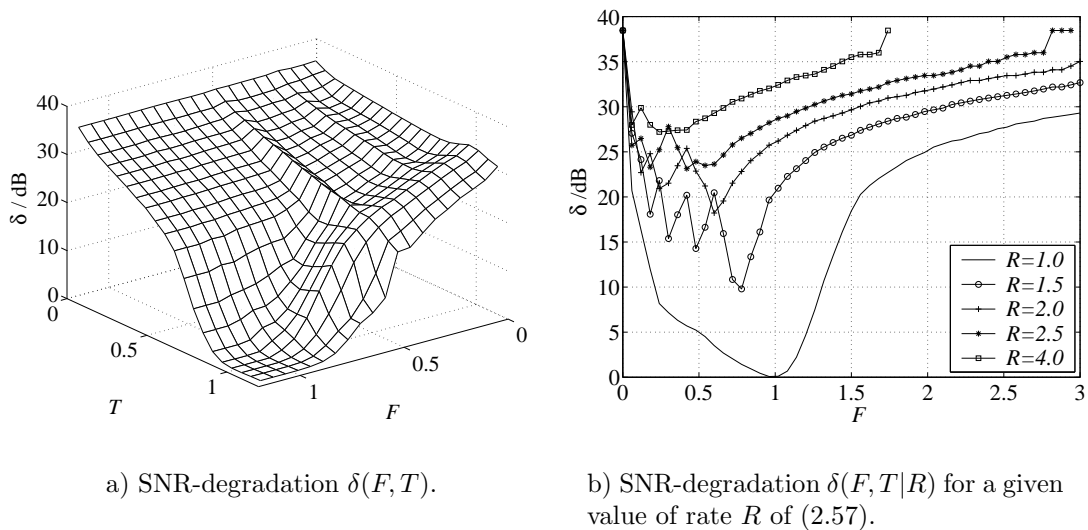


Fig. 4.17. $\delta(F, T)$ and $\delta(F, T|R)$ of a HY system with a sinc basic transmit signature $\underline{c}_0(t)$ of (3.13) versus the frequency separation F and time separation T ; $T_{\text{ref}} = 1/F_{\text{ref}} = 1$; MMSE-BLE; SNR=30 dB; $N_t = 8$, $N_f = 8$; AWGN channel.

value of $F = T$. By recalling (2.122), i.e.

$$\begin{aligned} \underline{A}_{n,n'} = & \exp[-j2\pi\Delta_f(n, n')FT(n_t(n') - 1)] \cdot \\ & \cdot \int_{-\infty}^{+\infty} \underline{c}_0(t)\underline{c}_0[t - \Delta_t(n, n')T] \exp[-j2\pi\Delta_f(n, n')Ft] dt, \end{aligned} \quad (4.25)$$

under the assumption of $\underline{c}_0(t) = \underline{c}_0(-t)$ and $\underline{c}_0(t)$ assuming only real values, we can rewrite (4.25) as

$$\begin{aligned} \underline{A}_{n,n'} = & \exp[-j2\pi\Delta_f(n, n')FT(n_t(n') - 1)] \cdot \\ & \cdot \int_{-\infty}^{+\infty} \underline{C}_0(f)\underline{C}_0[t - \Delta_f(n, n')F] \exp[-j2\pi\Delta_t(n, n')Tf] df. \end{aligned} \quad (4.26)$$

If $\underline{c}_0(t) = \underline{C}_0(f)$, then the role of T and F are changed and the interference in the system is the same. However, the functions $\Delta_f(n, n')$ and $\Delta_t(n, n')$ return different values for the same (n, n') so that the same interference is differently distributed within the system matrix $\underline{\mathbf{A}}$ of (2.14). The system matrix $\underline{\mathbf{A}}$ is different, but the interference for $F = T$ is the same.

In Fig. 4.17b, we consider different fixed values of the rate R of (2.57) and, by letting F vary we determine the SNR-degradation δ of (2.76). Also in this case we observe a degree of symmetry between Fig. 4.17b and Fig. 4.15b. The role of T and F seems exchanged. The variations of δ observed in Fig. 4.15b with the increasing of F appears now for the decreasing of F and more compressed. The smooth behaviour for small values of F in Fig. 4.15b can be noticed for high values of F in Fig. 4.17b. Although the system matrix

$\underline{\mathbf{A}}$ of (2.14) is different for HY systems with rect basic transmit signature $\underline{c}_0(t)$ of (3.10) and for HY systems with sinc basic transmit signature $\underline{c}_0(t)$ of (3.13), simulation results show very similar values of SNR-degradation δ of (2.68) and (2.76) and a high degree of symmetry. Indeed, as explained above, the amount of interference is the same but it is differently distributed within the system matrix $\underline{\mathbf{A}}$. The post-processing stage seems not to be influenced by the location of the interference but only by the amount of interference.

4.4.4 Gaussian basic transmit signature

Figs. 4.18 and 4.19 report the simulation results of a HY system with a gauss basic

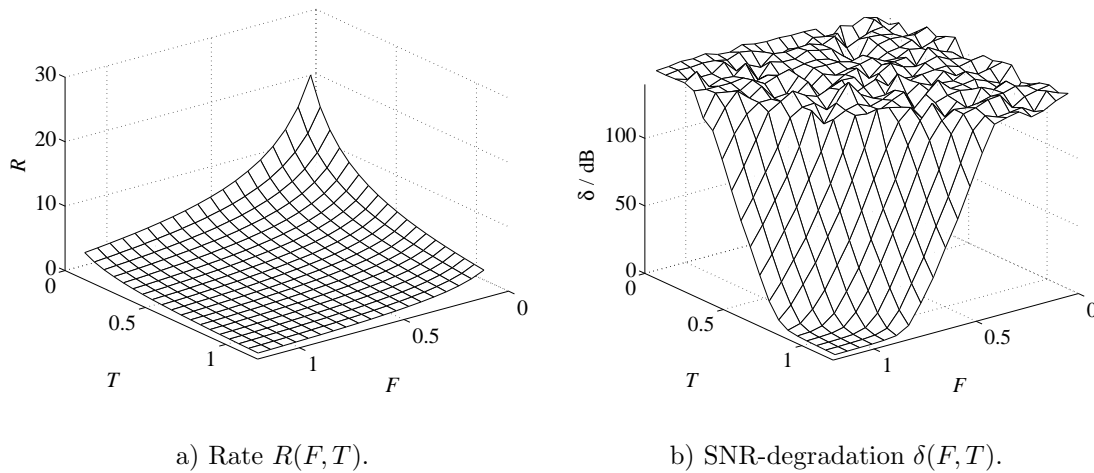


Fig. 4.18. $R(F, T)$ and $\delta(F, T)$ of a HY system with a gauss basic transmit signature $\underline{c}_0(t)$ of (3.18) versus the frequency separation F and time separation T ; $T_{\text{ref}} = 1/F_{\text{ref}} = 1$; $B_0 = 0.9$; ZF-BLE; $N_t = 8$, $N_f = 8$; AWGN channel.

transmit signature $\underline{c}_0(t)$ of (3.18) with $B_0 = 0.9$. We choose this value of B_0 so that, if $T = F$, the interference is equally distributed in time and frequency, cf. Subsection 3.3.4. From Fig. 4.18a we infer that the rate R is very similar to the rate R of Fig. 4.14a. As a matter of fact from (2.64) $R \approx 1/(FT)$ and it is independent of the choice of basic transmit signature $\underline{c}_0(t)$. For this reason we choose not to report the rate R of (2.57) of HY systems for any other gauss basic transmit signature $\underline{c}_0(t)$ of (3.18). Nevertheless, the approximation $R \approx 1/(FT)$ is valid only for high values of both N_t and N_f . In the considered cases, $N_t = N_f = 8$ cannot be considered high enough to completely avoid the influence of B_0 and T_0 and some difference can be noticed, e.g. the maximum value in Fig. 4.18a as compared with the maximum values of Figs. 4.14a and Figs. 4.16a. Fig. 4.18b reports the SNR-degradation δ of (2.68) versus T and F . The increment is smoother as compared to Figs. 4.14b and 4.16b and it reaches very high values of SNR-degradation δ . We also observe the corrugated surface in the range approximately of $F > 0.5$ and $T > 0.5$. For these values of T and F the system matrix $\underline{\mathbf{A}}$ of (2.14) is singular and the

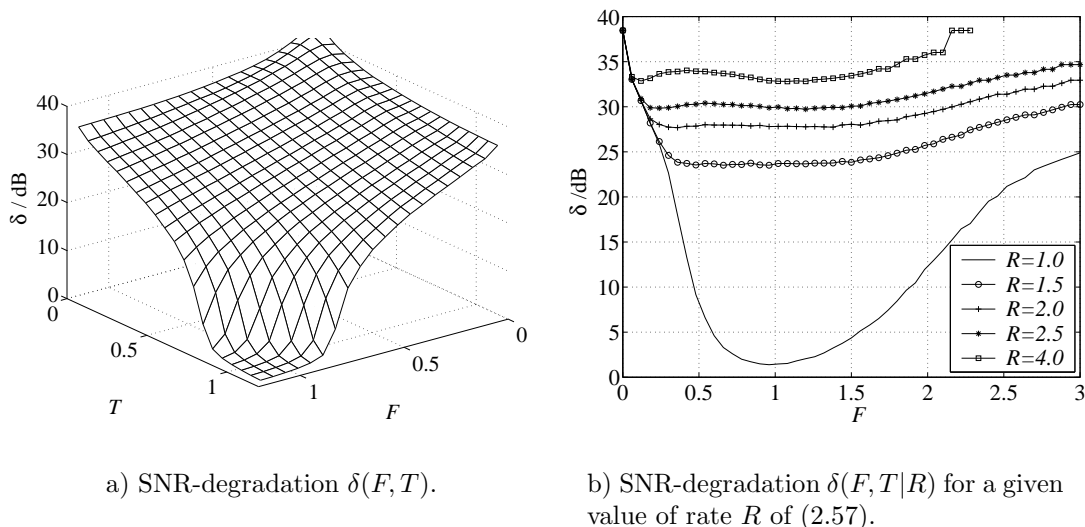


Fig. 4.19. $\delta(F, T)$ and $\delta(F, T|R)$ of a HY system with a gauss basic transmit signature $\underline{c}_0(t)$ of (3.18) versus the frequency separation F and time separation T ; $T_{\text{ref}} = 1/F_{\text{ref}} = 1$; $B_0 = 0.9$; MMSE-BLE; SNR=30 dB; $N_t = 8$, $N_f = 8$; AWGN channel.

ZF-BLE is not able to determine its inverse. Therefore the results diverge. We report them in the figure to complete the graphs, knowing however that they are meaningless and determined only by numerical calculation errors. Fig. 4.19a shows the performance of the MMSE-BLE for SNR=30 dB. In this case, the corrugated surface corresponding to high values of δ does not appear since the MMSE-BLE does not attempt to invert the system matrix $\underline{\mathbf{A}}$ of (2.14). The increment is very smooth in the whole range of considered values of T and F and the surface is quite symmetric with respect to T and F . This could be expected since the choice of B_0 ensures the same amount of ISI and ICI if $T = F$. The MMSE-BLE definitely outperforms the ZF-BLE for gauss basic transmit signature $\underline{c}_0(t)$ of (3.18) since the system matrix $\underline{\mathbf{A}}$ of (2.14) soon tends to singularity. Fig. 4.19b depicts the SNR-degradation $\delta(F, T|R)$ of (2.76). With the increasing of the rate R the SNR-degradation δ gets soon worse and worse. For $R = 1$, the best possible value is $F \approx 1$ to which corresponds $T \approx 1$. For $R > 1$ the SNR-degradation δ of (2.76) depends almost exclusively on the value of R and not on the time and frequency separation. This is determined by the characteristics of the gauss basic transmit signature $\underline{c}_0(t)$ of (3.18) which has the same shape both in time and frequency domain. By reducing F we increase T and the interference is mostly generated in the time domain. By increasing F , we decrease the time separation T and the interference is mostly generated in the frequency domain.

Figs. 4.20a and 4.20b show the SNR-degradation $\delta(F, T|R)$ for some given values of the rate R of (2.57) of a HY system with a gauss basic transmit signature $\underline{c}_0(t)$ of (3.18) with $B_0 = 0.7$ and $B_0 = 1.2$. We have chosen not to report the rate R of (2.57) and

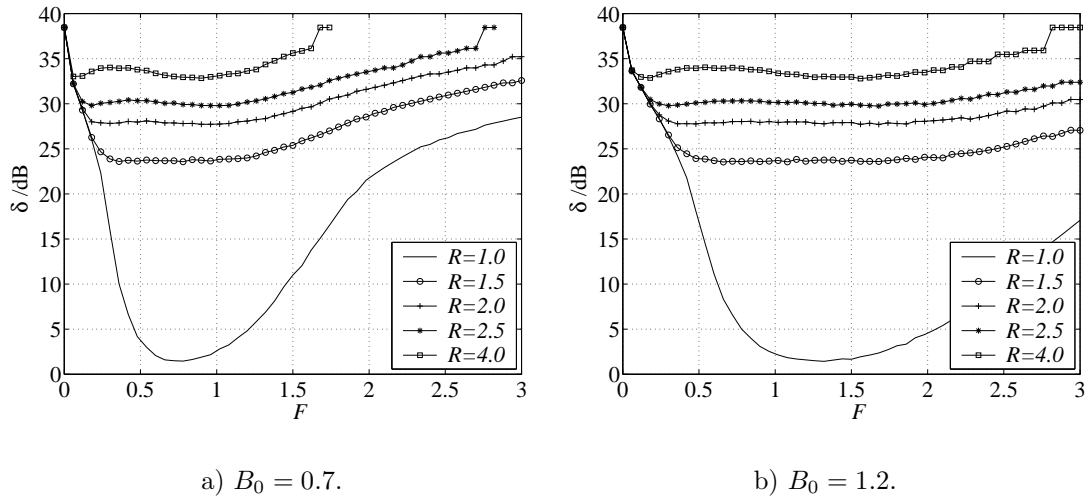


Fig. 4.20. $\delta(F, T|R)$ of a HY system with a Gauss basic transmit signature $\underline{c}_0(t)$ of (3.18) versus the frequency separation F and time separation T ; $T_{\text{ref}} = 1/F_{\text{ref}} = 1$; $B_0 = 0.7$; $B_0 = 1.2$; MMSE-BLE; SNR=30 dB; $N_t = 8$, $N_f = 8$; AWGN channel.

the SNR-degradation $\delta(F, T)$ of (2.68) and (2.76) for these configurations because the curves are very similar to Figs. 4.18 and 4.19a. The differences can be only noticed by comparing the two dimensional functions $\delta(F, T|R)$. We also observe that for HY systems the system matrix $\underline{\mathbf{A}}$ of (2.14) cannot be expressed as a function only of the rate R as in (4.3) and (4.20). Nevertheless, the dependency on σ remains very limited. By comparing Fig. 4.20a with Fig. 4.20b, the second is somehow an expanded version of the former. Let us focus on $R = 1$. The minimum in Fig. 4.20a is given for $F \approx 0.75$, while the minimum in Fig. 4.20b is given for $F \approx 1.25$. As expected, for a smaller 3 dB bandwidth B_0 the best combination of T and F is given for a relatively smaller value of F , while for a large B_0 the frequency separation F minimizing the SNR-degradation δ of (2.76) is larger than the time separation T . Fig. 4.19b, obtained with $B_0 = 0.9$ can be then recognized as an intermediate step between Fig. 4.20a and Fig. 4.20b.

4.4.5 Square root raised cosine basic transmit signature

Figs. 4.21 and 4.22 show the rate R of (2.57), the SNR-degradation δ of (2.68) and (2.76) and the SNR-degradation $\delta(F, T|R)$ of a HY system with an rrcos basic transmit signature $\underline{c}_0(t)$ of (3.21) with a roll-off factor $\alpha = 0.3$. The results are similar to the results of Figs. 4.16 and 4.17 since the sinc of (3.13) can be interpreted as an rrcos of (3.21) with roll-off $\alpha = 0$. Nevertheless, the faster time decay combined with the larger frequency occupation influences the results. The peaks in the SNR-degradation δ of Figs. 4.16b and 4.17a almost disappear in Figs. 4.21b and 4.22a. From Fig. 4.22b, we infer that the combination of F and T showing the lowest SNR-degradation δ of (2.68) and (2.76) is

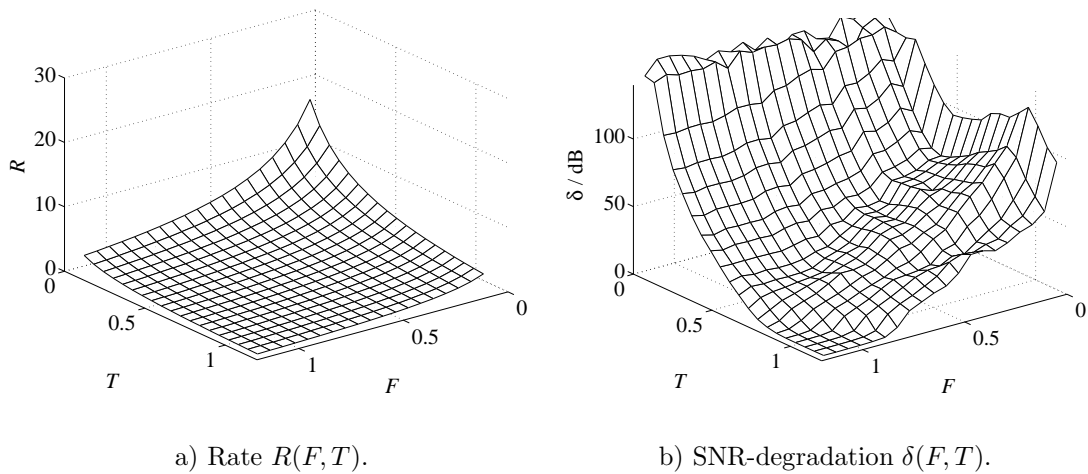


Fig. 4.21. $R(F, T)$ and $\delta(F, T)$ of a HY system with an rrcos basic transmit signature $\underline{c}_0(t)$ of (3.21) versus the frequency separation F and time separation T ; $T_{\text{ref}} = 1/F_{\text{ref}} = 1$; $\alpha = 0.3$; ZF-BLE; $N_t = 8$, $N_f = 8$; AWGN channel.

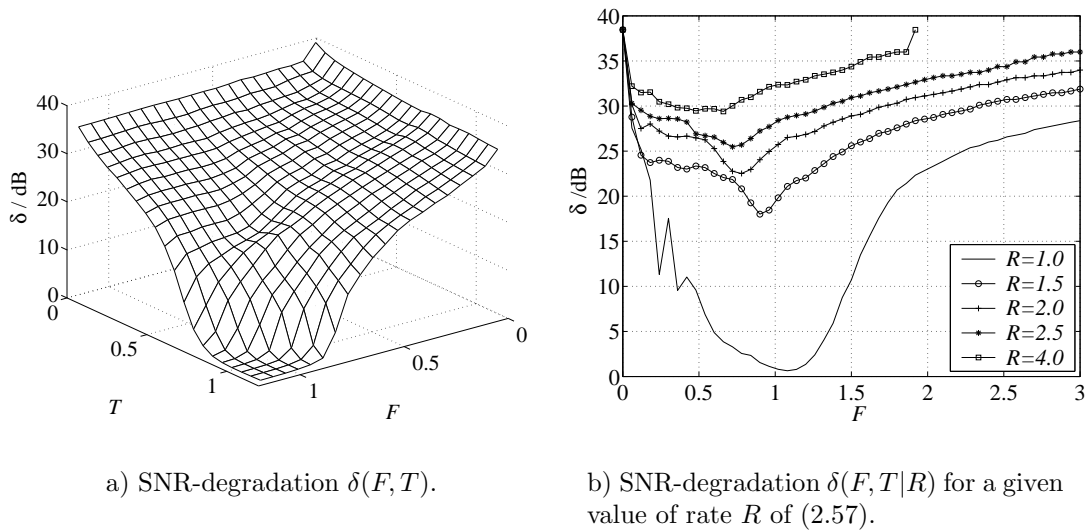


Fig. 4.22. $\delta(F, T)$ and $\delta(F, T|R)$ of a HY system with an rrcos basic transmit signature $\underline{c}_0(t)$ of (3.21) versus the frequency separation F and time separation T ; $T_{\text{ref}} = 1/F_{\text{ref}} = 1$; $\alpha = 0.3$; MMSE-BLE; SNR=30 dB; $N_t = 8$, $N_f = 8$; AWGN channel.

shifted to higher values of F as compared to Fig. 4.17b. The rrcos of (3.21) has a wider 3 dB bandwidth B_0 , which influences the performance since it generates a larger amount of interference in the frequency domain so that the system is more sensitive to the frequency separation F than to the time separation T .

The HY systems do not show as good performance as the SC and the MC systems. We have not found any combination of time separation T and frequency separation F

offering a promising trade-off between the SNR-degradation δ of (2.68) and (2.76) and the rate R of (2.57). This is due to the relationships between time and frequency domain. If we choose a time limited basic transmit signature $\underline{c}_0(t)$, it shows good performance for an SC carrier system because it limits the interference in the time direction. On the other hand it is frequency unlimited [Pro95], so that generating a significant amount of interference in the frequency direction.

4.5 Proposed approach as increment of the channel capacity

4.5.1 General

Subsection 3.4.2 shows how the channel capacity C of (3.44) is related to the rate R of (2.57) and the SNR-degradation δ of (2.68). In Sections 4.2 to 4.4, we have seen how the rate R of (2.57) and the SNR-degradation δ of (2.68) depend on the system configuration and on the choice of the basic transmit signature $\underline{c}_0(t)$. In the following subsections we investigate the performance of the considered configurations in terms of channel capacity C of (3.44). For each configuration and basic transmit signature $\underline{c}_0(t)$, we consider the corresponding SNR-degradation δ of (2.68) with a ZF-BLE and the rate R of (2.57) versus of the time separation T and/or the frequency separation F . Then, through (3.44), we determine the channel capacity C versus the time separation T and/or the frequency separation F . Since the channel capacity C of (3.44) depends also on the SNR γ_{MF} , we choose the two values SNR=10 dB and SNR=30 dB. At the aim of observing whether the proposed approach gives an improvement in terms of channel capacity C , we calculate the normalized channel capacity, cf. (3.44), defined as

$$C_{\text{norm}} = \frac{R \cdot \text{ld}(1 + \gamma_{\text{MF}}/\delta_{\text{ZF}})}{\text{ld}(1 + \gamma_{\text{MF}})}. \quad (4.27)$$

With (4.27), we can depict the normalized channel capacity C_{norm} of (4.27) given by the different considered SNR γ_{MF} in the same figure. We notice that the normalization factor $\text{ld}(1 + \gamma_{\text{MF}})$ of (4.27) represents the channel capacity C of (3.44) of the AWGN channel in absence of any interference, i.e. when the rate R of (2.57) is $R = 1$ and the SNR-degradation δ is $\delta = 0$ dB. Therefore, if C_{norm} of (4.27) is larger than one, then the proposed approach provides a method to increase the channel capacity C .

In the following we consider the configurations of SC, MC and HY systems and assume $T_{\text{ref}} = 1/F_{\text{ref}} = 1$, cf. (3.24).

4.5.2 Single carrier systems

In Fig. 4.23, we depict the normalized channel capacity C_{norm} of (4.27) for an SC system

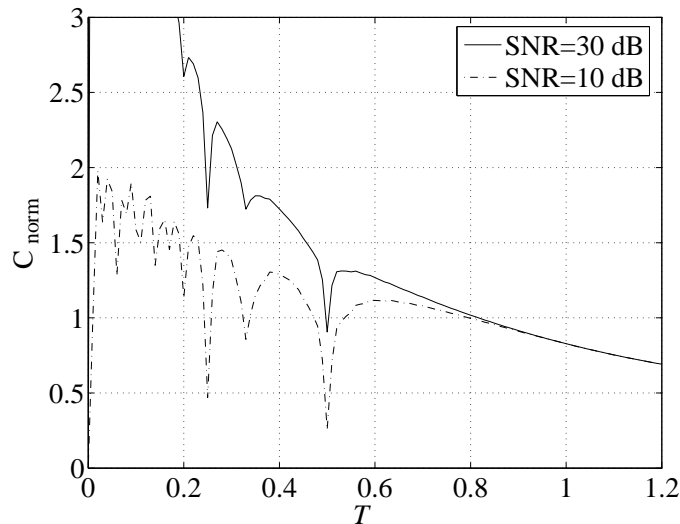


Fig. 4.23. Normalized channel capacity C_{norm} of (4.27) of an SC system with a rect basic transmit signature $\underline{c}_0(t)$ of (3.10) versus the time separation T ; $T_{\text{ref}} = 1$; ZF-BLE; SNR=10 dB and SNR=30 dB; $N = 64$; AWGN channel.

with a rect basic transmit signature $\underline{c}_0(t)$ of (3.10). The normalized channel capacity C_{norm} of (4.27) depends on the rate R of Fig. 4.1a and the SNR-degradation δ of (2.68) of Fig. 4.1b through (4.27). Therefore, we can recognize the presence of the peaks that cause an abrupt change in the values of the normalized channel capacity C_{norm} of (4.27). We notice that C_{norm} of (4.27) increases significantly for small values of T especially if we consider SNR=30 dB.

For SNR=10 dB the best case is given by a very small time separation T for which the channel capacity C of (3.44) almost doubles as compared to the conventional approach. The values have a high variation in correspondence of very small change in the time separation T . If we aim at designing a system able to improve the channel capacity C of (3.44), the choice of very small T is risky because small variations of the T , e.g. due to inaccurate time synchronization, generate very large variations of channel capacity C of (3.44). We could for instance choose a more conservative value such as $T = 0.4$. Then, the channel capacity C improves of 30% compared to the conventional approach, and it does not fall down to much lower values as the time separation T is slightly perturbed. For very small value of T the normalized channel capacity C_{norm} of (4.27) goes to zero as expected, cf. (3.45). Let us now focus on SNR=30 dB. The improvement is even higher in this configuration and it seems to diverge for very small values of T . In Chapter 5 we will consider this configuration in more detail, cf. Subsection 5.2. At the moment, we stress that the curve, after reaching its maximum value, converges to zero for small time

separation T . We were not able to show this behaviour in Fig. 4.23 since the maximum value is located at very small values of T .

In Fig. 4.24, we depict the normalized channel capacity C_{norm} of (4.27) obtained for

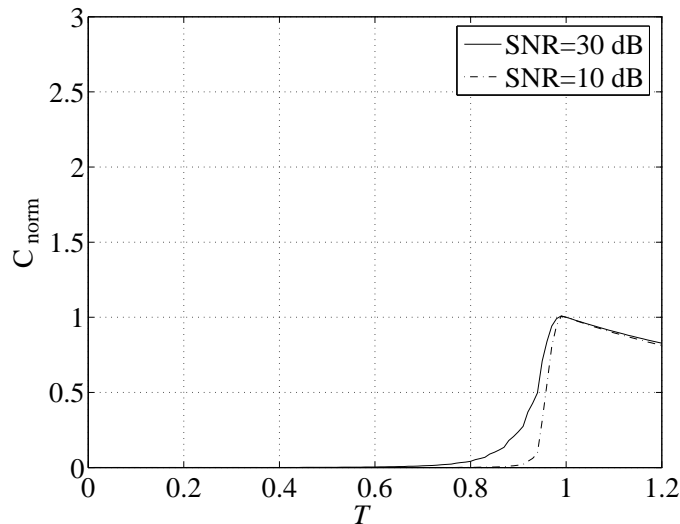


Fig. 4.24. Normalized channel capacity C_{norm} of (4.27) of an SC system with a sinc basic transmit signature $\underline{c}_0(t)$ of (3.13) versus the time separation T ; $T_{\text{ref}} = 1$; ZF-BLE; SNR=10 dB and SNR=30 dB; $N = 64$; AWGN channel.

an SC system with a sinc basic transmit signature $\underline{c}_0(t)$ of (3.13). The situation is much different from Fig. 4.23. By reducing the time separation T the channel capacity C of (3.44) decreases. The maximum value is given by $T = 1$, i.e. $R \approx 1$. This configuration corresponds to the standard configuration of no ISI in the AWGN channel. If $T > 1$, then $C < 1$ since the rate R of (2.57) decreases and the SNR-degradation δ increases, see Fig. 4.2. When $T < 1$, the rate R increases but not enough to compensate the also increasing SNR-degradation δ . From the simulation results of Fig. 4.24, we infer that a sinc basic transmit signature $\underline{c}_0(t)$ of (3.13) is not a promising choice to improve the channel capacity C in an SC system by reducing the time separation T . In Fig. 4.24 we also observe that the channel capacity C of (3.44) is slightly better for SNR=30 dB. For both values of SNR, with the decreasing of T the channel capacity C_{norm} of (4.27) tends to zero.

In Figs. 4.25, 4.26 and 4.27 we depict the normalized channel capacity C_{norm} of (4.27) of an SC system with a gauss basic transmit signature $\underline{c}_0(t)$ of (3.18) with $B_0 = 0.7$, $B_0 = 0.9$ and $B_0 = 1.2$, respectively. The channel capacity C_{norm} of (4.27) has very similar behaviour in the three different cases. It tends to zero as the time separation T decreases. However, there exists a range of $T < 1$ for which the channel capacity C of (3.44) is improved, i.e. it is larger than one. The maximum normalized channel capacity C_{norm} of (4.27) has the same value in the three different cases although it is obtained for different values of time separation T . It might be interesting to notice that the time

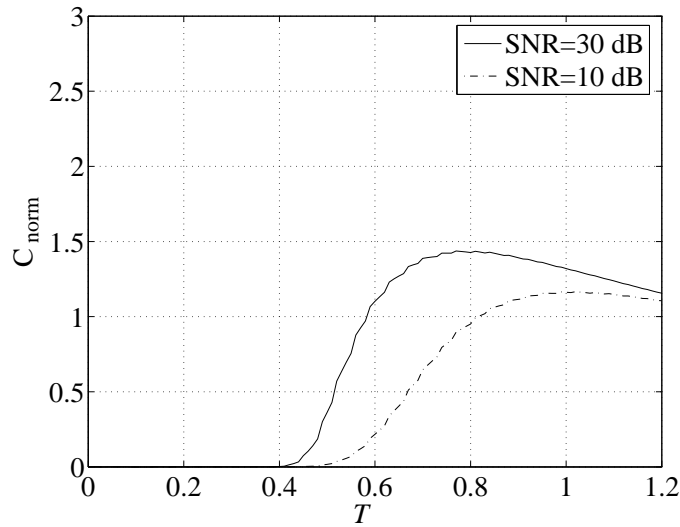


Fig. 4.25. Normalized channel capacity C_{norm} of (4.27) of an SC system with a gauss basic transmit signature $\underline{c}_0(t)$ of (3.18) versus the time separation T ; $T_{\text{ref}} = 1$; $B_0 = 0.7$; ZF-BLE; $N = 64$; AWGN channel; SNR=10 dB; SNR=30 dB.

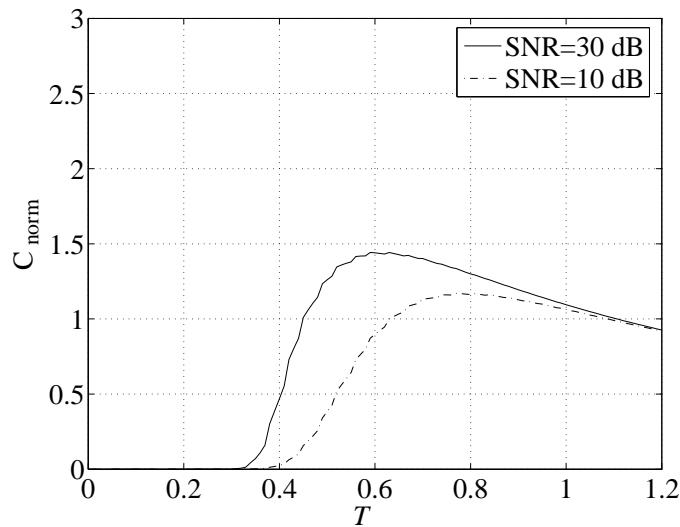


Fig. 4.26. Normalized channel capacity C_{norm} of (4.27) of an SC system with a gauss basic transmit signature $\underline{c}_0(t)$ of (3.18) versus time separation T ; $T_{\text{ref}} = 1$; $B_0 = 0.9$; ZF-BLE; $N = 64$; AWGN channel; SNR=10 dB; SNR=30 dB.

separation T offering the highest improvement of channel capacity C of (3.44) depends on the SNR. As before, the improvement is better for higher SNR, cf. (4.27). In Section 4.2, Figs. 4.3 to 4.5, we have shown that the relationship between the value of R of (2.57) and the SNR-degradation δ of (2.68), if a gauss basic transmit signature $\underline{c}_0(t)$ of (3.18) is employed, is independent of the standard deviation σ . However, a given range of values of rate R of (2.57) corresponds to different ranges of time separation T , since the relation between T and R is related to σ , cf. (4.1). As a consequence, depending on the value

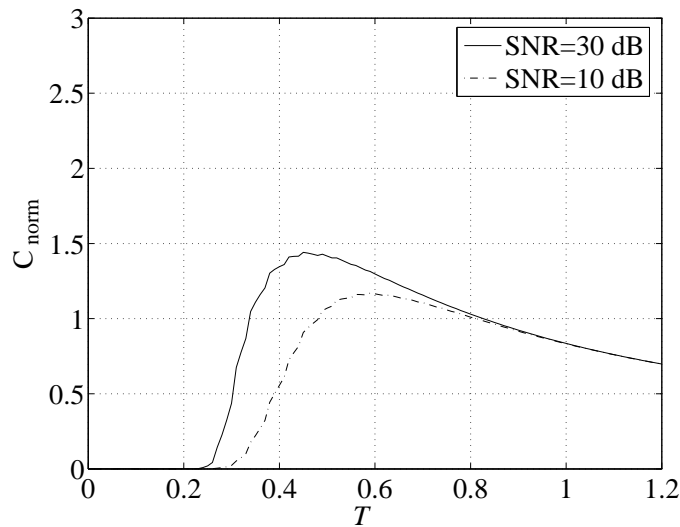


Fig. 4.27. Normalized channel capacity C_{norm} of (4.27) of an SC system with a gauss basic transmit signature $\underline{c}_0(t)$ of (3.18) versus time separation T ; $T_{\text{ref}} = 1$; $B_0 = 1.2$; ZF-BLE; $N = 64$; AWGN channel; SNR=10 dB; SNR=30 dB.

of B_0 , different ranges of T yield an improvement in the channel capacity C of (3.44). To better explain this aspect let us consider the approximate expression of the rate R of (2.57) of SC systems, i.e. $R = 1/(B_0T)$. Let us suppose to be interested in the range of T for which the rate R is $2 < R < 1$. From the expression of the rate R of (2.59), the corresponding range of time separation T is $1/B_0 < T < 1/(2B_0)$. Therefore, for a smaller value of B_0 , see Fig. 4.25, the range of time separation T returning a given range of rate R is larger. The choice of a gauss basic transmit signature $\underline{c}_0(t)$ of (3.18) in an SC system allows the choice of the corresponding time separation T that improves the channel capacity C of (3.44).

In Figs. 4.28 and 4.29 we consider an SC system with an rrcos basic transmit signature $\underline{c}_0(t)$ of (3.21) with $\alpha = 0.1$ and $\alpha = 0.3$, respectively. As expected, see Figs. 4.6 and 4.7, the results are similar to Fig. 4.24 in which we consider a sinc basic transmit signature $\underline{c}_0(t)$ of (3.13). The maximum value of channel capacity C of (3.44) corresponds to $T \approx 0.95$ if $\alpha = 0.1$ and to $T \approx 0.82$ if $\alpha = 0.3$. With the increasing of α the maximum value of channel capacity C of (3.44) is achieved for smaller time separation T . This is due to the fact that the larger the roll-off factor α , the faster the time decay of the rrcos basic transmit signature $\underline{c}_0(t)$ of (3.21), so guaranteeing a smaller amount of ISI generated by the data symbol specific transmit signatures $\underline{c}_n(t)$ of (2.24). However, due to the time unlimited nature of rrcos of (3.21), the amount of interference is always very high so that there is no value of the time separation T which ensures $C_{\text{norm}} > 1$.

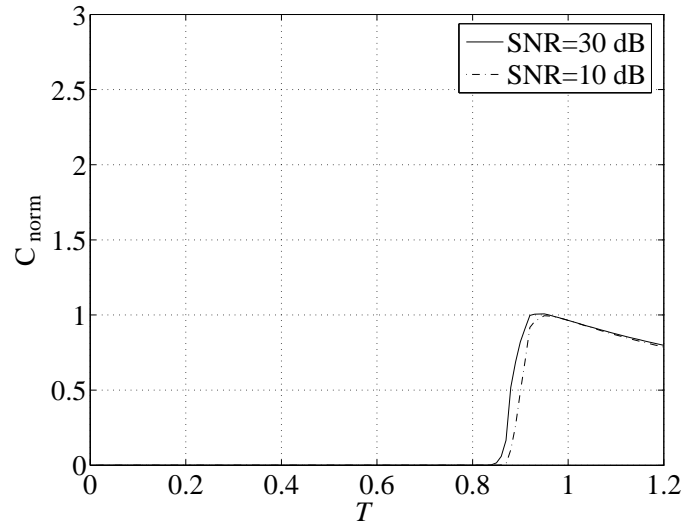


Fig. 4.28. Normalized channel capacity C_{norm} of (4.27) of an SC system with an rrcos basic transmit signature $\underline{c}_0(t)$ of (3.21) versus the time separation T ; $T_{\text{ref}} = 1$; $\alpha = 0.1$; ZF-BLE; $N = 64$; AWGN channel; SNR=10 dB; SNR=30 dB.

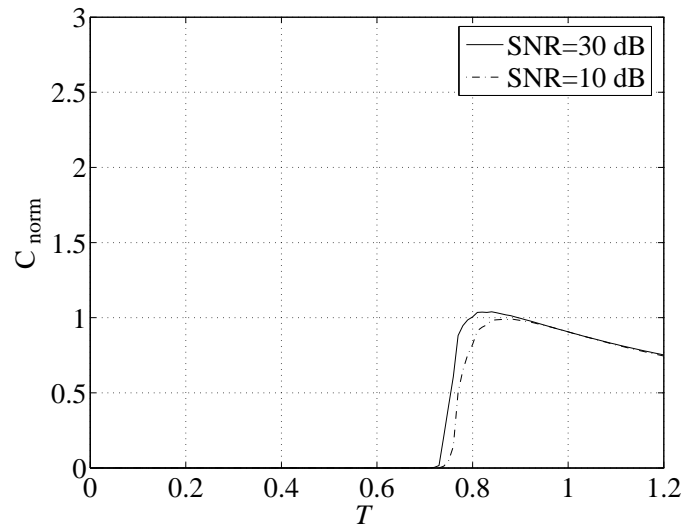


Fig. 4.29. Normalized channel capacity C_{norm} of (4.27) of an SC system with an rrcos basic transmit signature $\underline{c}_0(t)$ of (3.21) versus the time separation T ; $T_{\text{ref}} = 1$; $\alpha = 0.3$; ZF-BLE; $N = 64$; AWGN channel; SNR=10 dB; SNR=30 dB.

4.5.3 Multi-carrier systems

In Section 4.3 we have shown that MC systems can be interpreted as dual of SC systems and we have found the conditions under which SC and MC systems have the same system matrix $\underline{\mathbf{A}}$ of (2.14), cf. Subsection 4.3.5. Therefore, we do not report the simulation results obtained for MC systems with a rect basic transmit signature $\underline{c}_0(t)$ of (3.10) and a sinc basic transmit signature $\underline{c}_0(t)$ of (3.13) since they are equivalent to those depicted for SC systems with a sinc basic transmit signatures $\underline{c}_0(t)$ of (3.13) and a rect basic transmit signatures $\underline{c}_0(t)$ of (3.10), respectively. In the case of a gauss basic transmit signature $\underline{c}_0(t)$ of (3.18) we have seen, cf. Subsection 4.5.2, that the results, when expressed in terms of channel capacity C of (3.44), depend on the value of standard deviation σ . Therefore, they should differ in SC and MC cases. Nevertheless, the three chosen values of σ let us take into account dual situations. This means that the SC system with a gauss basic transmit signature $\underline{c}_0(t)$ of (3.18) and $B_0 = 0.7$ has performance almost identical to the MC system with a gauss basic transmit signature $\underline{c}_0(t)$ of (3.18) and $B_0 = 1.2$. For $B_0 = 0.9$ and $\underline{c}_0(t)$ of (3.18), SC and MC systems show very similar performance. For these reasons, we choose not to report the results obtained for MC systems with gauss basic transmit signature $\underline{c}_0(t)$ of (3.18). We consider only the rrcos basic transmit signatures $\underline{c}_0(t)$ of (3.21) whose time domain dual is not among the basic transmit signatures $\underline{c}_0(t)$ under investigation.

In Figs. 4.30 and 4.31, we report the normalized channel capacity C_{norm} of (4.27) of

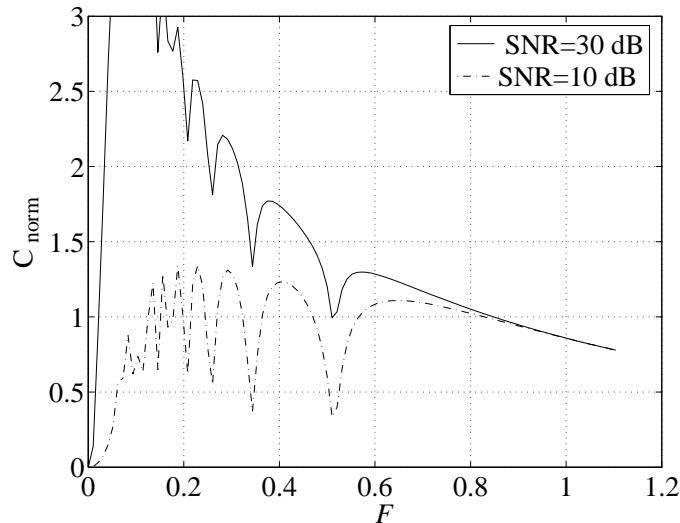


Fig. 4.30. Normalized channel capacity C_{norm} of (4.27) of an MC system with an rrcos basic transmit signature $\underline{c}_0(t)$ of (3.21) versus the frequency separation F ; $F_{\text{ref}} = 1$; $\alpha = 0.1$; ZF-BLE; $N = 64$; AWGN channel; SNR=10 dB; SNR=30 dB.

an MC system with an rrcos basic transmit signature $\underline{c}_0(t)$ of (3.21). In Fig. 4.30, we consider a roll-off factor $\alpha = 0.1$. The performance is quite similar to Fig. 4.23. This

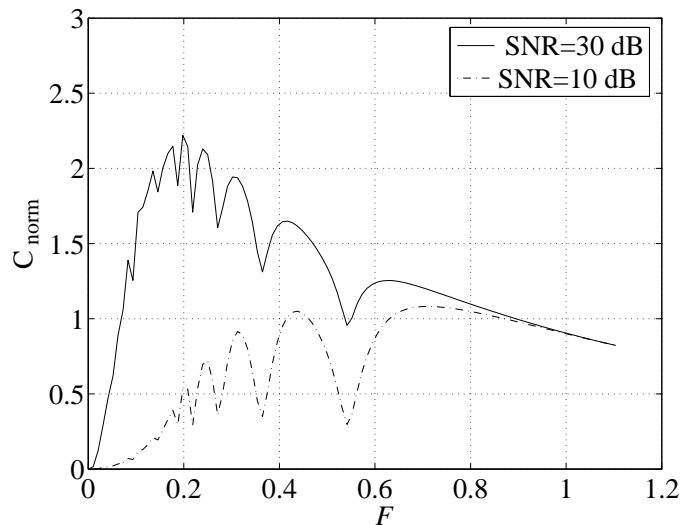


Fig. 4.31. Normalized channel capacity C_{norm} of (4.27) of an MC system with an rrcos basic transmit signature $\underline{c}_0(t)$ of (3.21) versus the frequency separation F ; $F_{\text{ref}} = 1$; $\alpha = 0.3$; ZF-BLE; $N = 64$; AWGN channel; SNR=10 dB; SNR=30 dB.

result is to be expected since the rrcos of (3.21) becomes a sinc of (3.13) when $\alpha = 0$ and the Fourier transform of a sinc(t) is a rect(f). For SNR=10 dB, the channel capacity C of (3.44) changes very quickly with the decreasing of the frequency separation F and it oscillates around the value one. We infer that exist some particular values of F which offer an improvement in terms of channel capacity C of (3.44). However, due to the peaks, for small values of F , the channel capacity C becomes very sensitive to the exact value of F . For SNR=30 dB, the improvement given by the reduction of the frequency separation F is much more significant. The channel capacity C of (3.44) reaches a maximum value, not shown in the figure, and then it converges to zero when all the symbols are transmitted at very close frequency locations. In Fig. 4.31, we consider $\alpha = 0.3$. The performance is not so good any more both for SNR=10 dB and SNR=30 dB. For SNR=10 dB, the ranges of F ensuring an improved channel capacity C of (3.44) are significantly reduced and it seems not convenient to further investigate the reduction of the frequency separation F . For SNR=30 dB, the channel capacity C doubles for $F \approx 0.2$ but also in this case the system is very sensitive to small variation of the chosen value of F .

In MC systems we can achieve a gain in terms of channel capacity C of (3.44) only when considering a frequency limited basic transmit signature $\underline{c}_0(t)$. This is dual with respect to what we inferred for SC systems, cf. Subsection 4.5.2, for which the best choice is given by a time limited basic transmit signature $\underline{c}_0(t)$.

4.5.4 Hybrid systems

In the case of HY systems the time and frequency separation, T and F , respectively, are jointly reduced to increase the rate R of (2.57), so causing an increment in terms of SNR-degradation δ of (2.68), cf. Section 4.4. The SNR-degradation δ can be very high, cf. Section 4.4.

In Fig. 4.32, we report the normalized channel capacity C_{norm} of (4.27) for a HY system with a rect basic transmit signature $\underline{c}_0(t)$ of (3.10). Also for HY systems, we consider two

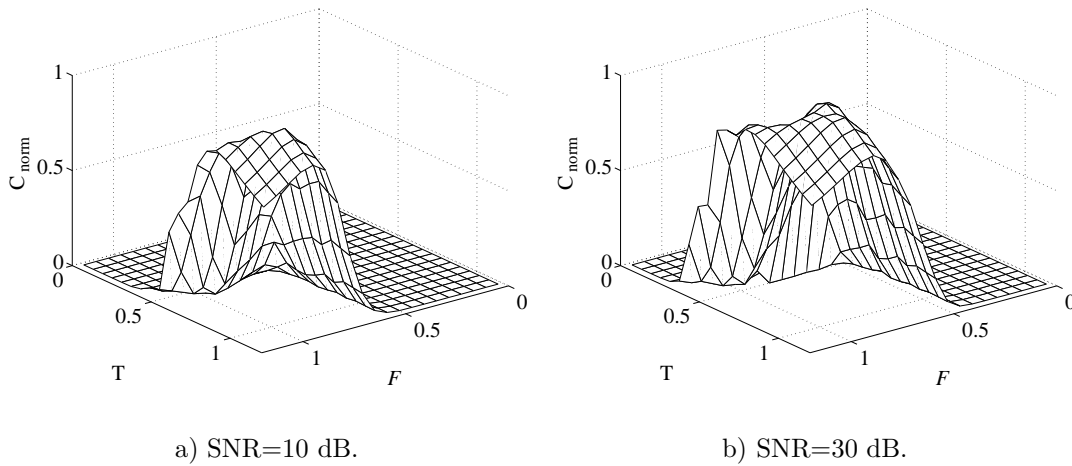


Fig. 4.32. Normalized channel capacity C_{norm} of (4.27) of a HY system with a rect basic transmit signature $\underline{c}_0(t)$ of (3.10) versus the frequency separation F and time separation T ; $T_{\text{ref}} = 1/F_{\text{ref}} = 1$; ZF-BLE; $N = 64$; AWGN channel; SNR=10 dB; SNR=30 dB.

values of SNR, i.e. SNR=10 dB and SNR=30 dB. We do not report the three dimensional surfaces representing the normalized channel capacity C_{norm} of (4.27) in the same figure to simplify the reading of the results. For both the SNR values the normalized channel capacity C_{norm} of (4.27) does not show any significant improvement. For T and F close to one, there exist some combinations of the time and frequency separations which ensure a normalized channel capacity C_{norm} of (4.27) only slightly larger than one. For $T < 1$ and $F < 1$, C_{norm} of (4.27) goes to zero very quickly as compared to SC and MC systems. This could be expected from Fig. 4.14b where we have seen that the SNR-degradation δ of (2.68) of the ZF-BLE diverges to very high values.

In Fig. 4.33, we report the normalized channel capacity C_{norm} of (4.27) for a HY system with a sinc basic transmit signature $\underline{c}_0(t)$ of (3.13). The normalized channel capacity C_{norm} of (4.27) is slightly larger than one only for a limited range of F and T . Fig. 4.33 is specular to Fig. 4.32. In particular, by comparing Fig. 4.33b with Fig. 4.32b we can notice that the role of F and T is exchanged.

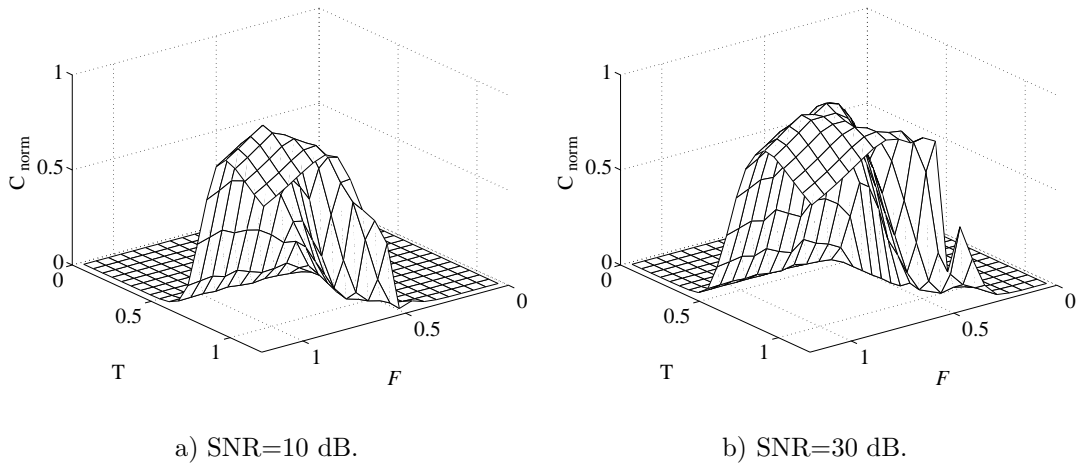


Fig. 4.33. Normalized channel capacity C_{norm} of (4.27) of a HY system with a sinc basic transmit signature $\underline{c}_0(t)$ of (3.13) versus the frequency separation F and time separation T ; $T_{\text{ref}} = 1/F_{\text{ref}} = 1$; ZF-BLE; SNR=10 dB and SNR=30 dB; $N = 64$; AWGN channel.

In Figs. 4.34, 4.35 and 4.36, we report the normalized channel capacity C_{norm} of (4.27) of

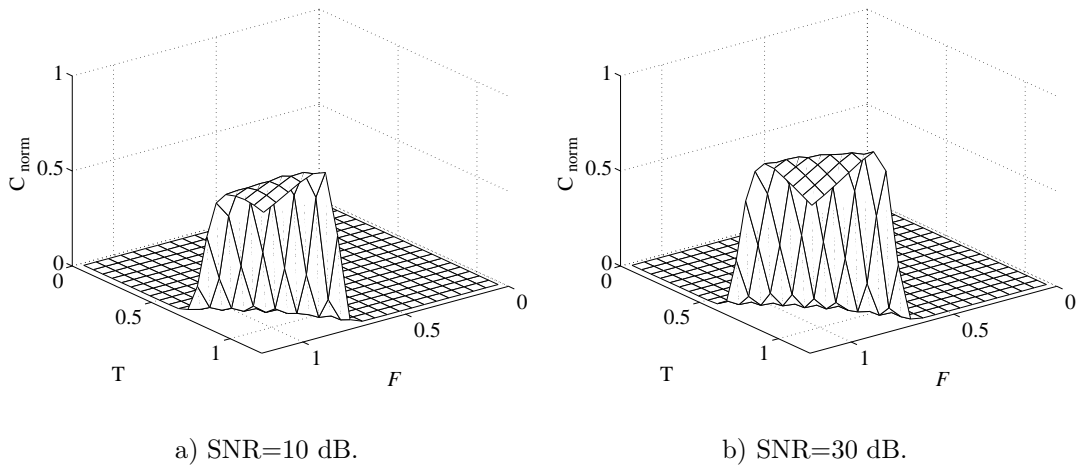


Fig. 4.34. Normalized channel capacity C_{norm} of (4.27) of a HY system with a gauss basic transmit signature $\underline{c}_0(t)$ of (3.18) versus the frequency separation F and time separation T ; $T_{\text{ref}} = 1/F_{\text{ref}} = 1$; $B_0 = 0.7$; ZF-BLE; SNR=10 dB and SNR=30 dB; $N = 64$; AWGN channel.

a HY system with a gauss basic transmit signature $\underline{c}_0(t)$ of (3.18) with $B_0 = 0.7$, $B_0 = 0.9$ and $B_0 = 1.2$, respectively. The normalized channel capacity C_{norm} of (4.27) is never larger than one for all values of B_0 . If we compare Fig. 4.34 with Figs. 4.35 and 4.36 we can notice how the dependency of the channel capacity C of (3.44) on the time separation T and the frequency separation F changes by varying B_0 . If B_0 is small, see Fig. 4.34, the channel capacity C decreases faster with the decreasing of the time separation T . This is due to the fact that for small B_0 , the time duration T_0 of the basic transmit signature $\underline{c}_0(t)$

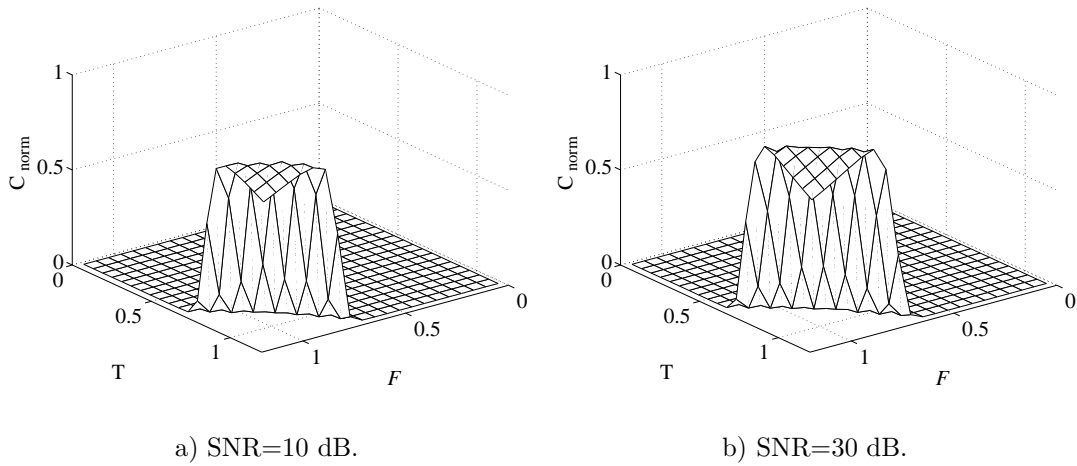


Fig. 4.35. Normalized channel capacity C_{norm} of (4.27) of a HY system with a gauss basic transmit signature $\underline{c}_0(t)$ of (3.18) versus the frequency separation F and time separation T ; $T_{\text{ref}} = 1/F_{\text{ref}} = 1$; $B_0 = 0.9$; ZF-BLE; SNR=10 dB and SNR=30 dB; $N = 64$; AWGN channel.

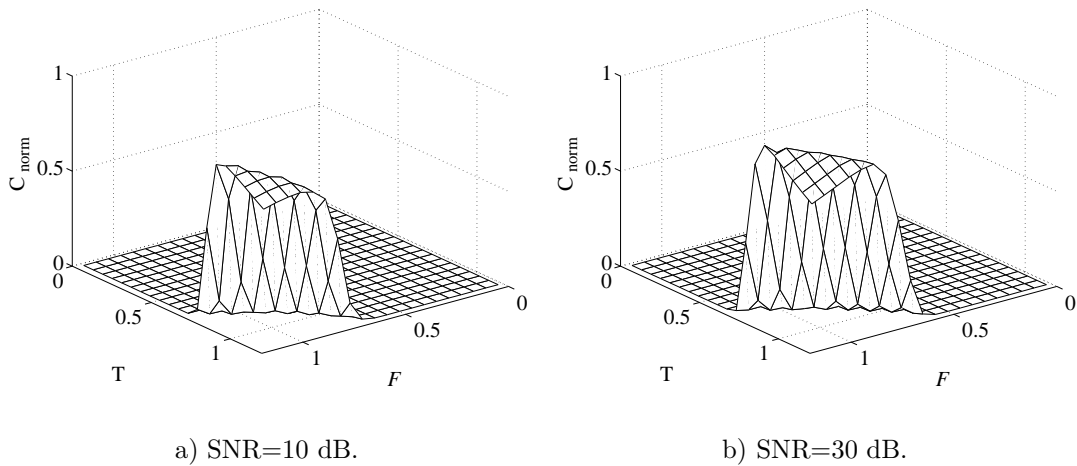


Fig. 4.36. Normalized channel capacity C_{norm} of (4.27) of a HY system with a gauss basic transmit signature $\underline{c}_0(t)$ of (3.18) versus the frequency separation F and time separation T ; $T_{\text{ref}} = 1/F_{\text{ref}} = 1$; $B_0 = 1.2$; ZF-BLE; SNR=10 dB and SNR=30 dB; $N = 64$; AWGN channel.

is large and the amount of interference generated in time domain is larger. For $B_0 = 0.9$, see Fig. 4.35, the interference is equally distributed in time and frequency direction, see Fig. 3.6. As a consequence, the normalized channel capacity C_{norm} of (4.27) shows the same dependency on the time separation T and frequency separation F . For $B_0 = 1.2$, see Fig. 4.36, with the larger 3 dB bandwidth B_0 most of the interference is generated by the frequency overlapping of the basic transmit signatures $\underline{c}_0(t)$. Therefore, the normalized channel capacity C_{norm} of (4.27) decreases faster when F decreases.

In Figs. 4.37 to 4.38, we report the normalized channel capacity C_{norm} of (4.27) of a

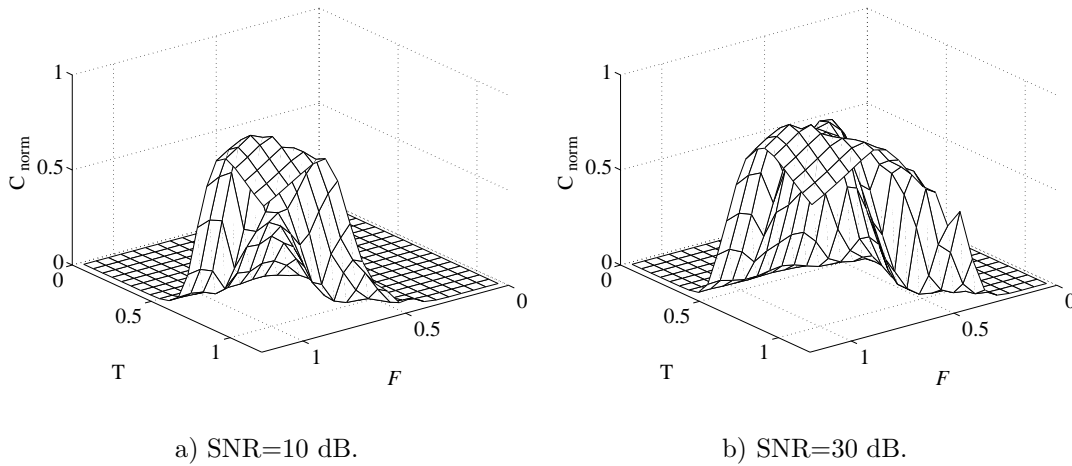


Fig. 4.37. Normalized channel capacity C_{norm} of (4.27) of a HY system with an rrcos basic transmit signature $\underline{c}_0(t)$ of (3.21) versus the frequency separation F and time separation T ; $T_{\text{ref}} = 1/F_{\text{ref}} = 1$; $\alpha = 0.1$; ZF-BLE; $N = 64$; SNR=10 dB and SNR=30 dB; AWGN channel.

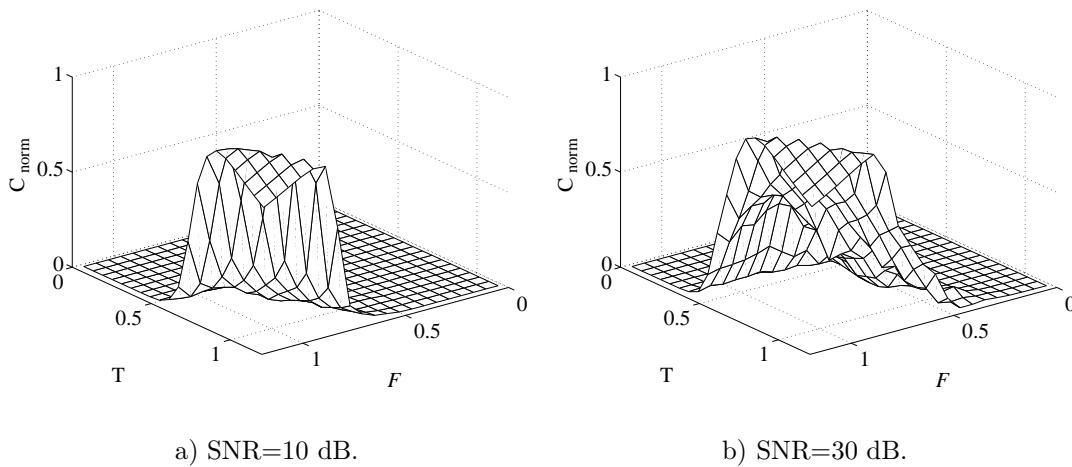


Fig. 4.38. Normalized channel capacity C_{norm} of (4.27) of a HY system with an rrcos basic transmit signature $\underline{c}_0(t)$ of (3.21) versus the frequency separation F and time separation T ; $T_{\text{ref}} = 1/F_{\text{ref}} = 1$; $\alpha = 0.3$; ZF-BLE; SNR=10 dB and SNR=30 dB; $N = 64$; AWGN channel.

HY system with an rrcos basic transmit signature $\underline{c}_0(t)$ of (3.21) and a roll-off factor $\alpha = 0.1$ and $\alpha = 0.3$, respectively. The normalized channel capacity C_{norm} of (4.27) gets slightly larger than one when F and T are close to one. For other values of T and F the normalized channel capacity C_{norm} of (4.27) is significantly smaller than one, i.e. it seems of no convenience to reduce the time and/or frequency separation. By comparing Fig. 4.37 with Fig. 4.38 we can notice also in this case the effect of an enlargement of the frequency

occupation due to the different value of the roll-off factor α . With the increasing of α , HY systems become slightly more sensitive to the reduction of the frequency separation F than to the reduction of the time separation T .

From Figs. 4.32 to 4.38, we have seen that in HY systems no one basic transmit signature $\underline{c}_0(t)$ of our choice, cf. Table 3.3, improves the channel capacity C of (3.44) if the time separation T and the frequency separation F are reduced. This does not imply that does not exist any basic transmit signature $\underline{c}_0(t)$ able to provide a larger channel capacity C also in HY systems. There might exist, but for the duality between time and frequency occupation it is very unlikely to find a basic transmit signature $\underline{c}_0(t)$ ensuring a significant gain in HY systems.

5 Discussion on simulations: Recommendations

5.1 General

In Chapter 4, we have presented the simulation results and discussed them to a certain extent to highlight in particular some peculiar relationships between different system configurations. In this chapter, we summarize the main results and investigate them in more detail in order to derive the most promising configurations. We finally conclude with some recommendations based on the attained results.

The sensitivity of SC, MC and HY systems to the reduction of the time separation T and/or frequency separation F was investigated in the previous chapter. We derived analytically the relationship between SC and MC systems and inferred that SC and MC systems have the same system matrix $\underline{\mathbf{A}}$ of (2.14) if the basic transmit signature $\underline{c}_0(t)$ of the SC system has the same shape as the Fourier transform of the basic transmit signature $\underline{c}_0(t)$ of the MC system. Therefore, investigating SC or MC systems is perfectly equivalent and in the following we avoid any consideration regarding MC systems since we are aware that the conclusions made on SC systems can be transferred to MC systems. The most promising configurations are given by SC systems with a time limited basic transmit signature $\underline{c}_0(t)$. HY systems are of no interest since the amount of interference in the time and frequency directions is very high for any proposed basic transmit signature $\underline{c}_0(t)$. In the remainder of the chapter, we focus our attention on SC systems with a rect basic transmit signature $\underline{c}_0(t)$ of (3.10) and examine in more detail the corresponding simulation results reported in Fig. 4.1, cf. Section 5.2. In Section 5.3, we draw the final conclusions suggesting some recommendations.

5.2 SC system with rectangular basic transmit signature

5.2.1 Properties

The most promising simulation results are given by the rect basic transmit signature $\underline{c}_0(t)$ of (3.10) applied to an SC system, see Figs. 4.1 and 4.23. However, in Chapter 4 we did not explain all the system characteristics emerging from the simulation results. In particular, we shall investigate the presence of the peaks in Fig. 4.1 and the behaviour of the normalized channel capacity C_{norm} in Fig. 4.23 for small values of time separation T .

The investigation starts from the analytical expression of the system matrix $\underline{\mathbf{A}}$ of (4.18) with $T_{\text{ref}} = 1$, i.e.

$$\underline{\mathbf{A}}_{n,n'} = \begin{cases} 1 - (n - n')T & \text{for } |n - n'|T < 1, \\ 0 & \text{else.} \end{cases} \quad (5.1)$$

We then evaluate the SNR-degradation δ of (2.68) of an SC system with a rect basic transmit signature $\underline{c}_0(t)$ of (3.10) by using (2.67), where the system matrix $\underline{\mathbf{A}}$ is derived from (5.1) instead of using (2.12). The results are shown in Fig. 5.1 which slightly differs

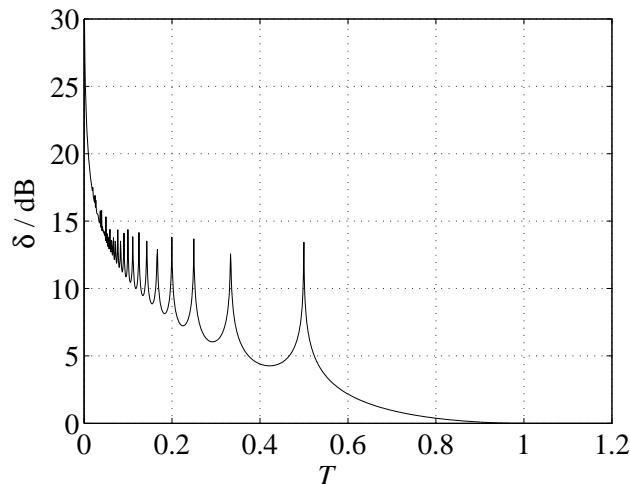


Fig. 5.1. SNR-degradation $\delta(T)$ of an SC system with a rect basic transmit signature $\underline{c}_0(t)$ of (3.10) versus the time separation T ; $T_{\text{ref}} = 1$; ZF-BLE; $N = 64$; AWGN channel. $\underline{\mathbf{A}}$ of (5.1) is assumed.

from Fig. 4.1 and Fig. 4.9. The small differences are due to numerical errors occurring when evaluating the integral in (2.12). Fig. 5.1 confirms the positions of the peaks which correspond to the values of the time separation T for which the number of interfering symbols changes. To justify the observed behaviour we would need to write the expression of δ of (2.68) in a closed form. The approach would be to express δ as in (2.80) and then, based on (5.1), find the dependency of δ on T . We were not able to follow this approach although the simple structure of the system matrix $\underline{\mathbf{A}}$ of (5.1) might allow to pursue this goal. The difficulties are related to the complexity of finding a closed form solution of the characteristic equation of $\underline{\mathbf{A}}$ of (5.1) without fixing the value of the number N and of the time separation T .

We follow a different approach. We consider two values of the time separation T corresponding to a peak and a valley of the SNR-degradation δ of Fig. 5.1. Then, we fix the number N . The value of N influences the numerical results but not the properties of the system matrix $\underline{\mathbf{A}}$ of (2.14). With these choices, we can investigate the properties of the system matrixes $\underline{\mathbf{A}}$ which generate the presence of peaks and valleys. In particular, we consider the inverse of the eigenvalues $1/\lambda_n$ of $\underline{\mathbf{A}}$ of (5.1), since their average value determine the SNR-degradation δ , cf. (2.79) and (2.80).

We choose $T = 0.5$, $T = 0.4$ and $N = 8$. The choice of $N = 8$ allows us to visualize all the elements of the involved system matrixes $\underline{\mathbf{A}}$. With $T = 0.5$, the system matrix $\underline{\mathbf{A}}$ of (5.1) reads

$$\underline{\mathbf{A}} = \begin{pmatrix} 1 & 0.5 & 0 & 0 & 0 & 0 & 0 & 0 \\ 0.5 & 1 & 0.5 & 0 & 0 & 0 & 0 & 0 \\ 0 & 0.5 & 1 & 0.5 & 0 & 0 & 0 & 0 \\ 0 & 0 & 0.5 & 1 & 0.5 & 0 & 0 & 0 \\ 0 & 0 & 0 & 0.5 & 1 & 0.5 & 0 & 0 \\ 0 & 0 & 0 & 0 & 0.5 & 1 & 0.5 & 0 \\ 0 & 0 & 0 & 0 & 0 & 0.5 & 1 & 0.5 \\ 0 & 0 & 0 & 0 & 0 & 0 & 0.5 & 1 \end{pmatrix}. \quad (5.2)$$

The interference on each symbol is generated only by the previous and the following symbols. $\underline{\mathbf{A}}$ of (5.2) generates an SNR-degradation δ of $\delta \approx 14$ dB, cf. Fig. 5.1, and corresponds to the right most peak. For $T = 0.4$, $\underline{\mathbf{A}}$ of (5.1) reads

$$\underline{\mathbf{A}} = \begin{pmatrix} 1 & 0.6 & 0.2 & 0 & 0 & 0 & 0 & 0 \\ 0.6 & 1 & 0.6 & 0.2 & 0 & 0 & 0 & 0 \\ 0.2 & 0.6 & 1 & 0.2 & 0.6 & 0 & 0 & 0 \\ 0 & 0.2 & 0.6 & 1 & 0.2 & 0.6 & 0 & 0 \\ 0 & 0 & 0.2 & 0.6 & 1 & 0.2 & 0.6 & 0 \\ 0 & 0 & 0 & 0.2 & 0.6 & 1 & 0.2 & 0.6 \\ 0 & 0 & 0 & 0 & 0.2 & 0.6 & 1 & 0.2 \\ 0 & 0 & 0 & 0 & 0 & 0.2 & 0.6 & 1 \end{pmatrix}. \quad (5.3)$$

Now, the interference on each symbol is generated by the two previous and the two following symbols. Therefore, it is greater than the interference of $\underline{\mathbf{A}}$ of (5.2). The corresponding SNR-degradation is $\delta \approx 4$ dB, which is 10 dB below the SNR-degradation δ given by (5.2). We infer that a larger amount of interference does not always imply a larger SNR-degradation δ of (2.68). In both cases $\underline{\mathbf{A}}$ is non-singular and the ZF-BLE removes all the interference generating a noise enhancement, i.e. the SNR-degradation δ . Since the SNR-degradation δ of (2.68) is proportional to the sum of the inverse of the eigenvalues $1/\lambda_n$ of $\underline{\mathbf{A}}$, cf. (2.80), in Fig. 5.2, we report the inverse of the eigenvalues of $\underline{\mathbf{A}}$ of (5.2) and of $\underline{\mathbf{A}}$ of (5.3). The λ_n are quite similar but for λ_1 which represents the minimum eigenvalue λ_{\min} of the system matrix $\underline{\mathbf{A}}$. For $T = 0.5$, λ_{\min} of $\underline{\mathbf{A}}$ of (5.2) is very close to zero, so causing the peak in the SNR-degradation δ , see Fig. 5.1. In other words, the condition number $|\lambda_{\max}/\lambda_{\min}|$ of $\underline{\mathbf{A}}$ is larger in the case of (5.2) than in the case of (5.3).

Figs. 5.1 and 5.2 show how the peaks and the valleys of the SNR-degradation δ of (2.68) are related to the eigenvalues λ_n of the system matrix $\underline{\mathbf{A}}$. By reducing the time separation T , e.g. from $T = 0.5$ to $T = 0.4$, and introducing on purpose a given amount of interference, we can influence the structure of the system matrix $\underline{\mathbf{A}}$ in such a way that the minimum eigenvalue λ_{\min} is increased. As compared with the ISI introduced by a

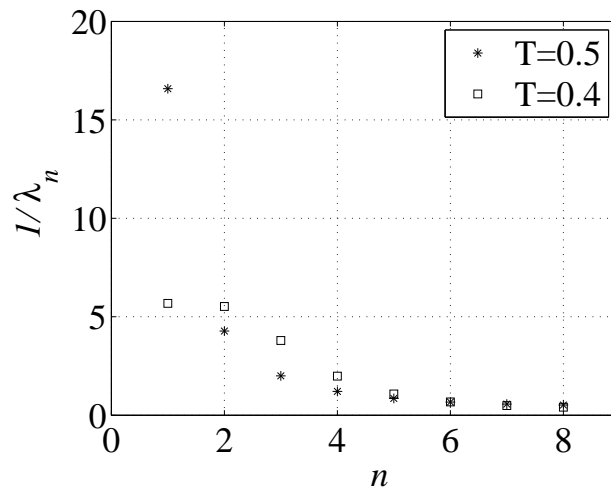


Fig. 5.2. Inverse of the eigenvalues λ_n of the system matrix $\underline{\mathbf{A}}$ of (5.1) of an SC system with a rect basic transmit signature $\underline{c}_0(t)$ of (3.10). $T_{\text{ref}} = 1$; $T = 0.5$; $T = 0.4$; $N = 8$.

multipath channel which depends on the current channel realization, in this case we have full control on the ISI through the choice of the basic transmit signature $\underline{c}_0(t)$ and the time separation T . Therefore, we can choose the values of the time separation T to build a system matrix $\underline{\mathbf{A}}$ with the minimum eigenvalues λ_{\min} not too close to zero.

5.2.2 Channel capacity

In this subsection, we re-obtain Fig. 4.23, in which we showed the normalized channel capacity C_{norm} of (4.27) of an SC system with a rect basic transmit signature $\underline{c}_0(t)$ of (3.10), starting from (5.1) instead of (2.12). We plot the results in Fig. 5.3 showing all the values of the normalized channel capacity C_{norm} of (4.27). In Fig. 5.3a we consider the whole range of T , while in Fig. 5.3b we focus on very small values of the time separation T to visualize the behaviour of the normalized channel capacity C_{norm} around its maximum. For SNR=10 dB, by reducing the time separation T , $C_{\text{norm}} \approx 2$ can be achieved. However, from Fig. 5.3b we infer that the value is not stable and the channel capacity C of (3.44) changes significantly for small variations of T . For SNR=30 dB, we observe that the channel capacity C of (3.44) tends to zero for $T \approx 0$, but by reducing T below 0.02. We can achieve a channel capacity C of (3.44) 11 times higher than the channel capacity C of (3.33) of the AWGN channel in absence of interference. However, also in this case the maximum value of channel capacity C is very sensitive to the time separation T . For a small variation of T we could end up in a region with much lower values of channel capacity C of (3.44). In the worst case, a small variation of T might cause the channel capacity C to go to zero.

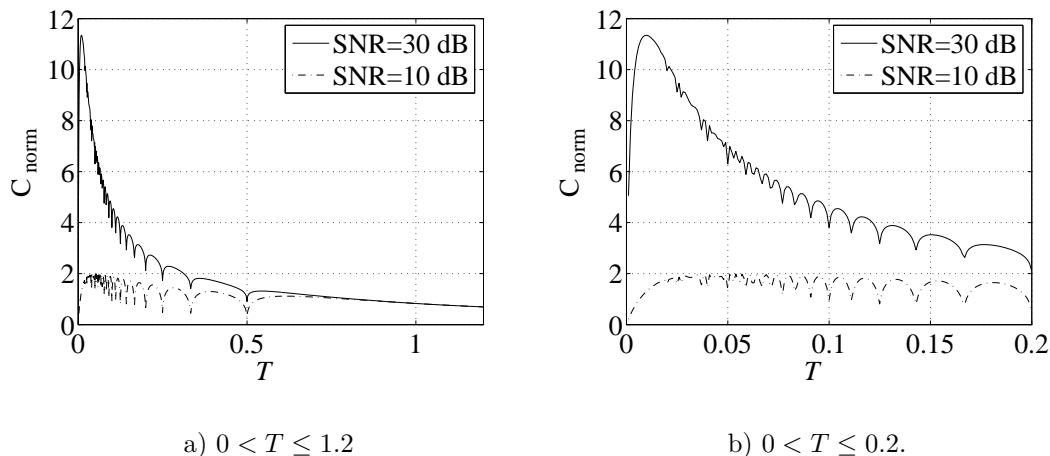


Fig. 5.3. Normalized channel capacity C_{norm} of (4.27) of an SC system with a rect basic transmit signature $\underline{c}_0(t)$ of (3.10) versus the time separation T ; $T_{\text{ref}} = 1$; ZF-BLE; SNR=10 dB and SNR=30 dB; $N = 64$; AWGN channel. $\underline{\mathbf{A}}$ of (5.1) is assumed.

We have shown that in SC systems by choosing a time limited basic transmit signature $\underline{c}_0(t)$ the trade-off between R of (2.57) and δ of (2.68) is promising and a higher channel capacity C of (3.44) can be achieved by reducing the time separation T . The maximum increment in channel capacity C of (3.44) is given for very small values of the time separation T . However, we do not recommend to choose a small value of T for two reasons:

1. The high value of the channel capacity C of (3.44) depends on the precise value of T . If the time separation T changes due to some impairments, e.g. bad time synchronization between the transmitter and the receiver, then the channel capacity C may significantly degrade.
2. From Fig. 5.1 and Fig. 5.3a, we infer that the maximum value of channel capacity C of (3.44) corresponds to an SNR-degradation $\delta \approx 20$ dB. To maintain the same system performance in terms of average bit error probability P_b , when transmitting with such a low time separation T , we shall increase the transmitted power of 20 dB. In any realistic scenario, 20 dB of increment in transmit power cannot be accepted.

We propose a more conservative approach. We choose $T = 0.4$ which does not offer the maximum value of channel capacity C of (3.44), but it returns a lower value of SNR-degradation δ of (2.68). Moreover, the corresponding value of the channel capacity C is less sensitive to the variations of T .

5.2.3 Possible applications

To show the potential of the proposed method of increasing the resource usage, we design a simple SC system and simulate its performance in terms of the average bit error probability P_b versus the average energy E_b per bit over the one sided noise power spectral density N_0 . We compare a system which satisfies the Nyquist assumptions of no ISI in an AWGN channel [BeC02, Pro95] with a system in which we employ the proposed method to reduce the time separation T beyond the Nyquist assumptions.

We consider the SC system of Fig. 5.4. The bits b_{n_b} , $n_b = 1 \dots N_b$, are stacked in

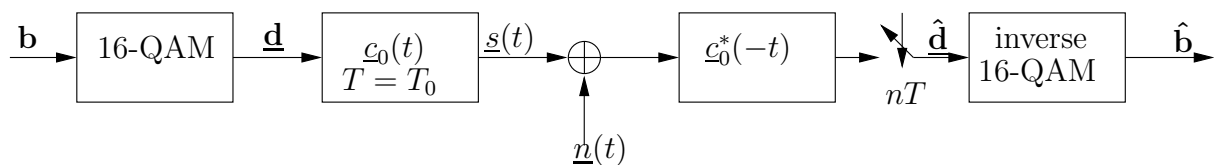


Fig. 5.4. SC system with a 16-QAM bit-mapping and a rect basic transmit signature $\underline{c}_0(t)$ of (3.10) with 3 dB time duration T_0 equal to the time separation T .

the bit vector

$$\mathbf{b} = (b_1 \dots b_{N_b})^T. \quad (5.4)$$

Each group of $\text{ld}(M_d) = 4$ bit of \mathbf{b} of (5.4) is mapped into a complex data symbol \underline{d}_n of $\underline{\mathbf{d}}$ of (2.1) through a 16-QAM bit-mapping [BeC02, Pro95]. The number N_b of bits is related to the number N of transmit data symbols through $N_b = N \cdot \text{ld}(M_d)$. The complex symbols \underline{d}_n are given as input to a filter [BeC02] with an impulse response determined by the basic transmit signature $\underline{c}_0(t)$. The transmitted signal $\underline{s}(t)$ reads as in (2.25). An AWGN channel is assumed so that $\underline{s}(t)$ is only corrupted by an AWGN $\underline{n}(t)$ and then enters the MF. After the MF, the signal is sampled at the multiples of the time separation T to obtain the estimates $\hat{\underline{\mathbf{d}}}$ of $\underline{\mathbf{d}}$. The inverse 16-QAM maps the complex estimates $\hat{\underline{\mathbf{d}}}$ in the bit estimates $\hat{\mathbf{b}}$. The basic transmit signature $\underline{c}_0(t)$ is chosen to be a rect of (3.10) with 3 dB duration $T_0 = T$. The described system is a conventional SC system [Pro95]. The Nyquist conditions are satisfied so that in an AWGN channel there is no ISI at the receiver and there is no need for any post-processing stage. The bit rate R_b is given by

$$R_b = \frac{\text{ld}(M_d)}{T}. \quad (5.5)$$

Under the assumption of 16-QAM and of $T = T_0$, we obtain from (5.5)

$$R_b = 4 \text{ bit}/T_0. \quad (5.6)$$

We further assume the data covariance matrix $\underline{\mathbf{R}}_d = \mathbf{I}$, cf. (2.22), and the energy per symbol defined as, cf. Subsection 2.6.4,

$$E_s = \int_{-\infty}^{+\infty} |\underline{c}_0(t)|^2 dt. \quad (5.7)$$

We indicate the signal power with P_s and the noise power with P_n and write the average SNR γ at the input of the MF as [BeC02, Pro95]

$$\gamma = \frac{P_s}{P_n}. \quad (5.8)$$

The average signal power P_s depends on the average signal energy E_s of (5.7) as [BeC02, Pro95]

$$P_s = \frac{E_s}{T}. \quad (5.9)$$

The average noise power P_n depends on the one sided noise power spectral density N_0 and the total bandwidth B_{tot} . We assume that the noise bandwidth is limited by the total system bandwidth B_{tot} . Since we have assumed an SC system in which $B_{\text{tot}} = B_0$, cf. (2.26), then [Pro95]

$$P_n \approx N_0 B_0. \quad (5.10)$$

With (5.9) and (5.10), (5.8) reads

$$\gamma = \frac{E_s}{N_0 B_0 T}. \quad (5.11)$$

From the definition of the rate R of (2.59) and indicating with $E_b = E_s/\text{ld}(M_d)$ the average energy per bit [BeC02, Pro95], we obtain

$$\gamma = \frac{E_b}{N_0} \text{ld}(M_d) R. \quad (5.12)$$

The relationship between γ and the ratio E_b/N_0 is a function of the order M_d of the bit-mapping and of the rate R of (2.57). In conventional SC systems in which the Nyquist assumptions are verified, the rate $R = 1$ and $\gamma = E_s/N_0$.

We evaluate the performance, see the dashed curve in Fig. 5.6, in terms of average bit error probability P_b [Skl04] versus the ratio E_b/N_0 of (5.12). In the case of the system of Fig. 5.4 with $R = 1$, the performance is the same as reported in [BeC02].

We now apply the proposed method to improve the performance of the SC scheme in Fig. 5.4. We first suppose to maintain the bit rate R_b constant. From (5.5), we infer that we could choose a QPSK [Pro95] and select a time separation $T = 0.5$. From Fig. 5.1, we infer that $T = 0.5$ corresponds to a high SNR-degradation δ of (2.68), therefore we choose $T = 0.4$, cf. Subsection 5.2.2. The resulting bit rate R_b is slightly increased, i.e.

$$R_b = 4.5 \text{ bit}/T_0. \quad (5.13)$$

The resulting SC communication scheme is depicted in Fig. 5.5, and its performance is evaluated in terms of average bit error probability P_b versus E_b/N_0 , cf. (5.12). In Fig. 5.5, we notice the presence of the post-processing stage which realizes a ZF-BLE. The equalizer is needed also in the presence of an AWGN channel since we are reducing the time

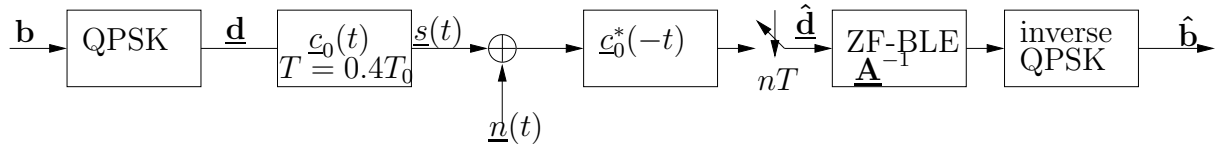


Fig. 5.5. SC system with a QPSK bit-mapping, a rect basic transmit signature $\underline{c}_0(t)$ of (3.10) and a time separation $T = 0.4T_0$.

separation T beyond the Nyquist assumption and ISI arises.

In Fig. 5.6 we depict the simulation results obtained when implementing the schemes of Figs. 5.4 and 5.5 and assuming the continuous time $t = lT_0/10$, $l = -\infty \cdots +\infty$. The

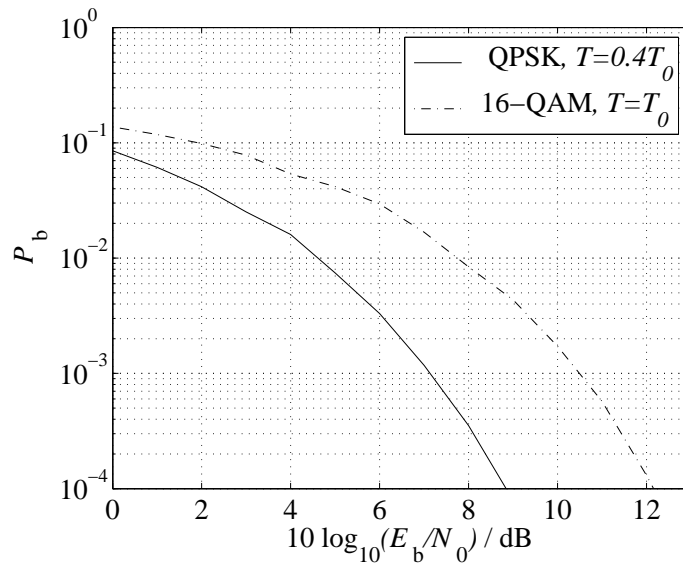


Fig. 5.6. Average bit error probability P_b versus $(E_b/N_0)_{\text{dB}}$. SC system with rect basic transmit signature $\underline{c}_0(t)$ of (3.10). 16-QAM with $T = T_0$ and QPSK with $T = 0.4T_0$.

proposed approach offers a slightly higher bit rate R_b of (5.5) while ensuring a gain in power efficiency barely higher than three dB. We notice that the E_b/N_0 ratio of (5.12) depends on the rate R of (2.57) which is higher in the QPSK than in the 16-QAM case. The three dB gain costs in terms of additional receiver complexity since, by reducing the time separation T , we have to introduce a ZF-BLE as in Fig. 5.5. However, the required increment in complexity is not very significant. The inverse of the system matrix $\underline{\mathbf{A}}^{-1}$ can be determined off-line and the ZF-BLE becomes a simple linear transformation.

5.3 Recommendations

The reduction of the time separation T or the frequency separation F enables the increment of the usage of the available resources R of (2.57) at a cost of a degradation in the SNR at the output of the post processing stage, i.e. the SNR-degradation δ of (2.68) and (2.76). The most promising configurations are SC systems with time limited basic transmit signatures $\underline{c}_0(t)$ and MC systems with frequency limited basic transmit signatures $\underline{c}_0(t)$. In these systems, the trade-off between R of (2.57) and δ of (2.68) and (2.76) achieved through the proposed method allows an improvement in terms of channel capacity C of (3.44) with respect to systems with a unitary rate $R = 1$ and $\delta = 0$ dB. The increment of R of (2.57) can be exploited to increase the transmission data rate or, equivalently, to reduce the total occupied bandwidth B_{tot} .

The analysis of the proposed method has assumed the presence of an AWGN channel, cf. Subsection 3.3.6. Propagation scenarios in which the impact of multipath propagation is negligible could be potential fields of application of the proposed method, e.g. indoor cellular links with very small cell size. The required increment in terms of complexity is not prohibitive since the system matrix $\underline{\mathbf{A}}$ of (2.14) is determined only by the choice of the basic transmit signature $\underline{c}_0(t)$ and the time separation T . Both these parameters are set by the design of the system so that the inverse of the system matrix $\underline{\mathbf{A}}^{-1}$ can be determined off-line. The receiver has to perform a linear time invariant transformation.

Our conclusion is that a more efficient usage of the available resources can be obtained by reducing the time separation T and/or the frequency separation F . The key idea of the thesis is to reduce T and/or F below the values which may ensure absence of ISI in an AWGN channel. The key result is that the reduction of T and/or F allows an increment in terms of channel capacity C of (3.44) at the additional cost of a post-processing stage which eliminates the ISI. Further work is necessary to investigate in more detail the impact of multipath propagation and to propose a realistic application.

6 Summary

6.1 English

The present thesis deals with a novel approach to increase the resource usage in digital communications. In digital communication systems, each information bearing data symbol is associated to a waveform which is transmitted over a physical medium. The time or frequency separations among the waveforms associated to the information data have always been chosen to avoid or limit the interference among them. By doing so, in the presence of a distortionless ideal channel, a single receive waveform is affected as little as possible by the presence of the other waveforms. The conditions necessary to meet the absence of any interference among the waveforms are well known and consist of a relationship between the minimum time separation among the waveforms and their bandwidth occupation or, equivalently, the minimum frequency separation and their time occupation. These conditions are referred to as Nyquist assumptions.

The key idea of this work is to relax the Nyquist assumptions and to transmit with a time and/or frequency separation between the waveforms smaller than the minimum required to avoid interference. The reduction of the time and/or frequency separation generates not only an increment of the resource usage, but also a degradation in the quality of the received data. Therefore, to maintain a certain quality in the received signal, we have to increase the amount of transmitted power. We investigate the trade-off between the increment of the resource usage and the correspondent performance degradation in three different cases. The first case is the single carrier case in which all waveforms have the same spectrum, but have different temporal locations. The second one is the multi carrier case in which each waveform has its distinct spectrum and occupies all the available time. Finally, the hybrid case when each waveform has its unique time and frequency location. These different cases are framed within the general system modelling developed in the thesis so that they can be easily compared.

We evaluate the potential of the key idea of the thesis by choosing a set of four possible waveforms with different characteristics. By doing so, we study the influence of the waveform characteristics in the three system configurations. We propose an interpretation of the results by modifying the well-known Shannon capacity formula and by explicitly expressing its dependency on the increment of resource usage and on the performance degradation. The results are very promising. We show that both in the case of a single carrier system with a time limited waveform and in the case of a multi-carrier system with a frequency limited waveform, the reduction of the time or frequency separation, respectively, has a positive effect on the channel capacity. The latter, depending on the actual SNR, can double or increase even more significantly.

6.2 German

In der vorliegenden Arbeit wird ein neuer Ansatz zum Steigern der Ressourcenverwendbarkeit in der digitalen Kommunikation betrachtet. In digitalen Kommunikationssystemen entspricht jede in Datensymbolen enthaltene Information einer über ein physikalisches Medium übertragenen Signalform. Die Zeit- oder Frequenzabstände zwischen den mit den Informationsdaten verbundenen Signalformen wurden immer so ausgesucht, daß gegenseitige Interferenzen vermieden oder möglichst begrenzt werden konnten. Hierdurch wird jede einzelne empfangene Signalform, unter der Annahme eines idealen verzerrungsfreien Kanals, so wenig wie möglich von der Anwesenheit der anderen Signalformen beeinflusst. Die notwendigen Bedingungen, um die Abwesenheit von Interferenzen zwischen den Signalformen und den von ihnen belegten Frequenzen zu gewährleisten, sind allgemein bekannt und sind durch das Verhältnis zwischen dem kleinsten Zeitabstand zwischen den Signalformen und den von ihnen beanspruchten Bandbreiten, bzw. zwischen dem geringsten Frequenzabstand und der von ihnen beanspruchten Zeit gegeben. Diese Bedingungen heißen Nyquist-Kriterien. Der Ausgangspunkt dieser Arbeit ist eine Abschwächung der Nyquist-Kriterien, so daß mit einem Zeit- und/oder Frequenzabstand zwischen den Signalformen gesendet wird, der unterhalb der das Auftreten von Interferenzen vermeidenden Mindestschwelle liegt. Die Verringerung des Zeit- und/oder Frequenzabstands ermöglicht nicht nur eine erwünschte Steigerung der Ressourcenausnutzung, sondern verursacht auch eine qualitative Beeinträchtigung der empfangenen Daten. Um eine bestimmte Qualität des empfangenen Signals zu gewährleisten, muß demnach die Sendeleistung erhöht werden. Wir untersuchen das Verhältnis zwischen der möglichen Erhöhung der Ressourcenausnutzung und der dabei auftretenden Degradierung der Systemperformanz in drei unterschiedlichen Fällen. Der erste Fall bezieht sich auf die Einträger-Übertragung, wobei die Signalformen auf derselben Frequenz, aber zu unterschiedlichen Zeitpunkten übertragen werden. Im zweiten Fall wird die Mehrträger-Übertragung untersucht, wobei jede Signalform auf einer unterschiedlichen Frequenz übertragen wird und dafür die gesamte zur Verfügung stehende Zeit beansprucht. Als dritter Fall wird ein hybrider Ansatz betrachtet, bei dem man jede Signalform zu einem eigenen Zeitpunkt und auf einer eigenen Frequenz überträgt. Die drei Fälle sind aus dem allgemeinen Systemmodell, das in dieser Arbeit beschrieben wird, ableitbar und somit direkt vergleichbar. Wir bewerten das Potential der dieser Arbeit zugrundeliegenden Idee anhand vierer Signalformen mit je unterschiedlichen Eigenschaften. Auf diese Art und Weise kann untersucht werden, wie die Signalformeneigenschaften jeweils die drei Systemkonstellationen beeinflussen. Die von uns vorgeschlagene Interpretation der Ergebnisse geht von einer Änderung der bekannten Kapazitätsformel nach Shannon aus, wobei explizit die Abhängigkeit zwischen der Erhöhung der Anzahl verfügbarer Ressourcen und der damit einhergehenden Degradation der Performanz berücksichtigt wird. Die Ergebnisse sind vielversprechend. Wir zeigen, daß sowohl im Fall des Einträger-Übertragungssystems mit einer zeitlich begrenzten Signalform als auch im Fall des Mehrträger-Übertragungssystems mit einer frequenzmäßig begrenzten Signalform die Auswirkung der Verringerung des Zeit- und/oder Frequenzabstands auf die Kapazität des Kanals positiv sind. Letztere kann, abhängig vom tatsächlichen SNR, auf das doppelte oder sogar noch mehr ansteigen.

Appendix

A.1 Abbreviations

| | |
|----------|----------------------------------------------------------------------------------------------------------|
| 2G | <u>2</u> nd <u>G</u> eneration |
| 3G | <u>3</u> rd <u>G</u> eneration |
| 4G | <u>4</u> th <u>G</u> eneration |
| ADSL | <u>A</u> ynchronous <u>D</u> igital <u>S</u> ubscriber <u>L</u> ine |
| AWGN | <u>A</u> dditive <u>W</u> hite <u>G</u> aussian <u>N</u> oise |
| BER | average <u>B</u> it <u>E</u> rror <u>R</u> ate |
| CDMA | <u>C</u> ode <u>D</u> ivision <u>M</u> ultiple <u>A</u> ccess |
| DFT | <u>D</u> iscrete <u>F</u> ourier <u>T</u> ransform |
| DL | <u>D</u> own <u>L</u> ink |
| DAB | <u>D</u> igital <u>A</u> udio <u>B</u> roadcasting |
| DAV | <u>D</u> igital <u>V</u> ideo <u>B</u> roadcasting |
| Ch | <u>C</u> hannel |
| FB | <u>F</u> ilter <u>B</u> ank |
| FDD | <u>F</u> requency <u>D</u> ivision <u>D</u> uplex |
| FDM | <u>F</u> requency <u>D</u> ivision <u>M</u> ultiplexing |
| FDMA | <u>F</u> requency <u>D</u> ivision <u>M</u> ultiple <u>A</u> ccess |
| FEC | <u>F</u> orward <u>E</u> rror <u>C</u> orrecting |
| FFT | <u>F</u> ast <u>F</u> ourier <u>T</u> ransform |
| FMT | <u>F</u> iltered <u>M</u> ulti <u>T</u> one |
| G-HY | <u>G</u> eneric <u>H</u> Ybrid |
| GPS | <u>G</u> lobal <u>P</u> ositioning <u>S</u> ystem |
| HY | <u>H</u> Ybrid |
| ICI | <u>I</u> nter <u>C</u> hannel <u>I</u> nterference |
| IFFT | <u>I</u> nverse <u>F</u> ast <u>F</u> ourier <u>T</u> ransform |
| ISI | <u>I</u> nter <u>S</u> ymbol <u>I</u> nterference |
| LAN | <u>L</u> ocal <u>A</u> rea <u>N</u> etwork |
| MAP | <u>M</u> aximum <u>a</u> Posteriori <u>P</u> robability |
| MC | <u>M</u> ulti <u>C</u> arrier |
| MF | <u>M</u> atched <u>F</u> ilter |
| ML | <u>M</u> aximum <u>L</u> ikelihood |
| MMSE-BLE | <u>M</u> inimum <u>M</u> ean <u>S</u> quare <u>E</u> rror <u>B</u> lock <u>L</u> inear <u>E</u> qualizer |
| OFDM | <u>O</u> rthogonal <u>F</u> requency <u>D</u> ivision <u>M</u> ultiplexing |
| O-QAM | <u>O</u> ffset <u>Q</u> AM |
| PAPR | <u>P</u> eak to <u>A</u> verage <u>P</u> ower <u>R</u> atio |
| PR | <u>P</u> erfect <u>R</u> econstruction |
| QAM | <u>Q</u> uadrature <u>A</u> mplitude <u>M</u> odulation |

| | |
|--------|------------------------------------------------------------------------------------------|
| QoS | <u>Q</u> uality of <u>S</u> ervice |
| QPSK | <u>Q</u> uadrature <u>P</u> hase <u>S</u> hift <u>K</u> ey |
| Rx | <u>R</u> eceiver |
| SC | <u>S</u> ingle <u>C</u> arrier |
| SIDMA | <u>S</u> ignature <u>D</u> ivision <u>M</u> ultiple <u>A</u> ccess |
| SNIR | <u>S</u> ignal to <u>N</u> oise plus <u>I</u> nterference <u>R</u> atio |
| SNR | <u>S</u> ignal to <u>N</u> oise <u>R</u> atio |
| TDD | <u>T</u> ime <u>D</u> ivision <u>D</u> uplex |
| TDM | <u>T</u> ime <u>D</u> ivision <u>M</u> ultiplexing |
| TDMA | <u>T</u> ime <u>D</u> ivision <u>M</u> ultiple <u>A</u> ccess |
| TMUX | <u>T</u> rans <u>m</u> ultiplex <u>e</u> r |
| Tx | <u>T</u> ransmitter |
| UL | <u>U</u> p <u>L</u> ink |
| VDSL | <u>V</u> ery high speed <u>D</u> igital <u>S</u> ub-scriber <u>L</u> ine |
| WSSUS | <u>W</u> ide <u>S</u> ense <u>S</u> tationary with <u>U</u> ncorrelated <u>S</u> catters |
| ZF-BLE | <u>Z</u> ero <u>F</u> orcing <u>B</u> lock <u>L</u> inear <u>E</u> qualizer |

A.2 Symbols

| | |
|----------------------------------------------------------------------|-----------------------------------------------------------------------------------------------------------------------------------------------|
| $\underline{A}_{n,n'}$ | correlation coefficient between the transmit data symbol $\underline{d}_{n'}$ and the receive data symbol $\underline{d}_{MF,n}$ |
| $\tilde{\underline{A}}_{n,n'}$ | modified correlation coefficient between the transmit data symbol $\underline{d}_{n'}$ and the receive data symbol $\underline{d}_{MF,n}$ |
| $\underline{A}_{n,n'}^{(k,k')}$ | correlation coefficient between the transmit data symbol $\underline{d}_{n'}^{(k')}$ and the receive data symbol $\underline{d}_{MF,n}^{(k)}$ |
| $\underline{\mathbf{A}}$ | system matrix |
| $\underline{\mathbf{A}}^{(k,k')}$ | system matrix from user k' to user k |
| $\underline{\mathbf{A}}^{(k)}$ | system matrix of user k |
| $\underline{\mathbf{A}}^{(MU)}$ | multi user system matrix |
| $\tilde{\underline{\mathbf{A}}}$ | modified system matrix |
| $\hat{\underline{\mathbf{A}}}$ | block structured matrix depending only on $\Delta_t(n, n')$ and $\Delta_f(n, n')$ and $\underline{\mathcal{C}}_0(t)$ |
| $\hat{\underline{\mathbf{A}}}_{\text{sub}}^{(n_t, n'_t)}(n_f, n'_f)$ | elements of the submatrix $\hat{\underline{\mathbf{A}}}_{\text{sub}}^{(n_t, n'_t)}$ |
| $\hat{\underline{\mathbf{A}}}_{\text{sub}}^{(n_t, n'_t)}$ | sub-matrix of $\hat{\underline{\mathbf{A}}}$ |
| $\underline{\mathbf{A}}_n$ | linear transformation which colours the noise |
| B | system bandwidth |
| B_0 | 3 dB bandwidth |
| $B_{0, n_f(n)}$ | 3 dB bandwidth of $\underline{\mathcal{C}}_{0, n_f(n)}(t)$ |
| B_C | coherence bandwidth of the multipath channel |
| B_{tot} | total bandwidth of the radiated signal |

| | |
|----------------------------------------------------------|-------------------------------------------------------------------------------------------------------|
| b_{n_b} | bit |
| \mathbf{b} | bit vector |
| $\hat{\mathbf{b}}$ | bit vector estimate |
| C | channel capacity |
| C_{norm} | normalized channel capacity |
| $\underline{C}_0(f)$ | Fourier transform of the basic transmit signature $\underline{c}_0(t)$ |
| $\hat{\underline{C}}_{0,\Delta_t}(f)$ | Fourier transform of $\hat{\underline{c}}_{0,\Delta_t}(t)$ |
| $\underline{c}_0(t)$ | basic transmit signature |
| $\hat{\underline{c}}_{0,\Delta_t}(t)$ | product of $\underline{c}_0(t)$ and $\underline{c}_0(t - \Delta_t(n, n')T)$. |
| $\underline{c}_{0,n_f(n)}(t)$ | basic transmit signature on sub-carrier $n_f(n)$ |
| $\underline{c}_n(t)$ | data symbol specific transmit signature |
| $\underline{c}_n^{(k)}(t)$ | data symbol specific transmit signature of user k |
| $\underline{c}_{r,n}(t)$ | data symbol specific receive signature |
| $\underline{c}_{r,n}^{(k)}(t)$ | data symbol specific receive signature of user k |
| $\tilde{\underline{c}}_{r,n}(t)$ | modified data symbol specific receive signature |
| \underline{d}_n | complex data symbol, $n = 1 \dots N$, |
| $\underline{d}_n^{(k)}$ | data symbol of user k |
| $\underline{\mathbf{d}}$ | data vector |
| $\underline{\mathbf{d}}^{(k)}$ | data vector of user k |
| $\underline{\mathbf{d}}^{(\text{MU})}$ | multi user data vector |
| $\hat{\underline{\mathbf{d}}}$ | final estimate of the data vector |
| $\hat{\underline{d}}_{\text{MF},n}$ | raw estimate of the data symbol \underline{d}_n after the MF |
| $\hat{\underline{\mathbf{d}}}_{\text{MF}}$ | raw estimate of the data symbol vector $\underline{\mathbf{d}}$ after the MF |
| $\hat{\underline{d}}_{\text{MF},n}^{(k)}$ | raw estimate of the data symbol $\underline{d}_n^{(k)}$ after the MF |
| $\hat{\underline{\mathbf{d}}}_{\text{MF}}^{(k)}$ | raw estimate of the data symbol vector $\underline{\mathbf{d}}^{(k)}$ after the MF |
| $\hat{\underline{\mathbf{d}}}_{\text{MF}}^{(\text{MU})}$ | multi user raw estimate of the data symbol vector $\underline{\mathbf{d}}^{(\text{MU})}$ after the MF |
| E_b | average energy per bit |
| E_s | average energy per symbol |
| $\underline{e}(t)$ | useful signal at the channel output |
| $\underline{e}^{(k)}(t)$ | useful signal of user k at the channel output |
| F | frequency separation between two consecutive basic transmit signatures |
| F_{ref} | reference frequency |
| $F^{(\text{MC})}$ | frequency separation between consecutive transmit signatures in MC systems |
| $F^{(\text{HY})}$ | frequency separation between consecutive transmit signatures in HY systems |
| $F_{n_f(n)}$ | frequency location of sub-carrier $n_f(n)$ |
| f_c | carrier frequency |
| f_D | Doppler shift |
| gauss | Gaussian basic transmit signature $\underline{c}_0(t)$ |
| $\underline{H}(f)$ | channel transfer function |

| | |
|----------------------------------------------------|----------------------------------------------------------------------------------------------|
| $\underline{H}_{n_f(n)}$ | value of the channel transfer function for the sub-carrier $n_f(n)$ |
| $\underline{h}(\tau, t)$ | impulse response of the linear time variant channel |
| $\underline{h}^{(k)}(\tau, t)$ | impulse response of the linear time variant channel experienced by user k |
| $\underline{h}_n(\tau)$ | impulse response of the MF for $\underline{c}_{r,n}(t)$ |
| k | user index |
| K | total number of users |
| L_n | energy loss factor |
| $\text{ld}(\cdot)$ | base two logarithm |
| $\ln(\cdot)$ | base e logarithm |
| M | oversampling factor in FBs |
| M_d | order of the bit-mapper |
| N | number of symbols per data block |
| N_0 | one sided noise power spectral density of the AWGN |
| N_K | number of symbols per user per data block |
| N_b | number of bit |
| N_f | number of sub-carriers |
| N_t | number of symbol time slots |
| n | data symbol index, $n = 1 \dots N$ |
| n_b | bit index |
| $n_t(n)$ | function that maps the data symbol index n to the correspondent symbol slot index $n_t(n)$ |
| $n_f(n)$ | function that maps the data symbol index n to the correspondent sub-carrier index $n_f(n)$ |
| $\underline{n}(t)$ | additive white Gaussian noise |
| $\tilde{\underline{n}}_n$ | element n of the modified receive noise vector $\tilde{\underline{\mathbf{n}}}$ |
| $\tilde{\underline{\mathbf{n}}}$ | modified receive noise vector |
| $\underline{\mathbf{n}}_{\text{MF}}$ | receive noise vector after the MF |
| $\underline{n}_{\text{MF},n}$ | receive noise sample affecting the receive symbol $\hat{d}_{\text{MF},n}$ |
| $\underline{n}_{\text{MF},n}^{(k)}$ | receive noise sample of user k affecting the receive symbol $\hat{d}_{\text{MF},n}$ |
| $\underline{\mathbf{n}}_{\text{MF}}^{(k)}$ | receive noise vector of user k after the MF |
| $\underline{\mathbf{n}}_{\text{MF}}^{(\text{MU})}$ | multi user receive noise vector after the MF |
| P_b | average bit error probability |
| P_n | noise power |
| P_s | transmitted signal power |
| R | rate |
| $R^{(\text{SC})}$ | rate of SC systems |
| $R^{(\text{MC})}$ | rate of MC systems |
| $R^{(\text{HY})}$ | rate of HY systems |
| $R^{(\text{G-HY})}$ | rate of G-HY systems |
| R_b | bit rate |
| $\underline{\mathbf{R}}_d$ | data covariance matrix |

| | |
|----------------------------------|------------------------------------------------------------------------------------|
| \mathbf{R}_n | noise covariance matrix |
| $\underline{R}_{n,n,n'}$ | element of the noise covariance matrix |
| $\tilde{\underline{R}}_{n,n,n'}$ | element of the modified noise covariance matrix |
| $\tilde{\mathbf{R}}_n$ | modified noise covariance matrix |
| $\underline{r}(t)$ | signal to be processed at the reciever |
| rect | rectangular basic transmit signature $\underline{c}_0(t)$ |
| rrcos | square root raised cosine basic transmit signature $\underline{c}_0(t)$ |
| $\underline{s}(t)$ | signal radiated by the Tx into the Ch |
| $\underline{s}^{(k)}(t)$ | signal radiated by the Tx of user k into the Ch |
| sinc | sinc shaped basic transmit signature $\underline{c}_0(t)$ |
| T | time separation between consecutive symbol specific transmit signatures |
| $T^{(SC)}$ | time separation between consecutive transmit signatures in SC systems |
| $T^{(HY)}$ | time separation between consecutive transmit signatures in HY systems |
| T_0 | 3 dB symbol duration |
| $T_{0,n_f(n)}$ | 3 dB duration of $\underline{c}_{0,n_f(n)}(t)$ |
| T_C | coherence time of the multipath channel |
| $T_{n_f(n)}$ | time separation between consecutive transmit signatures on sub-carrier $n_f(n)$ |
| T_{ref} | reference time |
| T_{pilot} | duration of the pilot sequence |
| T_{tot} | total duration of the radiated signal |
| t | absolute time |
| \mathbf{W}_0 | matrix representing the Wiener estimator |
| α | roll-off factor of the square root raised cosine |
| γ | SNR at the output of the post-processing unit |
| $\tilde{\gamma}$ | SNR at the output of the post-processing unit of the modified system model |
| γ_n | SNR of $\hat{\underline{d}}_n$ at the input of the receiver |
| γ_{MF} | SNR at the output of the MF under the assumptions of no ISI and no ICI |
| γ_{ZF} | SNR at the output of the ZF-BLE |
| γ_{MMSE} | SNR at the output of the MMSE-BLE |
| $\Delta_f(n, n')$ | relative frequency distance between $\underline{c}_n(t)$ and $\underline{c}'_n(t)$ |
| $\mathbf{\Delta}_f$ | matrix of the relative frequency distance $\Delta_f(n, n')$ |
| $\Delta_t(n, n')$ | relative time distance between $\underline{c}_n(t)$ and $\underline{c}'_n(t)$ |
| $\mathbf{\Delta}_t$ | matrix of the relative time distance $\Delta_t(n, n')$ |
| Δf | difference of absolute frequencies |
| Δt | difference of absolute observation times |
| δ | SNR-degradation |
| $\delta(\tau)$ | Kronecker delta function |
| δ_{f_D} | Doppler spread |
| δ_{MMSE} | SNR-degradation of the MMSE-BLE |

| | |
|--------------------------------|-------------------------------------------------------|
| $\tilde{\delta}_{\text{MF}}$ | modified SNR-degradation of conventional OFDM systems |
| $\tilde{\delta}_{\text{MMSE}}$ | modified SNR-degradation of the MMSE-BLE |
| δ_{ZF} | SNR-degradation of the ZF-BLE |
| $\tilde{\delta}_{\text{ZF}}$ | modified SNR-degradation of the ZF-BLE |
| λ_n | eigenvalue n of the system matrix \mathbf{A} |
| σ | standard deviation the Gaussian function |
| σ^2 | variance of the Gaussian function |
| σ_τ | delay spread of the multipath channel |
| τ_{max} | maximum excess delay of the channel |

References

- [AkV00] S. Akkarakaran, P.P. Vaidyanathan, "Bifrequency and Bispectrum Maps: A New Look at the Multirate Systems with Stochastic Inputs", *IEEE Transactions on Signal Processing*, vol. 48, no. 3, March 2000, pp. 723-736.
- [Ana01] G. Ananthaswamy, *Coded Modulation and Equalization for Highly Bandwidth Efficient Communication on Broadband Wireless Channels*, PhD Thesis, University of Massachusetts Amherst, May 2001.
- [Arm99] J. Armstrong, "Analysis of New and Existing Methods of Reducing Inter-carrier Interference Due to Carrier Frequency Offsets in OFDM", *IEEE Transactions on Communications*, vol. 47, no. 3, March 1999, pp. 365-369.
- [ATT03] A. Assalini, S. Pupolin, L. Tomba, "DMT and FMT Systems for Wireless Applications: Performance Comparison in the Presence of Frequency Offset and Phase Noise", *Proc. IEEE 6th International Symposium on Wireless Personal Multimedia Communications (WPMC'03)*, Yokosuka, Kanagawa, Japan, October 2003.
- [BaM02] P.W. Baier, M. Meurer, "Air interface enhancements for 3G and beyond 3G mobile radio communications", *Proc. 9th International Conference on Communications (ICT'02)*, Beijing, China, June 2002, pp. 284-291.
- [BaS99] S. Barbarossa, A. Scaglione, "On the capacity of linear time-varying channels", *Proc. IEEE International Conference on Acoustics, Speech and Signal Processing (ICASSP99)*, vol. 5, Phoenix, Arizona, USA, March 15-19, 1999, pp. 2627-2630.
- [BBB99] J. van de Beek, P.O. Börjesson, M.L. Boucheret, D. Landström, J.M. Arenas, P. Ödling, C. Östberg, M. Wahlqvist, S.K. Wilson, "A Time and Frequency Synchronization Scheme for Multiuser OFDM", *IEEE Journal on Selected Areas in Communications*, vol. 17, 1999, pp. 1900-1914.
- [BBC79] M.G. Bellanger, G. Bonnerot, M. Coudreuse, "Digital Filtering by Polyphase Network: Application to Sample Rate Alteration and Filter Bank", *IEEE Transactions on Acoustics, Speech and Signal Processing*, vol. ASSP-24, no. 2, April 1976 pp. 109-114.
- [BBT03] N. Benvenuto, P. Bisaglia, F. Tosato, "Sub-band Loading for Pre-equalized Uplink OFDM-CDMA Systems", *Proc. 4th International Workshop on Multi-Carrier Spread-Spectrum, MC-SS 2003*, Oberpfaffenhofen, Germany, September 2003, pp. 73-80.
- [BCT00] N. Benvenuto, G. Cherubini, L. Tomba, "Achievable Bit Rates of DMT and FMT Systems in the Presence of Phase Noise and Multipath", *Proc. IEEE 51st Vehicular Technology Conference (VTC'00 Spring)*, Tokyo, Japan, 2000, pp. 2108-2112.
- [BeC02] N. Benvenuto, G. Cherubini, *Algorithm for Communications Systems and their Applications*, John Wiley & Sons Inc., New York, 2002

- [BeD74] M.G. Bellanger, J.L. Daguët, “TDM-FDM Transmultiplexer: Digital Polyphase and FFT”, *IEEE Transactions on Communications*, vol. COM-22, no. 9, September 1974, pp. 1199-1205.
- [Bel63] P.A. Bello, “Characterization of randomly time-variant linear channels”, *IEEE Transactions on Communication Systems*, vol. CS-11, 1963, pp. 360-393.
- [Ben98] S. Ben Slimane, “OFDM Schemes with Non-Overlapping Time Waveforms”, *Proc. IEEE 47th Vehicular Technology Conference (VTC’98 Spring)*, Ottawa, Canada, May 1998, pp. 2067-2071.
- [BeS01] S. Beaver, T. Strohmer, “Optimal OFDM Pulse and Lattice Design for Doubly Dispersive Channels”, *Proc. Asilomar Conference Signals, Systems, Computers*, Pacific Grove, CA, 2001, pp. 1763-1767.
- [BeT02a] N. Benvenuto, S. Tomasin, “Efficient Pre-coding Schemes for FMT Broadband Wireless Systems”, *Proc. IEEE 13th International Symposium on Personal Indoor and Mobile Radio Communications (PIMRC’02)*, Lisbon, Portugal, September 2002, pp. 1493-1497.
- [BeT02b] N. Benvenuto, S. Tomasin, “Transmit Gain Optimization for Space Time Block Coding Wireless Systems with Co-channel Interference”, *Proc. IST Mobile & Wireless Telecommunications Summit*, Thessaloniki, Greece, June 2002.
- [BeT02c] N. Benvenuto, S. Tomasin, “On the Comparison Between OFDM and Single Carrier Modulation with a DFE Using a Frequency-Domain Feedforward Filter”, *IEEE Transactions on Communications*, vol. 50, no. 6, June 2002, pp. 947-955.
- [BeW02] I. Berenguer, I.J. Wassell, “FMT Modulation: Receiver Filter Bank Definition for the derivation of an Efficient Implementation”, *Proc. 7th International OFDM Workshop 2002*, Hamburg, Germany, September 2002, pp. 158-162.
- [BHF98] H. Bölcskei, F. Hlawatsch, H.G. Feichtinger, “Frame-theoretic analysis of oversampled filter banks”, *IEEE Trans. Signal Processing*, vol. 46, no. 12, Dec. 1998, pp. 3256-3268.
- [Bin90] J. A. C. Bingham, “Multicarrier Modulation for Data Transmission: an Idea whose time has Come”, *IEEE Communications Magazine*, vol. 28, 1990, pp. 5-14.
- [BKN94] J.J. Blanz, A. Klein, M.M. Naßhan, A. Steil, “Capacity of a cellular CDMA mobile radio system applying joint detection”, *COST 231 Temporary Document TD (94) 2*, Lisbon, 1994.
- [BoH95] H. Bölcskei, F. Hlawatsch, H. G. Feichtinger, “Equivalence of DFT filter banks and Gabor expansions”, *Proc. SPIE vol. 2569, “Wavelet Applications in Signal and Image Processing III”*, San Diego, California, USA, July 1995, pp. 128-139.

- [BoH97] H. Bölcskei, F. Hlawatsch, "Oversampled filter banks: Optimal noise shaping, design freedom, and noise analysis", Proc. International Conference on Acoustic Speech and Signal Processing (ICASSP97), Munich, Germany, vol. 3, April 1997, pp. 2453-2456.
- [BoH98] H. Bölcskei, F. Hlawatsch, "Oversampled modulated filter banks", Chapter in "Gabor Analysis: Theory, Algorithms, and Applications, H. G. Feichtinger and T. Strohmer, eds., Birkhäuser, 1998, pp. 295-322.
- [Bol99] H. Bölcskei, "Efficient design of pulse shaping filters for OFDM systems", Proc. SPIE, vol. 3813, "Wavelet Applications in Signal and Image Processing VII", Denver, Colorado, USA, July 1999, pp. 625-636.
- [Bos99] M. Bossert, Channel Coding for Telecommunications, Wiley and Sons, 1999.
- [BPH99] J.J. Blanz, A. Papathanassiou, M. Haardt, I. Furió, P.W. Baier, "Smart antennas for combined DOA and joint channel estimation in time-slotted CDMA mobile radio systems with joint detection", IEEE Transactions on Vehicular Technology, vol. 49, no. 2, 2000, pp. 293-306.
- [BTT01] N. Benvenuto, S. Tomasin, L. Tomba, "Receiver Architectures for FMT Broadband Wireless Systems", Proc. IEEE 53rd Vehicular Technology Conference (VTC'01 Spring), Rhode Island, Greece, May 2001, pp. 643-647.
- [BTT02] N. Benvenuto, S. Tomasin, L. Tomba, "Equalization Methods in OFDM and FMT Systems for Broadband Wireless Communications", IEEE Transactions on Communications, September 2002, pp. 1413-1418.
- [CaL91] E.F. Casas, C. Leung, "OFDM for Data Communications over Mobile Radio FM Channels-Part I: Analysis and Experimental Results", IEEE Transactions on Communications, vol. COM-39, NO. 5, May 1991, pp. 783-793.
- [Car96] G. Cariolaro, La teoria unificata dei segnali, UTET Libreria, Torino, Italy, 1996.
- [CCB95] P.S. Chow, J.M. Cioffi, J.A.C. Bingham, "A practical Discrete Multitone Transceiver Loading Algorithm for Data Transmission over Spectrally Shaped Channels", IEEE Transactions on Communications, vol. 43, NO. 2/3/4, February/March/April 1995, pp. 773-775.
- [CEO99] G. Cherubini, E. Eleftheriou, S. Ölcer, "Filtered Multitone Modulation for VDSL", Proc. IEEE Global Communication Conference (Globecom '99), Rio de Janeiro, Brazil, November 1999, pp. 1139-1144.
- [CEO00] G. Cherubini, E. Eleftheriou, S. Ölcer, J.M. Cioffi, "Filter Bank Modulation Techniques for Very High-Speed Digital Subscriber Lines", IEEE Communication Magazine, May 2000, pp. 98-104.
- [CEO02] G. Cherubini, E. Eleftheriou, S. Ölcer, "Filtered Multitone Modulation for Very High-Speed Digital Subscriber Lines", IEEE Journal on Selected Areas in Communications, vol. 20, 2002, pp. 1016-1028.

- [CFH02] E. Costa, A. Filippi, H. Haas, S. Ometto, E. Schulz, "Adaptive sub-band allocation in MC-CDMA/FDM systems", Proc. 7th International OFDM Workshop 2002, Hamburg, Germany, September 2002, pp. 16-20.
- [CFO03] E. Costa, A. Filippi, S. Ometto, M. Weckerle, E. Schulz, "Asynchronous up-link transmission in FMT-FDMA systems", Proc. IEEE International Symposium on Personal, Indoor and Mobile Radio Communications (PIMRC '03), Beijing, China 2003, pp. 1090-1094.
- [CFW03] E. Costa, A. Filippi, M. Weckerle, E. Schulz, "Comparison of FMT-FDMA and OFDMA in Asynchronous Uplink Applications", Proc. 8th International OFDM Workshop 2003, Hamburg, Germany, September 2003, pp. 93-97.
- [Cha66] R.W. Chang, "Synthesis of Band-Limited Orthogonal Signal for Multichannel Data Transmission", Bell System Technical Journal, December 1966, pp. 1775-1796.
- [CHS02] E. Costa, H. Haas, E. Schulz, A. Filippi, "Capacity Optimisation in MC-CDMA Systems", European Transactions on Telecommunications (ETT), vol. 13, no. 5, September/October 2002, pp. 455-463.
- [Cim85] L.J. Cimini, "Analysis and simulation of a digital mobile channel using orthogonal frequency division multiplexing", IEEE Transactions on Communications, vol. 33, no. 7, July 1985, pp. 665-675.
- [CoP02] E. Costa, S. Pupolin, "M-QAM-OFDM System Performance in the Presence of a Nonlinear Amplifier and Phase Noise", IEEE Transactions on Communications, vol. 50, March 2003, pp. 462-472.
- [COS89] COST 207, Digital land mobile radio communications, Final Report COST Action 207, Office for Official Publications of the European Communities, Luxembourg, 1989.
- [CTC91] J.S. Chow, J.C. Tu, J.M. Cioffi, "A Discrete Multitone Transceiver System for HDSL Applications", IEEE Journal on Selected Areas in Communications, vol. 9, August 1991, pp. 895-908.
- [CTF04] E. Costa, P. Trifonov, A. Filippi, "Location Based Adaptive sub-band Allocation for Multi-Carrier Multiple Access Systems", Proc. IEEE 15th International Symposium on Personal Indoor and Mobile Radio Communications (PIMRC'04), Barcelona, Spain, September 2004, pp. 599-603.
- [CvV98] Z. Cvetković, M. Vetterli "Oversampled Filter Banks", IEEE Transactions on Signal Processing, vol. 46, no. 5, May 1998, pp. 1245-1255.
- [DeZ94] U. Dersch, E. Zollinger, "Propagation mechanism in microcell and indoor environments", IEEE Transactions on Vehicular Technology, vol. 43, no. 4, 1994, pp. 1058-1066.
- [ECS98] R.B. Ertel, P. Cardieri, K.W. Sowerbi, T.S. Rappaport and J.R. Reed, "Overview of spatial channel models for antenna array communication systems", IEEE Personal Communications Magazine, vol. 5, no. 1, 1998, pp. 10-22.

- [FAB02] D. Falconer, S.L. Ariyavisitakul, A. Benymin-Seeyar, B.Eidson, "Frequency Domain Equalization for Single-Carrier Broadband Wireless Systems", IEEE Communications Magazine, April 2002, pp. 58-66.
- [FaK01] K. Fazel, S. Kaiser, "Multi-Carrier Spread Spectrum Systems", John Wiley and Sons Ltd., September 2001.
- [FaK02] K. Fazel, S. Kaiser, "Multi-Carrier Spread Spectrum Systems", John Wiley and Sons Ltd., September 2002.
- [FaK03] K. Fazel, S. Kaiser, "Multi-Carrier Spread Spectrum Systems", John Wiley and Sons Ltd., September 2003.
- [FCS04a] A. Filippi, E. Costa, E. Schulz, "Effects of the Reduction of the Time and Frequency Separation in Multi-Carrier Systems", Proc. 9th International OFDM Workshop 2004, Dresden, Germany, September 2004.
- [FCS04b] A. Filippi, E. Costa, E. Schulz, "Sensitivity of Multi-Carrier Systems to Time and Frequency Sub-Carrier Separation", Proc. 7th International Symposium on Wireless Personal Multimedia Communications (WPMC2004), Abano Terme, Padova, Italy, September 2004, pp. 431-435.
- [FCS04c] A. Filippi, E. Costa, E. Schulz, "Low Complexity Interleaved Sub-carrier Allocation in OFDM Multiple Access Systems", Proc. 60th Vehicular Technology Conference (VTC'04 Fall), Los Angeles, CA, September 2004.
- [FRB97] J. Fuhl, J.P. Rossi, E. Bonek, "High resolution 3-D direction-of-arrival determination for urban mobile radio", IEEE Transactions on Antennas and Propagation, vol. 45, no. 4, 1997, pp. 672-681.
- [ETS01a] European Telecommunications Standard Institute, "Radio Broadcasting Systems; Digital Audio Broadcasting (DAB) to mobile, portable, and fixed receivers", ETSI EN 300 401 V1.3.3, Sophia Antipolis, France, January 2001.
- [ETS01b] European Telecommunications Standard Institute, "Digital Video Broadcasting (DVB): Framing structure, channel coding and modulation for digital terrestrial television", ETS 300 744, Sophia Antipolis, France, January 2001.
- [ETS99] European Telecommunications Standard Institute, "HIPERLAN Type 2 Technical Specification; Physical (PHY) layer", ETSI DTS/BRAN-0023003, November 1999.
- [Gal68] R.G. Gallager, Information Theory and Reliable Communications, Wiley, New York, 1968.
- [GaR02] D. Galda, H. Rohling, "A low complexity transmitter structure for OFDM-FDMA uplink systems", Proc. IEEE 55th Vehicular Technology Conference (VTC '02), Birmingham, AL, USA, 2002, pp. 1737-1741.
- [GBR00] R. Grünheid, E. Bolinht, H. Rohling, K. Aretz, "Adaptive Modulation for the Hiperlan/2 Air Interface", Proc. 5th International OFDM Workshop 2000, Hamburg, Germany, September 2000, pp. 4-1-4-4.

- [GSB00] G.B. Giannakis, A. Scaglione, S. Barbarossa, "Robust OFDM Transmissions over Frequency-Selective Channels with Multiplicative Time-selective effects", Proc. International Conference on Acoustic Speech and Signal Processing (ICASSP2000), Istanbul, Turkey, June 5-9, 2000., pp. 2677-2680.
- [HCF02] H. Haas, E. Costa, A. Filippi, F. Abellan-Rodriguez, "The Impact of Channel Correlation on Space-Time Block Codes for Different Modulation Schemes", Proc. IEEE 56th Vehicular Technology Conference (VTC'02 Fall), Vancouver, Canada, September 2002, pp. 1907-1910.
- [HGI02] G.W. Hein, J. Godet, J. Issler, J. Martin, P. Erhard, R. Lucas-Rodriguez, T. Pratt, Status of Galileo Frequency and Signal Design, Brussels, September 2002, [http:// europa.eu.int/ comm/ dgs/ energy_transport/ galileo/ documents/ technical_en.htm](http://europa.eu.int/comm/dgs/energy_transport/galileo/documents/technical_en.htm).
- [Hir81] B. Hirosaki, "An Orthogonally Multiplexed QAM System using the Discrete Fourier Transform", IEEE Transactions on Communications, vol. COM-29, no. 7, July 1981, pp. 982-989.
- [Hoe92] P. Höher, "A statistical discrete-time model for the WSSUS multipath channel", IEEE Transactions on Vehicular Technology, vol. 35, 1992, pp. 461-468.
- [IAV00] T. Ihalainen, J. Alhava, A. Viholainen, X. Hongnian, J. Rinne, M. Renfors, "On the performance of filter bank based multicarrier systems in xDSL and WLAN applications", Proc. International Conference on Communications , New Orleans, Louisiana, USA, June 18-22, 2000, pp. 1120-1124.
- [IEE99] IEEE Standard 802.11a-1999, Part 11, "Wireless LAN Medium Access Control (MAC) and Physical Layer (PHY) specifications: High-speed Physical Layer in the 5 GHz Band", September 1999.
- [Kai98] S. Kaiser, "Multi-Carrier CDMA Mobile Radio Systems- Analysis and Optimization of Detection, Decoding, and Channel Estimation", Fortschritts-Berichte VDI, Reihe 10, Nr. 531, VDI-Verlag, Düsseldorf, 1998.
- [Kal95] G.K. Kaleh , "Channel Equalization for Block Transmission Systems", IEEE Journal on Selected Areas in Communications, vol. 13, 1995, pp. 110-121.
- [Kan04] G. Kang, Time and frequency domain joint channel estimation (ICE) in multi-carrier multi-branch systems, to appear as a PhD dissertation, University of Kaiserslautern 2004.
- [Kat97] R. Kattenbach, Charakterisierung zeitvarianter Indoor-Funkkanäle anhand ihrer System- und Korrelationsfunktionen, Shaker Verlag, Aachen, 1997.
- [Kay93] S.M. Kay, Fundamentals of Statistical Signal Processing: Estimation Theory, Prentice Hall, New Jersey, 1993.
- [KeH99] T. Keller, L. Hanzo, "Sub-band Adaptive Pre-equalised OFDM Transmission", Proc. IEEE 50th Vehicular Technology Conference (VTC'99-Fall), Amsterdam, Netherlands, 1999, pp. 334-338.

- [KKB96] A. Klein, K. Kaleb, P.W. Baier, "Zero Forcing and Minimum Mean-Square-Error Equalization for Multiuser Detection in Code-Division Multiple-Access Channels", *IEEE Transactions on Vehicular Technology*, vol. 45, 1996, pp. 276-287.
- [KIH82] R. Kohno, H. Imai, M. Hatori, "Cancellation techniques of co-channel interference in asynchronous spread spectrum multiple access systems", Institute of Electronics and Communications Engineers (IECE) Technical report, CS82-38, 1982, pp. 29-35.
- [KIH83] R. Kohno, H. Imai, M. Hatori, "Cancellation techniques of co-channel interference in asynchronous spread spectrum multiple access systems", *Transactions of the Institute of Electronics and Communications Engineers (IECE) Japan*, vol. J66-A, 1983, pp. 416-423.
- [Kle96] A. Klein, *Multi-user detection of CDMA-signals-algorithms and their application to cellular mobile radio*, Fortschrittberichte VDI, series 10, no. 423, VDI-Verlag, Düsseldorf, 1996.
- [KMT96] A. Klein, W. Mohr, R. Thomas, P. Weber and B. Wirth, "Direction-of-arrival of partial waves in wideband mobile radio channels for intelligent antenna concepts", *Proc. IEEE 46th Vehicular Technology Conference (VTC '96)*, Atlanta, 1996, pp. 849-853.
- [KoM98] W. Kozek, A.F. Molish, "Nonorthogonal pulse shapes for multicarrier communications in doubly dispersive channels", *IEEE Journal on Selected Areas in Communications*, vol. 16, 1998, pp. 1579-1589.
- [Koz96] W. Kozek, *Matched Weyl-Heisenberg Expansions of Nonstationary Environments*, PhD Thesis, Technical University of Vienna, September 1996.
- [KPU00] W. Kozek, G. Pfander, J. Ungermann, G. Zimmermann, "A Comparison of Various MCM Schemes", *Proc. 5th International OFDM Workshop 2000*, Hamburg, Germany, September 2000, pp. 20-1-20-4.
- [Kre95] E. Kreyszig, *Advanced Engineering Mathematics*, Seventh Edition, John Wiley & Sons, New York, 1993.
- [LaA03] C. Lange, A. Ahrens, "Orthogonal Bases for the Design of Multicarrier Transmission Systems", *Proc. 8th International Workshop 2003*, Hamburg, Germany, September 2003, pp. 254-258.
- [Lu02] Y. Lu, *Contributions to the application of the adaptive antennas ad CDMA code polling in the TD-CDMA downlink*, PhD thesis, http://kluedo.ub.uni-kl.de/volltexte/2002/1290/pdf/dissertation_7.pdf, 2002.
- [MBG96] T. Müller, K. Brüninghaus, H. Rohling, "Performance of Coherent OFDM-CDMA for Broadband Mobile Communications", *International Journal of Wireless and Personal Communications (WPC)*, Kluwer, vol. 2, no. 4, Dordrecht, The Netherlands, 1995/1996.
- [MoC58] R.R. Mosier, R.G. Clabaugh, "Kilex, a Bandwidth Efficient Binary Transmission System", *AIEE Transaction*, vol. 76, January 1958, pp. 723-728.

- [MRE98] T. May, H. Rohling, V. Engels, "Performance analysis of Viterbi decoding for 64-DAPSK and 64-QAM modulated OFDM signals", *IEEE Transactions on Communications*, vol. 46, no. 2, February 1998, pp. 182-190.
- [NeP00] R. van Nee, R. Prasad, *OFDM for Wireless Multimedia Communications*, Artech House, Boston, 2000.
- [NTT01] NTT DoCoMo, "The Path to 4G Mobile", *IEEE Communications Magazine*, vol. , March 2001, pp. 38-41.
- [Pap91] A. Papoulis, *Probability, Random Variables, and Stochastic Processes*, McGraw-Hill, Singapore, 3rd edition, 1991.
- [Pap00] A. Papathanassiou, Adaptive antennas for mobile radio systems using Time Division CDMA and joint detection, *Forschungsberichte Mobilkommunikation*, vol. 6, University of Kaiserslautern, 2000.
- [Par92] J.D. Parsons, *The mobile radio propagation channel*, Pentech Press, London, 1992.
- [Pfs01] S. Pfletschinger, J. Speidel, "Optimized Impulses for Multicarrier Offset-QAM", *Proc. IEEE Global Communication Conference (Globecom '01)*, San Antonio, Texas, USA, November 2001, vol. 1, pp. 207-211.
- [Pro95] J.G. Proakis, *Digital communications*, McGraw-Hill, New York, 3rd edition, 1995.
- [PSW99] A. Papathanassiou, R. Schmalenberger, M. Weckerle, P.W. Baier, "Advances in channel estimation techniques in TD-CDMA mobile radio systems with smart antennas", *Proc. International Workshop on Mobile Communications (IWMC'99)*, Chania, 1999, pp. 11-20.
- [Rap99] T.S. Rappaport, *Wireless communications: Principles & Practice*, Prentice-Hall, Inc., Upper Saddle River, New Jersey, 1999.
- [RBG97] H. Rohling, K. Brüninghaus, R. Grünheid, "Comparison of Multiple Access Schemes for an OFDM Downlink System", K. Fazel, G. Fettweis (Eds.): *Multi-Carrier Spread Spectrum*, Kluwer Academic Publishers, Dordrecht, The Netherlands, 1997, pp. 23-30
- [ReR94] C. Reiners, H. Rohling, "Multicarrier Transmission Technique in Cellular Mobile Communications Systems", *Proc. IEEE 44th Vehicular Technology Conference (VTC'94)*, Stockholm, Sweden, 1994, pp. 1645-1649.
- [RGG01] H. Rohling, R. Grünheid, D. Galda, "OFDM Air Interface for the 4-th Generation of Mobile Communication Systems", *Proc. 6th International OFDM Workshop 2001*, Hamburg, Germany, September 2001, pp. 1-28.
- [RGM97] H. Rohling, R. Grünheid, T. May, "Coherent and Incoherent Demodulation for an OFDM Transmission and System", 3. ITG-Fachtagung "Mobile Kommunikation" (EPMCC '97), Bonn, Germany, 1997, pp. 117-120.

- [Red02] A.J. Redfern, "Receiver Window Design for Multicarrier Communication Systems", *IEEE Journal on Selected Areas in Communications*, vol. 20, June 2002, pp. 1029-1036.
- [RMB99] H. Rohling, T. May, K. Brüninghaus, R. Grünheid, "Broad-Band OFDM Radio Transmission for Multimedia Applications", *Proceedings of the IEEE*, vol. 87, no. 10, October 1999, pp. 1778-1789.
- [RoG96a] H. Rohling, R. Grünheid, "Performance of an OFDM-TDMA Mobile Communication System", *Proc. IEEE 46th Vehicular Technology Conference (VTC'96)*, Atlanta, GA, 1996, pp. 1589-1593.
- [RoG96b] H. Rohling, R. Grünheid, "OFDM Transmission Technique with Flexible Subcarrier Allocation", *Proc. 3rd International Conference on Communications (ICT'96)*, Instambul, Turquie, April 1996, pp. 567-571.
- [RoG97] H. Rohling, R. Grünheid, "Performance Comparison of Different Multiple Access Schemes for the Downlink of an OFDM Communication System", *Proc. IEEE 47th Vehicular Technology Conference (VTC'97)*, Phoenix, AZ, 1997, pp. 1365-1369.
- [RoG98] H. Rohling, R. Grünheid, "Adaptive Coding and Modulation in an OFDM-TDMA Communication System", *Proc. IEEE 47th Vehicular Technology Conference (VTC'98 Spring)*, Ottawa, Canada, May 1998, pp. 773-776.
- [RoM97] H. Rohling, T. May, "Comparison of PSK and DPSK Modulation in a Coded OFDM System", *Proc. IEEE 47th Vehicular Technology Conference (VTC'97)*, Phoenix, AZ, 1997, pp. 870-874.
- [Sal67] B. Saltzberg, "Performance of an Efficient Parallel Data Transmission System", *IEEE Transactions on Communications Technology*, vol. COM-15, no. 6, December 1967, pp. 805-811.
- [Sch79] R.O. Schmidt, "Multiple emitter location and signal parameter estimation", *Proc. RADC Spectrum Estimation Workshop*, Griffiths AFB, New York, 1979, pp. 243-258.
- [Sch89] H. Schulze, "Stochastische modelle und digitale simulation von mobilfunkkanälen", in *Kleinheubacher Berichte*, no. 32, 1989, Germany (FR), Darmstadt, Germany, pp. 473-483.
- [SGB99a] A. Scaglione, G.B. Giannakis, S. Barbarossa "Minimum Redundancy Filterbank Precoder For Blind Channel Identification Irrespective of Channel Nulls", *Proc. IEEE Wireless Communications and Networking Conference (WCNC '99)*, New Orleans, Louisiana, USA, September 1999, pp. 787-791.
- [SGB99b] A. Scaglione, G.B. Giannakis, S. Barbarossa, "Redundant Filterbank Precoders and Equalizers Part I: Unification and Optimal Design", *IEEE Transactions on Signal Processing*, vol. 47, no. 7, July 1999, pp. 1988-2006.
- [SGB99c] A. Scaglione, G.B. Giannakis, S. Barbarossa, "Redundant Filterbank Precoders and Equalizers Part II: Blind Channel Estimation, Synchronization and Direct Equalization", *IEEE Transactions on Signal Processing*, vol. 47, no. 7, July 1999, pp. 2007-2022.

- [SGB99d] A. Scaglione, S. Barbarossa, G.B. Giannakis, "Filterbank Transceivers Optimizing Information Rate in Block Transmissions over Dispersive Channels", *IEEE Transactions on Information Theory*, vol. 45, no. 3, April 1999, pp. 1019-1032.
- [SGH02] C.V. Sinn, J. Götze, M. Haardt "Efficient Data Detection Algorithm in Single- and Multi-carrier Systems without the necessity of a Guard Interval", *Proc. IEEE International Conference on Acoustic Speech and Signal Processing (ICASSP'02)*, Orlando, Florida, USA, May 2002, pp. 2737-2740.
- [Sha48] C.E. Shannon, "A mathematical theory of communication", *Bell System Technical Journal*, vol. 27, July and October, 1948, pp. 379-423 and 623-656.
- [SHG02] C.V. Sinn, F. Hanschmann, J. Götze, "Efficient Algorithms Relating OFDM Channel Parameters to Filter Weights in single-Carrier Systems with Frequency Domain Equalization", *Proc. 7th International OFDM Workshop 2002*, Hamburg, Germany, September 2002, pp. 61-66.
- [Sk104] A. Sklavos, *Service Area Based OFDM Air Interface for Beyond 3G Mobile Radio Systems*, *Forschungsberichte Mobilkommunikation*, vol. 6, Alexandros Sklavos, Kaiserslautern 2004.
- [SMH02] D. Schafhuber, G. Matz, F. Hlawatsch, "Pulse-shaping OFDM/BFDM Systems for Time-varying Channels: ISI/ICI Analysis, Optimal Pulse Design, and Efficient Implementation", *Proc. IEEE 13th International Symposium on Personal Indoor and Mobile Radio Communications (PIMRC'02)*, Lisbon, Portugal, September 2002, pp. 1012-1016.
- [SMW01] A. Sklavos, I. Maniatis, T. Weber, P.W. Baier, E. Costa, H. Haas, E. Schulz, "Joint channel estimation in multi-user OFDM systems", *Proc. 6th International OFDM-workshop (InOWo '01)*, 2001, pp. 3-1-3-4.
- [StB96] A.J. Steil, J.J. Blanz, "Spectral efficiency of JD-CDMA mobile radio systems applying coherent receiver antenna diversity with directional antennas", *Proc. IEEE 4th International Symposium on Spread Spectrum Techniques & Applications (ISSSTA '96)*, Mainz, 1996, pp. 313-319.
- [Ste92] R. Steele (editor), *Mobile radio communications*, Pentech Press, London, 1992.
- [Ste95] B. Steiner, *Ein Beitrag zur Mobilfunkkanalschätzung unter besonderer Berücksichtigung synchroner CDMA-Mobilfunksysteme mit Joint Detection*, *Fortschrittberichte VDI*, series 10, no. 337, VDI-Verlag, Düsseldorf, 1995.
- [Ste96] A. Steil, *Spektrale Effizienz digitaler zellulare CDMA-Mobilfunksysteme mit gemeinsamer Detektion*, *Fortschrittberichte VDI*, series 10, no. 437, VDI-Verlag, Düsseldorf, 1996.
- [StJ67] S. Stein, J.J. Jones, *Modern communication principles*, McGraw-Hill, New York, 1967.

- [StJ94] B. Steiner, P. Jung, "Optimum and suboptimum channel estimation for the uplink of CDMA mobile radio systems with joint detection", *European Transactions on Communications*, vol. 5, 1994, pp. 39-49.
- [STS03] T. Strohmer, S. Beaver, "Optimal OFDM design for time-frequency dispersive channels", *IEEE Transactions on Communications*, vol. 51, 2003, pp. 1111-1122.
- [Sun01] Y. Sun, "Bandwidth-Efficient Wireless OFDM", *IEEE Journal on Selected Areas in Communications*, vol. 19, November 2001, pp. 2267-2278.
- [TCF03] P. Trifonov, E. Costa, A. Filippi, "Adaptive Coding in MC-CDMA/FDM Systems with Adaptive Sub-band Allocation", *Proc. 5th International Workshop on Multi-Carrier Spread-Spectrum, MC-SS 2003*, Oberpfaffenhofen, Germany, September 2003, pp. 133-140.
- [TCF04] P. Trifonov, E. Costa, A. Filippi, "Adaptive coding in MC-CDMA/FDM systems with adaptive sub-band allocation", to appear in *European Transactions on Telecommunications (ETT)*, Special Issues on MC-SS, vol. 15, no. 3, May-June 2004.
- [TLP00a] A. Tonello, N. Laurenti, S. Pupolin, "Analysis of the up-link of an asynchronous DMT OFDMA system impaired by time-offsets, frequency offsets, and multi-path fading", *Proc. IEEE 52nd Vehicular Technology Conference (VTC'00 Fall)*, Boston, Massachusetts, 2000, pp. 1094-1099.
- [TLP00b] A. Tonello, N. Laurenti, S. Pupolin, "Capacity considerations on the uplink of a DMT OFDMA impaired by time misalignments and frequency offsets", *Software radio technologies and services*, Springer-Verlag ed. 2000, pp. 93-104.
- [Tom01] L. Tomba, "On the Use of DMT or FMT for MC-CDMA Systems", *Proc. 3rd International Workshop on Multi-Carrier Spread-Spectrum, MC-SS 2001*, Oberpfaffenhofen, Germany, September 2001, pp. 147-154.
- [Ton01] A.M. Tonello, "Multicarrier multiuser asynchronous communications", Doctor of Research Degree Thesis, University of Padova, December 2001.
- [Ton02] A.M. Tonello, "Multiuser Detection and Turbo Multiuser decoding for Asynchronous Multitone Multiple Access Systems", *Proc. IEEE 56th Vehicular Technology Conference (VTC'02 Fall)*, Vancouver, Canada, September 2002, pp. 970-974.
- [Ton03] A.M. Tonello, "Exact matched Filter Performance Bound for Multitone Modulation in Fading Channels", *Proc. IEEE 6th International Symposium on Wireless Personal Multimedia Communications (WPMC'03)*, Yokosuka, Kanagawa, Japan, October 2003.
- [ToP02] A.M. Tonello, S. Pupolin, "Performance of Single User Detectors in Multitone Multiple Access Asynchronous Communications", *Proc. IEEE 55th Vehicular Technology Conference (VTC'02 Spring)*, Birmingham, Alabama, 2002, pp. 199-203.

- [TrF02] S. Trautmann, N.J. Fliege, "A New Equalizer for Multitone Systems Without Guard Time", *IEEE Communication Letters*, vol. 6, no. 1, January 2002, pp. 34-36.
- [Uns00] M. Unser, "Sampling-50 Years After Shannon", *Proc. IEEE*, vol. 88, no. 4, April 2000, pp. 569-587.
- [Vai93] P.P. Vaidyanathan, *Multirate Systems and Filter Banks*, Englewood Cliffs, NJ: Prentice Hall, 1993.
- [Vai01] P.P. Vaidyanathan, "Filter Banks in Digital Communications", *IEEE Circuit and System Magazine*, vol. 1, no. 2, Second Quarter 2001, pp. 4-25.
- [VeK95] M. Vetterli, J. Kovacevic, *Wavelets and Subband Coding*, Prentice Hill, 1995.
- [Ver98] S. Verdú, *Multiuser detection*, Cambridge University Press, 1998.
- [WaG00] Z. Wang, G.B. Giannakis, "Wireless Multicarrier Communications: where Fourier Meets Shannon", *IEEE Signal Processing Magazine*, May 2000, pp. 29-48.
- [Wec01] M. Weckerle, "Turbo methods for exploiting spatial and temporal covariance matrices in the TD-CDMA uplink with multi-element antennas", *Proc. 4th European Personal Mobile Communications Conference (EPMCC'01)*, Vienna, 2001, no. 29.1.
- [Wec02] M. Weckerle, *Utilization of Correlation Matrices in Adaptive Array Processors for Time-Slotted CDMA Uplinks*, *Forschungberichte Mobilkommunikation Band 11*, University of Kaiserslautern 2002.
- [WeE71] S.B. Weinstein, P.M. Ebert, "Data Transmission by Frequency-Division Multiplexing Using Discrete Fourier Transform", *IEEE Transactions on Communications Technology*, vol. COM-19, no. 5, October 1971, pp. 628-634.
- [WeM02] T. Weber, M. Meurer, "Iterative multiuser detection for TD-CDMA exploiting data estimate refinement techniques", *Proc. IEEE 56th Vehicular Technology Conference (VTC'02 Fall)*, Vancouver, 2002, pp. 1642-1646.
- [WeS00] S. Weiss, R. Stewart, "Fast Implementation of Oversampled Modulated Filter Banks", *IEEE Electronics Letters*, vol. 36, Issue 17, August 2000, pp. 1502-1503.
- [Wha71] A.D. Whalen, *Detection of signals in noise*, Academic Press, New York, 1971.
- [YoS01] D. Yoo, W.E. Stark, "Carrier Separated OFDM Systems for Multiaccess Wireless Communications", *Proc. IEEE 3rd International Conference on Mobile Wireless Communications Networks (MWCN'01)*, Recife, Brazil, August 2001, pp. 421-426.
- [Zol93] E. Zollinger, *Eigenschaften von Funkübertragungstrecken in Gebäuden*, *Doctoral Dissertation*, Eidgenössische Technische Hochschule Zürich, 1993.

- [ZoW95] W.Y. Zou, Y. Wu, "COFDM: an Overview", IEEE Transaction on Broadcasting, vol. 41. no. 1, March 1995, pp. 1-8.

Tabellarischer Lebenslauf

Name: Alessio Filippi

Adresse: Therese-Giehse-Allee 60
81739 München

Geburtsdatum: 3. Januar 1977

Geburtsort: Pordenone, Italien

Familienstand: verheiratet

Staatsangehörigkeit: italienisch

Schulbildung: September 1983 – Juni 1991 Grundschule in Padova, Italien
September 1991 – Juli 1996 Lyzeum in Padova, Italien

Schulabschluß: Abitur

Studium: September 1996 – März 2002
Studium der Elektrotechnik
an der Università degli Studi di Padova

Studienabschluß: Diploma di Laurea (Diplom, äquivalent Dipl.-Ing.)

Berufstätigkeit: September 2001 – November 2001
Werkstudent bei der Siemens AG, München

Dezember 2001 – Juni 2002
Diplomarbeiter bei der Siemens AG, München

Juli 2002 – Dezember 2004
freier Mitarbeiter der Siemens AG, München

seit Januar 2005
Mitarbeiter der Philips Research, Eindhoven, The Netherlands